Understanding the biochemical alterations in cancer cells chronically treated with PI3K/mTOR inhibitors

Maria Dermit

Queen Mary University of London

Barts and the London School of Medicine and Dentistry

Thesis submitted for the degree of Doctor of Philosophy

Principal Supervisor: Dr. Pedro R. Cutillas

Second Supervisor: Prof. John G. Gribben

Statement of originality

The research work presented in this thesis is the result of my own original work with the exception of:

- Figures 7.7, 7.9B, and 7.21: experiments performed by Benjamin Adley Omoregie as part of his MSc research project under the supervision of Maria Dermit and Pedro Cutillas.

- The sequencing experiments presented in Chapter 6 were performed at Source Biosciences, Nottingham. Bioinformatics analyses of these datasets were performed by Dr Ai Nagano.

- The fluidigm profiling experiments presented in Section 5.7 were performed and analysed by Hayley Campbell and Susan Critchlow.

The results presented in Chapters 3-5 of this dissertation have been published:

Dermit M, Casado P, Rajeeve V, Wilkes E.H., Foxler D.E., Campbell H., Critchlow S., Sharp T.V., Gribben J.G., Unwin R., Cutillas P.R. Oxidative stress downstream of mTORC1 but not AKT causes a proliferative defect in cancer cells resistant to PI3K inhibition. Oncogene (2016).

This thesis has a total of 68,518 words (including references).

Acknowledgements

First and foremost, I would like to thank my supervisor Pedro Cutillas for giving me the opportunity to do my research work in his lab. It has been few years of continuous learning, and I was really fortunate to be a PhD student of Pedro. I hope we keep discussing science and projects in the future. I would also like to thank John Gribben, my second supervisor, and Robert Unwin, who provided his guidance and contributed to the St Peters Trust and Barts studentship that supported my PhD.

I would also like to thank Vinni for her advice, for sharing her expertise, for being during long time the female friend within the ICSP [Integrative cell signalling and proteomics] group, and for helping the group staying afloat. Being surrounded by the members of ICSP – Arran, Maru, Ryan, Erika, and Dave – made the PhD time fully interesting. I would like to thank Pedro Casado for the paramount value of his scientific input to this work, and Ed, for being a great student model to follow as well as a friend during the early days of the PhD.

It was great being in the office with the "Girls of 326", where we shared both life and scientific experiences, and much cake. The Spaniards – Carmen, Cecilia, Ana, Teresa, Jose, Marina, and Jordi – made me feel like home many times and were excellent in making daily breaks and Friday nights great fun. Frankly, everybody in Barts Cancer Institute (BCI) contributed to provide a friendly and constructive research environment that substantially enriched the time of my PhD studies.

This thesis is dedicated to my dad and my mom, and it was made possible by the motivation and love of Pedro Tizei.

Why are you keeping this curiosity door locked?

Dustin Henderson (Stranger Things)

Abstract

The PI3K/mTOR signalling pathway plays a major role in biology and disease. Therefore, effective inhibitors that target proteins of this pathway have been developed. However, acquired resistance of cancer cells is a prevalent phenomenon that limits the durable response of these compounds.

It is becoming apparent that experimental approaches for comprehensive biochemical analysis contribute to understand the complex mechanisms that confer drug resistance, and advances in large-scale technologies including genomic sequencing and proteomics allow unprecedented molecular coverage without being biased for specific genes/cellular pathways.

Initially, the phenotypic response of sensitive and resistant cells to the absence or presence of a PI3K inhibitor (PI3Ki), as well as other kinases, was examined. This study revealed that PI3Ki-resistant cells experience extensive phenotypic changes upon withdrawal of the PI3Ki from the culture media.

The regulation of the proteome and phosphoproteome of sensitive and PI3Ki-resistant cells grown with or without the PI3Ki was analysed by shotgun mass spectrometry-based label-free quantitative technology. This analysis demonstrated that the proteomes and phosphoproteomes of drug-resistant cells are remodelled conditional to the presence of PI3Ki, and that the levels of enzymes with metabolic roles are modulated in resistant cells. Functional analysis of the metabolism of cells capable to survive in absence of PI3K/mTOR activity demonstrated that the bioenergetic activity of these cells is contingent on the presence of the selection drug.

The complete set of protein-coding regions of the genome (exome) of sensitive and PI3Ki-resistant cells was then sequenced. This study unveiled common alterations in exome regions across PI3Ki-resistant cell lines, as well as a degree of genomic heterogeneity between them.

Lastly, the impact of lactic acid, a metabolic product, on a defined signalling network of the MCF7 breast cancer cell line was analysed. This study described the capacity of this metabolite to change the activity of signalling network branches.

Table of contents

List of figures

List of tables

Abbreviations

ACLY: ATP-citrate synthase

ACN: Acetonitrile

AML: Acute myeloid leukaemia

AMPK: 5'-AMP-activated protein kinase

BAF: B-allele frequency

BCA: Bicinchoninic acid

BSA: Bovine serum albumin

BWA: Burrows-Wheeler Aligner

CAMK2: Calcium/calmodulin-dependent protein kinase II

CI: Combination index

CID: Collision-induced dissociation

CML: Chronic myeloid leukaemia

COSMIC: Catalogue Of Somatic Mutations In Cancer

CTAM: Compound target activity markers

DAPI: 4',6-diamidino-2-phenylindole

DAVID: Database for Annotation, Visualisation and Integrated Discovery

DDA: Data-dependent acquisition

DIA: Data-independent acquisition

DMEM: Dulbecco's modified Eagle's medium

DMSO: Dimethyl sulphoxide

DTT: Dithiothreitol

ECAR: Extracellular acidification rate

ECL: Enhanced chemiluminescence

EDTA: Ethylenediamine tetra-acetic acid

EGFR: Epidermal growth factor receptor

EPAS1: Endothelial PAS protein 1

ERLIC: Electrostatic repulsion-hydrophilic interaction chromatography

ESI: Electrospray ionisation

ETD: electron-transfer dissociation

FA: Formic acid

FASN: Fatty acid synthase

FABP5: Fatty acid-binding protein

FBS: Foetal bovine serum

FCCP: Carbonyl cyanide 4-(trifluoromethoxy) phenylhydrazone

FDR: False discovery rate

G6PD: Glucose-6-phosphate dehydrogenase

GPCR: G-protein coupled receptor

GEF: Guanine nucleotide exchange factor

GLUT4: Glucose transporter 4

GO: Gene ontology

HCD: Higher-energy collision dissociation

HER2: Human epidermal growth factor receptor 2

HIF: Hypoxia inducible factor

HILIC: Hydrophilic interaction chromatography

IAM: Iodoacetamide

ICAT: Isotope-coded affinity tag

IDH3A: Isocitrate dehydrogenase 3A

IMAC: Immobilised metal affinity chromatography

INPP4B: Inositol polyphosphate-4-phosphatase

IRS-1: Insulin receptor substrate 1

iTRAQ: Isobaric tag for relative and absolute quantification

KSEA: Kinase-substrate enrichment analysis

LC: Liquid chromatography

LC-MS/MS: Liquid chromatography-tandem mass spectrometry

LDHA: Lactate dehydrogenase A

LDH6B: Lactate dehydrogenase A-like 6B

LDHB: Lactate dehydrogenase B and

LOH: Loss of heterozygosity

LTQ: Linear trap quadrupole

MALDI: Matrix-assisted laser desorption ionisation

MAPK: Mitogen-activated protein kinase

MCT: Monocarboxylate transporter

MOAC: Metal oxide affinity chromatography

MS: Mass spectrometry

MRM: Multiple reaction monitoring

MSA: Multi-stage activation

mTOR: Mammalian target of rapamycin

NAC: N-acetyl cysteine

NRF2: Nuclear factor erythroid 2-related factor

NSCLC: Non-small-cell lung cancer

OCR: Oxygen consumption rate

PAGE: Polyacrylamide gel electrophoresis

PBS: Dulbecco's phosphate-buffered saline

PCA: Principal component analysis

PCK2: Phosphoenolpyruvate carboxykinase 2

PESCAL: Peak statistic calculator

PHD: Prolyl hydroxylases

PI3K: Phosphoinositide 3-kinase

PKB: Protein kinase B

PP2A: Protein phosphatase 2

PTEN: Phosphatase and tensin homolog

PTM: Post-translational modification

PTP1B: Protein tyrosine phosphatase 1B

PVDF: Polyvinylidene fluoride

Q-TOF: Quadrupole time-of-flight

ROS: Reactive oxygen species

RPMI: Roswell Park Memorial Institute medium

RPS6KB1: Ribosomal S6 protein kinase B1

RT: Retention time

RTK: Receptor tyrosine kinase

SAX: Strong anion exchange

SCX: Strong cation exchange

SD: Standard deviation

SGK1: Serum/glucocorticoid-regulated kinase 1

SGK3: Serum/glucocorticoid-regulated kinase 3

siRNA: small interfering RNA

SILAC: Stable isotope-labelled amino acids in culture

SREBP: Sterol regulatory element–binding proteins

SRM: Selected reaction monitoring

SNV: Single nucleotide variant

TBS-T: Tris-buffered saline-Tween

TCA: Tricarboxylic acid cycle

TFA: Trifluoroacetic acid

TKI: Tyrosine kinase inhibitor

TMT: Tandem mass tag

TSC: Tuberous sclerosis protein complex

TSQ: Triple stage quadrupole

TXNL: Thioredoxin-like protein

UPLC: Ultra-high pressure liquid chromatography

VHL: von Hippel–Lindau tumour suppressor protein

WES: Whole-exome sequencing

XIC: Extracted ion chromatogram

XF: Extracellular flux analyser

Chapter 1. Introduction

1.1 PI3K/AKT/mTOR pathway

PI3K/AKT/mTOR is a signalling pathway that regulates multiple biological processes, such as proliferation, migration, vesicular transport, and metabolism. The major biological functions of this signalling axis occur because of the lipid kinase activity of phosphoinositide 3-kinases (PI3Ks), which mediates the membrane distribution of phosphatidylinositol lipids to which downstream proteins bind specifically and get activated.

PI3Ks transfer a phosphate group from ATP to the 3-hydroxyl position of the inositol ring of phosphatidylinositol lipids, generating phosphoinositides known to have distinct cellular distribution [1] (Fig 1.1). The PI3K family is classified into three main classes (class I, class II, and class III) based on their primary structure, regulatory subunits, and phospholipid substrate specificity (Table 1.1) [2, 3].

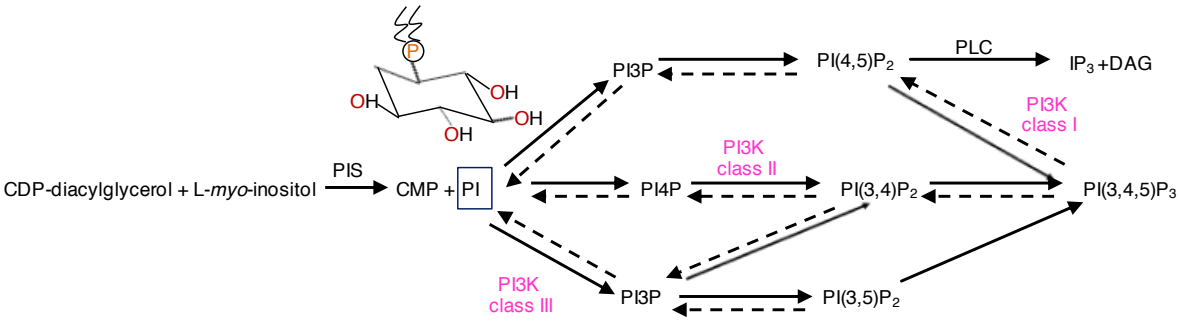

Figure 1.1 Synthesis of phosphoinositides from phosphatidylinositol. Phosphatidylinositol is a glycerophospholipid that has a glycerol backbone and a phosphate group binding two fatty acid tails. Metabolic reactions that lead to the synthesis of phosphatidylinositol and seven phosphoinositides are shown in this figure. Seven phosphoinositides are synthesised and have important signalling roles in different subcellular compartments. Reactions catalysed by the different classes of PI3K are shown. Reactions pointed out with dashed arrows have been shown *in vitro*, but their relevance *in vivo* remains unclear. CDP, cytosine diphosphate; CMP, cytosine monophosphate; DAG, diacylglycerol; IP3, inositol phosphate; PI, phosphatidylinositol; PI3K, phosphoinositide 3-kinase; PI4K, phosphoinositide 4-kinase; PIPK I/II, phosphatidylinositol phosphate kinase 1/2; PIS, phosphatidylinositol synthase; PLC, phospholipase C; PI3K, phosphoinositide 3-kinase.

Table 1.1 The PI3K enzyme family consists of three classes and eight isoforms. PI3K enzyme family is classified into three main classes — I, II, III — based on their structures, regulatory partners and substrate specificities that result in different products.

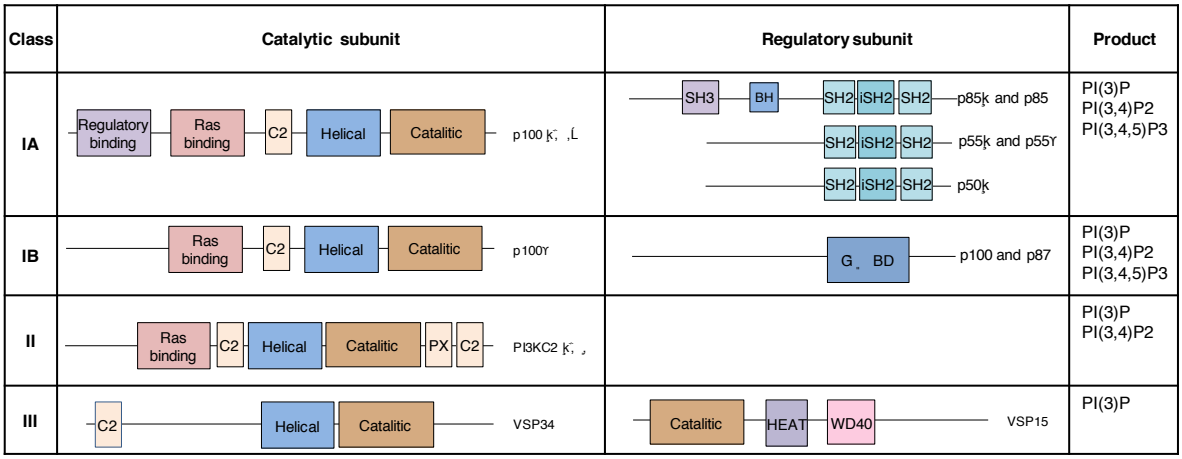

1.1.1 Classification of phosphoinositide 3-kinases

Class I PI3K is a heterodimer constituted by a regulatory and a catalytic subunit (Table 1.1). In mammals, class I PI3K is expressed throughout all cell types, and this class is further divided according to the regulatory subunit into class IA (p85 regulatory subunit) and class IB (p101 or p87 regulatory subunits). Upon the activation of GPCR (G protein–coupled receptor), RTK (receptor tyrosine kinase) or Ras proteins, class I PI3Ks are recruited to the plasma membrane, where they phosphorylate phosphatidylinositol (4,5)-bisphosphate [PI(4,5)P2] to generate phosphatidylinositol (3,4,5)-trisphosphate [PI(3,4,5)P3], as demonstrated in *in vivo* experiments [4]. The mechanisms of activation, regulation and products generated are further discussed in Section 1.1.2. The role of class I PI3K in normal physiology and disease has been extensively studied, and activating mutations are often found in a variety of cancers (e.g. mutations in *PIK3CA* gene that stimulate the kinase activity of p110α). The role of PTEN (Phosphatase and tensin homolog) — a lipid and protein phosphatase that opposes the PI3K reaction by the dephosphorylation of PI(3,4,5)P3 to PI(4,5)P2 [5] — has also been studied, and damaging mutations or loss of PTEN occurs in heritable and spontaneous tumours [6]. Given this, great effort has been put into understanding this signalling cascade, leading to the development of effective PI3K-targeted inhibitors [2].

In vertebrates, class II PI3K is comprised of three catalytic isoforms — PI3KC2α, PI3KC2β and PI3KC2γ — and no regulatory subunits [3]. The activity of class II PI3K is modulated through either the amino (N)- or carboxyl (C)-terminal domains [3]. Although the activation mechanisms of class II PI3K are not

fully understood, experiments demonstrated that upon activation of RTK or GPCR class II PI3Ks are recruited to the membrane, where they interact with plasma membrane proteins [7].

Evidence indicates that class II PI3K phosphorylates PI to PI(3)P and PI(4)P to PI(3,4)P_2 [8]. The PI(3)P product predominantly locates in the endosomes, where it serves as a scaffold for PX or FYVE domains contained in effector proteins, such as glycogen synthase kinase 3 (GSK3) and early endosome antigen 1 (EEA1) [1, 9]. Recent data shed light into the physiological function of this class, implicating PI3K-C2α in the primary cilium development [10], and PI3K-C2β being critical for insulin signalling and endosomal trafficking in *in vivo* models [11].

The single isoform class III, also called Vps34 (Vacuolar Protein Sorting 34), is encoded by *PIK3C3* gene in the human genome and is highly conserved throughout evolution, being present in metazoan, plants, and yeast [3]. Vps34 constitutes a heterodimer with its regulatory membrane-associated subunit Vps15. Vps15 is a Ser/Thr protein kinase that recruits Vps34 to membrane complexes to modulate its activity [3]. Mammalian Vps34-Vps15 dimer nucleates at least three distinct multiprotein complexes involved in autophagy [12], nutrient sensing through the mTOR network [13] or endocytic trafficking [14], depending on the identity of the accessory proteins that bind to the heterodimer. For example, one level of regulation of Vps34-Vps15 is via its association with Beclin-1, ATG-14, and AMBRA1; this complex activates autophagy, and this process inhibited by BCL-2 to sustain autophagic activity at levels compatible with cell viability [15]. The molecular mechanisms that regulate Vps34's activity are not completely elucidated, but the physiological relevance of this protein is inferred by its high degree of conservation and by the observation that homozygous deletion of *Vps34* gene results in unviable *Saccharomyces cerevisiae* and *Drosophila melanogaster* [3]. Interestingly, recent reports showed that Vps34 controls the activity of serum/glucocorticoid regulated kinase 3 (SGK3), which can be over-expressed to activate mTORC1 in systems that tolerate the inhibition of class I PI3K [16].

1.1.2 Phosphoinositide 3-kinases class I: activation, regulation and downstream signalling

In the absence of activating input, class I PI3K regulatory subunit p85 associates with p110 in the cytosol, impeding the lipid kinase activity of the latter, maintaining PI3K activation at basal levels [17]. Class I PI3K can be recruited and activated in plasma membrane in response to multiple input signals (Fig 1.2). First, stimulation of RTK by growth factors, hormones or inflammatory mediators induces the dimerisation and auto-phosphorylation of particular intracellular tyrosine residues of the membrane receptor, which promotes the recruitment to the receptor of p85 via its SH2 domains. These domains are present in p85's C-terminal region, where p85 makes contact with p110 [18]; the

interaction of the regulatory subunit with the RTK causes a conformational change in the PI3K complex, so that the catalytic subunit is released from the inhibitory contact of the regulatory subunit.

Another mechanism of activation some class I PI3Ks is through the action of GPCRs. These receptors are trimers of G_α, G_β, and G_γ subunits. Upon the detection and stimulation by a plethora of signalling mediators — including hormones, metabolites, chemokines, and neurotransmitters — a conformational change of G_α results in its binding to GTP via the GEF (Guanine nucleotide exchange factor) domain and dissociation from the $G_{\beta\gamma}$ complex, promoting GPCR activity and recruitment of downstream effectors. For instance, p110β couples GPCR downstream signalling through the same agonists as p110γ, driving PI3K signalling in tissues with low p110γ expression [19]. GPCRs can also transactivate RTKs, and this cross-talk between receptors integrates signalling that can modulate PI3K activity [20].

Finally, several class I PI3K isoforms can be activated by Ras family of GTPases (including HRAS, NRAS, and KRAS), whose genes are recurrently mutated in different human cancers types [21]. Active, GTP-bounded Ras mediates the activation of p110$\alpha/\gamma/\delta$ via the small domain Ras-binding domain present in the kinase [3]. *In vivo* studies suggest that selective regulation of Ras on different p110 isoforms has critical implications in Ras-driven tumorigenesis. For example, p110α interaction with Ras is believed to be required for Ras-driven *in vivo* tumour formation [22].

The products generated by PI3K can be metabolised by several lipid phosphatases including PTEN, 5-phosphatases such as the SH2 domain-containing inositol phosphatases type 1 and type 2 (SHIP1/2 — encoded by *INPP5D* and *INPPL* genes, respectively), and 4-phosphatases, such as the type II inositol polyphosphate 4-phosphatase (INPP4B) [23] (Fig 1.2). As mentioned previously, PTEN hydrolyses $PI(3,4,5)P_3$ to $PI(3,4)P_2$ [5], and its activity influences cell survival, metabolism and motility [24]. Interestingly, PTEN activity is controlled by the PI3K pathway, as demonstrated by decreased PTEN activity in p85 conditional knockout mice [25]. SHIP1/2 also dephosphorylates $PI(3,4,5)P_3$ but the product of their reaction is $PI(3,4)P_2$, and this phospholipid facilitates PDK1 and AKT signalling activity [23]. INPP4B dephosphorylates $PI(3,4)P_2$ producing PI(3)P. The phospholipid PI(3)P can activate SGK3 (which shares ~50% identity with the catalytic domain of AKT, but lacks the plekstrin homology [PH] domain) through its binding to the PX domain of SGK3 [26]. Therefore, INPP4B can act as an oncogenic driver through the activation of GSK3 in some tumours such as melanoma [27]. However, PI(3)P does not contribute to the signalling activity of either PDK1 or AKT. Finally, PI(3)P can be dephosphorylated by lipid-specific phosphatases myotubularins, which function in a wide range of endosomal trafficking events [28].

The product of class I PI3K activity, $PI(3,4,5)P_3$, causes the recruitment to the plasma membrane of signalling proteins that have the PH domain with affinity for the phospholipid. This domain is present in many signalling proteins including Ser/Thr kinases such as AKT and PDK1, Tyr kinases such as ITK and BTK, GEFs, and adaptor proteins [29]. Membrane-recruited proteins often result activated and trigger downstream signalling cascades. For example, AKT translocation to the cellular membrane allows its full activation by downstream kinases, in particular phosphorylation at Thr^{308} by PDK1, and phosphorylation at Ser^{473} by mTORC2 (the latter discussed in forthcoming Section 1.1.5) [30].

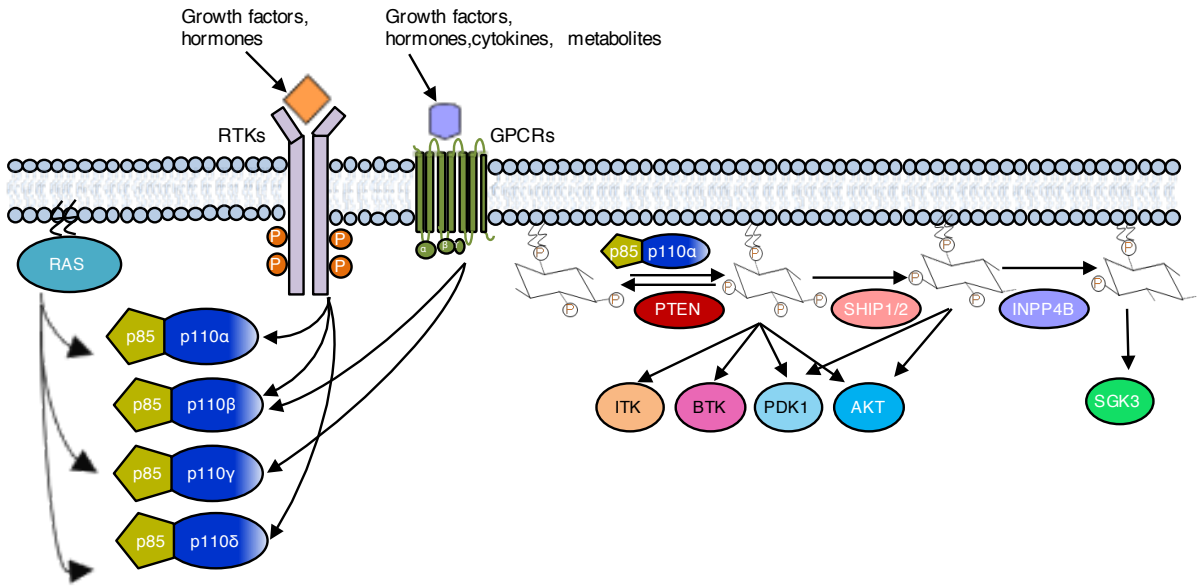

Figure 1.2 Class I PI3Ks are activated by RTK, GPCR, and RAS and the levels of phospholipids are regulated by PTEN, SHIP1/2 and INPP4B. p110α/γ/δ isoforms can bind and get activated by Ras. Class IA PI3Ks (α, β, δ) can be recruited to the plasma membrane and activated by RTKs upon the activation of RTK by growth factors or hormones. Class IA p110β and class IB p110γ can be recruited by activated GPCRs through their association to G_{by}. The amount of product of PI3K activity, $PI(3,4,5)P_3$, can be reduced by various lipid phosphatases ,namely PTEN and SHIP1/2, and other lipid phosphatases, such as INPP4B, dephosphorylate $PI(3,4)P_2$. These phosphoinositides trigger downstream cascades of signalling events involving kinases such as AKT, PDK1, ITK, BTK and SGK3. RTK, Receptor Tyrosine Kinase; GPCR, G-Protein Coupled Receptor. ITK, Tyrosine-protein kinase ITK/TSK; BTK, Tyrosine-protein kinase BTK; PDK1, Phosphoinositide-dependent protein Kinase-1; SGK3, Serum/Glucocorticoid regulated Kinase-3.

1.1.3 AKT

AKT, also named protein kinase B (PKB), is a Ser/Thr protein kinase activated in the plasma membrane and implicated in multiple cellular roles including survival, metabolism, growth and migration [31]. There are three highly conserved AKT isoforms, namely AKT1/2/3: AKT1/2 are ubiquitously expressed, whereas the expression of the AKT3 enzyme is restricted to certain tissues (e.g. brain). AKT activity is affected by its subcellular localisation and phosphorylation state. Fully active AKT phosphorylates

substrates that have the minimum sequence consensus motif R-X-R-X-X-S/T-X (being X any amino acid) [32]. There are 123 AKT-specific substrates derived from human cells reported in PhosphoSitePlus, a database that contains phosphorylation sites [33] (revised in June 2015). These AKT phosphorylation sites can stimulate or hinder its activity, and the overall AKT's output is believed to support cell viability.

AKT negatively regulates proteins involved in apoptosis. For instance, AKT-mediated phosphorylation of the BCL-2 protein family member BAD at Ser^{136} leads to its cytosolic capture and degradation by 14-3-3 proteins of the ubiquitin-proteasome pathway [34]; phosphorylation of caspase-9 at Ser^{196} by AKT blocks the apoptotic cascade inhibiting cell death [35]. AKT hampers the transcription of pro-apoptotic proteins — such as Bcl-2 homology domain 3 (BH3)-only proteins — by phosphorylation and translocation out of the transcription factor FOXO and the by phosphorylation of and translocation into the nucleus of MDM2, a negative regulator of p53 [35]. In addition, phosphorylation by AKT of the Cyclin-dependent kinase inhibitor 1B (p27Kip1 — encoded by the *CDKN1B* gene) prevents its nuclear import, allowing the cell cycle progression [36].

AKT also controls metabolism. For example, AKT phosphorylation of GSK3α at Ser^{21} and of GSK3β at Ser^{9} prevents glycogen synthesis, and this serves as a mechanism to control PI3K signalling [37]. AKT also mediates the transcription of enzymes involved in fatty acids biosynthesis, including fatty acid synthase (FASN) and ATP-citrate lyase (ACLY), through a mTORC1-dependent mechanism [38]. The translocation of glucose transporter 4 (GLUT4) to the plasma membrane in response to insulin is indirectly stimulated by AKT signalling to the GTPase AS160, facilitating glucose uptake [39].

The regulatory capacity of the PI3K/AKT downstream target mTOR is further described below.

1.1.4 Mammalian Target of Rapamycin (mTOR)

mTOR is a Ser/Thr protein kinase that belongs to the PI3K-related kinase family and nucleates at least two different multi-protein catalytic complexes, mTOR complex 1 (mTORC1) and mTOR complex 2 (mTORC2) [40]. mTORC1 consists of five components: mTOR, PRAS40, raptor, deptor and mLST8/GL whereas mTORC2 comprises mTOR, mSIN1, rictor, protor and mLST8. These two complexes coordinate different activating upstream signals (including growth factors and nutrients) to control key biological processes, such as cell survival, metabolism and migration. mTORC1's biology is better understood due to studies with rapamycin and its derivatives (a macrolide produced by the bacterium S*treptomyces hygroscopicus*). These compounds physically interact with the FK506-binding protein of 12 kDa (FKBP12) constituting the complex FKBP12-rapamycin that impedes mTORC1's activity [41]. Contrary to mTORC1, mTORC2 is not sensitive to the macrolide, although

inhibition of mTORC2 has been observed in some cells chronically exposed to rapamycin [42]. Although the mechanisms that lead to mTORC2's activation are not as well understood, some studies involving the genetic inhibition of mTORC2 suggested that mTORC2 is a growth-factor-sensitive but energy-insensitive complex that does not participate in core processes involving nutrients homeostasis [42, 43].

1.1.5 Mammalian Target of Rapamycin (mTOR): activation, regulation and downstream signalling

To understand the precision required to modulate the inputs upstream of mTORC1, the physiological downstream processes directed by mTORC1's activity are first considered. Under abundant energy conditions, mTORC1 is activated to drive the anabolic conversion of nutrients and energy into macromolecules — namely proteins, lipids, and nucleic acids [44]. Active mTORC1 promotes protein synthesis both through the specific 5'-cap-dependent mRNA translation and by enhancing the protein synthesis machinery capacity. Thus, mTORC1 specifically phosphorylates two downstream target regulators of translation: eIF4E binding proteins 1 and 2 (4E-BP1/2) at Thr^{37} and Thr^{46} and the ribosomal S6 kinases 1 and 2 (RPS6KB1/2) at Ser^{394} and Thr^{412} [45, 46]. On one hand, phosphorylated 4E-BPs are released from eIF4E, allowing the assembly of the complete translation initiation complex. On the other hand, activated RPS6KBs phosphorylate several proteins, including the RPS6 (40S ribosomal protein S6 — this being an activating phosphorylation), eEF2K (Eukaryotic elongation factor 2 kinase — this being an inhibitory phosphorylation) and PDCD4 (programmed cell death 4 protein — this being an inhibitory phosphorylation) to enhance protein translation efficiency [45]. mTORC1 promotes the protein synthesis on a global scale by facilitating ribosomal RNA transcription through the direct phosphorylation and deactivation of MAF1, a main repressor of RNA polymerase III transcription [47].

mTORC1 also stimulates nucleotide synthesis to regulate cell proliferation. For example, active RPS6KB1 phosphorylates and activates carbamoyl-phosphate synthase 2 (CAD), the rate-limiting enzyme for *de novo* synthesis of pyrimidines, increasing the nucleotides pool for DNA/RNA synthesis, as observed in *in vitro* and *in vivo* systems [48, 49]. mTORC1's activity can stimulate glycolysis to generate biosynthetic precursors and the production of the redox capacity – in form of NAPDH — required for cellular anabolic processes and to maintain the *de novo* lipids and nucleic acids synthesis. One of the mechanism used by mTORC1 to regulate glycolysis is by driving the synthesis of HIF-1α (Hypoxia-inducible factor 1-α) [50], which in turn induces the expression of multiple glycolytic enzymes [51].

Sterol regulatory element-binding proteins (SREBPs) promote the expression of genes involved in the *de novo* lipid and sterol synthesis upon their DNA-binding. The three human SREBPs isoforms are known to activate the expression of over 30 genes for enzymes that regulate the *de novo* lipid synthesis [52]. One study presented a mechanism by which mTORC1 controls the SREBP pathway through the lipin 1-dependent cellular distribution of SREBPs; active mTORC1 phosphorylates lipin 1 at Ser^{106} and Ser^{472}, preventing its nuclear activity and allowing the association of SREBPs to DNA [53]. Furthermore, mTORC1 increases the levels of glucose-6-phosphate dehydrogenase (G6PD), the rate-limiting enzyme in the oxidative pentose phosphate pathway (PPP) [54]. This process is dependent on SBREP, and thus mTORC1 coordinates the demand of NAPDH — obtained in the PPP — with the SREBPs synthesis.

In addition to contributing to the production of cellular building blocks, mTORC1 also inhibits autophagy. Autophagy is a catabolic process used by eukaryotic cells to degrade in the lysosome cellular constituents to macromolecules to strive against energy exhaustion, and to remove cellular disposable components [55]. mTORC1's best characterised mechanisms to block autophagy are: (i) through the direct phosphorylation of ULK1 at Ser^{757}, blocking the activity of this protein required for the initial steps of autophagosome formation [56] ; and (ii) through the phosphorylation and hindrance of transcription factor EB (TFEB), key in the transcription of lysosomal and autophagy-related genes [57] (Fig 1.3).

mTORC1's activity is modulated through the integration of multiple cellular signals, including growth factors (e.g. hormones and cytokines), energy stress (i.e. ATP/AMP ratio), oxygen stress (e.g. hypoxia) and amino acids (e.g. the essential amino acid leucine) (Fig 1.3). These processes stimulate mTORC1-mediated signalling by modulating the activity of the immediately upstream, ubiquitously expressed, small (21 KDa), Ras-superfamily GTPase member Rheb (Ras homolog enriched in brain) that, when on its GTP-bound state, activates mTORC1 [58]. Rheb is in turn regulated by TSC2, a GTP-ase stable in the TSC complex formed by TSC1/2 and the TBC1 domain family member 7 (TBC1D7), which promotes the conversion of Rheb-GTP to Rheb-GDP. Thus, in response to growth factors signals, AKT (through the PI3K-PDK1-AKT signalling cascade) and ERK (through the MEK-MAPK signalling cascade) potentiate the Rheb GTP-bound form through the phosphorylation of TSC2 [59, 60]. AKT can directly phosphorylate mTORC1 inhibitory subunit PRAS40 at Thr^{246}, facilitating the dissociation of PRAS40 from mTORC1, and binding of the former to 14-3-3 proteins for its degradation [61]. The MAPK (mitogen-activated protein kinase) signalling, on the other hand, phosphorylates and activates the essential scaffold subunit raptor, stimulating mTORC1 activity [62].

Alongside, mTORC1's activity in response to energy levels is mediated by the heterotrimeric 5'-AMP-activated protein kinase (AMPK), which senses the cellular ATP/AMP ratio [63]. When the ATP/AMP ratio is low, AMP binds to AMPK and allosterically activates it. Active AMPK phosphorylates TSC2 at multiple serines, leading to an inhibitory effect over mTORC1 [64]. In addition, AMPK directly phosphorylates raptor at two evolutionary conserved serines, leading to the association of raptor to 14-3-3 protein isoforms [65]. Alternative proteins that activate AMPK include: (i) CaMKKβ, through a mechanism mediated by Ca^{2+} cell-entry that anticipates the ATP demand [66]; and (ii) LKB1, through the phosphorylation of AMPK at Thr^{172} [67]. The activation of AMPK by CaMKKβ is also triggered under hypoxic conditions [68]. In low oxygen, the enhanced expression of HIF-1α transcription factor increases the expression of protein REDD1 (regulated in development and DNA damage responses 1), which itself binds and prevents TSC2 degradation, impeding mTORC1 activity [69]. Oxidative stress prompted by the accumulation of reactive oxygen species (ROS) can regulate mTORC1, in a manner that is dosage- and cellular compartment-dependent. Experiments have demonstrated that ROS inactivate TSC2 by direct oxidation of its cysteines, contributing to mTORC1 activity [70]. In contrast, it has been shown that peroxisome-located TSC2 reduces mTORC1 activity in response to ROS [71], and the raptor-mediated mTORC1 recruitment to stress granules decreases mTORC1 activity to prevent apoptosis caused by an hyperactivated mTORC1 [72]. Furthermore, the ATM Ser/Thr protein kinase, known to be a DNA damage sensor, functions as an oxidative stress sensor to repress mTORC1 activity via a TSC2-dependent mechanism [73].

Amino acids are crucial for the activity of mTORC1. The capacity of mTORC1 to sense the levels of amino acids is mediated by an additional protein complex, nicknamed the ragulator. This complex comprises a class of G proteins, the RagA-D GTPases and five regulatory subunits LAMTOR1–5 (late endosomal/lysosomal adaptor and MAPK and mTOR activator 1). Ragulator subunits recruit Rag GTPases to the lysosomal membrane, where the complete ragulator complex can sense the amino acids levels and activate Rheb accordingly [74]. Under energy depletion, the ATP-dependent TTT-RUVBL1/2 complex diminishes its interaction with mTORC1, decreasing the TTT-mTORC1 dimer necessary for mTORC1 activity. Indeed, the presence of adequate levels of essential amino acids (EEAs) is believed to be the rate limiting step for mTORC1 activation [75].

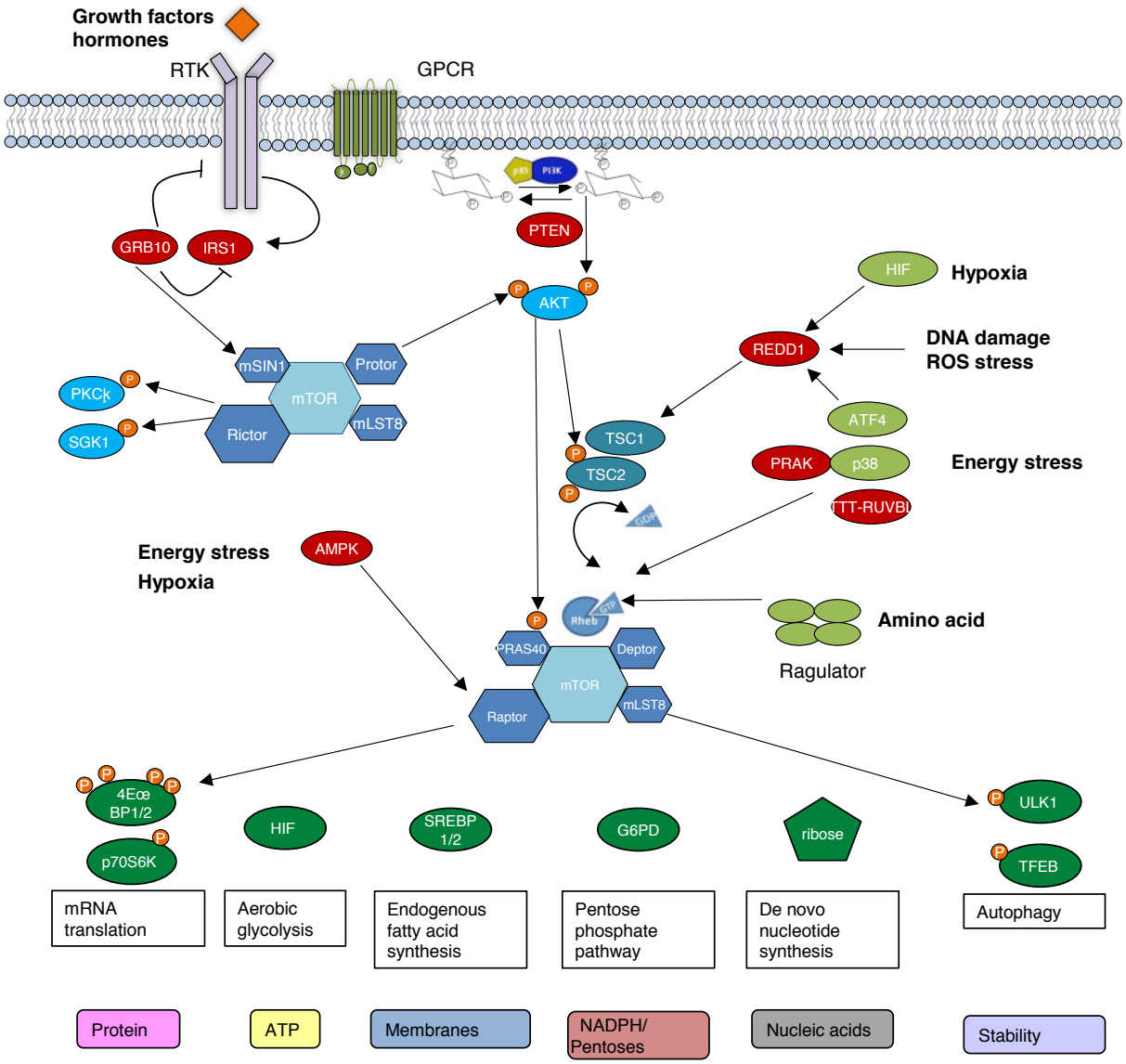

Figure 1.3 Activation, regulation and downstream signalling events trigger by mTORC1 and mTORC2. Activation of mTORC1 promotes several downstream signalling events including mRNA translation, glycolysis, lipid synthesis, activation of the pentose phosphate pathway, *de novo* pyrimidine synthesis and inhibition of autophagy. These processes engender the synthesis of energy (e.g. ATP), reducing moieties (e.g. NADPH) and macromolecules to build cellular components. The activation of mTORC2 is not that well understood and its position within the cell triggers the activation of several signalling cascades. For example, physical association with the ribosome and location in the mitochondrial associated ER-membranes (MAMs) activated the oncogenic PI3K signalling. Active mTORC2 triggers several members of the AGC kinase family (e.g. PKCα, SGK, and AKT). Various input signals participate in the regulation of mTORC1 including energy and oxidising stress, hypoxia and amino acid levels. One known mechanism by which mTORC2 is regulated is by the negative feedback loop from phosphorylated Grb10 and IRS-1 (by p70S6K) that prevents growth factor-promoted mTORC2's activity. GRB10 (Growth Factor Receptor Bound Protein 10); Insulin receptor substrate 1 (IRS-1); PKC (protein kinase C); SGK1 (Serum/Glucocorticoid Regulated Kinase 1); AMPK, AMP-activated protein kinase; TSC1/2, tuberous sclerosis protein 1/2; REDD1, regulated in development and DNA damage responses 1; HIF, Hypoxia-inducible factor 1; ATF4, Activating Transcription Factor 4; p38β, mitogen-activated protein kinases MAPK11; PRAK, p38-regulated/activated protein kinase; TTT, Tel2–Tti1–Tti2 4E-BP1, eIF4E-binding protein-1; p70S6K, 70 kDa ribosomal S6 kinase; SREBP1/2 sterol regulatory element-binding protein; G6PD, glucose-6-phosphate dehydrogenase; ULK1, Unc-51 Like Autophagy Activating Kinase 1; TFEB, transcription Factor EB.

mTORC2, on the other hand, is responsive to growth factor molecules, and phosphorylates hydrophobic motif sequences of the large family of AGC kinases — including AKT, PKCα and SGK1 [76]. For example, AKT phosphorylation at Ser^{473} by mTORC2 enables its complete activation (consequent to the phosphorylation at Ser^{308} by PDK1), and this contributes to cell survival, cell growth, and lipogenesis [40]. PKCα phosphorylation at Ser^{657} by rictor prompts morphological changes in the actin cytoskeleton [77]. Moreover, experiments in protor knockout mice revealed that protor enables mTORC2-mediated activation of SGK1 (serum/glucocorticoid regulated kinase 1) [78].

The molecular mechanisms that trigger mTORC2's activity are starting to be understood. A cofounding factor in the regulation of mTORC2 is its cellular localisation. One mechanism that engages mTORC2 activation is through the specific interaction of $PI(3,4,5)P_3$ with the PH domain of the mSIN1 subunit; this interaction releases the suppression of mSIN1 from mTORC2's kinase activity [79]. Other studies indicated that activation of mTORC2 requires its physical association with the ribosome; when located in that organelle, mTORC2 eases the stabilisation of nascent AKT proteins by the co-translational phosphorylation of AKT at Thr^{450}, preventing AKT ubiquitination [80]. When mTORC2 locates in a sub-compartment of the endoplasmic reticulum and associates with mitochondria it activates AKT upon growth factor stimulation and decreases mitochondrial inner membrane potential measured *in vitro* [81]. mTORC2's activity is further regulated by mechanisms upstream and downstream of PI3K signalling. For instance, mTORC1/S6K-mediated phosphorylation of IRS-1 and the adaptor protein GRB10 blocks the interaction with the p85 PI3K-regulatory subunit preventing mTORC2 activation and thus restraining insulin from simultaneously activating mTORC1 and mTORC2 signalling [82]. mTORC2's activity can be suppressed through insulin-independent mechanisms. For example, evidence suggests that stimuli such as EGF, PDGF and IGF-1 results in the phosphorylation of mSIN1 by AKT or by p70S6K; this promotes the dissociation of mSIN1 from mTORC2 to reduce mTORC2's activity [83].

1.1.6 Role of PI3K/AKT/mTOR in cancer

The mechanisms that induce oncogenic PI3K/AKT/mTOR signalling have been extensively reviewed [6, 84, 85] and include: (i) over-activating mutations in upstream receptors of the pathway including RTKs and GPRCRs; (ii) mutations in p110α 'hotspots' (i.e. H1047R, E545K and E542K) that confer constitutive kinase activity; (iii) loss of PI3K tumour suppressors (e.g. PTEN); (iv) over-activity of AKT (due to amplifications of AKT isoforms or activating mutations in AKT's PH domains); (v) over-activation of mTORC1 (due to inhibitory mutations in TSC1/2, activating mutations in mTOR itself, activating mutation in Rheb, over-expression of deptor, enhanced activation of some of its substrates such as

phosphorylation of 4E-BPs and p70S6K or activating mutations in V-ATPase); and (vi) activation of mTORC2 (due to aberrant EGFR signalling and loss of PTEN).

Overall, the PI3K pathway is crucial for the regulation of signalling events in response to cellular stimuli. Alterations of main nodes of this pathway is one of the most frequent events described in various human tumours [6], and deregulation of this pathway's activity alters a plethora of biological processes given its role in vital cellular functions including motility, growth and metabolism.

1.2 Cancer metabolism

1.2.1 Hallmarks of metabolic adaptations in cancer

The adaptation of cellular metabolism supplies the macromolecules and cofactors required to maintain the high rates of proliferation of cancer cells [86, 87]. Metabolic networks evolve driven by external and internal factors that select the malignant phenotype [88]. Hence, during tumour progression, cancer cells are selected based on their capacity to use the scarce nutrients usually present in the tumour microenvironment to produce biomass and maintain cellular proliferation. Metabolic remodelling not only allows cancer cell growth, but also substantially adapts the tumour extracellular milieu, generating an immune-permissive, favourable microenvironment (discussed further in Section 1.2.2).

To yield an efficient energetic conversion, non-tumorigenic cells favour the conversion of glucose to acetyl-CoA, the main substrate for the tricarboxylic acid (TCA) cycle. The reactions occurring in this cycle generate the reduction potential in the form of nicotinamide adenine dinucleotide (NADH) and flavin adenine dinucleotide ($FADH_2$); those factors are shuttled to the mitochondria where they produce an electrochemical gradient that ultimately results in the production of ATP through the ATPase complex. Cancer cells, similarly to genetically normal proliferating cells [89] and cells infected by some viruses [90], divert metabolic intermediates of the central carbon metabolism to the synthesis of diverse biomolecules, the generation of sufficient redox potential in form of nicotinamide adenine dinucleotide phosphate (NADPH), and the production of lactic acid by the activity of lactate dehydrogenase (LDH) [91]. Thus, glucose-6-phosphate (G6P), the first product of the glycolytic pathway, is found to be re-routed in cancer cells to generate both ribose-5-phosphate, a constituent of nucleotides, and NADPH in the PPP anabolic pathway (Fig 1.4). The hexamine biosynthesis pathway (HBP) for the generation of glycosylation substrates (e.g. heparan-sulphate and hyaluronic acid) can

be enhanced by an increase of the side-reaction from fructose-6-phosphate (F6P), the product of glycolysis-second reaction. As an example of this metabolic channelling in cancer cells, in an oncogenic mutant *Kras*^{G12D} pancreatic cancer mouse model, the biosynthesis of ribose to both maintain DNA replication and substrates for O- and N-protein glycosylation is facilitated by diverting glucose intermediates into the PPP and HBP, respectively [92]. The succeeding intermediate in the glycolytic pathway, glyceraldehyde-3-P, can be transformed to glycerol-3-phosphate to maintain the synthesis of phospholipid bilayer membranes (Fig 1.4) [86].

Glucose-derived carbon can be redirected from 3-phosphoglycerate to the synthesis of serine and glycine [93]. Serine has a unique metabolic role, since it provides one-carbon units for the synthesis of nucleotides, methyl donor groups and NADPH, and contributes to the TCA anaplerosis (i.e. replenishment of TCA intermediates). The gene that encodes for the first committed enzyme of the *de novo* serine biosynthesis, 3-phosphoglycerate dehydrogenase (PHGDH), locates in the chromosome locus 1p12, a genetic region that is recurrently amplified in diverse cancer subtypes, including ER- breast cancer cells [94] and melanoma-derived cells [93]. Amplification of PHGDH enhances the serine synthesis pathway, which is required for the proliferation of PHGDH-amplified malignant cells [93, 94].

Cancer cells not only divert the usage of metabolic middle-products, but also often increase the consumption of nutrients. Uptake of glucose, the most abundant available nutrient [95], is controlled by transmembrane transporters including the isoforms GLUT1-4, whose distribution is specific across different tissues and their regulation depends on extracellular and intracellular stimuli [96]. The expression and plasma membrane translocation of these transporters, as previously mentioned in Section 1.1.3, can be mediated by the activity of PI3K/AKT/mTOR pathway [97]. In addition, the levels of nutrient transporters and cellular dependency to specific nutrients (e.g. glucose) may be conditioned by the genetic background of cells. For example, previous data indicated that isogenic cells lines carrying an activating mutation in *PI3KCA* require glucose for their growth, possibly due to their highly glycolytic metabolism compared to non-mutated *PI3KCA* breast cancer cells [98].

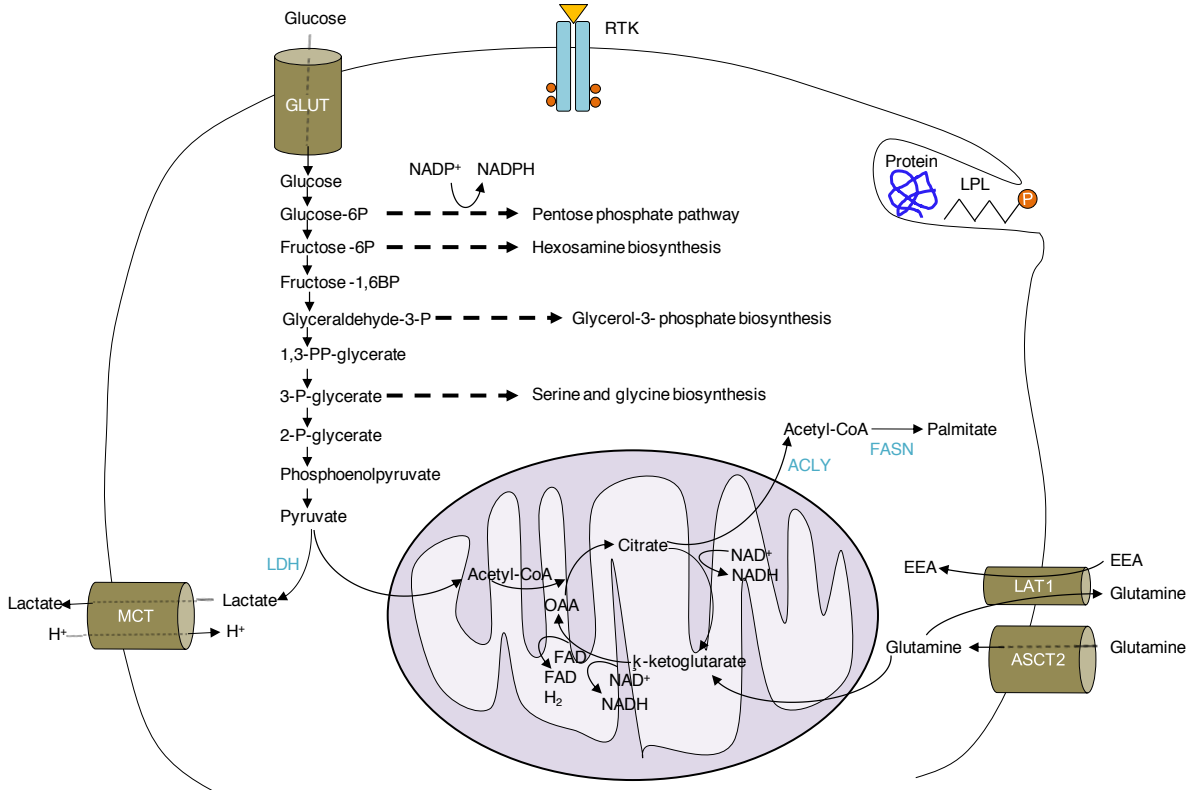

Figure 1.4 Adaptations of the metabolism of cancer cells. Cancer cells diversify multiple synthetic reactions from the central carbon metabolism, increase their nutrient demand and use nutrients available in the tumour microenvironment. In addition, cancer cells increase the expression of metabolic enzymes such as LDH and FASN, which facilitate the conversion of metabolic intermediates to generate biosynthetic precursors. LAT1 transporter coordinates the transport of EEAs (e.g. L-leucine) and glutamine. ACLY, ATP-citrate synthase; ASCT2, neutral amino acid transporter B; EEA, essential amino acid; FAD, flavin adenine dinucleotide; FASN, fatty acid synthase; GLUT, glucose transporter; LAT1, L-type amino acid transporter 1; LDH, lactate dehydrogenase; LPL, lysophospholipid; MCT, monocarboxylate transporter; NAD, nicotinamide adenine dinucleotide; NADP, nicotinamide adenine dinucleotide phosphate; OAA, Oxaloacetic acid; RTK, receptor tyrosine kinase.

Glutamine is a vital nutrient since it contains a carbon backbone and side amide nitrogen groups. As a result, it supplies the nitrogen for the glucosamine-6-phosphate (GlcN6P) biosynthesis, allowing the *de novo* synthesis of purine and pyrimidine nucleotides and synthesis of non-essential amino acids, and facilitates the import of essential amino acids. The uptake of neutral amino acids (e.g. glutamine) is controlled by ASCT2 (Alanine, serine, cysteine-preferring transporter 2) [99]. ASCT2 transcription is engaged by c-MYC transcription factor, which also controls the expression of proteins involved in the conversion of glutamine to glutamate, and stimulates mitochondria glutaminolysis (e.g. GLS1, PRPS2 and CAD) [100]. Some of these proteins (i.e. PRPS2 and CAD) participate in the first steps of purine and pyrimidine biogenesis. Therefore, c-MYC contributes to glutamine uptake and its utilisation in the purine and pyrimidine synthesis pathway. Enhanced ASCT2 expression has been observed in distinct cancer types, including breast cancer cells [99]; nevertheless, among the breast cancer subtypes studied, only basal triple negative breast cancer cells depended on ASCT2 activity to proliferate [99].

In addition to glutamine, cancer cells frequently increase the consumption of others amino groups-containing molecules. For instance, proliferating malignant cells incorporate higher amounts of extracellular arginine to produce polyamines (i.e. aliphatic carbon molecules that contain two or more amino groups), known to have pro-survival effects [101].

Cancer cells are able to survive in non-optimal nutrient conditions, exploiting available nutrients. As an example of this, metastatic ovarian cancer cells preferentially home in the omentum, a visceral-insulating organ predominantly composed of adipocytes, where the up-regulation of the transporter FABP4 (fatty-acid-binding protein 4) in omental and ovarian cancer cells facilitates fatty acids acquisition of the latter [102]. This helps to compensate the deficit of certain fatty acid species in ovarian cancer cells, such as unsaturated fatty acids, which synthesis is obviated in hypoxic conditions.

In addition to enhanced nutrient acquisition, the metabolic reprogramming of malignant cancer cells alters metabolite synthesis. Metabolic pathways of cancer cells, and the metabolites derived from them, are not merely the outcome of growth signals, but quite the opposite, they directly control cellular functions. As such, certain metabolites directly alter some epigenetic regulators to modulate gene expression rate, and they can be themselves a consequence of an aberrant genetic status. For example, mutations in the genes *IDH1/2* (isocitrate dehydrogenase 1/2) cause the conversion of α-ketoglutarate into 2-hydroxyglutarate (2-HG), instead of usual conversion isocitrate to α-ketoglutarate. In patients suffering from acute myeloid leukaemia (AML), mutations in *IDH1/2* genes impair the activity α-ketoglutarate-dependent DNA demethylase TET and block hematopoietic differentiation [103]. Furthermore, biallelic mutations in the succinate dehydrogenase (SDHD) — also known as mitochondrial Complex II — impede the conversion of succinate to fumarate. This blocks the TCA, triggering glycolytic pathways in normal-oxygen conditions and conferring growth advantage to infrequent benign head and neck tumours (a familial condition known as paraganglioma) [104].

Overall, the whole complex metabolic rewiring is a continuum whereby metabolic transformations, and the resulting metabolites, govern the phenotypic characteristics of cancer cells; the impact of metabolic modulators on cell physiology may be dictated by the tumour genotype and tissue of origin. For example, experiments have demonstrated that c-MYC induces diverse metabolic phenotypes in murine lung and liver tumours: lung tumours induced by c-MYC tended to accumulate glutamine, whereas liver tumours induced by c-MYC increased their lactate production [105]. The genetic background, interaction of cancer cells with the tumour microenvironment, and the *in vivo*

contribution of each metabolite to the tumour growth may explain the impact of metabolism in tumour formation [106].

1.2.2 Tumour microenvironment and metabolism

The metabolic status of tumour cells not only affects their own physiology but also modulates the behaviour of neighbouring cells. As previously discussed, there is a communication and exchange of nutrients between non-malignant cells (e.g. omental adipocytes) and malignant cancer cells (e.g. ovarian metastatic cells). Another example of metabolite exchange across tumour cells is the lactate shuttle between catabolic stromal cells and anabolic malignant cancer cells [107]. Although the mechanisms for cell-cell communication and the topological features of metabolic pathways may be cell- and context-specific, multiple processes contribute to the alteration of tumours extracellular milieu and the biology of adjacent cells. For instance, the elevated glucose and glutamine consumption of cancer cells to sustain increased glycolytic activity yields a high production of acids (e.g. lactic acid and carbonic acid). These acids, when exported, can impact the behaviour of cancer cells in a paracrine manner [108], and can alter the function of other cells present within the tumour microenvironment (see below). Therefore, a correct functionality of proteins implicated in the trafficking of metabolites (e.g. monocarboxylate transporters [MCTs] to control the flux of monocarboxylates, such as lactic acid) and metabolites-sensing receptors (e.g. GPCRs for metabolites and protons [H^+]) is critical to regulate the action of metabolites on cancer cells and the cells within their vicinity (Fig 1.5).

At physiological pH 7.4, the pKa= 3.86 of lactic acid implies the prevalence of the dissociated species ($lactate^- H^+$). Lactate concentration within the plasma under normal conditions is in the range 0.5-2 mMol/L [108]. Lactate is transported through the plasma membrane via MCTs. MCTs family is comprised by a total of 14 members (also known as solute carrier 16 ([SLC16] gene family) that transport single-carboxylate molecules, including pyruvate, L-lactate and ketone bodies across cellular membranes [109]. All MCT proteins are predicted to have well conserved 12 transmembrane helices and distinct intracellular loop sequences and N- and C-terminal regions. Lactate transporters bind to the accessory protein basigin, which facilitates their correct plasma membrane insertion allowing their function [109]. Four members of the MCT family (MCT1-4) locate in the plasma membrane and perform a proton-mediated transport of metabolites [109]. MCT1 is expressed in the majority of tissues of species studied and participates in lactate influx and efflux [110]. MCT2 is less ubiquitously expressed and is thought to play key roles in neurons at the postsynaptic density [109]. MCT3 expression is limited to the retinal pigment epithelium and choroid plexus epithelia [110]. MCT4's primary function is to export lactate and this transporter is greatly expressed in highly glycolytic cells,

such as white muscle fibres. The expression of this transporter is up-regulated in response to low oxygen tensions [111]. Differential levels of MTCs have been documented across cancer cell types; for example, evidence indicates that reduced expression of MCT1 is a hallmark of cancer cells resistant to inhibitors that target glycolytic enzymes [112].

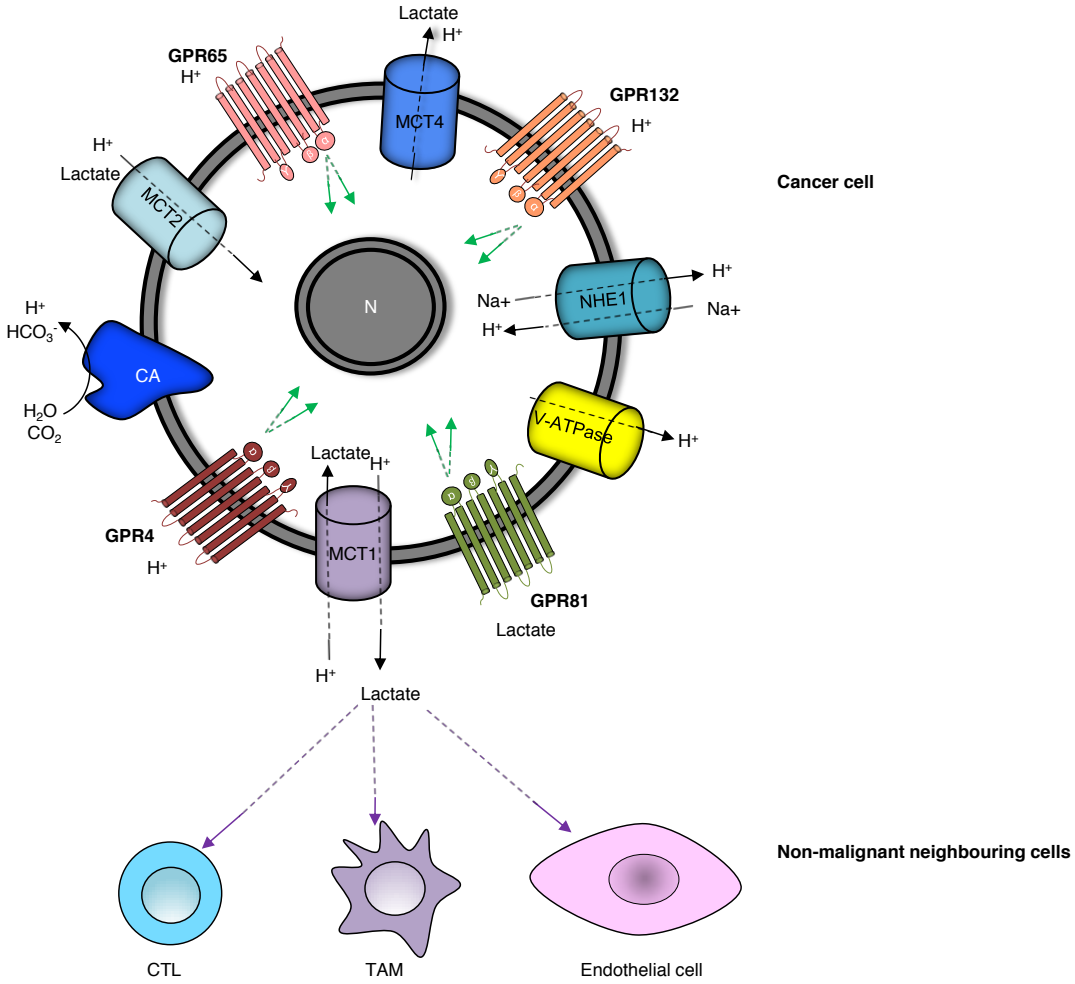

Figure 1.5 Schematic representation of the interaction of lactate and protons within a cancer cell and with tumour neighbouring cells. MCTs locate in cellular membranes and can transport lactic acid. Lactate cognate receptor (GPR81), some pH regulatory proteins (CA, NHE1 and V-ATPase), and pH sensing receptors (GPR4, GPR65, and GPR132) are represented. Reciprocally, products derived from the metabolism of cancer cells, such as lactate, have pleiotropic effects on the biology of normal cells of the tumour vicinity including cytotoxic T lymphocytes (CTLs), tumour associated macrophages (TAMs) and endothelial cells. CA, Carbonic anhydrase; N, nucleus; NHE1, Na+/H+ exchanger 1; MCTs, monocarboxylate transporters. Green dashed arrows represent the signalling cascades. Purple dashed arrows represent the effect of lactate in tumour surrounding cells.

To deal with greater acid concentration, cells rely on the activity of acid-ejecting/converting proteins. These include Na^+/H^+ exchangers (NHE1, also known as SLC9A1), Na^+/HCO_3^- (NBCn1, also known as SLC4A7) and carbonic anhydrases (CAs) [113]. Cells can also sense and respond to

surrounding metabolites trough membrane GPCRs. For example, lactate activates its cognate receptor GPR81, a G_i-type G protein [108], and protons can be sensed by additional GPCRs, including GPR4, GPR65 (also known as TDAG8), GPR68 (also known as OGR1), and GPR132 (also known as G2A) [114]. An example that gives insights into the functional relevance of these receptors is given by a recent study that demonstrated that lower levels of GPR81 receptor in three cervical carcinoma cell lines impede the lactate-mediated DNA double-strand break repair [115].

As mention above, cancer cells may benefit from a modified lactate-rich microenvironment through the alliance with vicinity cells. For example, recent *in vitro* studies showed a reduction of the tumour immunogenicity and cytokine production of human cytotoxic T lymphocytes (CTLs) caused by high concentrations of lactic acid in the tumour microenvironment [116]. Other study has demonstrated that a gradient of lactic acid produced by cancer cells promotes the tumour recruitment of tumour associated macrophages (TAMs) to prompt tumour growth and invasiveness through a mechanism mediated by HIF-1α and the pro-angiogenesis vascular endothelial growth factor (VEGF) [117].

1.2.3 Redox potential

The metabolic adaptations of cancer cells are tightly regulated to maximise mitochondrial activity to promote malignant progression whilst engaging antioxidant systems to metabolise oxidation-derived ROS products [118]. As mentioned in Section 1.1.5, the functional effects of ROS are dosage- and context-dependent. ROS are constantly created, transformed and eliminated by multiple cellular processes. At the most fundamental level, ROS are short-lived molecules derived from partially reduced oxygen with unpaired electrons. Based on the unpaired electrons present in the outer atomic orbital, ROS can be classified into radical ROS or non-radical ROS. In addition, the partial reduction state of oxygen from H_2O classifies ROS as superoxide anion ($^{\cdot}O_2^-$; three reduction states away from H_2O), hydrogen peroxidase (H_2O_2; two reduction states away from H_2O) and hydroxyl radical ($^{\cdot}OH$; one reduction state from H_2O) (Fig 1.6A).

ROS attain fundamental functions in living organisms. The signalling properties of ROS were first recognised in seminal experiments that demonstrated that ROS stimulation caused the phosphorylation of growth factor-dependent receptors (e.g. PDGFR and EGFR) and subsequent phosphorylation signalling due to $^{\cdot}O_2$-/H_2O_2-mediated inactivation of downstream phosphatases [119, 120]. One of the mechanisms by which ROS attain signalling activity is through the oxidation of the thiol side of Cys residues present in proteins (Cys-S^-) to sulfenic acid (Cys-SOH). This modification can lead to protein allosteric modifications, changing the expression, function and binding of proteins with

interacting partners [121, 122]. For example, the activity of PI3K/AKT/mTOR pathway increases in response to ROS due to the inactivation of PTEN upon its oxidation at Cys^{124}, a residue essential for PTEN catalytic activity [123], and due to the inactivation of phosphatase 2A (PP2A) and protein tyrosine phosphatase 1B (PTP1B) upon oxidation of cysteines present in their active sites [124].

Among the regulators of the expression of antioxidant genes, NRF2 (nuclear factor erythroid 2-related factor 2) is arguably the most important transcription factor involved in the control of transcription of many of antioxidant genes [125]. Under unstressed conditions, NFR2 is negatively regulated via its binding to KEAP1 (Kelch ECH associating protein 1), an adaptor protein that targets NRF2 for its degradation by the ubiquitin proteome system. NRF2, through the recognition and binding to DNA antioxidant response elements (AREs), promotes the expression of over 100 genes which protein products carry antioxidant function, including glutathione and catalase (see below). The bound complex between NRF2 and the very-rich Cys protein KEAP1 is disrupted upon oxidation of KEAP1's cysteines, releasing NRF2 to activate diverse antioxidants pathways to combat oxidative stress [125].

Excessive ROS levels are harmful for cell physiology. As mentioned before, ROS-derived oxidative stress activates ATM, which in turn phosphorylates p53 at Ser^{15} to stop cell cycle progression [126]. High levels of ROS can also enforce G1 cell cycle arrest by perpetual activation of cell-cycle inhibitor p16INK4A/Rb [127]. In addition to cell cycle, ROS impact on the stability of cellular lipids. Non-enzymatic peroxidation of membrane-abundant polyunsaturated fatty acids triggers downstream reactions that generate highly-reactive lipid electrophiles. These lipid-radicals avidly form adducts with nucleic acids, proteins, and lipids by creating covalent bonds with their nucleophilic moieties. The unsaturated 4-hydroxy-2-nonenal (4-HNE) is one of the most studied products derived from lipid peroxidation, and it known to trigger cellular apoptosis when present at high concentrations [128]. Finally, highly reactive free radicals react with heterocyclic DNA bases yielding altered nucleic acids and activating programmed cell death [129].

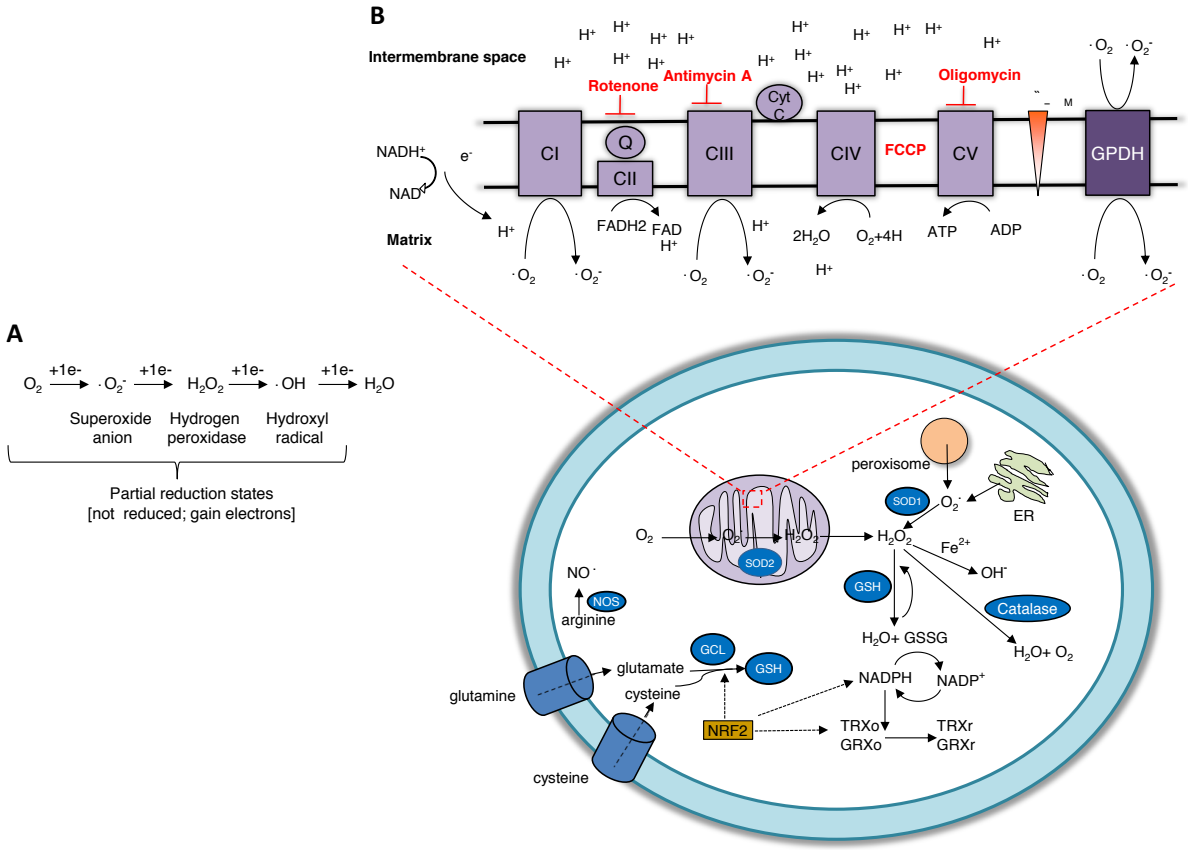

Figure 1.6 Mechanisms involved in cellular redox homeostasis. **(A)** Sequential reduction states of oxygen resulting from the addition of electron produces several ROS species including: superoxide anion ($O_2^{\cdot-}$), hydrogen peroxide (H_2O_2), and hydroxyl radical ($^{\cdot}OH$), which in turn can be reduced to water. In the electron transport chain (ETC), each electron is transferred to a more electronegative acceptor until O_2 undergoes a four-electron reduction at the complex IV to generate water. **(B)** The mitochondrial sites where $O_2^{\cdot-}$ is created by the acceptance of O_2 of leaking electrons from in the mitochondria are shown. Drugs that interfere with mitochondrial complexes are shown in red. Superoxide can be converted by superoxide dismutase 2 (SOD2) to H_2O_2, which is exported outside the mitochondria to be further reduced. SOD1 converts the cytoplasmic superoxide derived from peroxisomes and ER. Catalase reduces H_2O_2 to H_2O and O_2. Glutathione (GSH) is synthesised from glutamate and cysteine by glutamate cysteine ligase (GCL). The GSH redox cycle is comprised by GSH and glutathione disulphide (GSSG) and it is maintained by the reducing equivalents from NADPH. Similarly, thioredoxin (TRX) and glutaredoxin (GRX) transfer electrons from NADPH to their oxidised substrates. Nitric oxide (NO) derived from arginine and this reactive radical can be eliminated in the cytoplasm by nitric oxide synthase (NOS). Nuclear factor erythroid 2-related factor 2 (NRF2) (shown in yellow) controls various antioxidants pathways including the production of GSH, TRX and NADPH. Generation of NADPH arises from reactions involving glucose-6-phosphate dehydrogenase (G6PD), phosphoglycerate dehydrogenase (PHGDH), isocitrate dehydrogenase 1 (IDH1) and malic enzyme 1 (ME1) (data not shown). Cyt C, cytochrome C; FCCP, Carbonyl cyanide 4-(trifluoromethoxy) phenylhydrazone; PDH, glycerol-3-phosphate dehydrogenase; Q, quinone. $\Delta\Psi_M$, membrane potential.

The source of ROS can be extracellular — such as radiation, iron salts, and aerosols — or intracellular. The major intracellular contributors of ROS are the mitochondria, the endoplasmic reticulum (ER), peroxisomes and oxidases and oxygenases enzymes that generate ROS as part of their enzymatic reaction cycles (Fig 1.6B) [130]. Mitochondria are by far the largest source of intracellular

production of oxidants. In that organelle, electrons from NADH and $FADH_2$ are transported through energetic-favourable enzymatic electron-exchange reactions between electron donor/acceptor complexes located in the inner membrane, and electrons are used to pump protons into the mitochondrial intermembrane space. The series of consecutive reactions comprise the electron transport chain (ETC) and the electrochemical gradient of protons is transferred via chemiosmotic-coupling to the ATP synthase [131]. The entire process is often called oxidative phosphorylation because the energy of hydrogen oxidation is used to phosphorylate ADP to ATP [130]. Although the efficiency of the ETC during mitochondrial respiration is known to be high, electron leakage prompts the univalent reduction of O_2 to generate O_2^- [118]. In addition to the ETC complexes, other enzymes contribute to the pool of mitochondrial superoxide. As an example, the inner-membrane mitochondrial glycerol-3-phosphate dehydrogenase (GPDH) is able to couple electron transport and can generate superoxide [130]. Peroxisomes also contribute to the net amount of cellular ROS. Thus, whilst the activity of peroxisome proliferator-activated receptor alpha (PPARα) – member of the peroxisomal β-oxidation system – increases the amount of ROS, the activity of mammalian peroxisomes enzymes (e.g. catalase, superoxide dismutase 1, and peroxiredoxin 5) and non-enzymatic agents (e.g. glutathione, ascorbic acid, and plasmalogens) lower the free radical content in peroxisomes [132]. Finally, ROS are generated during the unfolded protein response as a consequence of thiol group transfers to folding substrates in the endoplasmic reticulum (ER) [133]. In addition to ROS elimination in the peroxisomes, ROS can be neutralised through main detoxification pathways that involve the activity of glutathione (GSH) and thioredoxin (TRX) (Fig 1.6B). GSH – a tripeptide composed by glutamate, cysteine and glycine – is the most abundant antioxidant molecule in the cell [122]. Like GSH, TRX contributes to protein reduction by thiol-disulphide exchange.

Finally, and as mentioned before, NRF2 controls the expression of antioxidant proteins that defend cells from oxidative damage. Although oncogenic mutations in *Nrf2* are less prevalent than mutations in *PI3KCA* or *KRAS*, gain-of-function mutations in the *Nrf2* gene or loss-of-function mutations in the *Keap1* gene are frequent occurrences in non-small-cell lung cancers (NSCLC) [134].

1.3 Targeted therapies in cancer

1.3.1 Oncogenic addiction in cancer cells

Tumours manage to proliferate through the activation of pro-survival pathways, which makes cancer cells more dependent to those cascades than other healthy cells. Examples include the human epidermal growth factor receptor 2 (HER2/ERBB2), which is frequently overactive in breast cancer cells, the activation of kinase BRAF that increases the activity of MAPK pathway in melanoma, the BCR-Abl fusion kinase that causes the constitutive activation of receptor-downstream pathways in leukaemia and PTEN loss and PI3K over-activation in prostate cancer cells [87]. Molecular targeted therapeutics aims to exploit the dependency of cancer cells on survival pathways. The survival outcome of patients suffering from cancer greatly improved due to targeted treatment with selective small-molecules inhibitors against pro-proliferative pathways (e.g. Gleevec, a type of tyrosine kinase inhibitor [TKI]) [135]. Kinases are particularly appealing drug targets for anti-cancer targeted therapies due to several factors. First, the structure and biochemistry of protein and lipid kinases is well characterised and a plethora of chemical inhibitors against kinases has been developed over the last 30 years. Moreover, isoform-specific kinase inhibitors have proved to effectively improve the target specificity. For example, while the small-molecule inhibitor against pan class I PI3K GDC-0941 inhibits p110α, β, δ, and γ with estimated IC_{50} values of 3 nM, 33 nM, 3 nM, and 75 nM, respectively [136], the PI3Kα isoform-specific inhibitor BYL719 inhibits p110α with estimated IC_{50} value of 5 nM [137] (Fig 1.7). It is important to note that the specific inhibition of p100δ isoform, highly expressed in leukocytes, with selective PI3Kδ inhibitors (e.g. Idelalisib) has demonstrated impressive clinical benefits for patients suffering from B-cell malignancies [138]. Owing to the great number of evidences in support of the role of aberrant activity of members of the PI3K/AKT/mTOR signalling axis in cancer cells, development of selective inhibitors targeting this signalling branch has raised much interest in pharmacotherapy, and in fact several small molecule kinase inhibitors and macrocyclic inhibitors specific against nodes of this pathway have been approved by the FDA for their clinical use [135].

However, the effectiveness of targeted therapeutics is limited by the confined knowledge of the cancer nature as well as by intrinsic characteristics of cancer cells including: (i) the inter-tumour heterogeneity, evidenced by differential responses of patients suffering from cancer with the same organ of origin; (ii) the spatial and temporal tumour intra-heterogeneity; (iii) the non-universal parameters that provide the basis for choosing the most suitable targeted therapy; (iv) the limited criteria to stratify patients; (v) the toxicity of combination targeted therapies; and (vi) the inevitable

emergence of drug resistance. The convergence of all these factors has profound implications in precision medicine.

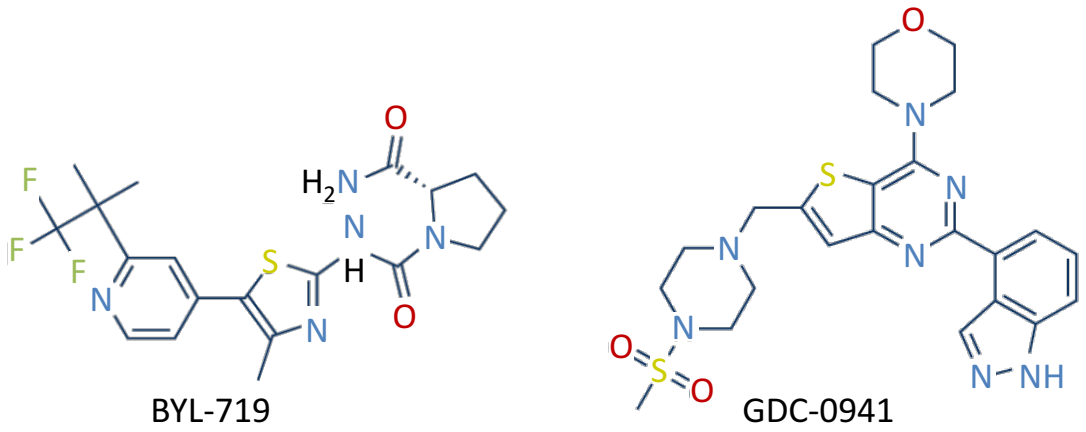

Figure 1.7 Examples of kinase-targeted inhibitors. Chemical structure of BYL-719 [$C_{19}H_{22}F_3N_5O_2S$] (left panel). Chemical structure of GDC-0941 [$C_{23}H_{27}N_7O_3S_2$] (right panel). BYL-719 and GDC-0941 bind to the ATP-binding pocket of PI3K, but BYL-719 only binds to the PI3Kα isoform, whereas GDC-0941 potentially binds to all class I PI3K isoforms.

Nevertheless, and in spite of the complex and highly diverse alterations that occur during the evolution of cancer cells, malignant cancer cells need to maintain a metabolic homeostasis to sustain cellular proliferation [139]. Targeting metabolic enzymes could be used as an anti-cancer treatment strategy to limit tumour growth, and it is further discussed in Section 1.3.2.

1.3.2 Non-oncogene addiction in cancer cells

Malignant cells rely on the activity of a set of cellular pathways to sustain their energetic requirements. Therapies that exploit the differences between the metabolism of cancer cells and non-malignant cells stand as promising anti-tumour agents, and in fact interfering with the metabolism of cancer cells has provided encouraging results in preclinical models and even proved successful in some clinical trials [140]. Such compounds can interfere with: (i) pathways that supply nutrients/produce energy; (ii) pathways involved in the synthesis of biomolecules required for cell growth; or (iii) transcription factors that regulate the expression of genes involved in metabolic processes (Fig 1.8).

For example, 'the lactate shuttle' can be blocked by the MCT1 target inhibitor AZD3965, which is currently undergoing phase I evaluation in the United Kingdom for patients with prostate and gastric cancers and diffuse large B-cell lymphoma [141]. One study revealed that blockade of this transporter disabled growth of lymphoblast-like cell lines due to intracellular lactate accumulation and reduction

of glutathione synthesis [142]. Alternatively, hindering lactic acid synthesis by preventing the activity of LDH with competitive inhibitors such as the gossypol-derived small molecule FX-11 or the pyruvate structural analogue oxamate has proven successful in preclinical studies in human-derived cancer cells [143, 144]. Interfering with the glycolytic pathway by preventing the activity of hexokinase (HK) by treating cells with the glucose analogue 2-deoxy-D-glucose (2-DG) showed therapeutic effects in combination with other anti-cancer agents, such as doxorubicin or paclitaxel [145]. Nonetheless, the difficulty to differentiate the extent of inhibition of tumoural from non-tumoural glycolysis achieved by those agents has limited the therapeutic benefit of such agents [95].

Drugs that restrict biomolecule synthesis are routinely used in clinical oncology. In fact, after the introduction in the clinic of the first vitamin-derivative that restricts DNA metabolism by Sidney Farber [146], chemotherapeutic agents that block nucleic acids synthesis and DNA repair (e.g. fluoropyrimidines, like 5-fluorouracil [5-FU] and antifolates like methotrexate) remain the gold standard treatment agents for patients with solid and haematological malignancies [147].

Among the regulators of cellular bioenergetics activity, mitochondrial activity can be modulated by several mechanisms. One of them is through the usage of arsenic trioxide (As_2O_3), which inhibits the mitochondrial complex IV and increases the electron leakage; this compound has proven beneficial in combination with all-trans retinoic acid (ATRA) in patients suffering from acute promyelocytic leukaemia (APL) [148]. Other mitochondrial enzymes are also targets in anti-cancer therapies. Oral, potent, selective inhibitors of mutated mitochondrial IDH2 enzyme are ongoing clinical trials in AML patients [149]. IDH-specific targeting provides an extraordinary opportunity to reduce the aberrant generation of 2-hydroxyglutarate (2-HG) metabolite without interfering with the metabolism of non-malignant cells.

Hindering cellular antioxidant defence can precipitate a redox-balance crisis leading to cancer cells death. For example, a recent study demonstrated that in models of highly glycolytic colorectal cancer cells harbouring $Kras^{G12D}$ mutation, exhaustion of the antioxidant GSH prompted a metabolic collapse and reduced xenografts tumour size, which can be rescued by the glutathione precursor N-acetyl-cysteine (NAC) [150] (Fig 1.8A). Conversely, scavenging optimal levels of superoxide elicited by metastatic progenitors prevented cancer cells migration in human- and mice-derived tumour models [151]. These examples serve to demonstrate that targeting oxidative stress responses of cancer cells may open a therapeutic window of opportunity to reduce tumour growth. Although the one-size fits-all usage of these products is likely flawed, the variability of the oxidative stress phenotype of cancer cells might be lesser compared to their genetic heterogeneity [86].

Transcription factors such as HIF-1α and c-MYC control the expression of several metabolic genes that provide fine adaptations to promote the proliferation of cancer cells [152]. Notwithstanding the appealing potential of targeting transcription factors to limit extensive gene expression, transcription factors are difficult to target because they do not directly bind small-molecule ligands, and therefore interfering compounds tend to be big molecules that join transcription factors binding surfaces. For example, chetomin –$C_{31}H_{30}N_6O_6S_4$ – is a metabolite produced by various species of *Chaetomium* that inhibits HIF transcriptional activities by precluding the HIF-interacting domain with the p300 coactivator [153]. c-MYC is up-regulated in multiple human cancers and is a master regulator that promotes catabolic processes [152]. Interestingly, c-MYC regulates the expression of about 15% of all known genes and it functions by amplifying the expression of already transcriptionally active genes through the stimulation of RNA pol II elongation [154]. Likewise for HIF, and in spite of the difficulties to develop chemical inhibitors against c-MYC, several small molecules that impede the binding of accessory proteins required for c-MYC's transcriptional activity have been developed [155, 156] (Fig 1.8B), and some are candidates for clinical trials (e.g. CPI-0610 targets chromatin-binding proteins and attenuates the expression of *c-MYC* oncogene) [157].

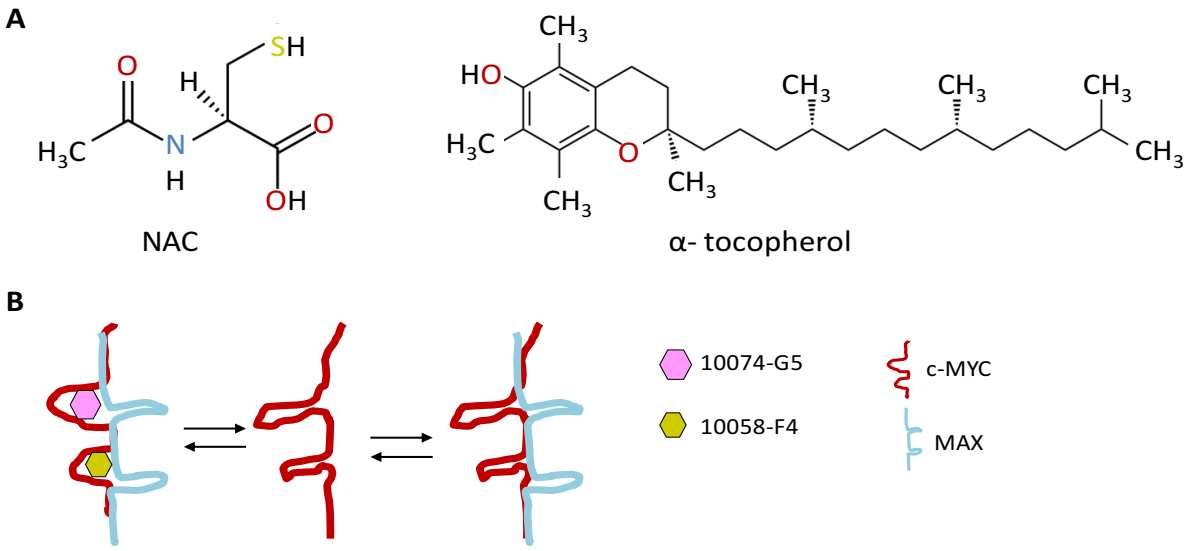

Figure 1.8 Examples of interactors and molecules that modulate the redox state. (A) NAC, N-Acetyl-L-cysteine (left panel) and α-tocopherol (also known as vitamin E) (right panel). NAC is a derivate of the amino acid L-cysteine and acts as a reducing agent due to its capacity to donate a thiol group. α-tocopherol is a strong peroxyl radical scavenger, especially effective in the inhibition of polyunsaturated fatty acids oxidation. (**B**) Compounds that disrupt the heterodimer formed between c-MYC and c-MYC associated protein X (MAX) (e.g. 10074-G5 and 10058-F4). These compounds disrupt the dimerisation equilibrium between c-MYC-MAX heterodimer, impeding the transcriptional activity of c-MYC. The compounds shown in this Figure were used in the studies presented in this thesis.

In summary, during the treatment of cancer cells with targeting agents that modulate protein activity it is important to: (i) elucidate which biological pathways are altered in cancer cells at the time of analysis and treatment; (ii) accurately measure the products derived from the activity of those

pathways; and (iii) predict which cancer cells will be sensitive to combination/alternative therapies. It is also critical to unravel the molecular events that are activated in cancer cells that acquire resistance to targeted therapies in order to delay or even overcome treatment failure.

1.3.3 Intrinsic and acquired drug resistance

Intrinsic or innate resistance is caused by pre-existent mechanisms in cancer cells prior to exposure to a given drug. This type of resistance accounts for the absence of complete response after treatment with a specific targeted therapy of a population of cancer cells within tumours that are not absolutely dependent on the targeted aberrant signalling pathway. Patients with intrinsic resistance are stratified based on genetic mutations to receive treatment and fail to benefit from such therapy. For instance, clinical observations demonstrated that the clinical benefit rate (defined as absence of disease progression ≥6 months) of ER+ breast cancer cell after treatment with BYL719 was 44% for those patients with *PIK3CA*-mutated tumours and 20% for those with the *PIK3CA* wild-type [158]. Indeed, chemosensitive responses to kinase-targeted therapies rated only up to 75% in *EGFR* mutated pulmonary adenocarcinoma treated with erlotinib, an efficient EGFR inhibitor [159]. This lack of complete response to targeted therapies prompts the need for greater knowledge and finer tumour molecular profiling, adequate patient classification, and underscores the importance of the discovery of molecular biomarkers that render information during disease and treatment.

There are at least three mechanisms that account for the existence of drug intrinsic resistance, namely: (i) relief of negative feedback loops; (ii) activity of cooperative signalling pathways; and (iii) aberrant mutations in apoptotic genes. The inhibition of feedback regulation is a common mean of intrinsic resistance described for some small-molecules targeting the PI3K and MAPK signalling pathways, whereby membrane receptors are permanently activated. For example, inhibition of mTORC1 with rapamycin reduces the phosphorylation of S6K1-mediated feedback loop to IRS-1, enhancing the activity of the latter and raising the activation of MAPK signalling [160]. The activity of parallel pathways is known to mediate resistance to the inhibition of a given kinase. For instance, primary AML cells intrinsically resistant to PI3K inhibition activated MEK/ERK and PKC [161]. Finally, genetic instability such as the deletion polymorphism of the *BCL2L11* gene (which encodes for the BIM pro-apoptotic protein) that results in a BIM isoform without the pro-apoptotic BCL2-homology domain is enough to confer intrinsic resistance to tyrosine kinase inhibitors in various cancer cell types [162].

Acquired or adaptive resistance emerges throughout the treatment duration. Thus, patients who initially benefit from therapy often stop responding. There are several mechanisms that explain the

development of acquired drug resistance to targeted-therapy in cancer cells. First, mutations of the targeted protein in certain amino acid residues reduce or impede the drug binding (Fig 1.9). As an example of this, mutations in the translocated Philladelphia chromosome (BCR-ABL) in M351T, T315I, or E255K often arise in chronic myeloid leukaemia (CML) patients after long periods of imatinib treatment. These mutations impede the initial drug binding and effective response [163]. Similarly, the missense mutation T790M in the gatekeeper EGFR kinase domain is present in about half NSCLC patients and makes lung adenocarcinomas resistance to erlotinib or gefitinib-based treatments [164]. Mutations that block drug binding in PI3K have been discovered in some model organisms [165]. One study documented that mTOR's F2108L somatic mutation conferred resistance to the mTORC1 allosteric inhibitor everolimus after 18 months of efficient patient response [166]. Acquired resistance to ibrutinib, an irreversible Bruton tyrosine kinase (BTK) inhibitor, in patients suffering from chronic lymphocytic leukemia (CLL) was associated to cysteine-to-serine mutation in the 481 residue of BTK [167]. Loss of phosphatases that counteract the activity of the targeted kinase can explain the emergence of resistance. A remarkable example is the convergent PTEN lost by diverse genetic alterations in 14 metastatic sites in a patient whose tumours had become resistant to a PI3K inhibitor [168].

Up-regulation of RTKs is another mechanism through which cancer cells stop responding to kinase-targeted therapies. Various RTKs, including PDGFRβ, IGF-1R, and HGFR have been documented to be over-expressed in resistant melanoma cells to compensate for the inhibition of BRAF [169]. By contrast, the activation of alternative kinases that make up for the inhibited activity of targeted kinases is an alternative mechanism used by cancer cells to reactivate the targeted signalling pathway. For instance, the activity of p110β isoform can rebound PIP3 levels mediating resistance to p110α inhibitors [170]. Cancer cells that have common point-mutation BRAF (V600E) in melanoma, can overcome MAPK inhibition via mutational activation or over-expression of pathway activators (such as NRAS, CRAF), splicing of alternative BRAF isoform immune to inhibitors (e.g. p61 BRAF-V600E) or through mutation of kinases downstream of BRAF (e.g. COT, MEK1, and MEK2) [169]. Lastly, hyperactivation of alternative or compensatory signalling cascades can sustain the drug-resistant phenotype of cancer cells. Indeed, preclinical *in vivo* models have shown a synergistic regression of *Kras*^{G12D}-induced lung tumours after two weeks of combination treatment with inhibitors that target the PI3K and the MAPK pathways, indicating an existing cross-talk between these signalling pathways [171]. Synergistic induction of death of cells resistant to PI3K/mTOR inhibition has also been observed using in combination PI3K and c-MYC molecule inhibitors [172].

Overall, these examples serve to emphasise that profiling of somatic mutations may not be sufficient to infer the sensitivity of cancer cells to a given treatment, and this may have direct implication in the design of lines of chemotherapy.

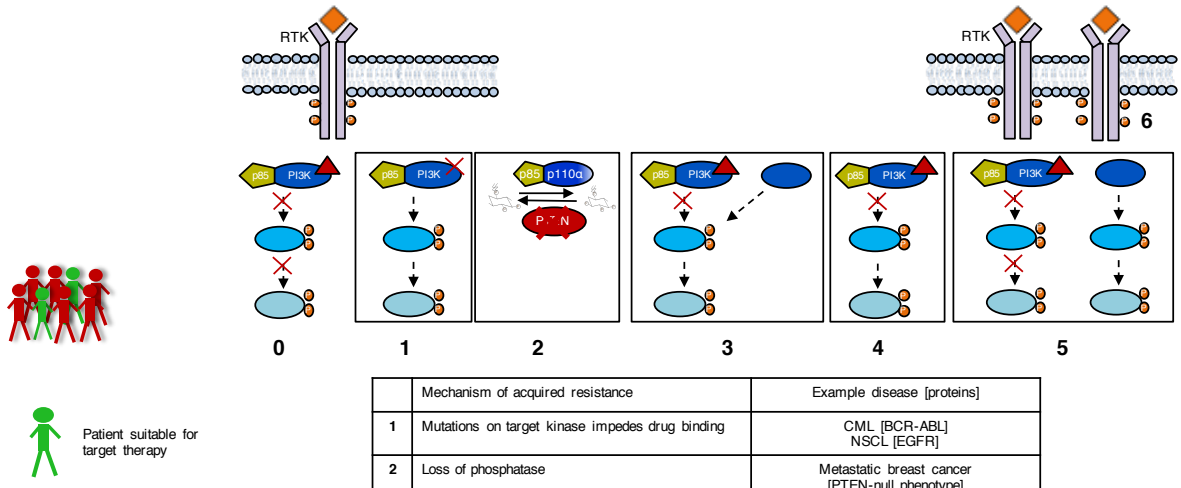

	Mechanism of acquired resistance	Example disease [proteins]
1	Mutations on target kinase impedes drug binding	CML [BCR-ABL] NSCL [EGFR]
2	Loss of phosphatase	Metastatic breast cancer [PTEN-null phenotype]
3	Upregulation of compensatory kinase	Melanoma (BRAF(V600E)) [NRAS, CRAF,+BRAF, alternative splicing]
4	Activation of downstream kinase	Melanoma (BRAF(V600E)) [+MAP3K8, activating mutation in MEK1/2]
5	Emergence of parallel pathways	Melanoma (BRAF(V600E)) [+PI3K/AKT/mTOR signalling]
6	Amplification of membrane receptor	Melanoma (BRAF(V600E)) [+EGFR, IGF-1R, and PDGFR]

Figure 1.9 Mechanisms of acquired resistance. Within population of patients suffering from cancer, some patients (represented in red) have intrinsic resistance to a given drug treatment and do not respond to treatment. On the other hand, those patients that are stratified to receive a given treatment (represented in green) eventually will acquire resistance to treatment. Targeted therapies specifically bind their target (e.g. PI3K, represented by a red triangle) and impede downstream signalling, normally causing cell death (0). However, secondary mutations on the targeted kinase impede the inhibitor binding and the signalling inhibition (1). Loss-of-function mutations or deletions of phosphatases that counteract the kinase activity lead to resistance to kinases inhibitors (2). Mutations or over-expression of kinases able to compensate the signalling activation rescue the pathway activity (3). Activation of downstream components of the signalling pathway also restore the signalling activity (4). Hyperactivation of parallel signalling cascades (usually mediated by up-regulation of membrane receptors) recover the activity of signalling cascades (5). Amplification of membrane receptors facilitate the activity of downstream signalling cascades (6). CML, chronic myeloid leukaemia; NSCLC, non-small cell lung carcinoma; PDGFR, Platelet-derived growth factor receptors.

1.3.4 Lines of chemotherapy

In the clinic parlance “drug resistance” is frequently used almost interchangeably to “progressive disease” [174]. The usual procedure in cancer treatment after disease progression is to commence an alternative therapy by the administration of drugs which cancer cells are non-cross-resistant to (Fig

1.10A). The rationale for this is that the initial anti-cancer agents are no longer effective to reduce the malignant cells and thus a distinct treatment plan is required. The lines of therapy chosen after treatment failure are based on observations made from randomised studies conducted to estimate the efficacy of alternative treatments. There are several clinical intervention approaches to handle progressive diseases. The first one consists of shifting to a distinct therapeutic agent: when the first-line therapy fails, second-line therapy may be used instead. The choice of alternative agents may be guided by the drug pharmacodynamics (i.e. the effect of the drug at a given time and concentration), pharmacokinetics (i.e. the drug's distribution and metabolism), and can be influenced by the patient's comorbidities, neutropenia, smoking record, and patient's preference [175]. For example, the treatment options for NSCLC patients who become refractory to first-line treatment with platinum-based chemotherapy include docetaxel, pemetrexed or erlotinib as second-line chemotherapy [175].

An additional plan of action is to continue with the initial treatment despite disease progression (Fig 1.10B). Continuing with first-line trastuzumab beyond disease progression in ERBB2 positive breast cancer patients in combination with lapatinib showed superior survival and response rates compared to patients that switch to lapatinib (i.e. 51.6 weeks for treatment beyond progression versus 39.0 weeks for lapatinib monotherapy) [176]. At present, there is not comprehensive methodology to predict an adequate balance between drug efficacy and drug toxicity. Thus, delivering optimal dose-combinations in the clinic has been exceedingly difficult because overlapping drugs toxicities enforce treatment interruption and dose reductions for most cancer patients [177, 178].

Finally, when patients relapse, a temporal treatment discontinuation (i.e. treatment-free interval) is potentially followed by rechallenge with the same drug. A period of drug holiday (i.e. drug removal) is the principal reason cited for re-sensitisation of cancer cells to the initial therapy. In fact, *in vitro* data demonstrated that drug withdrawal provokes drug re-sensitisation of models of resistance to targeted-therapies [179-183]. Xenograft models of renal-cell carcinoma and hepatocarcinoma that had acquired resistance to TKIs (i.e. sorafenib or sunitinib) gained sensitivity after a treatment break, highlighting the plasticity of the resistance phenotype [184, 185]. Moreover, intermittent dosing of lapatinib and trastuzumab combination treatment improved the anti-tumour capacity in two HER2-overexpressing xenografts compared to the continuous treatment [186]. Preclinical data suggested that drug resistance can be delayed by intermittent dosing [187], and a small case series reported that two melanoma patients were re-sensitised to BRAF-selective inhibitors after rechallenge [188]. Intermittent and reduced drug doses contribute to lower the toxicity of single or combination of molecular targeted agents. This, along with the rising cost of anti-cancer treatments [189], emphasises the urgent need to design innovative dosing schedules for precision medicine (Fig 1.10C).

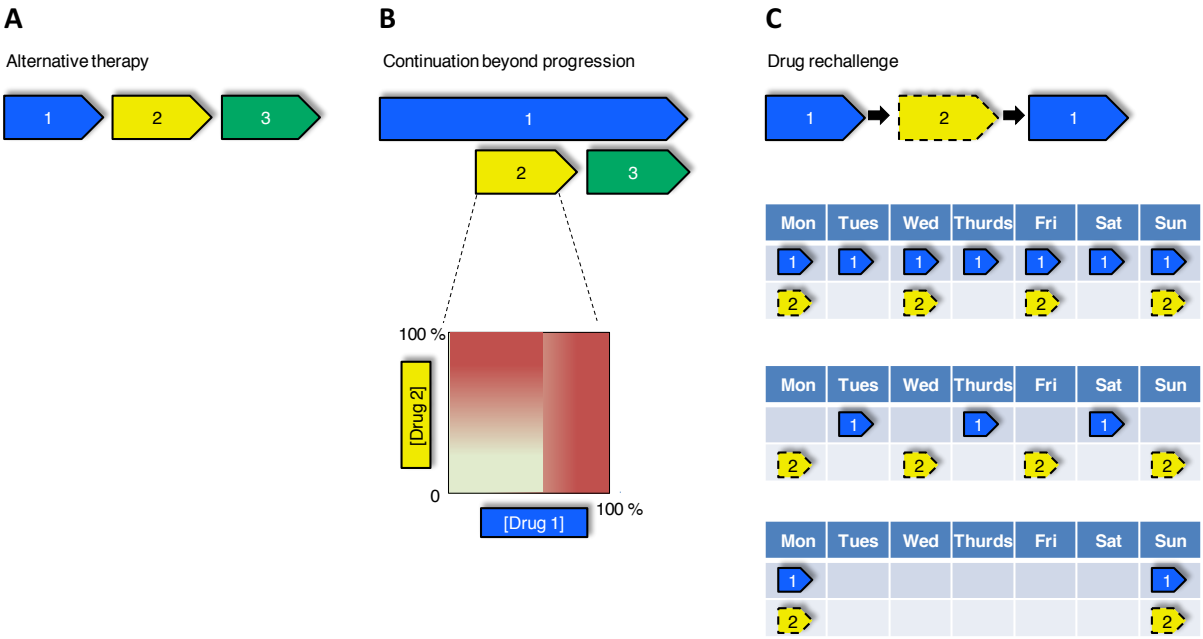

Figure 1.10 Overview of the treatment regimens used in medical oncology. (**A**) When the initial front therapy drug 1 stops to have a beneficial effect reducing tumour progression, treatment is switched to different drugs 2, 3, etc. (**B**) In combination trials, the initial agent can be maintained, even when disease continue, together with an alternative drug, which may improve the response rate of the alternatives agents. The lower image shows the traditional approach to determine the optimal response dose tolerable based on drugs toxicities. (**C**) An alternative dosing strategy consists in scheduling intermittent drug administrations. A gap in therapy 1, potentially followed by a period of treatment with additional drug, could potentiate the effect of the initial therapy. Black arrows represent drug-free periods. The lower image shows improved therapy designs to achieve optimal response to drug derived from modelling of large drug-response datasets. For example, some patients would benefit from periodic withdrawal of drug 2, while others would benefit with alternating dual treatment.

Current FDA-approved chemotherapy dosage schedules may not be optimised to forestall the emergence of resistance, as demonstrated by a study that used mathematical modelling to predict the resistance response to alternative dosing schedules [181]. Nevertheless, much effort has been made in recent years to create and refine models based on system biology approaches to predict better dose combinations and schedules [178, 190, 191].

Understanding the evolutionary dynamics of molecular pathways that emerge during drug resistance may contribute to a superior success of targeted therapies. As outlined before, given the cross-communication of molecular pathways, better knowledge of biochemical networks would help to explore potential vulnerabilities of cancer cells. To this end, the field of translational research is starting to use high-resolution mass spectrometry-based proteomics, which is a methodology that has an unbiased nature and high information content. These facts, coupled with adequate bioinformatics analyses, allow the comprehensive profile of, in theory global, protein species in biological systems.

1.4 Proteomics

1.4.1 Principles of proteomics using mass spectrometry

Proteomics is the study of the complete set of proteins of a biological system at a given time and condition. Mass spectrometry is a technology that nowadays is extensively used for studying proteins. By definition, mass spectrometry (MS) is an analytical technique that measures the mass to charge ratio (*m/z*) of ions in gas-phase. A mass spectrometer is composed of three essential components: an ion source, a mass analyser and a detector. The ion source is a device that transforms the sample molecules present in liquid or solid phase into gas-phase ions, which are then transported to the mass analyser by the application of a discharge voltage to the ion transfer capillary at atmospheric or low pressure. Ions are separated in the mass spectrometer according to their *m/z*, following the laws that control charged species in vacuum in electric and magnetic fields (i.e. Lorentz force law and Newton's second law). Finally, when each separated ion packet hits the detector, this calculates the relative ion abundance by measuring the current generated for each hit. A mass spectrum of an ion is a plot of its *m/z* (on the x axis) against its relative abundance (on the y axis). Using the mass spectra, the charge of each ion (z) can be determined; hence the mass (m) of each ion can be calculated from the *m/z*. The analysis of the mass spectra provides the identification and the quantification information of the compounds contained in a sample. This technique is used in industry and research for specific and unbiased analyses of complex chemical and biochemical mixtures.

There are two methods presently used to perform "soft" ionisation of macromolecules contained in a sample: electrospray ionisation (ESI) and matrix assisted laser desorption/ionisation (MALDI). ESI applies high voltage to a liquid-phase analyte as it passes through an electrically conductive capillary, to create a mist of multiply charged ions in gas phase [192]. MALDI uses a pulse laser to vaporise a sample embedded in solid matrix containing acidic groups and then protonate those molecules which are then accelerated by the application of a voltage and analysed [193]. MALDI have been applied for peptide mass fingerprinting, but this ionisation technique is not suitable for high-throughput proteomic analysis given that it is difficult to couple to liquid-chromatography and that its reproducibility depends on the efficiency of matrix-to-analyte proton transfer, which is often variable. In fact, the ionisation method of choice for proteomic analysis is nano-ESI, a variant of ESI performed at lower flow rates (~0.3 µL/min). This capability increases the sensitivity of analysis due to higher ionisation efficiency, less ion suppression and higher analyte concentration [194, 195].

To identify peptides within a complex sample, peptide masses are measured and its components consequently fragmented. This occurs inside the quadrupole or ion trap mass analyser, and there are three main types used in mass spectrometry, namely the quadrupole ion trap, the penning ion trap and the orbitrap. Many of these instruments are often used in combination with more than one analyser.

In the quadrupole ion trap, two (2D-ion traps) or four (3D-ion traps) rods form a chamber where ions are trapped. Constant direct current and radio-frequency electric fields are applied to trap ions according to their *m/z* ratio by sweeping the radio-frequency [196]. By applying an alternating current, trapped ions are subject to be fragmented (CID fragmentation, see Section 1.4.4). A hyphenated variation of this is the triple stage quadrupole (TSQ), which, as the name suggests, has three sequential quadrupoles (Fig 1.11). When quadrupole ion traps are in selection mode, they have high sensitivity and therefore are efficient instruments for the quantification of known component fragments. However, when in scanning mode, they have low resolution and relatively low mass accuracy, and therefore they are not adequate for peptide discovery through fragmentation.

The Penning ion traps are a variation of the quadrupole ion traps, whereby electric field is applied to an ion chamber placed in the centre of a magnetic field (*B*). Ions are trapped in that magnetic field upon their excitation with an electric field orthogonal to *B*. The *m/z* of each ion and the strength of the magnetic field *B* determine the cyclotron frequency at which each ion rotates; rotating ions induce a charge on the detection electrodes (the image current), which can be converted into a mass spectrum using a Fourier transformation. Therefore, this technique is often referred as Fourier transform ion cyclotron resonance (FT-ICR).

Lastly, the orbitrap consists of an axial inner electrode surrounded by a barrel-shape outer electrode [197]. Orbitrap instruments trap ions using an electric field and subsequently eject them into the orbitrap, where ions oscillate around the central electrode according to their *m/z*. Like for FT-ICR analysers, the image current induced by the oscillating ions on the detection electrodes can be transformed by a Fourier transformation function into a mass spectrum. In the LTQ-Orbitrap mass spectrometer, a linear quadrupole is combined with an orbitrap; in this instrument, the intact masses are measured in the orbitrap and ions are fragmented in the quadrupole trap.

Orbitraps have turned prominent analysers in the proteomics field during the last decade given their high mass resolution (for example, for the Q exactive Plus the optical resolution is up to 140,000 FWHM at *m/z* 200), high mass accuracy (1-2ppm), high sensitivity, and relatively high dynamic range.

1.4.2 Sample preparation for proteomics

Proper sample preparation is a crucial step for successful proteomics analyses. There are two methods to prepare and analyse samples for a given proteomics experiment: bottom-up and top-down. The bottom-up approach is the most commonly used method in proteomics; in this strategy, proteins are proteolytically digested by a selected enzyme resulting in a complex mixture of peptides (that are ~8–25 residues long), which are then used to identify/quantify the proteins within a given sample. There are several considerations that need to be taken into account during bottom-up sample preparation [198]. The first consideration is the method used for protein extraction; as such, tissue-derived samples are subject to vortexing and liquid nitrogen treatment in order to achieve complete tissue disruption. Otherwise, cells are usually lysed with buffers that contain denaturing chaotropes (e.g. urea) to increase protein solubility. However, chaotropes can interfere with the enzymatic activity required for protein digestion. One strategy to remove those blocking agents is to immobilise proteins in a solid support, either in a gel in the case of polyacrylamide gel electrophoresis (PAGE), using a filter for detergent removal in the case of filter-assisted sample preparation (FASP) [199], or the more advanced pipette-based filters that remove interfering agents while minimizing sample loss and contamination [200]. Another strategy is to perform an in-solution protein enzymatic digestion, so that the disrupting substances are diluted and their negative impact on the proteolytic yield is reduced. Solubilised and denatured proteins are consequently reduced and alkylated with agents such as dithiothreitol (DTT) and iodoacetamide (IAM), respectively. The second consideration is the selection of enzyme used to digest protein mixtures. The most currently used enzyme is trypsin, which cleaves proteins at the C-side of arginine and lysine residues [201]. Other proteases, such as Arg-C, chymotrypsin, or Glu-C, may be desired for certain proteomics experiments. For example, Arg-C has been used to facilitate the study of modifications in histone peptides given that this enzyme exclusively cleaves at Arg, leaving intact Lys-containing peptides [202].

In the top-down approach there is no digestion step, and therefore this technique can in principle be used to characterise primary structure of intact proteins, differentiate between proteoforms, and obtain structure information and ligand/cofactor-binding affinities [203].

1.4.3 Liquid chromatography-MS

Despite the continuous improvements in mass spectrometers performance — including better mass accuracy, higher mass resolving power, improved sensitivity, and faster scanning speed — deep sequencing of complex proteomes (e.g. mammalian proteomes) still requires a previous separation

step before the analytes enter into the MS. Intrinsic chemical properties of proteins such as polarity, hydrophobicity, and charge can be exploited to fractionate entire proteomes into more simplified formats. Among the separation techniques integrated with mass spectrometry, liquid chromatography (LC) is a widely used online method (i.e. the complex sample fractionation is directly coupled to the mass spectrometer). In the LC-MS/MS, compounds are separated based on their hydrophobicity: the liquid-phase analyte in the organic carrier solvent (mobile phase) is separated on its moving through the silica-bead-filled hydrophobic chromatography column (the stationary phase, in reverse-phase). The elution of the mobile phase (usually achieved using acetonitrile [ACN] or methanol) is done in a gradient that usually starts at low proportion of organic phase and progresses linearly to a higher organic concentration. The time at which each analyte elutes from the column is called the retention time (t_R) and is a distinctive characteristic of each peptide: hydrophilic peptides elute earlier from the column and hydrophobic peptides are retained longer in the column. Hence, the chromatographic separation expands the dynamic range and sensitivity of mass spectrometers. Alternative offline methods such as immunological/inorganic affinity purification or 1D/2D electrophoresis/chromatography also reduce sample complexity, but the integration with the MS analysis is not fully automated (see Section 1.4.6). Although tandem LC-MS/MS requires longer workflow times and greater quantity of starting sample material, continuous development of LC technology (such as the introduction of ultrahigh-pressure liquid chromatography [UPLC] with sub-2 µm bead resins) helps to improve sample recovery, speed, and parallelisation [204].

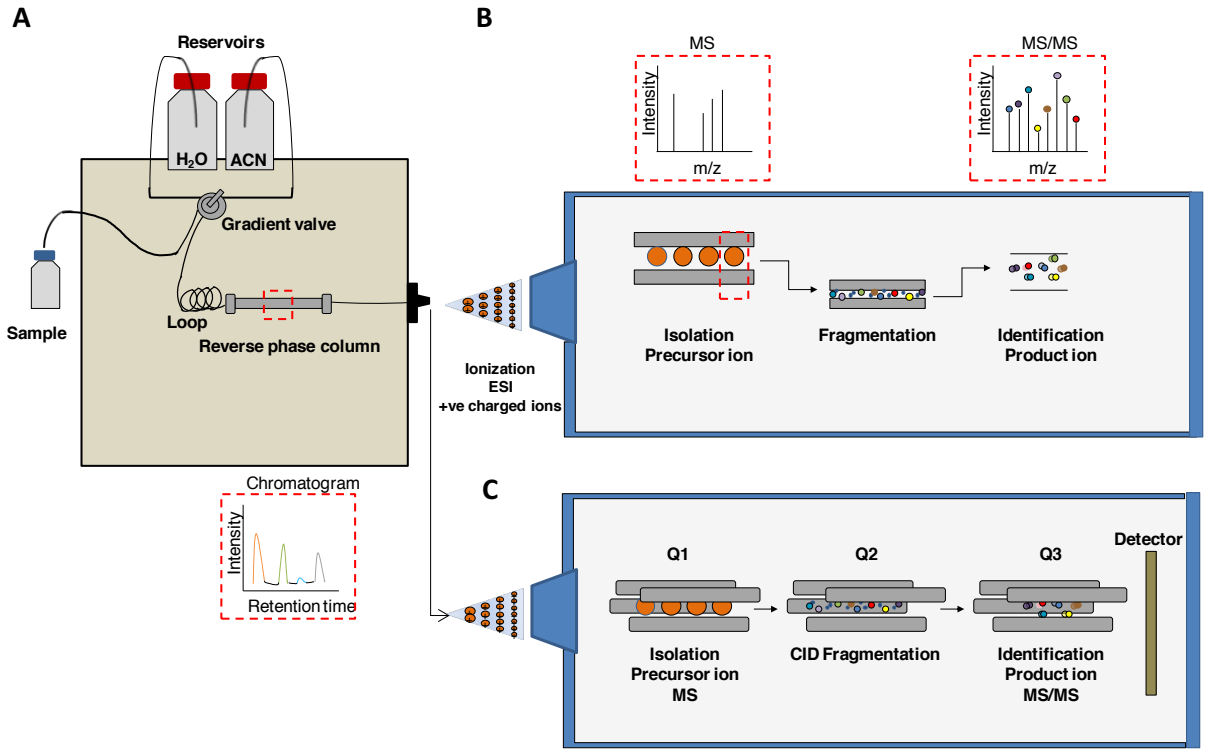

Figure 1.11 Principles of tandem LC-MS. Each sample is separated by reverse-phase liquid chromatography (LC) previous ionisation and injection into the mass spectrometer (MS). (**A**) LC: Sample is injected into the sample injection loop on a mixed gradient regulated by the gradient valve. The sample then enters into the analytical column, where peptides bind to the non-polar stationary phase under aqueous buffer and increasing concentration of organic solvent (e.g. ACN) elute each peptide at a given retention time depending on their hydrophobicity. Hydrophobic peptides are retained longer in the column. Eluted peptides pass through the ESI emitter where voltage is applied (typically 1 to 2 kV). Charged droplets pass through the ion transfer capillary and are directed into the MS. (**B**) MS: Gas-phase ions enter the mass spectrometer where their *m/z* intensities are measured in the first MS scan. A given precursor is selected and isolated for fragmentation and the intensities of fragmented ions are measured in the second MS/MS scan. The sequence of the precursor ion is inferred from the MS2 data by manual sequence assembly or by comparison with a database. (**C**) Ions can also be directed into a triple quadrupole mass spectrometer. This instrument allows high sensitivity quantitative detection of peptides and small molecules, such as metabolites and drugs. Each quadrupole contains four cylindrical, metal parallel rods connected electrically, which allow the ions travelling through the centre of quadrupole analyser. Ions are guided into the first quadrupole (Q1), which acts as a mass filter allowing the streaming of ions of certain *m/z*. Ions with a stable trajectory arrive to the middle quadrupole (Q2), which is used as a gas collision cell for CID fragmentation of precursor ions. Q3 is another mass filter and directs fragmented ions towards the detector. ESI, electrospray ionisation.

1.4.4 Qualitative identification analysis

Qualitative proteomics for the identification of proteins and peptides can be carried out either in a targeted or untargeted manner. Experiments designed for targeted proteomics usually aim to discover with high precision the amount of known proteins within a sample. Untargeted proteomics, conversely, is a global and powerful approach that allows the unbiased identification of tens of thousands proteins at once within a relatively short time. Qualitative assignment of protein sequences

is possible due to the existence of tandem mass spectrometry (MS/MS or MS2) analysis, which separates and fragments ions in a multiple-step process. In the first step, peptide ions are selected for their further fragmentation (i.e. chemical dissociation of energetically unstable ions) in the second step. There are two ways how mass spectrometers select sample peptides for fragmentation, namely data dependent acquisition (DDA) and data independent acquisition (DIA). During DDA mode, the instrument is automated so that only a specific number of peptide ions — for example, 20 in a "top 20" experiment — that generate the most intense MS signal are selected for fragmentation. The DDA approach has the significant limitation that its performance deteriorates as sample complexity increases because the less abundant ions are usually not selected for fragmentation; this limits further peptide identification and quantification (the so called under-sampling problem). Development of more sensitive instruments with lower duty cycle (the operating time of the mass spectrometer) have greatly ameliorated the output of this approach. Optimised algorithms for protein/peptide quantification, such as PESCAL [205] have also contributed to a large extent to undermine the undersampling problem (see Section 1.4.5). DDA-based proteomics approaches resulted in two drafts of the human proteome, which reported 84% [206] and 92% [207] coverage of annotated protein-coding sequences of the human genome. In DIA strategies, however, all parent ions in an MS run are subject to fragmentation. One popular DIA method is SWATH, which fragments and acquires all the ion spectra in sequential acquisition windows (that usually span 25 *m/z*) through the MS run [208]. In DIA, peptides are identified by matching the transition ions to pre-existing public spectral repositories generated using DDA methods. Among the benefits of DIA are broader dynamic range of signals, better reproducibility for identification, and improved sensitivity and accuracy for quantification [209]. However, the resulting MS2 data are difficult to interpret and need to be deconvoluted [210].

Ions are subject to fragmentation when they acquire additional energy, which cause their backbone breakage either by heterolysis or homolysis. Fragmentation can occur in the ion source (i.e. in-source fragmentation) or in the collision zone (i.e. post-source fragmentation), the latter being normally used in a proteomics experiment. In fact, ion-source fragmentation is technically not a tandem MS/MS technique because some ions (i.e. metastable ions) dissociate before being selected, contrarily to post-source fragmentation, whereby energy is added to the ions after MS analysis. Ion fragmentation rate is determined by the peptide molecular size, amino composition, and by the fragmentation method employed. There is an array of methods used to transfer kinetic energy into ions, being the two mostly methods used in proteomics analysis transfer of electrons from an electron donor (e.g. electron transfer dissociation [ETD] or electron capture dissociation [ECD]) and collision with a neutral gas (often helium, nitrogen or argon) (e.g. collision-induced dissociation [CID] or higher-energy collision dissociation [HCD]). Selection of the fragmentation method is optimised depending on both

the instrument of analysis and the analyte, as different types of fragment ions can be generated depending on the fragmentation method. For example, during CID — the most popular form of fragmentation over the last years — peptides are broken at the amide-backbone, whereas in ETD peptides are broken at the carboxyl-backbone. HCD is a type of CID whereby higher voltage is applied to trap ions in the C-trap, where they are fragmented before being injected into the orbitrap for high resolution mass detection and generation of MS2 spectra.

These spectra can be used to derive the sequence of amino acids of a given peptide without any prior knowledge, using the so called *de novo* sequencing, where the mass of each amino acid is calculated using the mass difference between two consecutive peaks. Until recently, *de novo* sequencing was performed manually, which make this identification approach very laborious and time consuming, especially for large datasets. However, this approach can identify novel peptides as well as peptide mutations, and recent automation achieved by computer programs such as PEAKS [211] reduces the time-consuming problem and other issues such as incorrect ion assignment.

Peptides can be also identified by processing MS2 raw spectra into peak lists that can be searched in databases containing theoretical peptides spectra generated by *in silico* digestion with a particular enzyme and fragmented with a specific fragmentation mode [212]. This is a highly automated process and several software packages with different peptide identification scoring including Mascot [212], SEQUEST [213], and X!Tandem [214] can be used for peptide identification. Mascot, widely used in the proteomics community, scores a peak list using the MOWSE score. Initially, this search engine compares the experimental peptide/proteome data with each entry in the database (± a given mass tolerance), calculates a Mascot score derived from the probability that the peptide match is achieved by chance — the lower the probability, the higher the Mascot score. This approach has proven to be extremely advantageous given the relatively fast, high throughput identification of peptides. In addition, a false discovery rate (FDR) can be calculated by searching the data in a reverse or randomised (i.e. “decoy”) database to estimate the number of false positives identified with the real database.

1.4.5 Quantitative identification analysis

Large-scale quantification of proteomes has made possible to address fundamental questions of biological systems [206, 207]. There are two main methods applied in quantitative proteomics: label-based and labelled-free techniques (Fig 1.12). Label-based approaches introduce in the samples affinity tags that have known and distinctive isotopic mass. Differentially labelled protein or peptides are combined and posteriorly analysed in the LC-MS/MS. Peptide intensities are compared to heavy ion peptides (in isotopic labelling) or to a reporter ion (in isobaric labelling), which permits the relative calculation of peptide abundances. One of the first labelling method developed, isotope-coded affinity tags (ICAT) is an isotopic labelling method based on the covalent attachment at protein cysteine residues of heavy and light isotope tags (deuterium and hydrogen, respectively) attached to a biotin tag for purification [215]. The mass difference between the heavy and light isotope-tagged samples is resolved at the MS level. Because samples are processed at the MS level, ICAT has several technical limitations, including large tags interfering with the subsequent fragmentation, and it is limited to label cysteine-containing proteins. Moreover, hydrophobic proteins are underrepresented in ICAT due to poor recovery of peptides from avidin. Isobaric labelling with tandem mass tag (TMT) [216] and isobaric tags for relative and absolute quantitation (iTRAQ) [217] aim to amend some of these limitations, by the usage of reporters ions that are released during MS2 step, which permit the identification and quantification of reporter groups of known mass [217]. Although these methods have been used in multiple studies, isobaric tagging approaches present various drawbacks, including variability in the labelling efficiency — and therefore variability in the quantification — and limited/erroneous quantification due to co-isolation and fragmentation of precursors that have similar mass [218].

Proteins can also be labelled *in vivo* during protein synthesis using the well-established method called stable isotope-labelled amino acids in cell culture (SILAC) [219]. SILAC involves the incorporation of two differentially labelled amino acids (usually lysine or arginine) into metabolically active cells during culture. One population of cells is fed with media supplemented with unlabelled amino acids whereas another population of cells is fed with media supplemented with heavy amino acids, being this mass shift being detectable by the mass spectrometer. Equal amount of harvested cells/proteins are mixed, processed, and the relative protein abundance is calculated by comparing heavy labelled peptide ions to their unlabelled counterparts. In this manner, proteins are labelled as they are synthesised, which ameliorates purification issues and issues with labelling kinetics [219]. The two major limitations of the SILAC approach are that its application to primary tissue samples is not

straightforward and that only a limited number of comparisons is possible within an experiment (usually between 2-3 samples).

In sum, label-based approaches offer several possibilities to successfully perform quantitative proteomics analysis, allowing multiplexing to improve quantitative precision. However, there are crucial limitations including increased complexity and time for sample preparation, limited number of comparisons, relatively high cost of reagents and constrains for clinical samples, which ultimately restrict the application of these approaches to answer many biological questions.

On the other hand, the label-free methods rely neither on chemical derivatisation nor on metabolic incorporation of stable isotopes, but instead aim to either compare the abundance of peptides/proteins between samples or to perform absolute protein quantification at a global scale [220]. Two fundamentally different strategies are currently used in label-free quantitative proteomics: spectral counting and extracted ion chromatograms (XICs). Spectral counting follows the assumption that the abundance of a peptide is directly correlated with the number of MS2 scans triggered by that peptide [221]. After counting the MS2 events for all peptides, the abundance of each protein is calculated by averaging the spectral counts of all peptides belonging to each protein. This method is intuitive and easy-to-apply; however, the quantitative capacity of spectral counting is often considered semi-quantitative because the most abundant peptides are more likely to be selected for MS2 (due to the undersampling problem). There have been several attempts to improve the usability of spectral counting for quantitation, although accurate quantification of ion abundances using these method is often not feasible [222].

The XICs label-free method constructs extracted ion chromatograms of the precursor peptide ions. Thus, XICs integrate *m/z* over the chromatographic time for each peptide and extrapolate peptide or protein abundance by calculating either the peak area or peak height for each eluted peptide. In this approach, *m/z* tolerance and *tR* windows to generate XICs are selected based on the LC-MS performance. Given that complex samples tend to have isobaric peptides within a given *tR* window, narrowing the *m/z* window contributes to reducing erroneous selection of peaks for quantification. This principle is followed in the accurate mass and time tag (AMT) approach, which is a targeted and label-free method developed for the accurate selection of LC-MS parameters for peptide/protein quantification [223]. Separately, selective reaction monitoring (SRM) is a specific targeted label-free method normally done in triple quadrupoles, whereby the first and the third quadrupoles specifically select precursor ions to be fragmented and monitored to calculate their abundance [224]. Like SRM,

multiple reaction monitoring (MRM) monitors multiple product ions from a precursor ion, providing greater confidence in the quantification.

PESCAL (Peak Statistic Calculator) is computer program used to quantify proteins in an untargeted manner developed in the Cutillas group that automates the generation of XICs and can be used for the quantification of peptide/proteins of complex samples [205]. Initially, a database of peptides identified in the MS/MS data is populated with peptides *m/z*, charge state (z), *tR* and name of sample where the peptide was identified. The *tR* of common peptides are calculated across samples to compensate for chromatography variability. The *tR* used to calculate the XICs (with windows of ± 7-10 ppm), however, is specific for each sample and is a result of extrapolation with linear models formed between standards present in the sample. To increase the quantification accuracy of this method, peaks must contain a minimum number of data points to be considered for quantification. Moreover, the ratios of second and third isotopes of each peptide are correlated with the theoretical distribution and used in the quantification, which improves the robustness of the peak-picking, increasing the correct assignation of isobaric peptides [205].

Among the advantages of the PESCAL method, stands the fact that the number of possible samples to be compared is theoretically, unlimited. This strategy allows peptide quantification and identification even if the peptide was not selected for MS/MS fragmentation, which greatly reduces the under-sampling problem. Moreover, it can be applied to samples derived from clinical material. There is, however, some margin of error in the assignment of the peptide *tR* and retention time shifts when analysing large datasets, which can be reduced by robust LC instrumentation. Certain inaccuracy in the peptide assignment to each MS peak is possible, although improvements on high mass-accuracy MS instrument (sub-ppm) reduce this problem. The sample preparation could be long if many samples are to be analysed given that, as for all label-free methods, samples must be processed independently. Performing data replicates has proved to enhance the quality of quantitative data [225], despite increasing experimental timing. Overall, PESCAL is a reproducible, label-free quantification method that has reported robust quantification (CV of 22% across replicates, which is enhanced after data normalisation) and accurate quantitative readout [225]. Indeed, PESCAL has been successfully used to address multiple biological questions [161, 226-228].

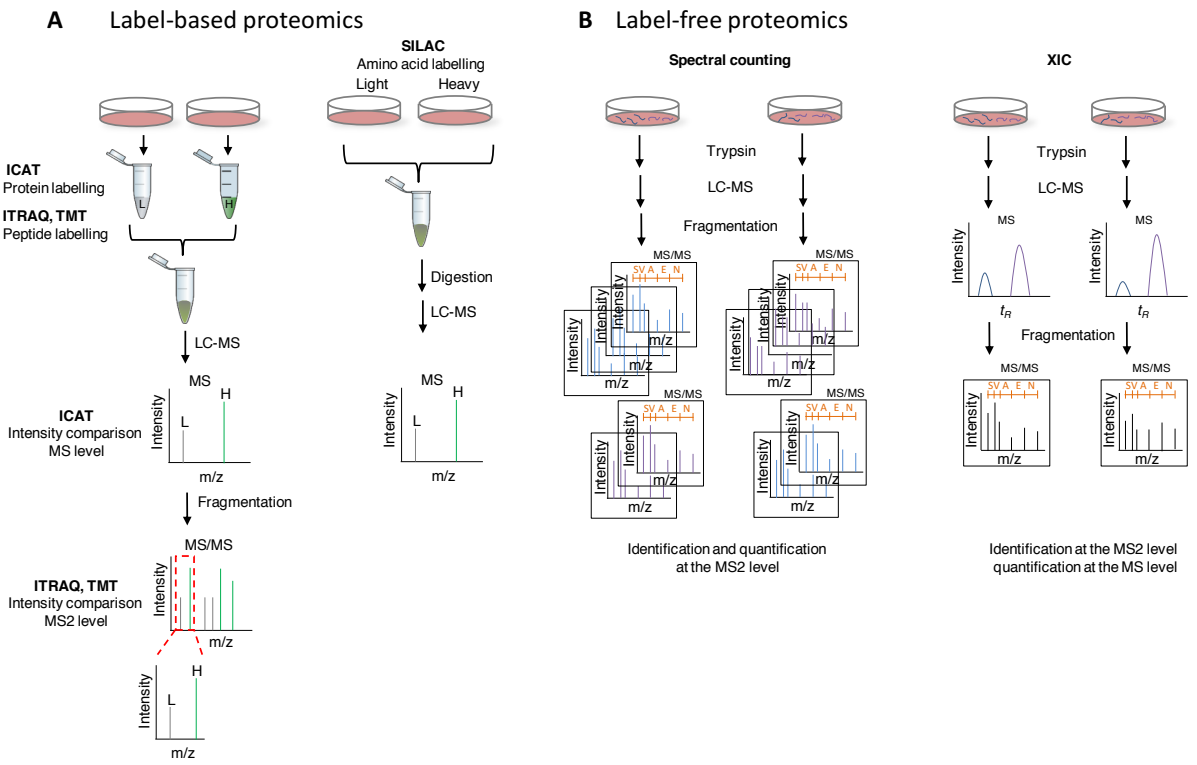

Figure 1.12 Representation of label-based and label-free methods used for quantitative proteomics. (**A**) In label-based methods proteins (in ICAT) or peptides (in iTRAQ and TMT) are labelled. Samples are mixed and prepared for analysis on a mass spectrometer. The isotopes differential abundance is compared at the MS level (in ICAT) or at the MS2 level (in iTRAQ and TMT). Zoom in the *m/z* region of dissociation of reporter ions used for quantification (left panel). In metabolic-labelling techniques, the culture media contains regular or heavy isotopes of lysine or arginine. Isotope incorporation into proteins occurs during protein synthesis. Samples are mixed, digested, and analysed on a mass spectrometer. The differential abundance between heavy and light isotopes is calculated from the MS data. (**B**) Quantitation strategies based on label-free methods included spectral counting and extracted ion chromatograms (XICs). Samples are lysed, proteins are digested and peptides are independently run on an LC-MS/MS system. In this example, the blue proteins are more abundant than the purple proteins and the relative abundance of the peptides is reflected by the number of the MS2 spectra (in spectral counting) or by the area under the XIC. ICAT, isotope-coded affinity tagging; iTRAQ, isobaric tags for relative and absolute quantification; SILAC, stable isotope-labelled amino acids in cell culture; TMT, tandem mass tagging.

1.4.6 Phosphoproteomics

Phosphoproteomics is the study of the global dynamic post-translational modification (PTM) of proteins whereby phosphate is added via a covalent bound. Phosphorylation of proteins is catalysed by kinases, removed by phosphatases, and often causes protein conformational changes. Protein phosphorylation has a pivotal role in diverse cellular responses, and can alter proteins activity, stability, interactions, and localization [229]. Consequently, the dynamic of protein phosphorylation is tightly regulated by networks of kinases and phosphatases that act within time frames of milliseconds to seconds [230]. Evolutionary studies on phosphorylation revealed a high degree of conservation of phosphorylation sites compared to the non-phosphorylated counterparts in higher eukaryotes,

suggesting that the phosphoproteome is a major phenomenon in cellular evolution [231]. To date, however, there is some controversy about the function of phosphorylation sites [232, 233], although some hypotheses point to lineage- or specie-specific role of phosphorylation events. As an example of this, the cyclin-dependent kinase (CDK) consensus motif of phosphorylation of mini-chromosome maintenance protein 3 (MCM3) was found essential in *S. cerevisiae* for the protein's location and function, but not required in *S. pombe* or in *H. sapiens* [234]. Thus, although the function of many phosphorylation events is yet to be understood, some evidences indicate that phosphorylation may be major event for the regulation of proteins' activity across organisms.

It is estimated that phosphorylation affects half of eukaryotic proteins [235], and the human genome encodes for 518 protein kinases but only about 200 protein phosphatases for phosphorylated proteins or lipids [236]. Phosphorylation occurs mostly on serine residues (more than 80% of the total phosphorylation events), followed by threonine residues (about 10%) and tyrosine residues (less than 5%) [237]. Phosphorylation at histidine residues has also been reported [238]. Protein phosphorylation is one of the most studied regulatory processes in cellular physiology, and faulty signalling transduction has been associated to pathological conditions including cancer [239], diabetes [240], and neurodegenerative disorders [241]. Deregulation of signalling pathways can arise from mutations on kinases/phosphatases or by alteration in epigenetic modulators of the expression/activity of these enzymes. At a wide level, the phosphoproteome flux is highly interconnected and activation of kinases and phosphatases not only impacts immediate downstream targets, but also extensive parts of the signal transduction modulated by phosphorylation [242]. This challenges the precise characterisation of the associations between elements of a signalling network. Computational methods such as one termed PHONEMeS (from phosphorylation networks for mass spectrometry) are based on the training on kinase–substrate relations to predict interactions from phosphoproteomics data, contribute to uncover biologically meaningful signalling networks [227].

To perform comprehensive analyses of phosphorylation events, it is critical to acknowledge the dynamic nature of the phosphate bound, unstable at high temperature and high pH, and the rapid kinetics of phosphatases compared to kinases [243]. Hence, to preserve phosphorylation states, it is essential to maintain cold and non-alkaline pH conditions and use compounds to maintain inhibit phosphatase activity.

Moreover, it is important to note that phosphorylated peptides are usually less abundant compared to their non-phosphorylated counterparts [229]. Therefore, selective enrichment methods are required to detect phosphopeptides in a LC-MS system. There are several approaches to enrich for

phosphorylation events, namely chemical derivatisation, chromatography, immunological affinity purification, and inorganic affinity purification [244].

Chemical derivatisation consists of the modification of the phosphate group to be enriched. The idea behind this method is that substituting the phosphate group improves the peptide ionisation and further MS2 fragmentation (Fig 1.13A). A well-established chemical derivatisation technique consists of β-elimination of phosphate mediated by hydroxyl ion at high temperature conditions, followed by Michael addition of nucleophile thiol-derived affinity tags [244]. This technique has several drawbacks including sample loss and addition of maleimide residues. Nevertheless, chemical derivatisation has been widely used to enrich for phosphopeptides and other PTMs (e.g. glycosylation) [245].

Immunological-based affinity purification relies on the selective recognition of phosphorylated residues by specific antibodies raised against pSer, pThr or pTyr [246] (Fig 1.13B). Although it is believed that Tyr kinases evolved after Ser/Thr kinases, and phosphorylation in tyrosines the less frequent modification in phosphoproteome of higher eukaryotes [237], the number of specific antibodies that recognise pTyr residues is by far greater than those for pSer or pThr, possibly given the higher immunogenicity of the Tyr aromatic ring [247]. Antibody purification of pTyr has been successfully used for the study of pTyr residues, primarily due to the absence of alternative pTyr-specific enrichment methods [248, 249]. More recently, molecular imprinted polymers (MIPs, also referred to as “plastic antibodies”) have been used to efficiently enrich for phosphopeptides within clinical samples [250].

Phosphopeptides can also be separated using different chromatography fractionation strategies, such as those based on phosphopeptides’ charge, pKa or hydrophobicity. Charged-based separation approaches exploit the charge-difference between phosphorylated and non-phosphorylated peptides. In this way, cations in strong cation exchange (SCX) [251], and anions in strong anion exchange (SAX) [252], are retained in an opposite-charged stationary phase (Fig 1.13C). Retention time in the column is proportional to the ionic strength, and ions can be eluted using a pH or salt gradient. Thus, and given the negative nature of the phosphoryl group, SAX chromatography selectively retains phosphopeptides in the polar column. It has been demonstrated that the specificity of each method improves when in combination with other methods, particularly when the amount of phosphopeptides in the sample is limited [253]. Additional chromatography fractionation techniques based on hydrogen-bonding are used to retain charged or polar ions in a stationary phase. For example, electrostatic repulsion-hydrophilic interaction chromatography (ERLIC) causes the electrostatic repulsion of amino groups that have a similar charge state to the charged stationary

phase [254] and hydrophilic interaction chromatography (HILIC) involves the hydrophilic interaction of analytes (e.g. phosphopeptides) with the hydrophilic stationary phase [255]. Phosphorylated peptides are retained in ERLIC and HILIC columns based on the number of negatively-charged groups. Similarly to SCX and SAX, ERLIC and HILIC by themselves lack specificity for phosphopeptide enrichment, but can yield a good coverage of the phosphoproteome when coupled with additional enrichment methods as recently demonstrated for some pre-fractionation strategies [256].

Because phosphate groups are pH-dependent and negatively-charged they can also be enriched by chelation with positively-charged metal ions contained in solid matrices. The most commonly used methods based on this principle are immobilised metal ion affinity chromatography (IMAC), metal oxide affinity chromatography (MOAC), or combinations of both (Fig 1.13D). IMAC resins chelate metal ions such as Fe^{3+}, Ni^{2+}, Cu^{2+}, Zn^{2+}, Al^{3+}, Ga^{2+} and Ti^{4+}, which in turn form ion-pair interactions with phosphate groups. Although Fe^{3+}-IMAC was the first developed and has been frequently used for phosphopeptide enrichment, Ti^{4+}-IMAC has proved greater reproducibility and in-depth phosphoproteome screening due to the high affinity of the titanium ions for phosphate groups [257]. Nevertheless, the specificity of IMAC to enrich for phosphopeptides is limited since N- and S-containing amino acids (e.g. cysteine) and peptides containing acidic amino acids (e.g. Glu and Asp) bind to the transition metals. Acidic pH and high concentration of organic solvent eluent effectively reduce binding of acidic non-phosphorylated to the metal ions [258].

Phosphopeptides can by enriched by an alternative affinity chromatographic method called metal oxide affinity chromatography (MOAC), which is based on the affinity of multivariate metal oxides (e.g. TiO_2, ZrO_2 or AlO_3) to phosphate groups. TiO_2 remains the most widely used method given its demonstrated high efficiency to enrich for phosphorylation [259]. Like IMAC, specific and non-specific binding can occur in TiO_2-MOAC. Addition of trifluoroacetic acid (TFA) and 2,5-dihydroxybenzoic acid (DHB) into the loading solution significantly reduces the number of specific and non-specific binding of acidic non-phosphorylated peptides, improving the selectivity for phosphate groups [260]. Although multiply-phosphorylated peptides tend to tightly bind to TiO_2, efficient elution of phosphopeptides from TiO_2-MOAC is usually achieved using basic eluents, such as NH_4OH [261], and through the use of multiple round of elution steps [262]. A robust and sensitive single-shot TiO_2-MOAC based method for label-free phosphoproteomics analyses was optimised in the Cutillas laboratory [225]; this phosphoenrichment method was used in the studies presented in this thesis (see methods Section 2.9.3).

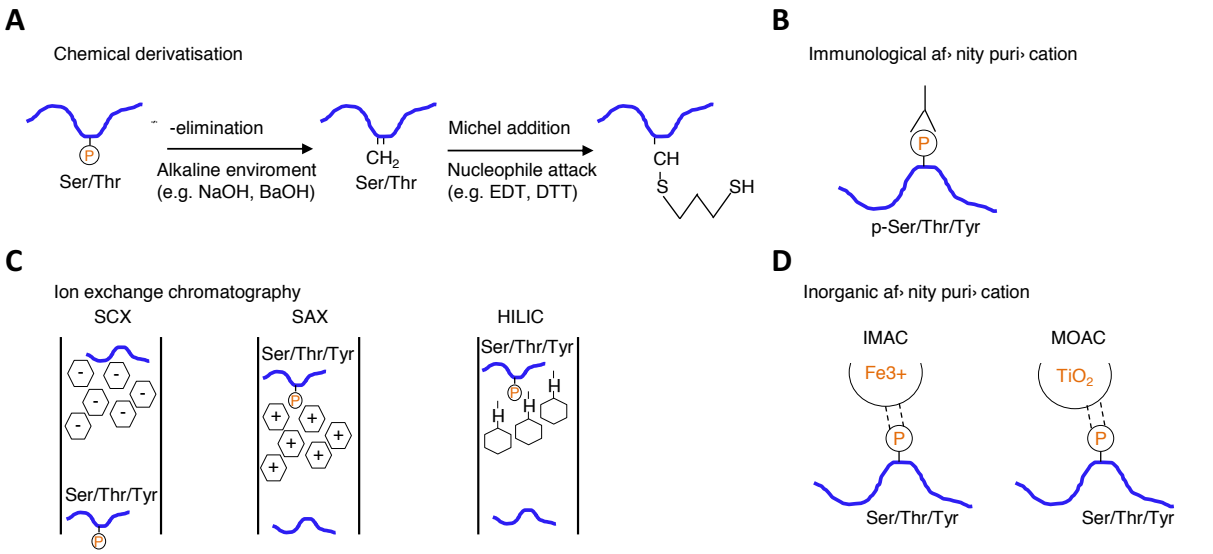

Figure 1.13 Common strategies used for phosphopeptides enrichment. The selection of phosphoenrichment method depends on the sample and type of phosphopeptides. The four main used fractionation methodologies used for phosphoenrichment include chemical derivatisation, chromatography separation, antibody-based affinity purification and inorganic affinity purification.

In addition to the analytical methods to enrich for phosphopeptides, several considerations need to be taken during the mass spectrometry and bioinformatics analysis of phosphoproteomics data. Given the negative charge of phosphate, phosphopeptides are less well fragmented than non-phosphorylated peptides. Therefore, fragmentation methods can be optimised for the sequencing of phosphopeptides, for example using neutral loss scanning or multistage activation. When phosphopeptides are subject to the widely-used CID fragmentation method they undergo a neutral loss of 80 Da for HPO_3 or of 98 Da for H_3PO_4 due to β-elimination reactions. Triple quadrupoles and linear ion traps can be programmed to detect phosphopeptide species that experience such losses [263]. In the multistage fragmentation method termed Pseudo MS(n) [264], CID fragmentation is applied and the neutral losses are subject to further fragmentation, generating a composite spectrum containing informative spectra of all ion series. Improved CID-based activation methods contribute to reducing the prevalence of neutral loss ions in the MS2 spectra. For example, HCD fragmentation increases the accuracy, mass resolution, and site location of measured ions [265]. Alternative fragmentation approaches such as electron transferring (usually from fluoranthene radical-anions) via ETD triggers the peptide amide backbone fragmentation, bypassing labile PTMs. ETD, however, has limited applicability to singly-charged peptides, often yield in tryptic digestions [266].

Another challenge is the correct assignment of the site of phosphorylation and is complicated given that phosphate groups in gas phase are potentially capable of switching between side groups

therefore rendering artificial pairs of isomeric phosphopeptides (i.e. peptides identical in sequence but carrying the phosphate group in different amino acids) [267]. The development of computer programs such as Mascot or Sequest has contributed to correct phosphopeptide site assignments. The effectiveness of the Mascot delta score used by Mascot and the A score used by Sequest to calculate the most likely phosphorylation site location providing a false location rate (FLR) associated to the probability of correct location of the phosphorylation was studied Savitski *et al*. [268], and demonstrated their efficacy to report phosphopeptide sites likelihood.

As mentioned before, computational methods to investigate cellular signalling by phosphoproteomics have been developed in the last years [227]. One approach to estimate the kinase activity called kinase substrate enrichment analysis (KSEA), which is based on changes on known kinase substrates, was developed in the Cutillas group [161], and was used in the experiments performed in the studies presented this thesis (see methods Section 2.10.3 for detailed description). This method assumes that the activity status of a given kinase can be inferred from the phosphorylation of its known substrates. It should be noted that this method does not directly measure kinase activity, as opposed to other techniques [269], but uses phosphoproteomic targets and kinase-substrate annotations (e.g. those included in PhosphoSitePlus [33]) to predict kinase activities. The performance of the KSEA method and similar predictive algorithms has been recently benchmarked by Hernandez-Armenta and co-workers that demonstrated the good performance of KSEA, and indicated that the number known kinase substrates and the source of evidence of interactions being *in vivo*, *in vitro,* or *in silico* influence the predictions outcome [270].

1.5 Metabolic based assays

1.5.1 Seahorse-based metabolic analysis

Metabolism is conceived as the array of life-maintaining chemical reactions occurring in a biological system. There are currently several methods to specifically measure the rate of respiration as well as the glycolytic activity of a biological system. One of the first methods used to analyse the amount of oxygen in a liquid, being blood or other liquid, was designed by Clark in 1953 [271]. A Clark electrode consists of two electrodes surrounded by an electrolyte solution covered by an oxygen-permeable Teflon solution. Oxygen concentration in a liquid-phase is directly inferred from the amount of current generated by oxidation of the metal (e.g. platinum). One of the main disadvantages of this technique is the short life of the Teflon membrane, which becomes coated with protein after few years.

Following the same principle, Oroborus instruments permit measurements of O_2 perturbations of tissue-derived samples or even direct measurements on isolated mitochondria [272]. Methods based on fluorescence such as MitoSOX and MitoXpress measure the amount of mitochondrial superoxide and extracellular O_2, respectively. Finally, extracellular flux analysers (XF) developed by Seahorse Bioscience are fully integrated 24 or 96-well instruments that quantify, in real time and simultaneously mitochondrial respiration and glycolysis, the main energy-producing pathways in cells. In these machines, the Oxygen Consumption Rate (OCR) is a measurement of cellular mitochondrial activity, while the Extracellular Acidification Rate (ECAR) is a measurement of cellular glycolytic activity. Thus, XF analysers determine the extracellular flux changes in oxygen and protons in the media immediately surrounding attached cells. Each Seahorse experiment comprises a disposable sensor cartridge, integrated with pairs of fluorescent biosensors for oxygen and protons coupled to a fibre-optic waveguide. The excitation wavelength values for oxygen and protons are 532 nm and 470 nm, respectively and fluorescent transmission signals are 650 nm for oxygen and 530 nm for protons. Oxygen consumption and proton extrusion result in rapid real-time measurable changes in oxygen tension and pH within a microchamber generated by the sensor cartridge in each of the microplate wells and after treatments with a series of drugs that interfere with different components of the mitochondrial oxidative chain. Usually, the baseline OCR and ECAR readings are established before the injection of mitochondrial drugs. Optimal confluency (number of seeding cells) is a critical parameter that needs to be optimised for Seahorse experiments in order to minimise measurements noise [273]. Another critical parameter to optimise is the amount of mitochondrial drugs supplemented. Specially, the range of FCCP [carbonyl cyanide 4-(trifluoromethoxy) phenylhydrazone] concentration that effectively uncouples mitochondrial oxidative phosphorylation without killing the cells may be specific for each cell line, and the concentration of FCCP to use on a Seahorse experiment requires to be optimised.

Accurate quantification of the cellular bioenergetic profile has been facilitated over the last years by the Seahorse technology. Nevertheless, this method comes with some limitations including relatively high cost of reagents. A comparison between the different assays to quantify the cell bioenergetic status is resumed in Table 1.2 and Table 1.3.

Table 1.2. Comparison between different metabolic assays**.**

Feature	Seahorse	MitoXpress	MitoSOX	Ouroboros	Clark electrode
Equipment	Seahorse machine	Fluorescent reader	Confocal microscope	Ouroboros machine	Clark electrode and chamber
Dynamic drug addition during experiment	No	Yes	Yes	Yes	Yes
Disposable plates	Yes	Yes	Yes	No	No
High-throughput	Yes	Yes	Yes	No	No
Real time	Yes	Yes	Yes	Yes	Yes
Label-free	Yes	No	No	Yes	Yes
Time	~2.5 h	~2h	~2h	Long	Long
Sensitivity	High	Low	High	High	Low for cells; high for enzyme/ chemical reactions
Reproducibility	High	High	High	High	Low for cells; high for enzyme/ chemical reactions
Price of consumables	High	Medium	High	Low	Low

Table 1.3. Comparison between the information potentially obtained with different metabolic assays.

Information	Seahorse	MitoXpress	MitoSOX	Ouroboros	Clark electrode
Basal Respiration	Yes	Yes	No	Yes	Yes
ATP Production	Yes	No	No	Yes	Yes
Proton Leak	Yes	No	No	Yes	Yes
Maximal Respiration	Yes	Yes	No	Yes	Yes
Spare Respiratory Capacity	Yes	Yes	No	Yes	Yes
Oxygen consumption	Yes	Yes	No	Yes	Yes
Mitochondria content	No	Yes	No	No	No
ROS production	No	No	Yes	Yes	No
Glycolytic capacity	Yes	No	No	Yes	No
Fatty acid oxidation	Yes	No	No	No	No

1.5.2 MS quantification of metabolites

Metabolomics is the study of metabolites (i.e. small molecules that are substrates and products of metabolic reactions) in a biological system at a given physiological state. Metabolites are effective mediators in the intercommunication between the genome and proteome of a biological entity and its environment. Because each metabolite is, by definition, the result of a metabolic reaction, metabolites are direct fingerprints of the cellular metabolic activity. Profiling the metabolites of cellular system contributes to greater understanding of the metabolic status of biological systems [274], and can help to identifying biomarkers of disease aggressiveness [275].

As for LC-MS proteomics, correct sample preparation is paramount for ensuring good sensitivity and reproducibility of metabolomics results. There are two main categories employed for metabolites quantification depending whether one metabolite or all the metabolites of a given biological system are to be measured. The approaches used to analyse a selected metabolite are hypothesis-driven, and the chemical properties of the compound to be investigated are known and used to guide the customisation of sample preparation to minimise matrix effects. Perhaps the most commonly used extraction technique to isolate metabolites is liquid-liquid extraction, which relies on differential solvents solubility [276]. Most of the LC-MS platforms used for metabolites analyses can perform sample ionisation in both negative and positive modes and the adequate selection of the polarity mode for efficient metabolite ionisation is determined by its physico-chemical properties. Metabolites can be quantified in comparison to standards of known concentration of the metabolite of interest, or thorough internal standards spiked in each sample [276, 277].

Global metabolomics, on the other hand, allows the analysis of global metabolites of biological systems without prior knowledge of their nature. In this strategy, metabolites are isolated and analyse to generate the spectral data comprised of complex superimposed ion chromatograms [278]. There are two main analytical platforms often used to calculate the concentration of multiple metabolites: NMR and LC-/GC-MS. Given the good coverage of LC–MS-based methods compare to NMR, this approach has recently enjoyed increased popularity as the methodology for metabolomics analysis [278].

Metabolic fluxes can be measured by means of isotopologues (i.e. metabolites containing stable isotopes — such as ^{13}C, ^{2}H, ^{18}O and ^{15}N — and their non-labelled counterparts). Metabolic flux studies have allowed the investigation the activity of metabolic enzymes and their relationships with their

substrates. For example, [1-^{13}C] glutamine was used to uncover that under hypoxia, glutamine is the preferential carbon source for the synthesis of fatty acids in various cancer cell lines [279].

1.6 Genomic sequencing

Genomics is the study of the complete genetic material of a biological entity. The genome of an organism includes both the genes (i.e. the coding regions) and the non-coding regions of the DNA (e.g. introns and regulatory elements). Although sequencing of whole-genomes advances the understanding of recurrent mutations in non-coding genomic regions, a proportionally high number of studies have focused on the exploration of DNA regions that contain protein-encoding genes (i.e. exomes, which represent ~2% of the genome), since this approach can identify recurrent variants in multiple diseases, for instance hereditary diseases [280]. The overview of the methodology employed for exome sequencing is shown in Fig 1.14. Among the advantages of whole exome-sequencing (WES) analyses are the lower cost of sequencing compared to whole-genome sequencing, being more manageable for bioinformatics processing, and ultimately of rather easier interpretation compared to complete sequenced genomes. Indeed, computational advances in the recent years have contributed to ease the predictions of the functional implications of genetic variants, in particular in the context of cancer [281-284].

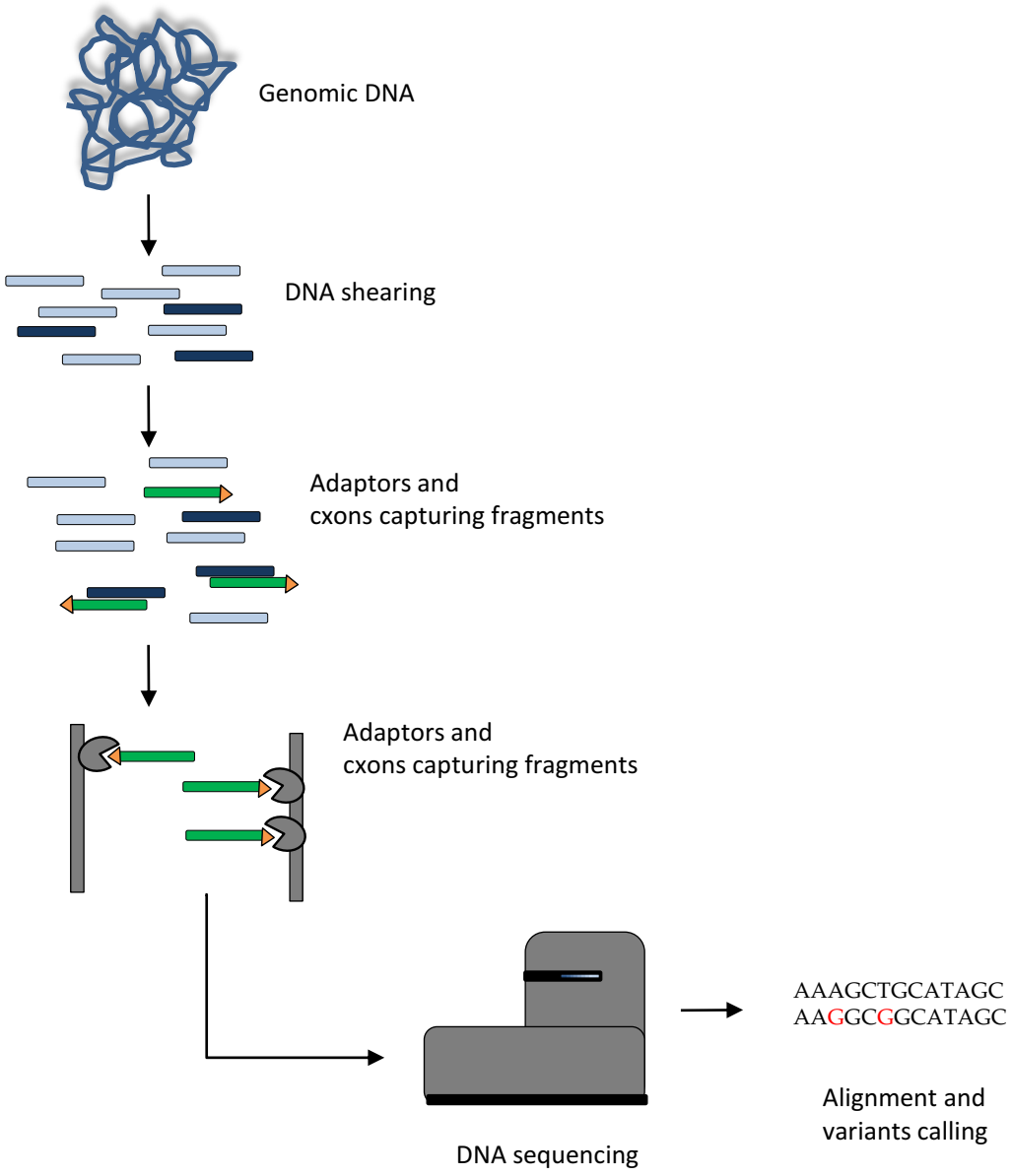

Figure 1.14 Overview of the main steps involved in the whole-exome sequencing methodology. Initially, DNA is extracted, sheared, and the fragments of adequate length are used to construct a genomic library. DNA fragments are flanked by sequence adaptors, which allow the hybridisation of each fragment with probes that are compliment to all genome exons. Captured DNA is then sequenced and the sequence reads are mapped to the reference genome to detect for possible genome variants.

Thesis project aims

The aim of this thesis is to understand the molecular adaptations that allow cancer cells to compensate for chronic PI3K inhibition. The specific objectives to cover this aim are the following:

1) To characterise the phenotype of MCF7 parental cells and three cell lines that had acquired resistance to 1 μM GDC-0941, a PI3K inhibitor (PI3Ki).

2) To understand the biochemistry of PI3Ki-sensitive and PI3Ki-resistant cells by means of LC-MS/MS-based proteomics and phosphoproteomics approaches. This project also seeks to characterise the biochemistry of PI3Ki-resistant cells when these cells are treated with the PI3Ki or on its absence.

3) To explore the metabolic characteristics of sensitive and resistant cells. For this objective, the Seahorse metabolic flux analyser is to be used to study the energy phenotype of such cells, the transcript profiling of metabolic genes is to be measured and the proliferation response to manipulating metabolic gene/protein or metabolic products of those cells.

4) To characterise the genomic background of sensitive and resistant cells to PI3K treatment by whole exome sequencing analysis.

5) To determine what are the signalling properties of lactic acid. The signalling response of the MCF7 model system is to be measured by means of LC-MS/MS-based phosphoproteomics and proteomics.

Overview of the methods used in the experiments presented in this thesis

Approaches	**Principle**
Methodologies used to characterise cellular functionalities	
Vi-CELL counter Guava Cell Cycle assay Guava Nexin assay	Cellular incorporation of trypan blue dye DNA staining Integrity of cellular membranes
Biochemical methodologies	
(Phospho)-proteomics and proteomics Gene expression DNA sequencing Bioenergetic assay (Seahorse)	Phosphorylation state and levels of proteomes Transcripts levels Genetic background Measuring of mitochondrial and glycolytic activity

Chapter 2. Materials and Methods

2.1. Culture media used for experimentation

Table 2.1 Specification of nutrient used to supplement media to culture cells.

Name	Manufacturer	Reference	Glucose [mM]	Glutamine [mM]	Sodium pyruvate [mM]
DMEM	Sigma	6429	25	4	1
DMEM no glucose, no phenol red, no glutamine	Life technologies	A14430	0	0	1
XF assay medium	Seahorse Biosciences	102365-100	25	2	1
RPMI 1640	Sigma	8750	11.10	2	0

2.2. Nutrients used for experimentation

Table 2.2 Specification of nutrients used to complement culture A14430 media.

Name	Manufacturer	Reference
D-(+)-Glucose	Sigma	G7528
L-Glutamine	Sigma	G7513
Sodium pyruvate solution	Sigma	S8636
Phenol Red	Sigma	P3532

2.3. Inhibitors and chemical compounds

Table 2.3 Specification of inhibitors, quenchers of free radicals, free radicals, and acids used to treat cells in culture.

Name	Manufacturer	Reference	Dilution	Concentration	Primary target
GDC-0941	Chemdea	CD0245	DMSO	1 µM	PI3K α/δ
BYL719	Selleckchem	2814	DMSO	1 µM	PI3Kα
Ku-0063794	Chemdea	CD0274	DMSO	1 µM	mTORC1/2
MK-2206	Selleckchem	S1078	DMSO	1 µM	AKT 1/2/3
A-VII	Cayman	14870	DMSO	1 µM	AKT 1/2
Everolimus	Selleckchem	S1120	DMSO	20 nM	mTORC1
10058-F4	Sigma	F3680	DMSO	25 µM	c-MYC
10074-G5	Sigma	G3798	DMSO	20 µM	c-MYC
Chetomin	Sigma	C9623	DMSO	10 nM	HIF-1/2α
GSK-650394	Sigma	650394	DMSO	0.5 µM	SGK
Trametinib	Selleckchem	S2673	DMSO	0-20 µM	MEK
KN-93	Tocris	139298	DMSO	0-200 µM	CAMKII α/β/γ/δ
N-acetylcysteine	Sigma	A0737	Water	200 µM	Free radicals
Oligomycin	Sigma	75351	DMSO	5 µM	Mitochondria CV
Carbonyl cyanide 4-(trifluoromethoxy) phenylhydrazone (FCCP)	Sigma	C2920	DMSO	2 µM	Mitochondria uncoupler
Antimycin A	Sigma	A8674	DMSO	1 µM	Mitochondria CII
Rotenone	Sigma	R8875	DMSO	1 µM	Mitochondria CoQ10
(±)-α-Tocopherol	Sigma	T3251	DMSO	0-20 µM	Free radicals
H_2O_2	Sigma	216763	Water	130 µM	Free radicals
L-lactic acid	Alfa Aesar	L13242	Water	0-30 mM	
Hydrochloric acid 37 %	Sigma	258148	Water	0-9.7mM	

2.4. Materials and Reagents

Table 2.4 Specification of materials and reagents used.

Name	Manufacturer	Reference	Information
2',7'-Dichlorofluorescin diacetate (DCFH-DA)	Sigma	D6883	Non- fluorescent dye used to visualized intracellular oxidative species
4% paraformaldehyde	Santa Cruz	Sc-281692	Reagent used to fix cells
4-15% mini-PROTEAN TGX pre-cast gradient gels	Biorad	4561084	Gels used in western blot
ACQUITY UPLC Peptide BEH C18 (1.7 µm, 130 Å, 75 µm X 150 mm)	Waters	186003543	Analytical column used for XL LC separations
nanoACQUITY UPLC Symmetry C18 Trap Column (5 µm, 100 Å, 180 µm x 20 mm)	Waters	164569	Trap column used for XL LC separations
Acclaim PepMap100 C18 analytical columm (3 µm, 100 Å, 75 µm× 25 cm)	Dionex	164261	Analytical column with a nanoViper connection used for Q Exactive + LC separations
Acclaim PepMap µ-Precolumns (5 µm, 100 Å,300 µm x 5 mm)	Thermo	160454	Trap column used for Q Exactive + LC separations
Bicinchoninic acid (BCA) protein assay	Thermo	23225	Assay used for protein quantification
Crystal violet	Sigma	C3886	Cell proliferation
CellTiter 96 AQueous One solution reagent	Promega	G3580	Reagent used to determine celular metabolic activity
DNeasy Blood & Tissue Kit	Quiagen	69504	DNA isolation
Dual luciferase reporter assay	Promega	E1910	Luciferase reporter
EDTA-trypsin (0.05%/0.02%)	Sigma	L11-004/T4299	Cell detacher
Empty spin filter-tips TF2EMT	Glygen	TF2EMT	Empty tips with filter used to prepared TiO_2 phosphoenrichement columns
Eppendorf LoBind microcentrifuge tubes	Sigma	Z666505	Low binding microcentrifuge tubes used to collect samples for protein analysis
FujiFilm X100 FUJI RX X-RAY FILM (18 X 24 cm)	Fisher	12715325	X-ray film for western blot
Guava Cell Cycle Reagent for Flow Citometry	Millipore	4500-0220	Reagent used to determine cell cycle distribution
Guava Nexin Reagent for Flow Citometry	Millipore	4500-0450	Reagent used to determine cell apoptosis
Heat-inactivated (HI) Foetal Bovine Serum (FBS), E.U. approved	Gibco	10500-064	Sera with growth factor used for tissue culture
Immobilised trypsin-tosyl lysine chloromethylketone (TLCK)	Thermo	20230	In-solution trypsin used to digest peptides
Interferin transfection reagent	Polyplus	40901	Reagent used to transfect cells with siRNA
Nano-Glo Luciferase assay	Promega	N1110	Reagent used to determine luciferase activity
Oasis-HLB 1cc cartridges	Waters	WAT094225	Cartridges used to desalt and extract peptides
ONE-Glo EX Luciferase assay	Promega	E8110	Reagent used to measure luminesce
Passive Lysis Buffer 5X	Promega	E1941	Reagent used to lyse cells transfected with DNA
Penicillin/streptomycin	Sigma	P4333	Antibiotics
Phenylmethylsulfonyl fluoride (PMSF)	Sigma	93482	Serine protease inhibitor used in Western blot
Ponceau S solution	Sigma	P7170	Reagent used to visualized protein bands
Poly-L-lysine solution	Sigma	P8920	Polymer used to assist cell adhesion to solid surphaces
Polysine Adhesion Slides (25 mm X 75 mm X 1mm)	Thermo	10143265	Slides used to visualize microscope samples
PVDF transfer membrane	Millipore	IPVH00010	Transfer membrane for western blot
SuperSignal West Pico ECL substrate	Pierce	34080	Horsereadish peroxidase (HRP) reagent for western blot
siRNA against HIF-1α(4082 bp)	Sigma	NM_001530	Sequence used to transiently inhibit HIF-1-α
Titansphere TiO_2 (Titanium Dioxide, TiO_2)	GL Science	502075010	Method used to perform phosphoenrichement method
ViaFect tranfection reagent	Promega	E4981	Reagent used to tranfect DNA into cells

siRNA against GPR81	Quiagen	3124607	Sequences used to transiently inhibitsGPR81
Mounting medium with	Vector laboratories	DAPI H-1200	Staining for DNA
Alexa Fluor® 488 Phalloidin	Thermo	A12379	Staining for F-actin

2.5 Antibodies

Table 2.5 Specification of antibodies and concentration used.

Name	Manufacturer	Reference	Concentration	Procedure
p-AKT Ser^{473}	Cell Signalling Technologies	4058	1/1000	Western blot
p-PRAS40 Ser^{246}	Cell Signalling Technologies	2640	1/2000	Western blot
p-4EBP1 Thr^{37}/Thr^{46}	Cell Signalling Technologies	2855	1/1000	Western blot
FASN	Cell Signalling Technologies	3189	1/1000	Western blot
LDHB	Abcam	ab53292	1/1000	Western blot
c-MYC	Cell Signalling Technologies	5605	1/1000	Western blot
HIF-1α	Cell Signalling Technologies	3716	1/500	Western blot
HIF-1α (siRNA experiments)	BD Transduction Laboratories	610959	1/500	Western blot
MCT1	Astrazeneca	MCT1	1/100	Western blot
MCT2	Astrazeneca	MCT2	1/100	Western blot
MCT2	Astrazeneca	MCT2	1/100	Western blot
GPR81	Santa Cruz	sc-32647	1/100	Western blot
α-Tubulin	Cell Signalling Technologies	2144	1/1000	Western blot
Vinculin	Cell Signalling Technologies	V9131	1/500	Western blot

2.6 Cell Culture

2.6.1 Cell lines

MCF7 cells were obtained from the ATCC (HTB-22). PI3Ki-resistant cells were previously made resistant to 1 μM GDC-0941 or 1 μM Ku-0063794 [226]. MCF7 sensitive and resistant cells were grown

in DMEM (Dulbecco's modified Eagle's medium) supplemented with 10% FBS and penicillin/streptomycin (each at 100U/mL) at 37°C, in humidified atmosphere at 5% CO_2. Resistant cell lines G1, G2 and G3 were routinely maintained with 1 µM GDC-0941 or with 1 µM DMSO when GDC-0941 was removed from culture media. Resistant cell lines K1, K2 and K3 were routinely maintained with 1 µM Ku-0063794 or with 1 µM DMSO when Ku-0063794 was removed from culture media.

Sensitive and resistant pairs derived from oesophagus cancer cell lines, KYSE70 (ATCC 30-2001) and KYSE180 (Invitrogen 11875-093) and pairs of head and neck cancer cell lines (H&N), CAL33 (ATCC 30-2002) and LB771-HNC (ATCC 30-2006) were a kind gift from the Baselga laboratory. Head and neck cancer cell lines (H&N), LB771-HNC and CAL33 were grown in DMEM supplemented with 10% FBS and penicillin/streptomycin (each at 100U/mL) and 2 mM L-glutamine at 37°C, in humidified atmosphere at 5% CO_2. Oesophagus KYSE70 and KYSE180 were grown in RPMI 1640 (Roswell Park Memorial Institute medium) supplemented with 10% FBS and penicillin/streptomycin (each at 100U/mL) and 1% L-glutamine at 37°C, in humidified atmosphere at 5% CO_2. Resistant cell lines KYSE70, KYSE180, LB771-HNC and CAL33 were routinely maintained with 1 µM BYL719 or with 1 µM DMSO when BYL719 was removed from culture media.

2.6.2 Growing and seeding of cells

Adherent cells growing in flasks were washed twice with PBS before addition of 0.05% EDTA-trypsin and incubation for 5 min at 37°C to allow cell detaching from the flask. Trypsin was inactivated by the addition of approximately three volumes of media. After centrifugation at 1,300 rpm for 5 min, cell pellets were resuspended in fresh media and cell numbers were calculated using Beckman Coulter Vi-CELL XR instrument. For proliferation experiments, appropriated number of cells was seeded in the 6 well plates to avoid reaching confluence on a total volume of 2 mL. Thus, 200,000 cells were seeded in each well and proliferation was measured after 5 days, 100,000 cells were seed in each well and proliferation was measured after 7 days and 30,000 cells were seed in each well and proliferation was measured after 7 and 14 days. After the appropriate time, media was removed from the wells, which were then washed with approximately 1mL PBS, before the addition of 300 µL of trypsin. After 5 min incubation at 37°C and 5% CO_2, 700 µL of media were added and cells in suspension were counted in the Vi-CELL counter.

For signalling experiments where lactic acid and HCl were used to induce MCF7 parental cells, these were maintained for 24 h in DMEM media supplemented with 0.5% FBS and 1% penicillin/streptomycin before the addition of the pertinent acid.

2.6.3 Storage of cells in liquid nitrogen

Cells maintained in culture at confluence of approximately 70% were collected (according to Section 2.6.2) and cell pellets were resuspended in 10% DMSO/90% FBS. Cryogenic vials were named with cell identify, date of freezing and surname and 1 mL of cells in suspension was added to the cryovials, that were placed in freezing containers with isopropanol. Containers were cooled overnight at -80°C at a cooling rate of approximately -1°C/min. Cryovials were then placed in boxes located in liquid nitrogen cryotank for long-term storage. To resuscitate frozen cells, those were thaw at room temperature for approximately 10 min and transferred to 10 mL fresh media. Cells were centrifuged at 1,300 rpm for 5 min, resuspended with fresh media and then transfer to flasks for culture.

2.6.4 Treatment with inhibitors, free radicals and free radical scavengers

If required, stocks of chemical compounds were initially diluted (according to Table 2.3) up to an adequate treatment concentration.

2.6.5 siRNA experiments

Cells were seeded in 6-well plates (200,000 cells/well). By means of filtered tips, 20 nM siRNA against HIF-1α or scrambled siRNA were mixed by pipetting in Optimen serum-reduced media (200 mL) and transferred into 2 mL sterilised eppendorf tubes. Interferin reagent (2 mL) was added into the eppendorf tubes that were then vortex for 10 s. Mixtures were spinned down for approximately 10 s and incubated at room temperature for 10 min. Fresh media was replaced and mixtures containing siRNA were dropwise added into the wells. Six hours after transfection, fresh DMEM media was replaced with fresh media. After 72 h post-transfection (80-90% confluence), cells were collected for western blot analysis of HIF-1α.

For siRNA against GPR81, a total of 200,000 MCF7 cells were treated with 35 nM of a siRNA pool created from four sequences against GPR81: Hs_GPR81_1:TGGGATCTATTGATCTATCAA; Hs_GPR81_2:CAGGCCGAATGAGGCTCTTTA; Hs_GPR81_3:CAGCGTGTCTGCTAGACTCTA; Hs_GPR81_5: AGGGTCATTAGTCAACTCTTA (see Table 2.4). After 72 h, receptor knockdown was tested by Western blot.

2.6.6 Luciferase reporter assay of HIF transcriptional activity

MCF7 sensitive and PI3Ki-resistant cells were seeded in 24-well plates (100,000 cells/well). Cells were transfected either with plasmids that contain the HIF-binding consensus sequence (5'-T/G ACGTGCGG-3') which located in promoter regions of genes known as Hypoxia Response Elements (HREs), located upstream of the gene encoding for the firefly luciferase or with plasmid control that contain the promoter of the constitutively active simian-virus 40 (SV40), located upstream the gene encoding for *Renilla* luciferase. An amount of 30 ng of HRE-Nanogloluciferase and 10 ng of SV40-firefly luciferase were mixed by pipetting in Optimen media (50 mL/well) in plastic Bijou tubes. ViaFect reagent (3:1; ViaFect: DNA) was added, vortex briefly and incubated for 20 min at room temperature. Mixtures were added into the cells and incubated for 6 hours. If required, plates were placed in low oxygen incubator (1% O_2). Following 48 h after transfection, 10 μL of One-Glo was incubated for 2 min and then 1X Passive Lysis Buffer was added. The intensity of the correspondent reporter was quantified by the Nano-Glo Dual-Luciferase Reporter Assay System. Luciferase and Renilla emissions (i.e. λmax= 535 nm and 613 nm, respectively) were measured using a Dynex Revelation 4.06 luminometer following manufacturer's instructions. Measurements were acquired for three technical independent replicates.

2.6.7 Determination of cell cycle and apoptosis

For cell cycle measurements, 2,000 cells/well MCF7 sensitive and resistant cells were seeded in a 96-well plate. Plate was centrifuged at 4,500 g for 5 min and pellets were washed once with PBS. Guava Cell Cycle reagent containing propidium iodide (150 μL/well) was incubated in the dark for approximately 30 min, before the analysis in the Guava easyCyte flow cytometer. The distribution of the histogram markers was centred for the resting population (cells in G_0/G_1) at DNA content of value of 1,024. A total of 5,000 events were acquired per sample and generated FSC files were analysed using the CytoSoft software.

For apoptosis measurements, 2,000 cells/well resuspended in 100 μL were plated into a 96-well plate. Cells were washed once with PBS before the addition and resuspension of 150 μL of Guava Nexin reagent containing Annexin V and 7-aminoactinomycin D (7-AAD) dyes. Annexin V stains extracellular phosphatidylserine and is an indicator of plasma membrane integrity, whereas 7-AAD is a plasma membrane impermeable compound that exclusively labels unviable cells. Cells were incubated with Guava reagent for roughly 30 min in the dark, before analysing the samples in the Guava easyCyte flow cytometer. The intensity of the forward scatter (FSC) was selected to exclude any cellular debris and to locate viable cell on the top left corner of the dot plot. A total of 2,000 events

were acquired per sample and saved as FCS files that were further analysed by means of the CytoSoft software.

2.6.8 MTS assays

A total of 2,000 cells/well was seeded in 96-well plates and treated with the indicated compounds. After the indicated time, 25 µL of MTS assay reagent were added into the wells following manufacture's protocols. After 1.5 h and 3 h, absorbance at 490 nm was quantified.

2.6.9 Crystal violet assays

Crystal Violet assay is a method to quantify the amount of DNA. A total of 2,000 cells/well were plated in 96-well plate and left overnight. After 3 days of treatment with the appropriate inhibitor, cells were washed with PBS once, and 100 µL of cold 4% paraformaldehyde (PFA) were added into the plates which were left on ice covered in foil for 30 min. PFA was discarded and 75 µL of crystal violet solution (0.5% w/v; 20% MeOH; 80% ddH_2O) were added into the well and incubated for 10 min at room temperature. Crystal violet was removed and was washed from the plates by immersion into distilled water. Crystal violet stain was extracted by adding 100 µL/well of Sorenson's buffer (0.1M $Na_3C_6H_5O_7$; 50% EtOH; 50% ddH_2O) and left on agitation at 300 rpm for 30 min. Absorbance at 540 nm was then quantified.

2.7 Metabolism assessment

2.7.1 Collection of culture media for experimentation to measure lactic acid

The relevant cell-lines were seeded in 6-well plates at 200,000 cells/well. After five days treatment with the indicated concentrations of the specified drugs or vehicle (DMSO), 2 mL media were collected into 15 mL falcon tubes. Lactic acid was extracted from 100 µL of the collected media. Samples were mixed thoroughly and subsequently deprotonated with 600 µL of a cold mixture of methanol: acetonitrile (1:1, by volume) and centrifuged at room temperature for 10 min at 14,000 rpm. The supernatant was pipetted into a reaction vial and evaporated to dryness under a gentle stream of nitrogen at a temperature of 50°C. The derivatised residue was reconstituted with 150 µL acetonitrile: water (1: 2, by volume). Samples were analysed on a TSQ mass spectrometer (Thermo Fisher Scientific). Chromatograms were acquired and processed with Excalibur (Thermo) and quantification

was done measuring the area under the curve and comparing to a standard curve with range 0-200 mM.

2.7.2 Oxygen Consumption Rate (OCR) and Extracellular Acidification Rate (ECAR)

OCR and ECAR were measured using the Seahorse XF24 extracellular flux analyser (Seahorse Bioscience, Billerica, MA, USA) (Fig 2.1). Cells were seeded at 80,000 cells/well into the Seahorse XF24 V7 multi-well culture plate and allowed to adhere. Five hours after culture, 100 µL of culture medium were added and cells were incubated overnight at 37°C in 5% CO_2. Sensors embedded in the Seahorse assay plate were moisturised overnight with the calibration solution at 37°C in the Seahorse XF Prep Station, a non-CO_2 incubator. The following day, cells were rinsed with Seahorse assay media and Seahorse assay media (as described in Table 2.1) was replaced. Culture plate was equilibrated in the Seahorse XF Prep Station for one hour without CO_2 at 37°C and the assay plate was calibrated in the Seahorse XF Extracellular Flux Analyser for 30 min, prior to evaluation. After establishing four baseline OCR and ECAR readings, mitochondrial inhibitors were injected.

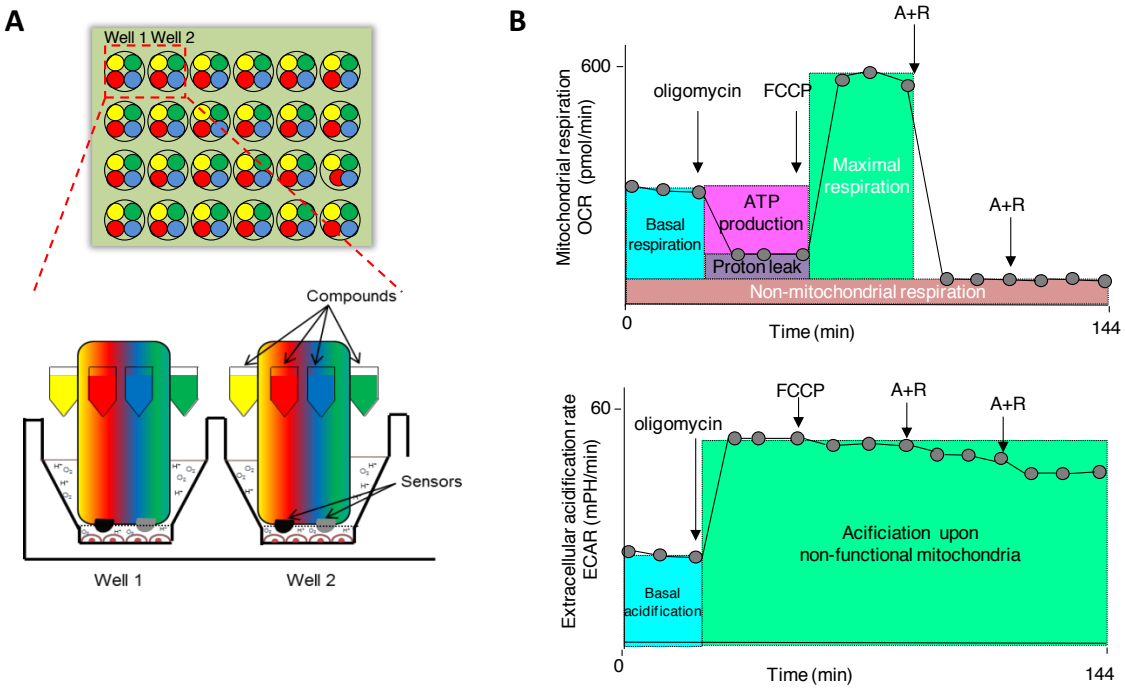

Figure 2.1 Overview of the Seahorse plate design and experimental output. (**A**) Seahorse XF analysers use a microchamber created between the sensors and the cells to measure their bioenergetic profile in a precise, sensitive and relatively non-destructive manner. Up to four compounds can sequentially be added per well. (**B**) Real time OCR (upper panel) and ECAR (lower panel) measurements are obtained in response to compounds that interfere with mitochondrial ETC constituents: oligomycin, FCCP [carbonyl cyanide 4-(trifluoromethoxy) phenylhydrazone], antymycin (A), and rotenone (R).

2.7.3 Determination of expression of metabolic genes using the Fludigm platform

Gene expression of 76 metabolic genes was quantified on the multiplex Fluidigm platform. DNA extract of three independent experiments was added to the amplification chip and used consequently in the multiplex qPCR reaction which was used consequently to convert to the Ct (cycle threshold) values. Ct values were used to normalise the expression levels.

ΔΔCT=(CT(target, untreated)−CT(reference, untreated))−(CT(target,treated)−CT(reference, treated)). Final ratio between control and treatment of gene expression levels is calculated as $2^{\Delta\Delta CT}$.

2.7.4 ROS measurement

Circular 13 mm^2 diameter coverslips were placed into 6-well plates and 200 µL of Poly-L-lysine solution (0.1% w/v; H_2O) were added. After 30 min incubation at 37°C, a meniscus of the polymer was formed. Plate wells were then washed once with PBS and 100,000 cells/well were consequently seeded. After the appropriated treatment time, the fluorescent dye dichlorodihydrofluorescein diacetate (DCFH-DA) 10 µM was added and incubated for 30 min. Upon transfusion into the cells, cellular esterases oxidise the DCFH-DA compound into DCFH, which is further oxidised by nitrate species (NO_2^-), carbonate species (CO_2^-) and oxygen species (OH^-) into the highly fluorescence molecule DCF [285]. Coverslips were collected using forceps, washed with ice cold PBS and transferred to microscope slides. Cells were observed in an upright microscope Nikon eclipse Ci-S/Ci-L (Nikon Instruments) selecting maximum excitation and emission spectra of 495 nm and 529 nm, respectively, at x1.3 gain. Fluorescence was quantified using the Image J 1.48V Software, by means of plotting the histogram of each image.

2.8 Western Blot

Cells in 6-well plates were placed on ice and washed twice with 2 mL of PBS containing 1mM Na_3VO_4 and 1mM NaF. After these washes, basic lysis buffer (50 mM Tris-HCl pH 7.4; 150 mM NaCl; 1 mM EDTA pH 8.0; 1% Triton X100) supplemented with protease (Complete Mini EDTA-free; Roche) and phosphatase inhibitors (1 mM Na_3VO_4; 1 mM NaF; 1 mM β-glycerol-phosphate; 2.5 mM $Na_4P_2O_7$; 1 µM okadaic acid) was added to the wells and maintained for 30 min on ice. RIPA buffer (50 mM Tris-HCl pH 7.4; 150 mM NaCl; 1 mM EDTA; 1% NP-40; 0.5 % DDC; 0.1 % SDS) and Laemmli lysis buffer (1M Tris-HCl pH 7.5; 1% glycerol; 10% SDS) were also complemented with phosphatase inhibitors and used

to lyse cells to extract GPR81 membrane protein. Cells extracts were scrapped and transferred to 1.5 mL low protein binding eppendorfs and centrifuged at 4°C at 13,000 rpm for 10 min. Protein quantification was performed using the BCA assay and 30-45 µg of protein were loaded into 4-15% precast polyacrylamide gradient gels (Mini-PROTEAN TGX™, Biorad); runs were set at 100 V and proteins were transferred to PVDF membranes (Millipore). Before the addition of primary antibody, membranes were blocked with 5% milk in TBS-Tween for 1 h. Primary antibodies were incubated overnight in the cold room and the appropriate secondary antibody were incubated for 1 h at room temperature. Enhanced chemiluminescence reagent (SuperSignal West Pico Chemiluminescence, Thermo Scientific) was added to the membranes for 1 min and protein bands were visualised by means of X-ray films (Super RX; Fujifilm) or by an Amersham Imager 600. Concentrations and manufacturer details are included in Table 2.5. If applicable, concentration of protein bans was done with Image J 1.48 V. The area under the peak was quantified for each band and normalised by the intensity of α-Tubulin.

2.9 Mass spectrometry experiments

2.9.1 Cell lysis for proteomics and phosphoproteomics

Cells growing in 175 mL flasks or 100 mm treated tissue culture plates were washed twice with cold PBS supplemented with phosphatase inhibitors (1 mM Na_3VO_4; 1 mM NaF) before addition of urea lysis buffer (8 M Urea in 20 mM HEPES pH 8.0) supplemented with phosphatase inhibitors (1mM Na_3VO_4; 1mM NaF; 1 mM β-glycerol-phosphate; 2.5 mM $Na_4P_2O_7$). After ice incubation for 30 min lysed cells were scrapped and transferred to 2 mL low protein binding eppendorf tubes. Cell extracts were homogenised by sonication (3 intermittent pulses, 15 s each or 10 cycles of 30 s pulses and 40 s pause) and centrifugation at 13,000 x g for 5 min at 4°C was applied to remove insoluble material. After transferring the supernatants to fresh low protein binding eppendorf tubes, protein concentration was quantified by BCA assay.

2.9.2 Protein digestion and peptide desalting for proteomics and phosphoproteomics

A total of 450 µg proteins per sample was used for the phosphoproteomics experiments of MCF7 sensitive and resistant cells. A total of 250 µg proteins per sample was used for the phosphoproteomics experiments of MCF7 parental cells induced with 5 mM lactic acid, 0.97 mM HCl, 20 mM lactic acid or 9.7 mM HCl. A total of 200 µg proteins per sample was used for the proteomics

experiments of MCF7 sensitive and resistant cells. A total of 100 µg proteins per sample was used for the proteomics experiments of MCF7 parental cells induced with 20 mM lactic acid or 9.7 mM HCl. Proteins were sequentially reduced with 10 mM DTT for 1 h at 25°C at 1,200 rpm and alkylated with 10 mM IAM for 30 min at 25°C at 1,200 rpm agitation. To allow tryptic digestion, concentration of urea was decreased to 2 M by adding 20 mM HEPES pH 8.0. Tryptic digestion was performed at 37°C at 1,200 rpm overnight with Immobilised tosyl-lysinechloromethyl ketone (TLCK)–trypsin [20 p-toluenesulfonyl-L-arginine methyl ester (TAME) units/mg]. Next day, samples were transferred to ice and a cold centrifugation at 2,000 x g for 5 min was applied to remove trypsin beads by precipitation. For desalting of peptide mixtures either C18 spin tips (Thermo Fisher Pierce) or Oasis-HLB cartridges (Waters, Manchester, UK) joined to a vacuum manifold were used. Briefly, peptides were loaded in the pre-activated (100% ACN) and pre-equilibrated (0.1% TFA; 1% ACN) columns or tips. Peptides were washed (0.1% TFA; 1% ACN) and eluted with 250 µL glycolic acid buffer (1 M glycolic acid; 50% ACN; 5% TFA) for phosphoenrichment procedure or with elution buffer (70% ACN; 0.1% TFA) for proteomics experiments.

2.9.3 Phosphopeptide enrichment by TiO_2

Peptide mixtures were normalised up to 500 µL with glycolic acid buffer and samples were incubated with 50 µg of TiO_2 beads (50% slurry in 1% TFA) for 5 min. Sample slurries were then loaded into empty spin tips, which were previously activated with 200 µL of ACN. Phosphopeptides were washed by centrifugation with 100 µL glycolic acid solution, 100 µL ammonium acetate solution (100 mM ammonium acetate; 25% ACN) and 100 µL of 10% ACN for 3 min at 1,500 x g. To recover phosphopeptides from the columns four consecutive elution steps of 50 µL of elution buffer (5% NH_4OH in 1% ACN) were applied and to remove non-soluble material recovered elutes were centrifuged for 2 min at 13,000 x g. After freezing supernatants for 15 min on dry ice, samples were dried in a speedvac and kept at -80°C.

2.9.4 Sample reconstitution

For the Orbitrap Q Exactive Plus mass spectrometer system, sample pellets were resuspended in 20 µL of reconstitution buffer (3% ACN; 0.1% TFA) for the phosphoproteomics experiments of MCF7 sensitive and resistant cells or sample pellets were resuspended in 13 µL of reconstitution buffer (3% ACN; 0.1% TFA) for the experiments of MCF7 parental cells induced with lactic acid or HCl, injecting 4 µL into the system. Sample reconstitution was optimised in the second case in the host laboratory to achieve a more concentrated sample preparation. For the proteomics experiments cells were

sequentially reconstituted with 20 µL 0.1% TFA and those 20 µL were further diluted 1/10 by taking 3 µL and adding 27 µL reconstitution buffer; 2 µL of those dilutions (1 µg of total protein) were injected into the system.

2.9.5 Thermo Q-Exactive plus and XL mass spectrometers

The Thermo LTQ-Orbitrap XL and Q exactive Plus instrument have some components in common (Fig 2.2). Basically, these incorporate ion guide lenses and an injection flatapole, a quadrupole mass filter, a C-trap, and an orbitrap mass analyser. Gas phase ions are captured and introduced in the mass spectrometer, where they are initially focused by a lenses system. While the ion optics of the LTQ-Orbitrap XL are based on high pressure, the ion optics of the Q exactive Plus incorporates stacked-ring radio frequency (RF) ion that efficiently focus the ions into a tight beam avoiding ions losses. In the LTQ-Orbitrap XL ions are directed into the linear trap quadrupole (LTQ), which comprises three-dimensional rod quadrupoles where selected voltages are applied to trap ions. The ion frequency given by their *m/z* determined the ion motion within the trap [286]. Thus, the function of the LTQ is to accumulate ions before sending them to the orbitrap for mass analysis. In the Q exactive Plus, however, a bend flatapole filters neutral species before selection in the quadrupole, increasing analysis robustness. Moreover, in the Q exactive Plus the hyperbolic-assembled rod quadrupoles have been replaced by a segmented quadrupole which is able to achieve narrow isolation windows, which increase the quantitative analysis accuracy. As for the precursor selection and fragmentation, in the LTQ-Orbitrap XL those occur in the linear ion trap (CID fragmentation), whereas in the Q exactive Plus, both MS and MS/MS are acquired in the orbitrap, which permit nearly instantaneous mass selection and expands the C-trap ability of storing ions populations derived from multiple precursor ions before tangentially injecting them into the orbitrap. When the LTQ-Orbitrap XL is using a DDA method, the instrument switches between MS and MS/MS modes: in MS mode packages of ions are sent to the C-trap to be further transferred into the orbitrap, whereas in MS/MS mode peptides are selected for isolation and fragmentation. In the DDA method used on the LTQ-Orbitrap XL instrument full MS spectra (*m/z* 375-1,800) were acquired with 30,000 resolution at *m/z* 400. The 5 most intense ions for each full MS scan survey were selected for CID fragmentation (35% normalised energy collision) and MS/MS analysis in the LTQ (*m/z* 50-2,000). A dynamic exclusion of 30 s was enabled to minimise repeated sequencing of peptides with an exclusion list of 500 precursor ions and a mass window of 10 ppm. This generated a duty cycle of 2.5 s. In the DDA method performed on the Q exactive Plus, full scan survey spectra (*m/z* 375-1,500) was selected with a 70,000 resolution. The 20 most intense ions for each MS scan were selected for HCD using an isolation width of 1.6 Da and MS/MS analysis (*m/z*

200-2,000) with a resolution of 17,500. A 30 s dynamic exclusion was enabled with an exclusion list of 10 ppm mass window. This produced a duty cycle of 2.1 s.

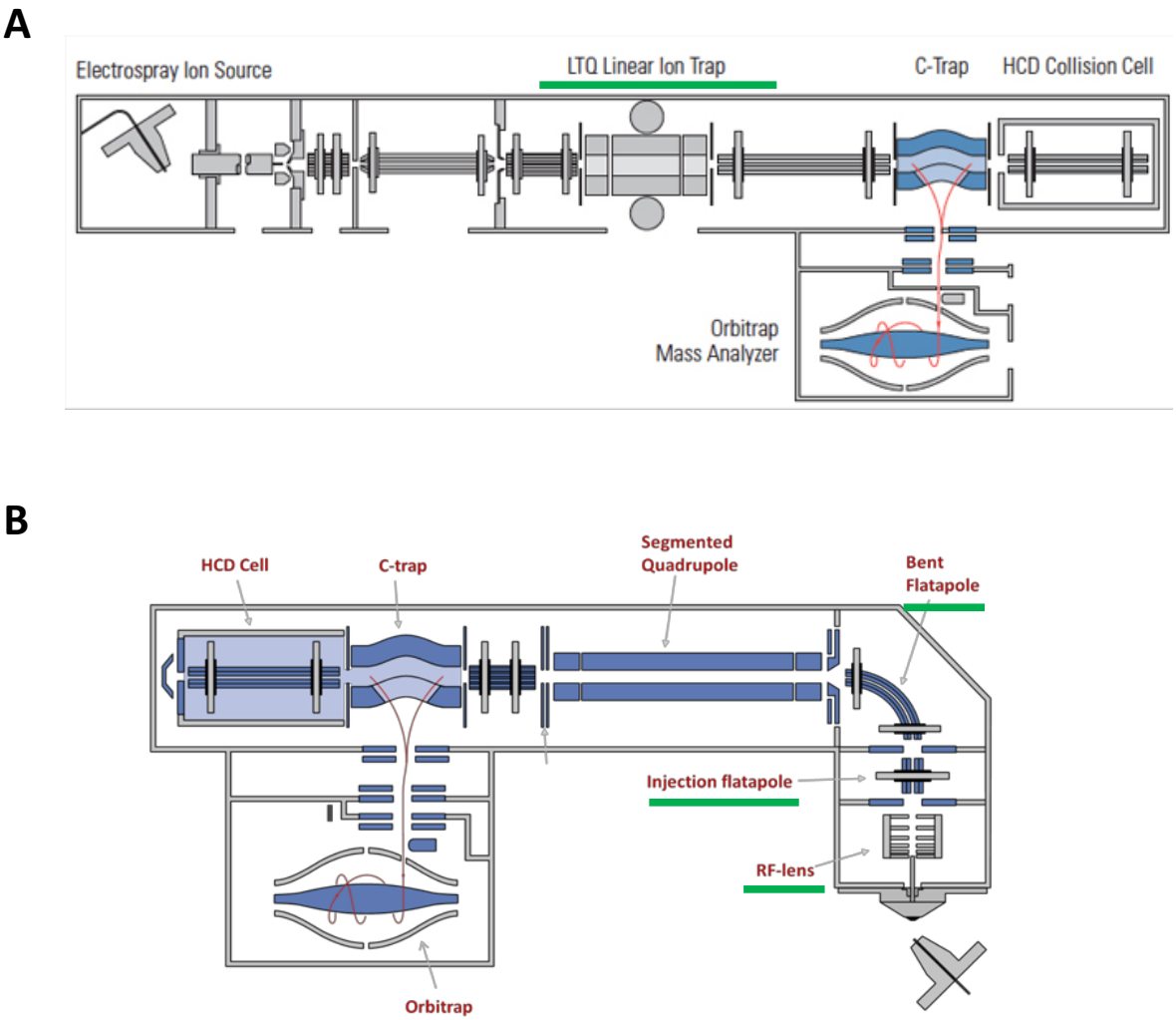

Figure 2.2 Scheme of the LTQ-Orbitrap XL and Q exactive Plus. Details of the major design elements of the LTQ-Orbitrap XL (**A**) and the Q exactive Plus (**B**). The main differences between the instruments are highlighted on green. Diagrams adapted from: planetorbitrap.com

2.9.6 LC separations

A dionex UltiMate 3000 RSLC nano is coupled to an Orbitrap Q Exactive Plus mass spectrometer (Thermo Fisher Scientific). For the LC solvent A (0.1% FA) and solvent B (100% + 0.1% ACN) were used as mobile phases. A total of 4 µL of reconstituted phosphopeptide solution were loaded in an Acclaim PepMap µ-Precolumn for 2 min at a back pressure of 15 bar and a nanoflow of 10 µL/min. Then phosphopeptides were separated in an Acclaim PepMap 100 column using a gradient that went from 3% to 23% B for 120 min with a background pressure of 155 bar and a nanoflow of 0.3 µL/min. Finally, the column was washed with 23-85% B for 7 min and equilibrated with 3% B for 3 min.

Phosphopeptides were transferred to the online connected to a Q Exactive Plus system. For phosphoproteomics and proteomics analysis, chromatographic peaks were about 30 s at the base which allowed the construction of extracted ion chromatograms (XICs) with at least 10 data points.

A liquid chromatography (UPLC, nano Acquity, Waters) is coupled to an LTQ-Orbitrap XL mass spectrometer (Thermo Fisher Scientific). For LC separation, solvent A (0.1% FA) and solvent B (100% ACN +0.1% FA) were used as mobile phases. Peptides were loaded in a nano ACQUITY UPLC Symmetry C18 Trap Column for 8 min with a nanoflow of 2 µL/min. Peptides were separated using an ACQUITY UPLC Peptide BEH C18 nano ACQUITY Column. For peptide elution, it was established a gradient from 5 to 35% of solvent B for 150 min with a background pressure of 4000 psi and a nano flow of 0.3 µL/min. Lastly, the column was washed with 35-85% B for 10 min and equilibrated with 1% B for 15 min. Peptides were transferred to the online coupled LTQ-Orbitrap XL system.

2.10 Data Analysis

2.10.1 Mascot database searches

Mascot Daemon 2.5.0 and Mascot Distiller 2.5.1.0 were used to smoothen and centroid the MS/MS data and generate peaklist files (in MGF format). Mascot 2.5 search engine was used to match peaks with peptides contained in proteins annotated in the SwissProt Database (SwissProt_2012Oct.fasta for proteomics or uniprot_sprot_2014_08.fasta for phosphoproteomics analysis) with a FDR of ~1%. The parameters used to search for protein were up to two missed cleavages for trypsin; one fixed modification (carbamidomethyl Cys); two variable modifications for (PyroGlu on N-terminal Gln; oxidation of Met); mass tolerance of 10 ppm for the precursor ion and mass tolerance of 25 mmu for the fragment ion. The parameters used to search for phosphoproteomics were the same as for protein searches but selecting five variable modifications for PyroGlu on N-terminal Gln; oxidation of Met; Phosphorylation on Ser, Thr, and Tyr. Peptides were then curated using an in-house developed Perl script that exclude identifications that have a Mascot delta score <10.

2.10.2 Protein and phosphopeptide quantification

PESCAL, an in-house computer program written in Python v2.7, was used to construct the extracted ion chromatograms (XICs) of the first, second and third isotopes of each peptide identified across all samples. The retention times (*tR*) of each phosphopeptide in each sample were predicted by aligning

the enolase standard peptides spiked into each sample and then including the chromatograms for each phosphopeptide in each sample (Fig 2.3). The window to construct each XIC had a mass-to-charge (*m/z*) tolerance of 7 ppm and *tR* tolerance of 1.5 min. Peak areas from XICs were normalised to the sum of all values in a sample and averaged between replicates and fold change between conditions was calculated. Statistical significance between conditions was assessed with a Student's *t*-test and considered significant when $P < 0.05$.

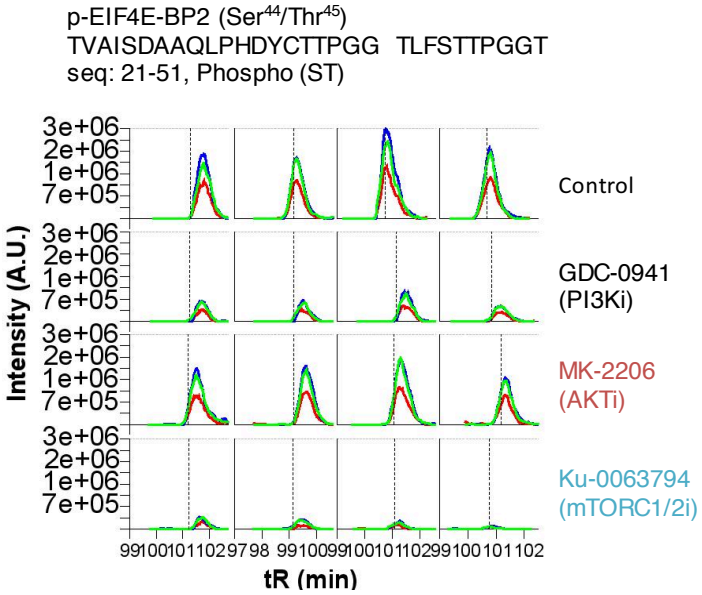

Figure 2.3 Example of XICs created by PESCAL. XICs are generated from the MS data, from the three first isotopes of each peptide (first isotope [all ^{12}C]: blue; second isotope [one ^{13}C]: red; third isotope [one ^{13}C]: green).

2.10.3 KSEA and Clustering Analysis

KSEA algorithm was used to categorise phosphopeptides into groups of phosphopeptides identified as substrates of a particular kinase downloaded from the public repository PhosphoSitePlus [33] or from in-house experiments [226]. The significance of enrichment for each kinase were calculated using a *Z*-score formula as $Z = [(mS - mP) * \sqrt{m}]/d$, mS being the mean of each kinase group $\log_2$ fold-changes against control, mP the mean of $\log_2$ of the entire data set mean changes, m the number of phosphopeptides of each substrate group, and d the standard deviation (SD) of the mean of the total data set $\log_2$ fold-changes (Fig 2.4). *Z*-scores were transformed to *P*-values using a function in excel.

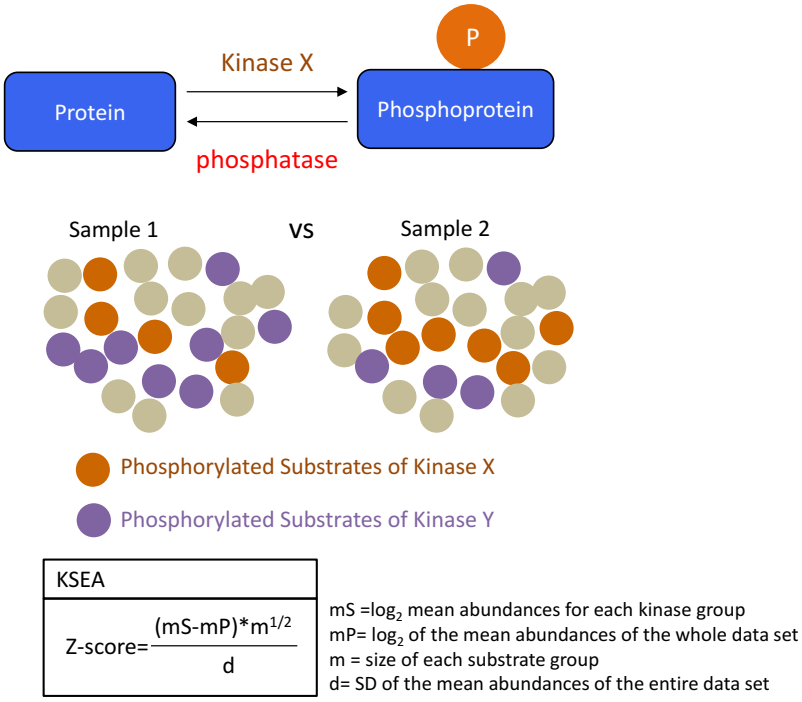

Figure 2.4 Schematic representation of the KSEA principle. The $\log_2$ mean intensities of exclusive peptides phosphorylated at sites phosphorylated by each kinase is normalised to the SD of the intensities of phosphopeptides in the whole dataset and by the number of known substrates of the given kinase.

Unsupervised *k*-means clustering algorithm was used to distribute the quantified peptides (for proteomics experiments) or phosphopeptides (for phosphoproteomics experiments) across a number of clusters based on the cluster with the nearest mean to each peptide or phosphopeptide. The significance of enrichment for kinase substrates, ontologies and pathways was determined for each cluster by means of an in-house script (written in VBA) that use the hypergeometric test approach to calculate the extent of enrichment by the formula $e=\log_2([a/b]/[c/d])$, where a is the number events of a particular ontology, pathway or group in a given cluster, b is the total number of events in a the cluster, c is the number of events specific of the ontology, pathway or group and d is the total number of events.

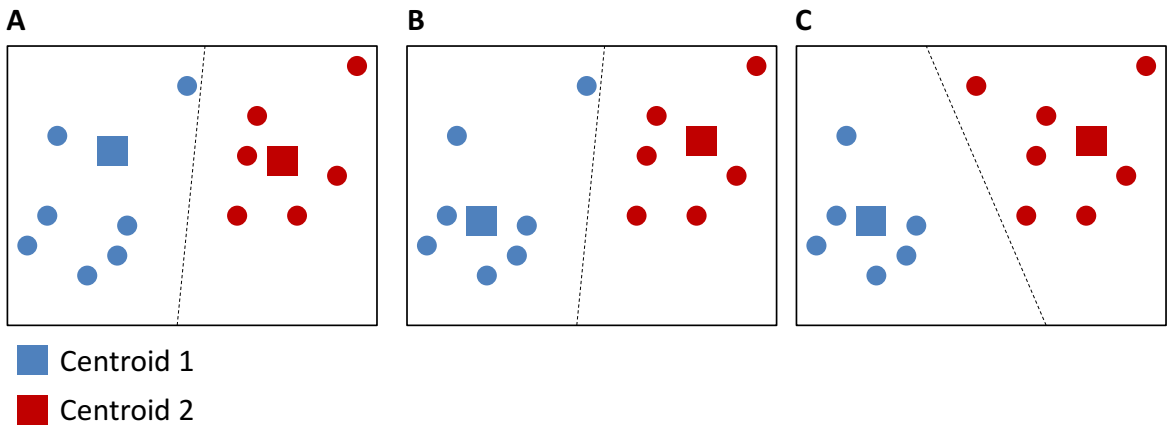

Figure 2.5 Principle of *K*-means clustering for data partition. Initially, several centroids or *K* (2 in this case) are randomly generated. (**A**) The data (represented by circles) is clustered by association with the nearest mean and the space distance is calculated by the Euclidean distribution. (**B**). Then, the centroids are distributed to become the new mean within the cluster. (**C**) Steps (**A**) and (**B**) are repeated until reaching convergence. Dashed lines represent the Euclidean distribution of space.

2.11 WES sample preparation, reads mapping, somatic variants and copy number alteration detection

200 µg of DNA from MCF7 sensitive and G resistant cells was extracted using a commercial DNA purification kit (Quiagen). DNA amount was quantified using the Qubit fluorometric system (Thermo Fisher). Raw FASTQ reads were aligned using the Burrows-Wheeler Aligner (BWA) [287] to the reference human genome version hg19. Output alignments in SAM format were sorted and converted to BAM. PCR duplicates were marked and removed using Picard algorithm (http://picard.sourceforge.net.). Local alignment around indels and base quality were recalibrated using the GATK algorithm [288]. Somatic single nucleotide variants (SNVs) and indels were identified with the Strelka algorithm [289]. To calculate the VAFs, the number of variant reads was divided by the total number of obtained reads. Copy number alterations (CNAs) were identified using the VarScan2 algorithm [290]. Analysis of CNAs and LOHs regions was done using the ASCAT R package [291].

Chapter 3. Characterisation of the phenotype of models of acquired resistance to PI3K chronic inhibition

3.1 Introduction and aims of the study

Populations of cells within tumours display a vast phenotypic heterogeneity resulting from both genetic (i.e. mutations in drivers and passengers genes) [292, 293] and non-genetic causes— including epigenetic modifications [294], cancer stem cells [295] and stochastic biochemical processes [296].

As mentioned in Section 1.3.5, there is an urge to understand the diverse range of mechanisms by which cancer cells acquire resistance to therapies, since that knowledge may contribute to discover druggable vulnerabilities of cancer cells.

The aim of the work presented in this Chapter was to characterise the phenotype of cell lines that had acquired resistance to PI3K targeted inhibitor, in the presence and in the absence of the selection drug. To accomplish this, different phenotypic features — including proliferation, cell size, protein content, cell cycle and apoptosis — of three independent cell lines derived from chronic treatment of the MCF7 cell line with the PI3K Class IA specific inhibitor GDC-0941 (referred to as PI3Ki hereafter) exposed to PI3Ki treatment as well as drug withdrawal were examined. MCF7 sensitive parental cells were named P, PI3Ki-resistant cell lines grown with the PI3Ki were named G1+, G2+ and G3+ cells and PI3Ki-resistant cell lines grown without the PI3Ki were named G1-, G2- and G3- cells (Fig 3.1).

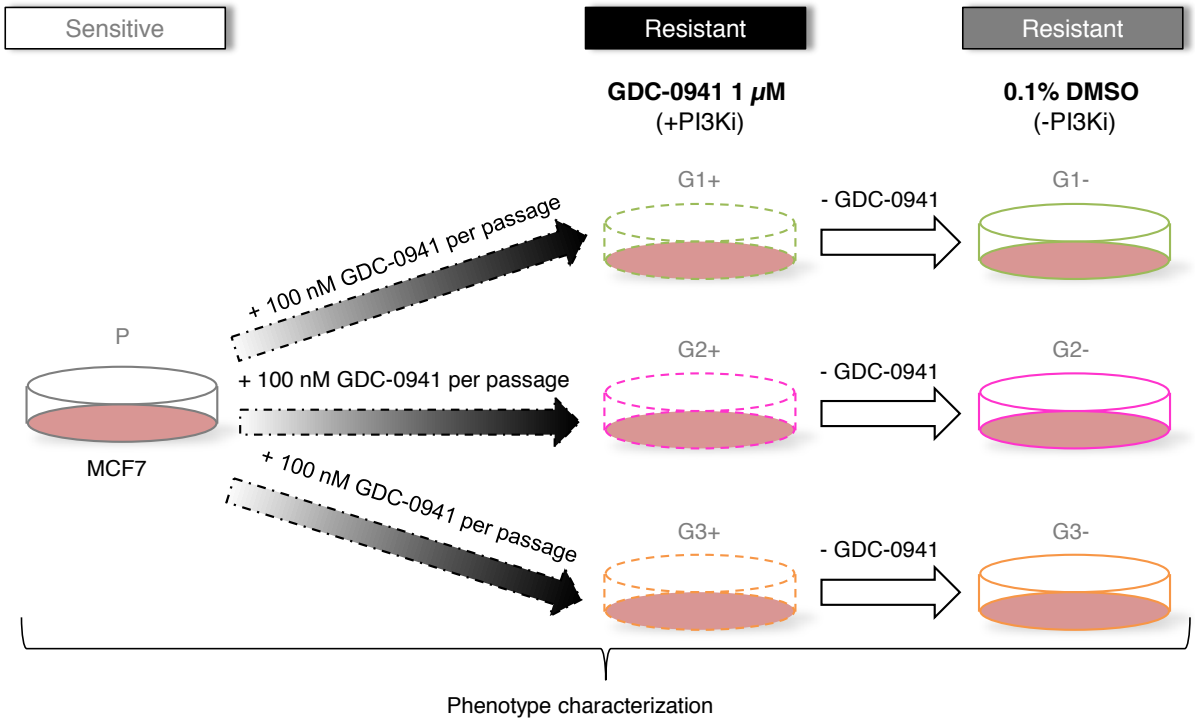

Figure 3.1 Experimental approach followed to characterise cells that had acquired resistance to a PI3K inhibitor at the phenotype level. Three models of resistance to 1 μM GDC-0941 had been previously derived in the Cutillas laboratory by increase treatment of parental MCF7 cells with 100 nM GDC-0941 at each culture passage up to a final concentration of 1 μM GDC-0941 [226]. Resistant cells were routinely maintained with 1 μM GDC-0941 (+PI3Ki). To examine the phenotype of PI3Ki-resistant cell in the absence of the selection drug, the PI3Ki was removed from the three cultures that were instead treated with DMSO control (-PI3Ki). P: Parental MCF7 cells. G1, G2, G3: PI3Ki-resistant MCF7 –derived cells.

3.2 Validation of resistance phenotype

Initially the sensitivity of cells to PI3Ki was ascertained by measuring cell viability after exposing the cells to increasing concentrations of the drug. Equal number of parental and resistant cells (0.02 x 10^6 per well) were seeded in 96-well plates containing 200 μL of growth media and treated with increasing concentrations (between 0 and 10 μM) of GDC-0941 for 5 days. The experiment was performed in triplicate. Proliferation was measured by means of a crystal violet assay (see Section 2.6.9).

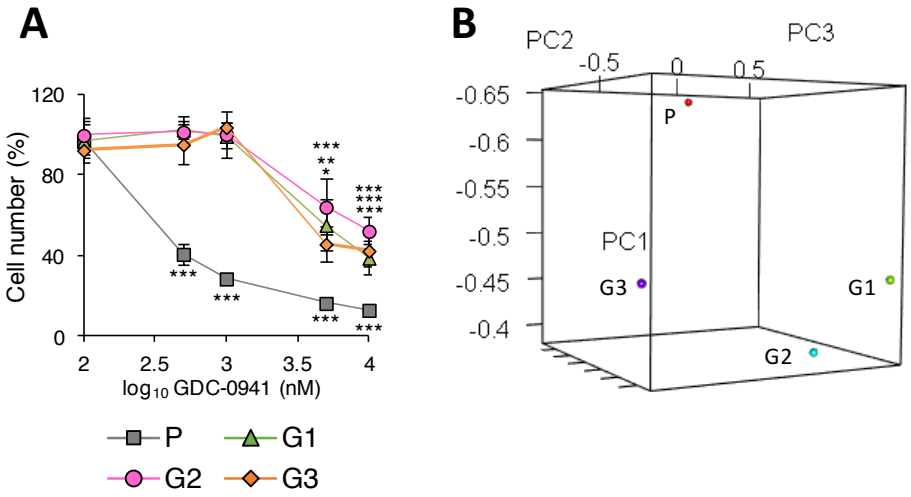

Figure 3.2 MCF7 parental cells are sensitive to PI3Ki treatment whereas the proliferation of resistant cells is not hampered by treatment up to 1 µM GDC-0941. (**A**) Viability of parental and PI3Ki-resistant cells treated with several concentrations of GDC-0941. Data are represented as mean ± SD (*n*=3, three independent technical replicates) relative to DMSO control. *P*-values were calculated using an unpaired, two-tail Student's *t*-test against control (DMSO); * $P < 0.05$; ** $P < 0.01$; *** $P < 0.001$. (**B**) PCA for the data presented in (**A**). P, parental MCF7 cells; G1, G2, G3, PI3Ki-resistant cells.

These data demonstrated that parental cells were sensitive to the PI3Ki, given that treatment of these cells with PI3Ki reduced the number of parental cells (P $\log_{10}$ IC_{50}= 2.5 nM) (Fig 3.2A). The results of this experiment also showed that PI3Ki-resistant cells were indeed resistant to the PI3K inhibitory compound, although there was a degree of heterogeneity between resistant cells lines (G1 $\log_{10}$ IC_{50}= 3.8 nM; G2 $\log_{10}$ IC_{50}= 4.0 nM; G3 $\log_{10}$ IC_{50}= 3.8 nM), as evidenced by the distribution of response values in the dimensional space upon the performance of a principal component analysis (PCA) (Fig 3.2B).

3.3 Determination of cross-resistance to additional kinase inhibitors

It was then sought to determine whether cells that had proved to be resistant to the PI3Ki were resistant to additional compounds that target nodes of the PI3K/AKT/mTOR signalling pathway. To this end, the same number of parental and PI3Ki-resistant cells (0.2 x 10^6 per well) was cultured in 6-well plates and kept for 5 days after treatment with the indicated concentration of inhibitors (Table 3.1). Each experiment was performed in triplicate. The number of viable cells was then measured using the Beckman Vi-CELL counter according to manufacturer's instructions. For these experiments, treatment of each compound was performed separately, each one with a DMSO control. These controls were then used to normalise the resulting dataset of compound-treated cells.

Analysis of these data showed that parental cells were sensitive to the panel of targeted kinase inhibitors (Fig 3.3). This analysis also showed that PI3Ki-resistant cells were more resistant than parental cells to the inhibition of kinases downstream of PI3K. For example, although the mTORC1/2 inhibitor reduced the proliferation of PI3Ki-resistant cells, the number of viable parental cells after treatment with this compound was ~12% relative to untreated cells, whereas the number of G1, G2 and G3 resistant cells after treatment with mTORC1/2i was ~42%, ~89% and ~49%, respectively. This analysis also demonstrated different sensitivity of parental cells to kinase inhibitors, as parental cells were most sensitive to the PI3Ki followed by mTORC1/2i, AKTis, mTORC1i and SGK1i.

These experiments showed that PI3Ki-resistant cells were cross-resistant to inhibitors of kinases downstream of PI3K, suggesting that PI3Ki-resistant cells evolved to survive in the absence of activity of this signalling pathway.

Name	Drug	Concentration
PI3Ki	GDC-0941	1 μM
AKTi1	A-VII	1 μM
AKTi2	MK-2206	1 μM
mTORC1/2i	KU-0063794	1 μM
mTORC1i	Everolimus	20 nM
SGKi	GSK 650394	0.5 μM

Table 3.1 Inhibitors used in this experiment. Abbreviation for the compound to represent the name of the intended targeted kinase, name of the inhibitor, and concentrations used in the experiment.

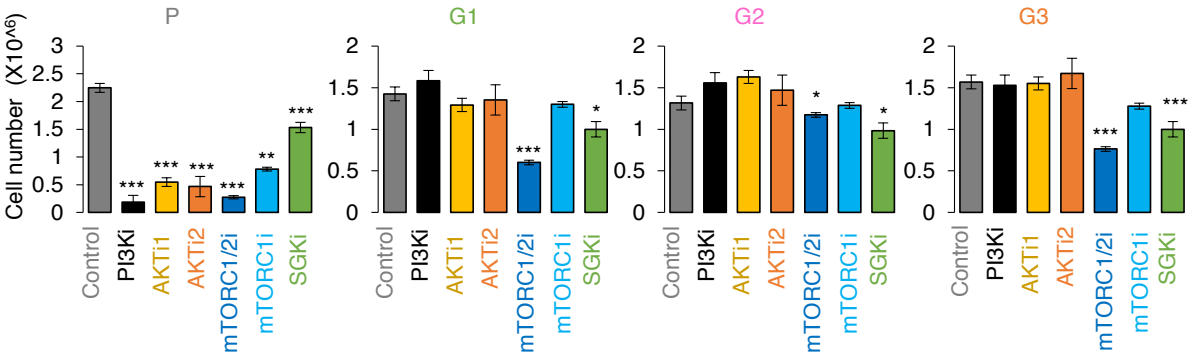

Figure 3.3 Resistant cells had acquired cross-resistance to kinase inhibitors. Number of parental and resistant cells as a function of treatment or 5 days with the panel of kinase inhibitors presented in Table 3.1. Data are represented as mean ± SD (*n*=3, three independent biological replicates). *P*-values calculated using an unpaired, two-tail Student's *t*-test between treatment and control (DMSO); * $P < 0.05$; ** $P < 0.01$; *** $P < 0.001$.

3.4 Defining the effects of drug holidays on resistant cells

3.4.1 Proliferation of resistant cells during drug holidays

The data presented in Fig 3.3 suggested that the proliferative rate of some resistant cells (G1 and G2) diminished upon removal of PI3Ki from the culture media. To characterise the effect of drug holidays (i.e. treatment removal) on PI3Ki-resistant cells in more depth, a series of experiments were carried out. Initially, the proliferation rate of parental and resistant cells grown in the presence (referred to as G1+, G2+ and G3+ cells) or in the absence of PI3Ki (referred to as G1-, G2- and G3- cells) was compared. To accomplish this, 6-well plates were seeded with equal number of parental and resistant cells (0.2×10^6 per well) and cells were maintained with either 1 μM GDC-0941 or 0.1% DMSO for 0, 1, 3 or 5 days.

In line with the data presented in Fig 3.2 and Fig 3.3, parental cells showed a negligible proliferation when they were cultured with PI3Ki whereas PI3Ki-resistant cells proliferated when treated with PI3Ki (Fig 3.4A). The proliferation rate of each PI3Ki-resistant cell line was subtly heterogeneous. For instance, G3+ cells proliferated at slower rate compared to G1+ and G2+ cells. These data also showed that resistant cells, even when grown in the absence of PI3Ki, did not recover the proliferation rate of parental cells.

An experiment was carried out to assess the effects of longer time exposure to drug holidays on the proliferative capacity of resistant cells. To avoid confluence (and thus prevent growth being stopped by contact inhibition) a relative low number of cells (0.03×10^6 per well) was seeded in 6-well plates and maintained with either 1 μM GDC-0941 or 0.1% DMSO during 7 or 14 days, with daily media replacements. These experiments clearly demonstrated that drug holidays influenced the proliferation of PI3Ki-resistant cells (Fig 3.4B). Thus, drug holidays resulted beneficial for the proliferation of G3- cells but detrimental for G1- and G2- cells. These data indicated that some of the PI3Ki-resistant cells developed a proliferative defect during drug holidays, and that the proliferation of G1 and G2 resistant cells benefit from the presence of PI3Ki in the media.

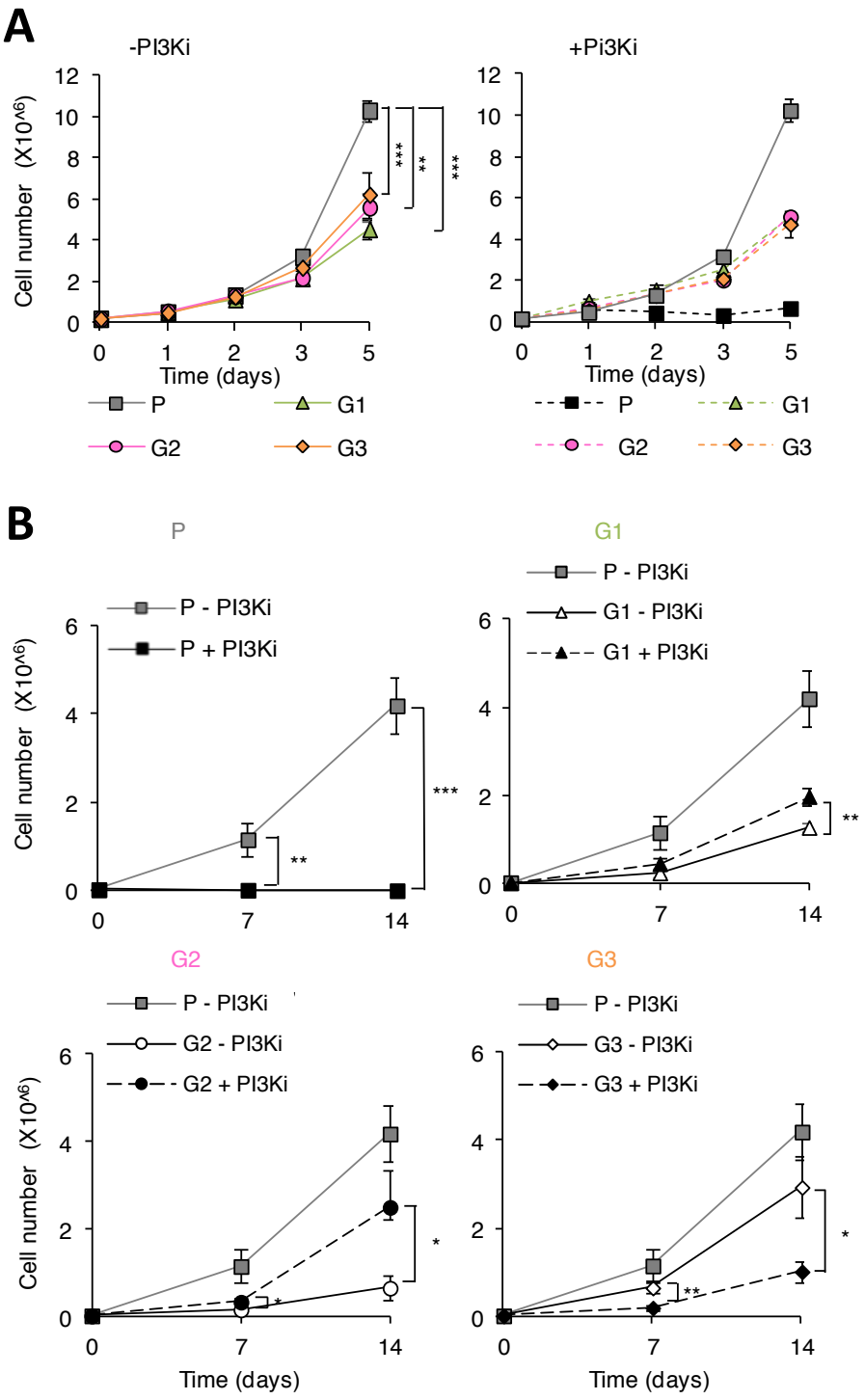

Figure 3.4 Resistant cells do not recover the proliferation rate of parental cells and in some cases develop a proliferative defect during drug holidays. (**A**) Number of parental and resistant cells growing in the absence or presence of 1 µM GDC-0941 (PI3Ki) measured after 5 days. (**B**) Number of parental and resistant cells growing in the absence or presence of 1 µM GDC-0941 (PI3Ki) measured after 7 and 14 days, replacing the media every day. Data are represented as mean ± SD (*n*=3, three independent biological replicates). *P*-values were calculated using an unpaired, two-tail Student's *t*-test against control (DMSO); * $P < 0.05$; ** $P < 0.01$; *** $P < 0.001$.

3.4.2 Cellular size and protein content of resistant cells during drug holidays

The effect of drug holidays on cell size and cellular protein amount was also investigated. Parental and PI3Ki-resistant cells were maintained in the presence or absence of PI3Ki for 5 days. Cells were visualised using a light microscope and cell size was calculated as the mean cell diameter, measured by means of the Beckman Vi-CELL counter. Exposure of PI3Ki-resistant cells to drug holidays resulted in a significant increase in the size of G1- and G2- cells (by about 10%, *P*= 0.001) compared to the same cells grown with the PI3Ki, whereas G3- cells had a slight but non-significant increase in cell size (by about 2.6%, *P*=0.26) (Fig 3.5A). Net protein content also increased for G1-G3 resistant cells after being exposed to drug holidays, as shown in Fig 3.5B. These experiments revealed that drug holidays contributed to cell biomass production, and that PI3Ki-resistant cells used that biomass to increase cell size but not to proliferate.

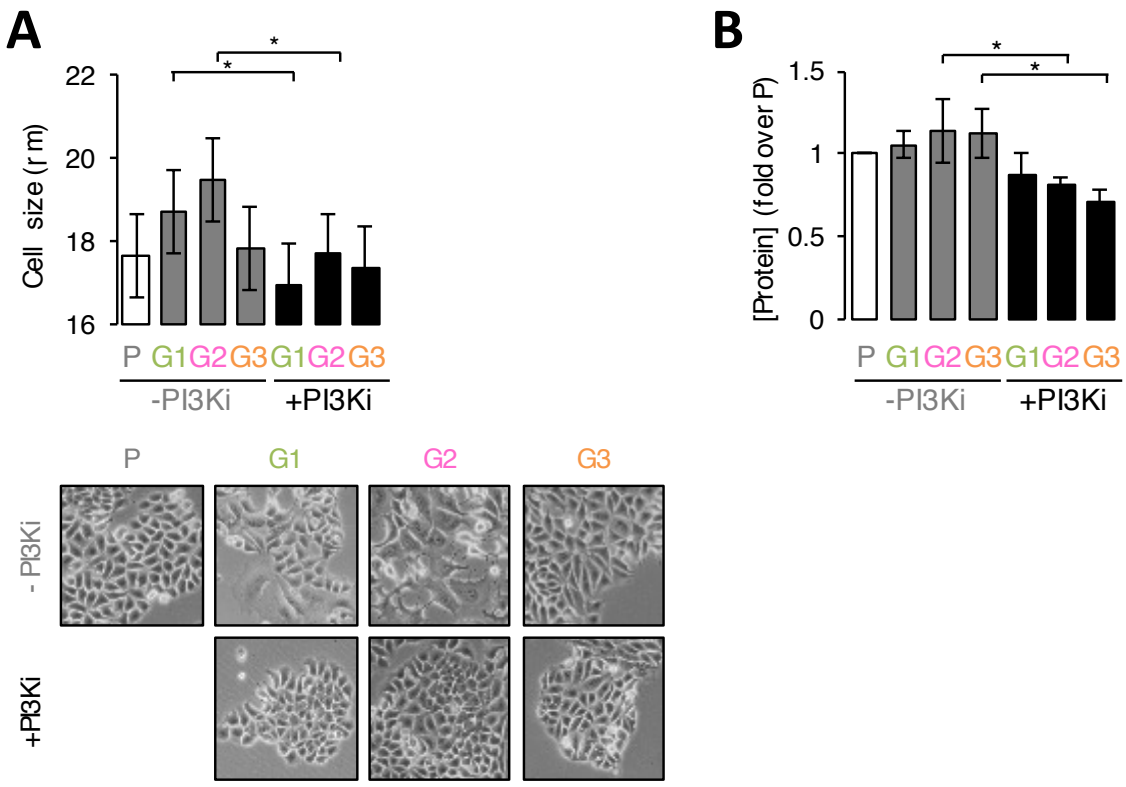

Figure 3.5 Resistant cells increase their size and protein content during drug holidays. (**A**) Representative images and diameter size of parental and resistant cells maintained in culture for 5 days in the absence or presence of 1 µM GDC-0941 (PI3Ki). (**B**) Protein content of parental and resistant cells growing in the absence or presence of 1 µM GDC-0941 (PI3Ki) measured after 5 days. Data are represented as mean ± SD (*n*=3, independent biological replicates). *P*-values were calculated using an unpaired, two-tail Student's *t*-test against control (DMSO); * $P < 0.05$.

3.4.3 Cell cycle and apoptosis of resistant cells during drug holidays

Further analysis of the cell cycle progression and cellular apoptosis (as detailed in Section 2.6.7) of parental and PI3Ki-resistant cells upon exposure to drug holidays revealed a significant reduction in the cell cycle progression from G_0/G_1 to S phase in G1- cells (by ~25%, *P*=0.0004) and in G2- cells (by ~40%, *P*=0.0014) following PI3Ki withdrawal from these cells, whereas the cell cycle progression from G_0/G_1 to S phase of G3- cells increased (by ~41%, *P*=0.052) compared to G3+ cells (Fig 3.6A). The percentage of PI3Ki-resistant cells undergoing apoptosis, however, was not significantly affected by the drug holiday conditions (Fig 3.6B).

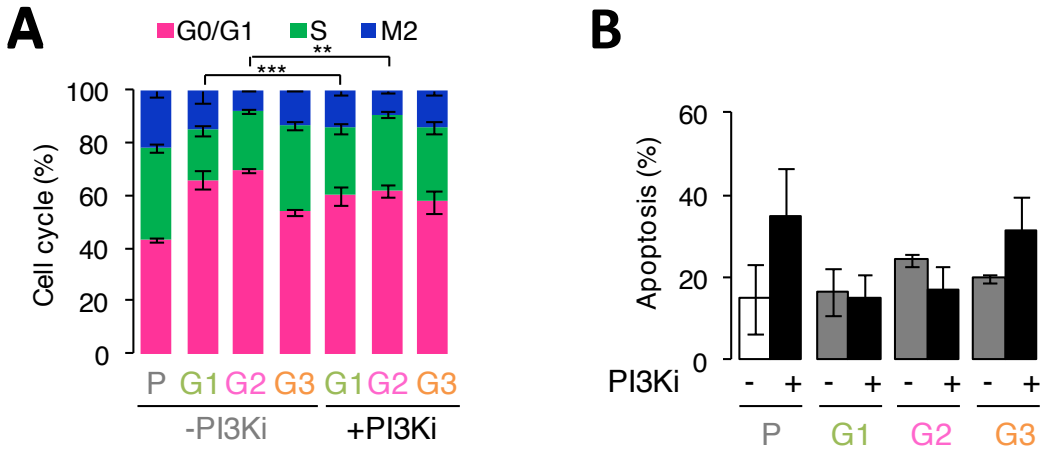

Figure 3.6 Drug holidays stop the cell cycle progression of resistance cells but it does not promote apoptosis. (**A**) Cell cycle distribution of parental and resistant cells after culture for 5 days in the absence or presence of 1 µM GDC-0941 (PI3Ki). (**B**) Percentage of apoptosis for parental and resistant cells maintained in the absence or presence of 1 µM GDC-0941 (PI3Ki) for 5 days. Data are mean ± SD (*n*=3, three independent technical replicates). *P*-values were calculated through an unpaired, two-tail Student's *t*-test comparing presence and absence of GDC-094. Significance is shown for the percentage of cells in S phase; ** *P* <0.01; *** *P*< 0.001.

3.5 Conclusions

The aim of the experiments presented in this Chapter was to characterise the phenotype of cell models of acquired resistance to PI3K-targeted inhibition.

PI3Ki-resistant cells could survive the presence of a PI3Ki, whereas parental cells were sensitive to treatment with PI3Ki, as demonstrated by the cell viability response to treatment with a range of PI3Ki concentrations (Fig 3.2). In addition, PI3Ki-resistant cells were more resistant than parental cells to treatment with compounds that target kinases of the PI3K/AKT/mTOR pathway (Fig 3.3). However, PI3Ki-resistant cells proliferate at slower rate than parental cells, even after PI3Ki withdrawal from the culture media (Fig 3.4). Moreover, some PI3Ki-resistant cells — i.e. G1 and G2 cells — proliferated at lower rate when they were not treated with the PI3Ki (Fig 3.4), suggestive of a potential addiction of

these cells to the PI3Ki. Protein quantification assays revealed that resistant cells increased the amount of protein during drug holidays (Fig 3.5B); instead of using this increased in cell biomass to proliferate, PI3Ki-resistant increased their size. Consistent with the observation of a reduced proliferation of some resistant cells during drug holidays, Guava–based cell cycle assay data revealed that drug withdrawal promoted cell cycle arrest and consequent stagnation of proliferation kinetics of G1- and G2- cells (Fig 3.6A). Apoptosis of PI3Ki-resistant cells, however, was not enhanced by drug holidays (Fig 3.6B).

Having established that drug holidays are an important determinant of the phenotype of cancer cells that had acquired resistance to a PI3K inhibitor, the changes on the proteome and signalling rewiring of PI3Ki-resistant cells grown in the presence of 1 μM GDC-0941 or DMSO control were investigated and this is the topic of the next chapter.

Chapter 4. Determination of changes in the proteome and phosphoproteome of PI3Ki-resistant cells

4.1 Introduction and aims of the study

The results presented in Chapter 3 characterised the phenotypic responses of models of PI3Ki-resistant cells to the presence of PI3Ki or its absence. Phenotypic changes occurring in several diseases, such as the development of a particular metabolic features in metabolic diseases [11], modification of migration programs during metastasis [297] involve the alteration of numerous proteins comprised in molecular pathways that regulate a particular phenotype (e.g. anabolic/migratory phenotype).

The aim of the work presented in this Chapter sought to understand how cells can survive in the absence of PI3K signalling. It was hypothesised that the observed phenotypic differences of PI3Ki-resistant cells exposed to the presence of PI3Ki or to drug holidays from PI3Ki could be recapitulated at the signalling and proteome levels. To explore this, two experiments were designed to quantitatively compare the proteomes and phosphoproteomes of parental and three PI3Ki-resistant cell lines maintained in the absence or in the presence of 1 μM GDC-0941 for 5 days using LC-MS/MS in quadruplicate replicates (Fig 4.1).

The quantitative data from proteomics and phosphoproteomics experiments were analysed using Excel, VBA, and R functions. Two type of comparisons were made: (i) the difference in protein and phosphopeptides abundances between resistant cells — both in the absence (referred as G1-, G2- and G3- cells) and in the presence of GDC-0941 (referred as G1+, G2+ and G3+ cells) – and parental cells (referred as P cells); and (ii) the difference in protein and phosphopeptides abundances in PI3Ki-resistant cells after being withdrawn from PI3Ki.

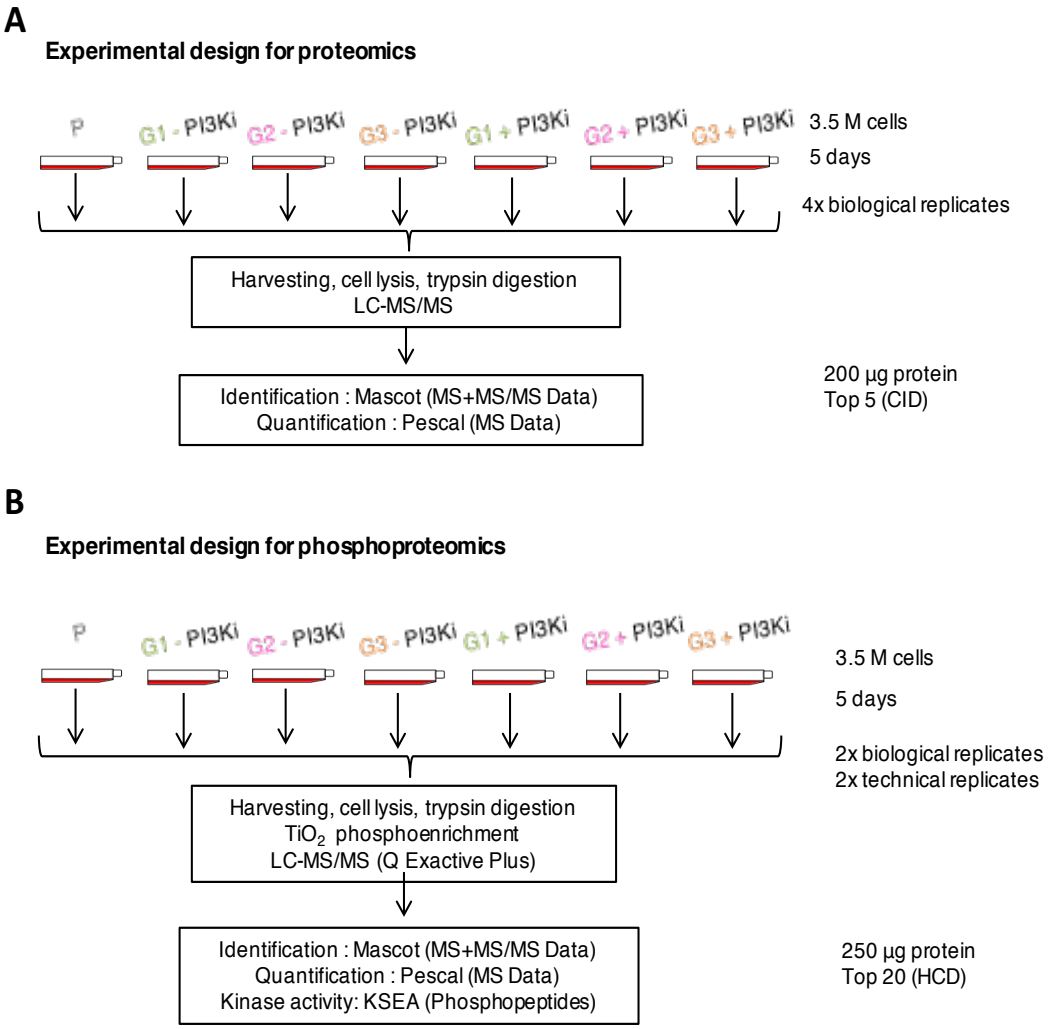

Figure 4.1 Overview of the workflow followed to analyse the proteomes and phosphoproteomes of MCF7 parental and PI3Ki-resistant cells. (**A**) Parental and resistant cells were seeded in 175 cm^2 flasks at 70% confluence and kept in culture for 5 days either with 1 µM GDC-0941 or 0.1% DMSO. The experiment was performed in quadruplicate. Cells were then collected and lysed, proteins were digested with trypsin and peptides desalted by solid-phase extraction. (**B**) Same experimental conditions as in (**A**) modified for phosphoproteome analysis (cells were grown in duplicate).

4.2 Proteomic profiling of sensitive and resistant cells during drug treatment and withdrawal

To characterise the modifications in protein levels in resistant cells, the proteomes of parental and PI3Ki-resistant cells were analysed (Fig 4.1A).

4.2.1 Data quality control

Previous to the analysis of data derived from MS experiments, quality controls of these datasets were carried out at 6 levels: (i) visualisation of total ion chromatograms (TIC) and quantification of the area

under the total ions chromatogram; (ii) determination of the MS fragmentation performance; (iii) assessment of the identity assignation to each peptide or phosphopeptide; (iv) assessment of the chromatography linearity by calculating the linear relation in retention times across all samples; (v) evaluation of the normality distribution of peptides or phosphopeptides intensities and; (vi) determination of intensity normalisation efficiency to remove technical noise.

First, the mass spectrometer performance was estimated by determining the sum of the total area under the chromatographic peaks for each scan. TIC intensities were visualised by Xcalibur and quantification of the sum of chromatographic areas demonstrated that the mean intensity was in the E13 range, which was comparable to reported values obtained from instruments used in the study (Fig 4.2A). Second, the summary of MS and MS/MS scans (quantified by RawMeat) demonstrated an average ratio of 1.45 MS2 to MS which pointed out to adequate fragmentation efficiency (Fig 4.2B). Third, the number of peptide ions whose identity was assigned with high confidence (FDR<0.05) for each of the total 28 LC-MS/MS runs that generate the database was calculated. A total of 13,843 unique peptide ions were identified with FDR<0.05, which was a comparable number to what obtained in similar type of experiments (Fig 4.2C) [226]. Fourth, the precision of the bioinformatics predictions implemented in the PESCAL algorithm used to populate the database with retention times for each peptide ion across all the samples was estimated. These predictions are made by fitting a linear model of the pairwise alignment of the retention times of common peptides. The linearity of the pairwise alignments between peptide retention times of two samples served to demonstrate the accuracy of the linear model (Fig 4.2D, left image). The high correlation between all linear alignments between each pair of samples illustrated consistency in the linearity of *tR* alignments (Fig 4.2D, right image). Fifth, and after label-free quantification by the PESCAL algorithm, the data were $\log_2$ transformed. Normal distribution of the data was deduced by visual inspection of the peptide intensities, which enabled following parametric statistical analyses (Fig 4.2E). Six, the $\log_2$-transformed data was normalised and inspection of these data proved the capacity of normalisation to make distributions across the samples homogenous in statistical properties (Fig 4.F).

Overall, the steps followed to assess the quality of these experiments advocate the good quality of the MS dataset and that the pre-processing applied to remove confounding variables allowed a robust downstream data analysis.

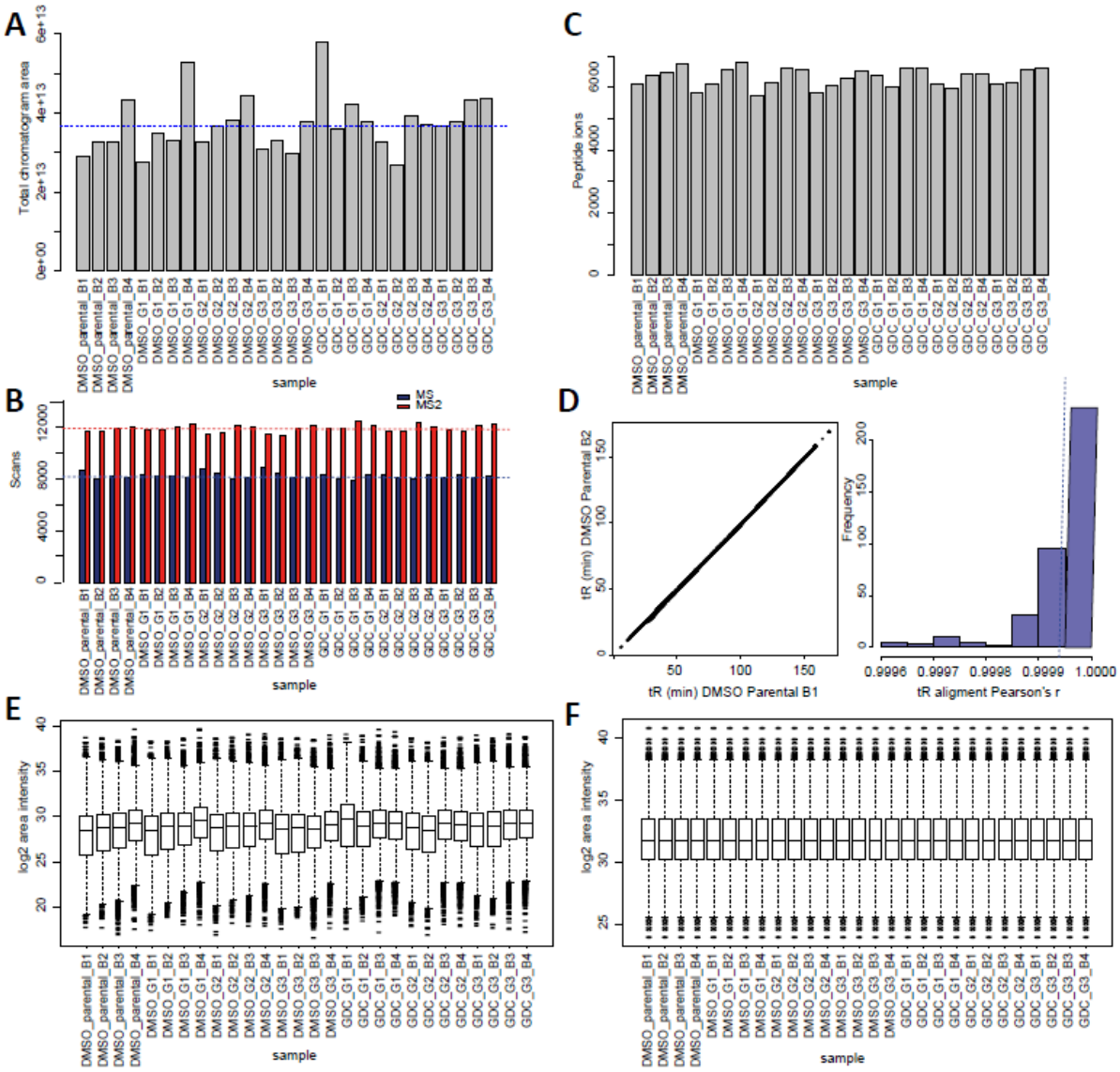

Figure 4.2 Quality control MS data used to analyse the proteomes of MCF7 parental and GDC-0941 resistant cells grown in the presence or in the absence of PI3Ki. (**A**) Quantification of total area under the chromatographic peaks contained in 28 proteomics MS runs. (**B**) Number of MS and MS2 scans quantified by RawMeat. (**C**) Quantification of the number of identified peptide ions (FDR<0.05) that generate the database created from the 28 MS runs. (**D**) Representative alignment between retention times of two experimental samples (left panel) and histogram distribution of the correlation between the alignment of retention times of all experimental samples (right panel). (**E**) Box plots demonstrating the distribution of log_2-transformed peptide peak intensities pre-normalisation. (**F**) log_2 distribution of peptides peak intensities post-quantile normalisation.

4.2.2 Differential abundance

The peptides contained in the proteomics dataset were further grouped into 3,314 proteins. A summary of the differential abundance analysis is shown in Fig 4.3. These results gave an overview of the differences between the proteomes of parental and PI3Ki-resistant cells. Interestingly, the number of differently abundant proteins between PI3Ki-resistant cells maintained in the presence or absence

of PI3Ki was distinct, indicating changes in the proteomes of PI3Ki-resistant cells as a result of drug treatment.

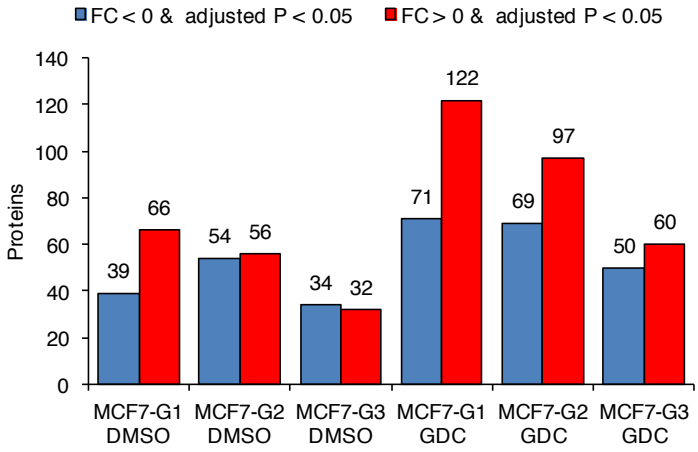

Figure 4.3 Differential abundance analysis of the proteomics data. The number of proteins containing more than one peptide and mascot score >45 either significantly (FDR<0.05) decreased (blue bars) or increased (red bars) in abundance compared to parental cells (*ntotal* =359). FC, $\log_2$ fold change vs P; adjusted *P*, is the corrected *P*-value for multiple testing by the Benjamini-Hochberg method.

4.2.3 Relation between the proteomes of resistant cells

To obtain an overview of the proteomes of parental and resistant cells, a PCA of the data presented in Fig 4.3 was performed. This analysis revealed that, as expected, proteomic sample replicates grouped closer in the PCA space (Fig 4.4). This analysis also showed that PI3Ki-resistant cells separated well from parental cells on the first principal component (PC1), indicating that acquisition of resistance was the principal factor determining diversity in the proteomes of parental and resistant cells. Moreover, the second principal component (PC2) also discriminated differences between PI3Ki-resistant cells; G1+ and G2+ cells located close together and far apart from G1-, G2- and G3 cells.

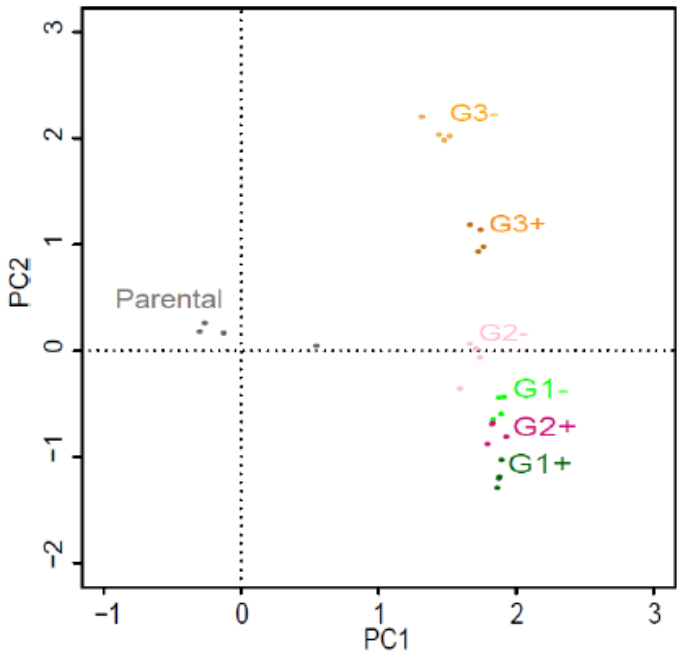

Figure 4.4 The proteome profile of MCF7 parental cells is different from the proteome of PI3Ki-resistant cells. Scatter plot of the two principal components of the proteomics data shown in Figure 4.3. Plotted dots represent replicated values for each condition. PC1, principal component 1; PC2, principal component 2.

Table 4.1 Pathway enrichment analysis discriminates over-represented biological pathways in PI3Ki-resistant cells because of PI3K withdrawal.

G1	G2	G3
GO:0009267~cellular response to starvation	GO:0043038~amino acid activation	GO:0019748~secondary metabolic process
GO:0042594~response to starvation	GO:0006418~tRNA aminoacylation for protein translation	
GO:0031669~cellular response to nutrient levels	GO:0043039~tRNA aminoacylation	
GO:0031668~cellular response to extracellular stimulus	GO:0006399~tRNA metabolic process	
	GO:0006564~L-serine biosynthetic process	
	GO:0034660~ncRNA metabolic process	
	GO:0006563~L-serine metabolic process	
	GO:0007010~cytoskeleton organization	
	GO:0009070~serine family amino acid biosynthetic process	
	GO:0008219~cell death	
	GO:0016265~death	
	GO:0006268~DNA unwinding during replication	
	GO:0006270~DNA replication initiation	
	GO:0032508~DNA duplex unwinding	
	GO:0032392~DNA geometric change	
	GO:0006541~glutamine metabolic process	
	GO:0006412~translation	

To determine the cellular functions potentially modulated in PI3Ki-resistant cells, a pathway enrichment analysis of proteins presented in Fig 4.3 was carried out using the Database for Annotation, Visualisation and Integrated Discovery (DAVID) resource, an online application containing gene lists generated from prior knowledge [298]. This analysis revealed that proteins modulated in PI3Ki-resistant cells, in comparison to proteins in parental cells, were involved in metabolic processes including glucose metabolism, monosaccharide metabolism and oxidation-reduction processes (Appendix 1). Analysis of the pathways containing proteins modulated because of drug holidays (i.e.

resistant cells grown in the presence and the absence of PI3Ki, n=54, FDR adjusted P<0.05) revealed that proteins involved in cellular response to starvation, amino acid activation and secondary metabolic processes were overrepresented in PI3Ki-resistant cells in response to the drug holiday treatment (Table 4.1).

To provide additional evidence of modulated metabolic features in PI3Ki-resistant cells, various proteins involved in diverse metabolic processes were extracted from the proteomic dataset and their mean $\log_2$ fold-change (against the parental cells) represented. The data shown in Fig 4.5A demonstrated that PI3Ki-resistant cells increased the levels of proteins involved in the production of lactic acid (e.g. LDHA — lactate dehydrogenase A, LDHB — lactate dehydrogenase B and LDH6B — lactate dehydrogenase A-like 6B), fatty acid metabolism (e.g. FASN — fatty acid synthase, FABP5— fatty acid-binding protein, and ACLY — ATP-citrate synthase), TCA cycle (e.g. IDH3A — isocitrate dehydrogenase 3A) and electron transport chain (e.g. TXNL— thioredoxin-like protein). The data also showed that upon drug removal, PI3Ki-resistant cells increased the levels of proteins involved in the pentose phosphate pathway (PPP) (e.g. G6PD — glucose-6-phosphate dehydrogenase) and gluconeogenesis (e.g. PCK2 — phosphoenolpyruvate carboxykinase 2) (Fig 4.5A).

To confirm some of the changes observed in the proteomics experiment, Western blots were carried out for two proteins involved in the production of fatty acids and the glycolytic pathway: FASN and LDHB. The results shown in Fig 4.5B were in agreement with the patterns of protein expression shown in Fig 4.5A, supporting the accuracy of the MS data.

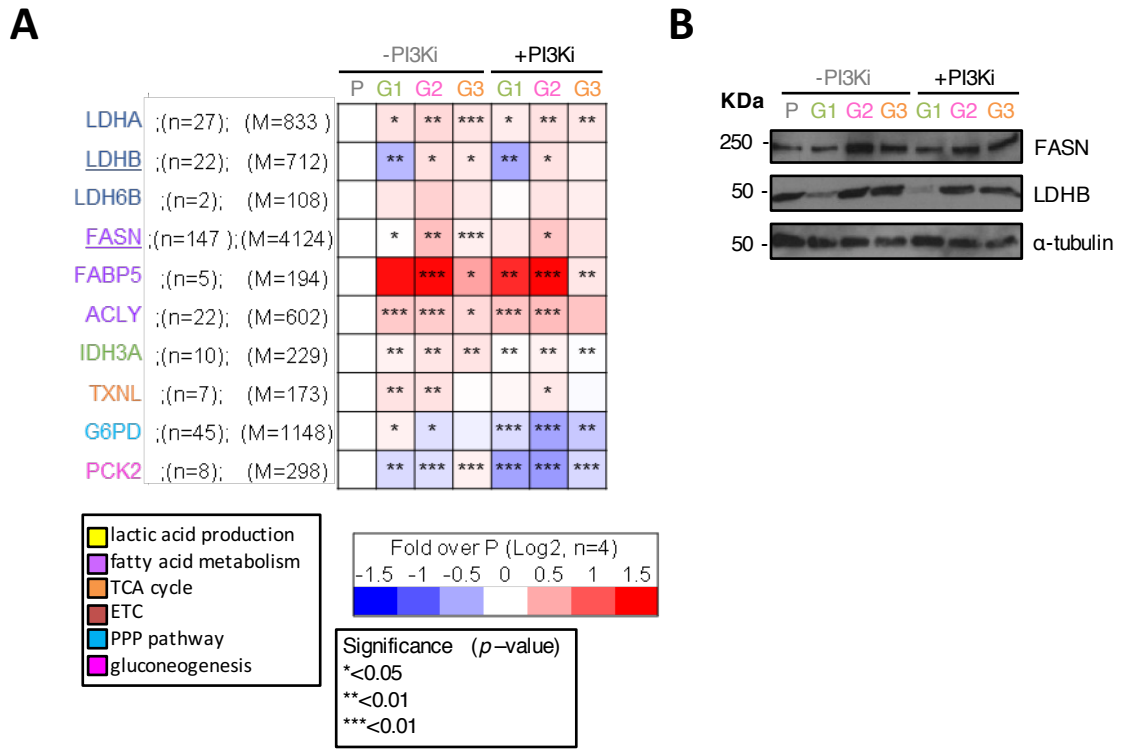

Figure 4.5 Proteins involved in metabolic processes are modulated in PI3Ki-resistant cells. (**A**) Heatmap of selected proteins involved in various metabolic processes. Gene names of proteins are coloured based on the metabolic pathway in which they are involved. Protein information is arranged as follows: gene name; number of unique peptides (n); Mascot protein score (M). Data represents the $\log_2$ fold ratio protein intensity of resistant cells over protein intensity of parental cells. (**B**) Western blots against FASN and LDHB for parental and resistant cells. Loading control for each cell is shown.

4.2.4 Systematic classification of the proteomes of resistant cells

To systematise the classification of the proteomics dataset and further explore the relationship of proteomes of PI3Ki-resistant cells, cell proteomes were organised into six groups by means of unsupervised *k*-means clustering. Grouping the proteomics data in this manner facilitates unravelling proteins associations. Thus, proteins that significantly increased in PI3Ki-resistant cells compared to parental cells were comprised in cluster 1 (small cluster, 10 proteins) and cluster 2 (containing 276 proteins), and proteins that decreased were included in cluster 5 (containing 143 proteins) and cluster 6 (small cluster, 13 proteins) (Fig 4.6A). The complete clustering analysis of the proteomics dataset is included in Appendix 2. An ontology analysis [299] of the functions and processes associated to the proteins enriched in PI3Ki-resistant cells (cluster 2), demonstrated that proteins involved in regulation of translational initiation (GO: 0006446 and GO: 0003743) were enriched in PI3Ki-resistant cells (Fig 4.6B-C), in line with the data showed in Table 4.1. Interestingly, the analysis of proteins that increased in PI3Ki-resistant cells (cluster 2), using an alternative annotated-pathways database (i.e. Nci pathway interaction database) [300] revealed that proteins associated to HIF-1-α transcription factor network

and validated targets of c-MYC transcriptional activation increased in PI3Ki-resistant cells (Fig 4.6D). On the other hand, analysis of proteins that decreased in PI3Ki-resistant cells (cluster 5) revealed that proteins of the extracellular matrix disassembly (Fig 4.6E) and Ca^{2+} ion binding (Fig 4.6F) decreased in PI3Ki-resistant cells. Moreover, proteins associated with the caspase cascade in apoptosis decreased in PI3Ki-resistant cells (Fig 4.6G).

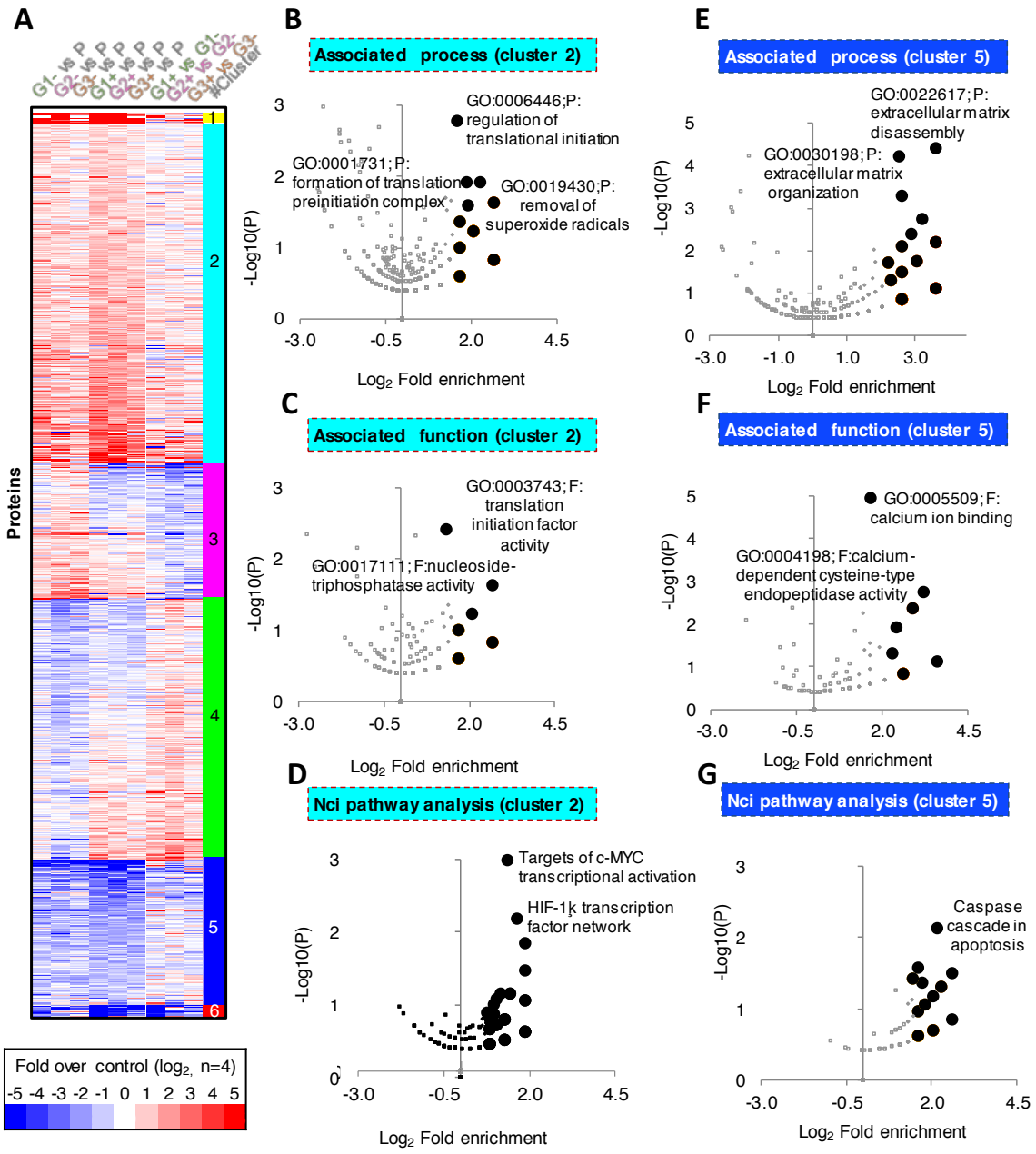

Figure 4.6 *K*-means consensus clustering for the proteomes of MCF7 parental and resistant cells identifies six subgroups. (**A**) *k*-means algorithm grouped proteins that increased (clusters 1-2) or decreased (5-6) in resistant cells compared to parental. (**B**) Volcano plots of associated gene ontology (GO) processes of proteins comprised in cluster 2. (**C**) Associated functions of the same proteins as in (**B**). (**D**) Nci pathway of the same proteins as in (**B**). (**E**) Volcano plots of associated GO processes of proteins comprised in cluster 5. (**F**) Associated functions of the same proteins as in (**E**). (**G**) Nci pathway of the same proteins as in (**E**).

The levels of c-MYC in parental and resistant cells were then evaluated and presented in Section 4.3. The functional role of c-MYC and HIF-1-α transcription factors on PI3Ki-resistant cells was further evaluated and these data will be discussed in Chapter 5.

4.3 Evaluation of c-MYC levels in resistant cells by immunoblotting

The analysis of the proteomics data presented in Section 4.2.4 suggested that c-MYC activity increased in PI3Ki-resistant cells. Given the documented role of this transcription factor in the development of PI3Ki resistance in breast cancer cells [301], the levels of c-MYC protein in parental and PI3Ki-resistant and cells were measured by Western blot. The data in Fig 4.7 demonstrated that PI3Ki-resistant cells had higher levels of c-MYC protein compared to the parental cells. Moreover, PI3Ki-resistant cells showed an increase c-MYC protein when treated with the PI3Ki (Fig 4.7). This suggested that the function of c-MYC could be important for PI3Ki-resistant cells to survive in a background of PI3K inhibition.

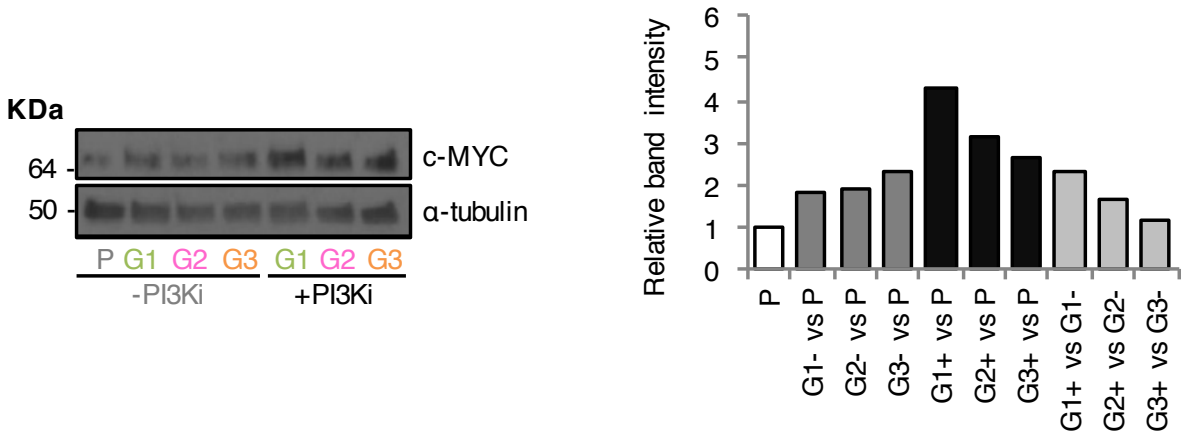

Figure 4.7 c-MYC protein levels are enhanced in PI3Ki-resistant cells treated with PI3Ki. Western blot for c-MYC and α-tubulin (loading control) of parental and resistant cells (left panel). Log_2 fold-change of c-MYC protein levels in parental and PI3Ki-resistant cells normalised by levels of α-tubulin (right panel).

4.4 Phosphoproteomic profiling of sensitive and resistant cells during drug treatment and removal

To understand the signalling changes that occurred in resistant cells, the phosphoproteomes of parental and PI3Ki-resistant were then analysed (Fig 4.1B).

4.4.1 Data quality control

As for the proteomic experiment discussed above, the quality control of the phosphoproteomics experiment performed to explore the phosphoproteomes of parental and PI3Ki-resistant cells in the presence and absence of PI3Ki demonstrated the good quality of the phosphoproteomics dataset and the validity of the pre-processing implemented before data analysis. This quality control is shown in Appendix 3.

4.4.2 Differential abundance

Analysis of this experiment retrieved 7,056 peptides, of which 5,674 were phosphorylated. The data shown in Figure 4.8 served as preliminary indication of the differential modulation of the phosphoproteomes of PI3Ki-resistant cells in comparison to the phosphoproteome of parental cells. These data also revealed the modulation of the phosphoproteomes of PI3Ki-resistant cells grown in the presence or absence of PI3Ki treatment.

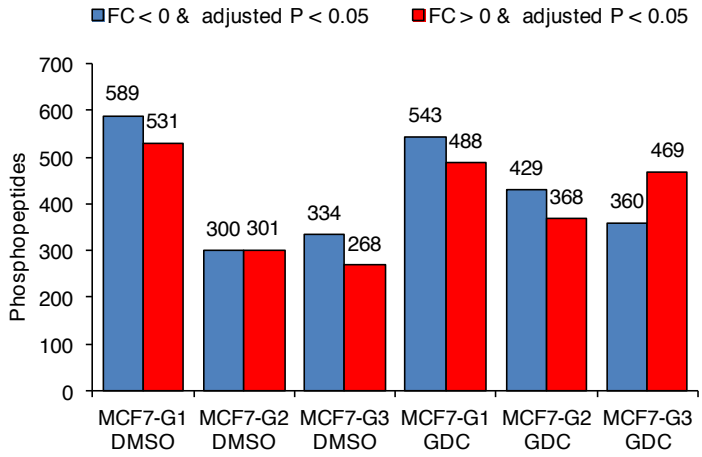

Figure 4.8 Differential abundance analysis of the phosphoproteomics data. The number of phosphopeptides either significantly (FDR<0.05) decreased (blue bars) or increased (red bars) in abundance compared to parental cells are shown (*ntotal* = 3,008). FC, $\log_2$ fold-change vs Parental; adjusted *P*, is the corrected *P*-value for multiple testing by the Benjamini-Hochberg method.

4.4.3 Examination of the status of PI3K/AKT/mTOR signalling in resistant cells

To investigate if PI3K remained inhibited in PI3Ki-resistant cells treated with PI3Ki, several phosphorylation sites known to be substrates of kinases of this signalling cascade, were extracted from the phosphoproteomics dataset, and their differential phosphorylation status analysed. For example, the abundance of phosphorylation on a site of AKT1S1 (most probably Ser^{246}, also known as PRAS40), EIF4EBP1 seq 64-99 (most probably on Thr^{68}/Thr^{70}), GSK3α seq 17-50 (most probably Ser^{21}),

GSK3β seq 7-27 (most probably Ser[9]) and RPS6KB1 Thr[444]/Ser[447] was reduced upon exposing PI3Ki-resistant cells to PI3Ki (Fig 4.9A).

Moreover, Western blots performed against AKT Ser[473], PRAS40 Thr[246] and p-4E-BP1 Thr[37/46], which are phosphorylation sites on proteins known to be downstream of PI3K, demonstrated a decreased in the phosphorylation of these sites after treatment of the PI3Ki-resistant cells with PI3Ki, indicating that signalling activity downstream of PI3K remained inhibited on those conditions (Fig 4.9B). These data also showed a recovery in the phosphorylation on these sites upon drug removal from culture, suggesting that the pathway activity is restored after drug withdrawal. The immunoblotting data reflected the pattern observed in the phosphoproteomics data that PI3K signalling was inhibited during PI3Ki treatment and reactivated upon PI3Ki removal from the culture media (Fig 4.9B).

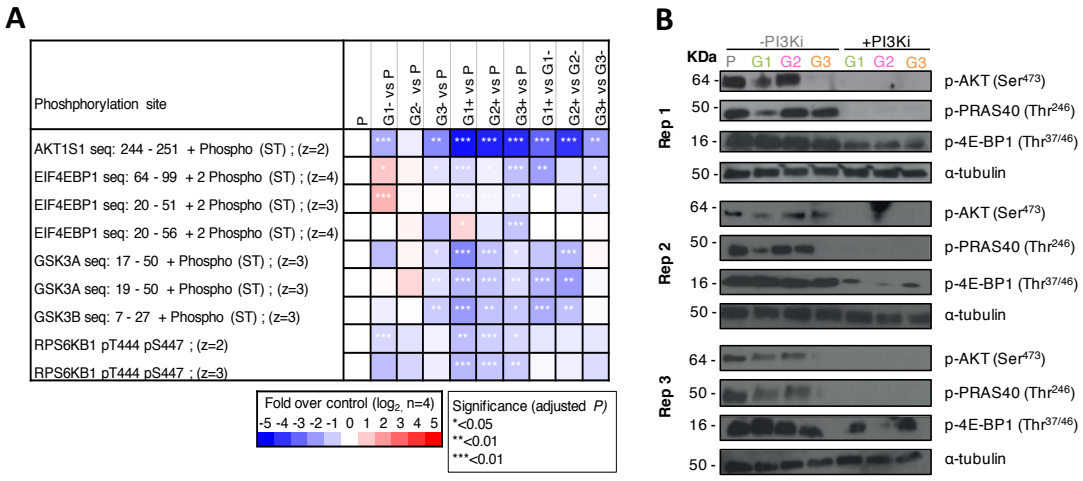

Figure 4.9 PI3K/mTOR signalling decreased in PI3Ki-resistant cells treated with PI3Ki and recovered after removal of the compound. (**A**) Heatmap of selected phosphorylation sites associated with the PI3K pathway activity. Information of the phosphopeptide is shown follows: gene name with sequence fragment and modification; phosphopeptide charge. Potential phosphorylation sites are reported as sites of phosphorylation if Mascot δ-score > 10. (**B**) Western blots (3 biological replicates) for phosphorylation sites markers of activity downstream of PI3K and α-tubulin loading control.

4.4.4 Examination of the status of c-MYC phosphorylation status in resistant cells

The phosphoproteomics dataset contained the phosphorylation of c-MYC at Thr[58]/Ser[62]. These sites are associated with c-MYC gene expression transactivation [302] and increased in PI3Ki-resistant cells (Fig 4.10). These data also showed that the c-MYC phosphorylation increased in resistant cells grown in culture media containing PI3Ki.

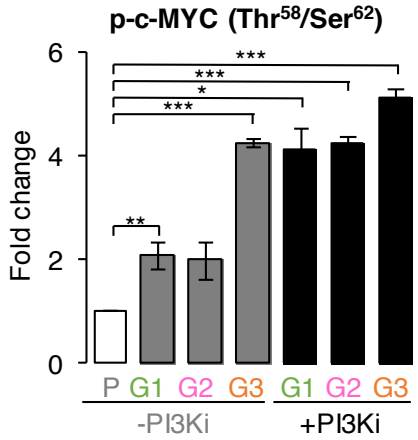

Figure 4.10 c-MYC phosphorylation increases in PI3Ki-resistant cells. Levels of p-c-MYC (Thr^{58}/Ser^{62}) in PI3Ki-resistant cells relative to parental cells. Phosphorylation data are represented as mean (n=4) ± SD. * $P < 0.05$; ** $P < 0.01$; *** $P < 0.001$.

4.4.5 Associations of the phosphoproteomes of resistant cells

To understand the relationships between the phosphoproteomes of PI3Ki-resistant cells, the consensus phosphorylation motifs present in the phosphoproteomics dataset were analysed. Hierarchical clustering of the mean $\log_2$ fold-change across common 173 specific phosphorylation motifs revealed similar patterns of association between PI3Ki-resistant cells to those observed previously (Figs 3.2 and 4.4). For example, the consensus phosphorylation motifs of G1+ and G2+ resistant cells grouped close together, whereas the same cells grown in the absence of PI3Ki (i.e. G1- and G2- resistant cells) grouped close and far from the cells treated with the PI3Ki (Fig 4.11). G3 resistant cells located far from G1 and G2 resistant cells in the dendogram. This result suggested that the abundance of peptides containing similar kinase recognition motifs was different across PI3Ki-resistant cells, and that treatment with PI3Ki changed the phosphoproteome profile of PI3Ki-resistant cells.

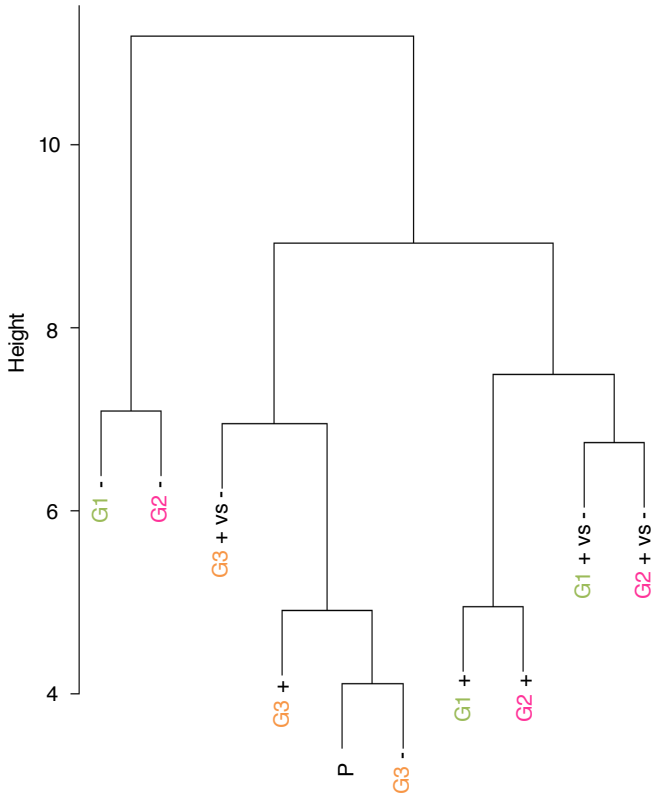

Figure 4.11 Relationship between the phosphoproteomes of parental and PI3Ki-resistant cells grown in the presence or in the absence of PI3Ki. Agglomerative hierarchical clustering of the Pearson correlation for the mean $\log_2$ fold-change of consensus phosphorylation motifs contained in the 7,056 peptides identified in the phosphoproteomic experiment (see text for details).

4.4.6 Classification of the phosphoproteomes of resistant cells

As with the analysis of the proteomes outlined above, to group the phosphoproteomics dataset of parental and PI3Ki-resistant cells, the phosphoproteomes of these cells were grouped into 6 clusters: groups that contained phosphopeptides that significantly increased (clusters 1-2; cluster 1: 101 peptides; cluster 2: 571 peptides; cluster 3: 426 peptides) or decreased (cluster 4 and cluster 6; cluster 4: 564 peptides; cluster 6: 69 peptides) in PI3Ki-resistant cells compared to parental cells (Fig 4.12A). The complete clustering analysis of the phosphoproteomic dataset is included in Appendix 4. Analysis of the phosphorylation sites present in cluster 1 using the KSEA algorithm to infer kinase activity [205], revealed an enrichment of substrates specific of MEK and CAMKII, suggesting a greater activity of these kinases in PI3Ki-resistant compared to parental cells (Fig 4.12B). The functional relevance of these kinases in PI3Ki-resistant cells was further evaluated and results will be discussed in Section 4.5.

Analysis of the biological processes associated to cluster 2 showed that processes involving oxidative stress (e.g. GO: 0016209 antioxidant activity and GO: 0005507 copper ion binding processes) were enriched in PI3Ki-resistant cells as a result of PI3Ki removal from the culture media (Fig 4.12C).

Among the phosphorylated proteins associated with increased redox activity in resistant cells upon PI3Ki withdrawal, were the member of the Prdx family peroxiredoxin-6 (PRDX6) phosphorylated at Thr^{44}, the selenoprotein S phosphorylated at Ser^{140} and the phosphorylation of TP53 most likely at Ser^{315}, the latter being a phosphorylation that inhibits stress-induced apoptosis responses [303] (Appendix 5). In agreement with the increased metabolic processes in PI3Ki-resistant cells during drug holidays observed in the proteomics dataset (Table 4.1), the phosphoproteomics dataset suggested that the metabolic activity of PI3Ki-resistant cells was enhanced upon PI3Ki removal from the culture media.

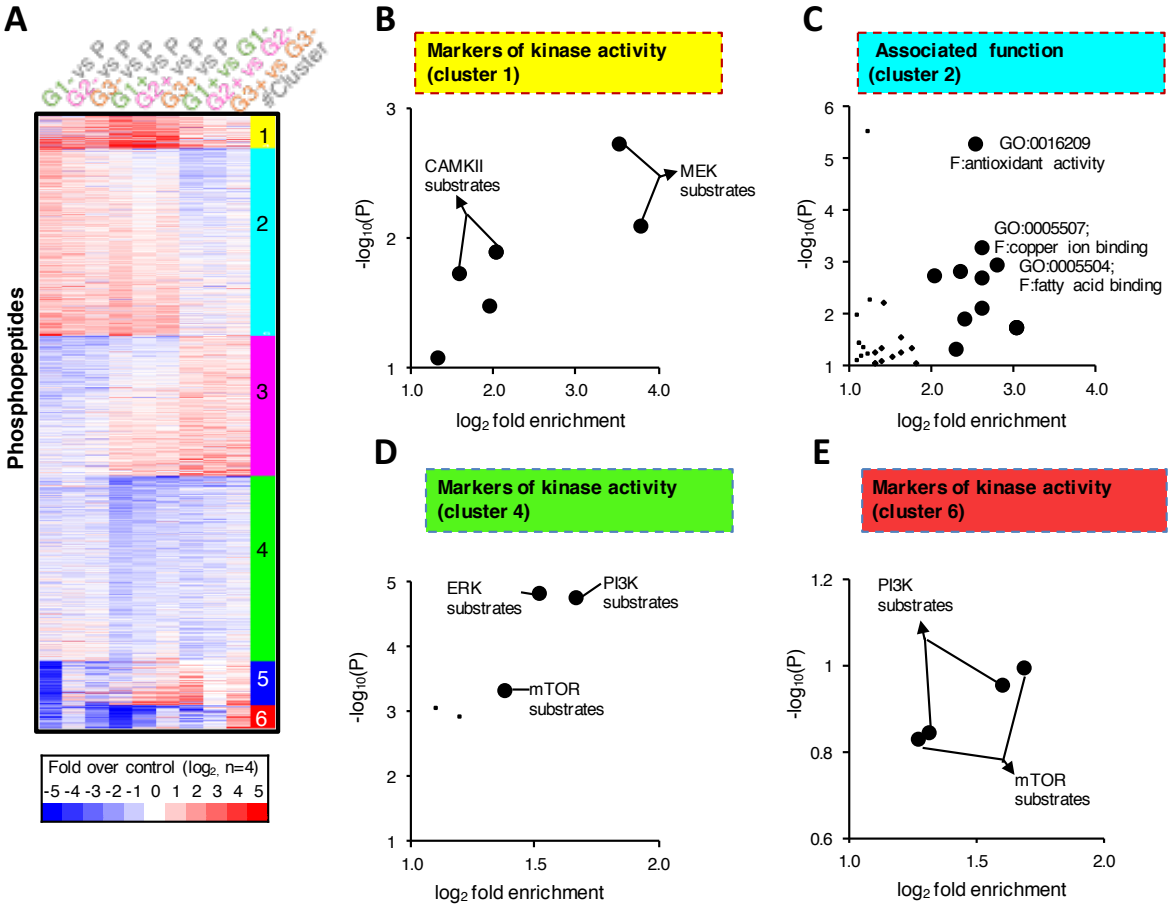

Figure 4.12 *K*-means consensus clustering for the phosphoproteomes of MCF7 parental and resistant cells identifies six subgroups. (**A**) *k*-means algorithm grouped phosphopeptides that increased (cluster 1-2) or decrease (4-6) in PI3Ki-resistant cells compared to parental. (**B**) KSEA analysis of phosphopeptides that increased in PI3Ki-resistant cells (cluster 1). (**C**) GO analysis of processes of phosphopeptides increased in PI3Ki-resistant cells relative to parental and upon the exposure of resistant cells to PI3Ki-treatment break (cluster 2). (**D**) KSEA analysis of phosphopeptides decreased in PI3Ki-resistant cells (cluster 4). (**E**) KSEA analysis of phosphopeptides decreased in PI3Ki-resistant cells (cluster 6).

Examination of the phosphorylation sites that decreased in PI3Ki-resistant cells (cluster 4 and cluster 6) revealed that the phosphorylation of substrates of PI3K and mTOR were reduced in PI3Ki-resistant

cells compared to parental cells, as expected (Fig 4.12D-E). Interestingly, the activity of AKT inferred as a function of the status of sites specifically phosphorylated by this kinase, was not reduced in PI3Ki-resistant cells treated with PI3Ki.

4.5 Effects of MEK and CAMKII inhibition on resistant cells

MEK and CAMKII, as well as PI3K, locate downstream of growth factor receptors (e.g. ERBB2), and a synergistic anti-tumour activity of the combination therapy with PI3K and MEK inhibitors has been demonstrated *in vitro* and *in vivo* [304]. It was therefore hypothesised that the MAPK and Calcium signalling pathways may be compensating for the lack of PI3K activity in PI3Ki-resistant cells.

To explore whether these kinases could mediate resistance to PI3K inhibition, the response to treatment with inhibitors against these kinases was determined in parental and PI3Ki-resistant cells by means of an MTS assay. For these experiments, the same number of parental and PI3Ki-resistant cells (0.02×10^6 per well) were seeded in triplicate in 96-well plates and treated with the indicated concentration of kinase inhibitors for 2 days. The results of these experiments showed that MEKi or CAMKIIi potentiated the effect of PI3Ki (Fig 4.13), suggesting that the activity of these kinases contribute to maintain the PI3Ki-resistant phenotype.

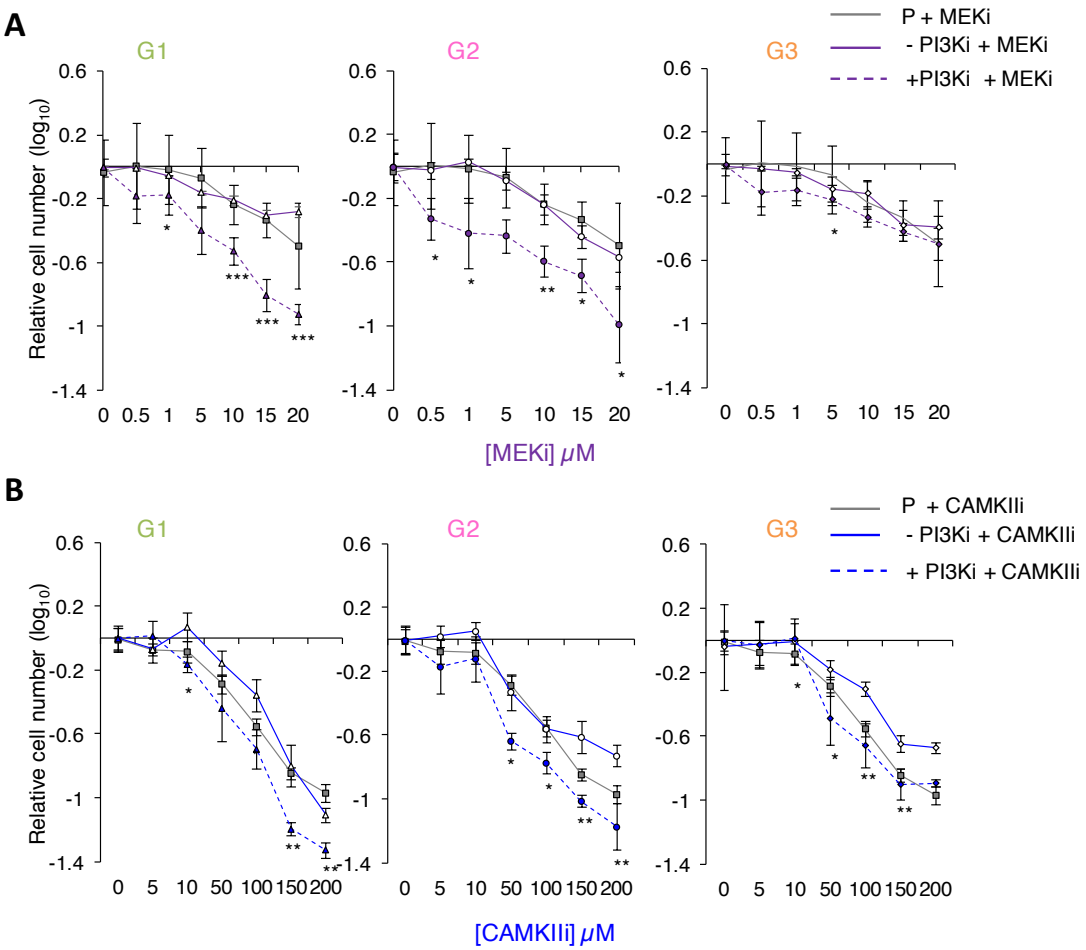

Figure 4.13 MEK and CAMKII inhibitors potentiate the effect of the PI3K inhibitor reducing the proliferation of PI3Ki-resistant cells. Relative cell number of parental and resistant cells measured after 2 days of treatment with MEK inhibitor (**A**) or CAMKII inhibitor (**B**), normalised to control. Data are represented as mean ± SD (*n*=3, three independent technical replicates). *P*-values were calculated for PI3Ki-resistant cells treated with PI3Ki alone against combination treatment using an unpaired, two-tail Student's t-test. * $P < 0.05$; ** $P < 0.01$; *** $P < 0.001$. PI3Ki, GDC-0941 (1 μM); MEKi, GSK1120212; CAMKIIi, KN-93.

4.6 Conclusions

The overall aim of the experiments described in this Chapter was to characterise the biochemistry of PI3Ki-resistant cells using MS-based proteomics and phosphoproteomics approaches (Fig 4.1). These experiments revealed numerous differences between the proteomes of parental and PI3Ki-resistant cells (Figs 4.3). Pathway enrichment analysis of cells proteomes unveiled that proteins involved in metabolic and transcriptional processes were increased in PI3Ki-resistant cells during drug holidays (Table 4.1). Moreover, analysis of the proteomes of resistant cells using the NCI pathway database and GO terms revealed that proteins included in processes associated with translation, and c-MYC and HIF transcriptional activity increased in PI3Ki-resistant cells compared to the proteome of parental cells (Fig 4.6A-D).

Similarly to what was observed for the proteomes of PI3Ki-resistant cells, the phosphoproteomes of these cells were different from parental cells, as revealed by the number of differentially modulated phosphopeptides of these cells (Fig 4.8). Markers of activity of kinase members of the PI3K/AKT/mTOR signalling cascade derived both from the phosphoproteomics dataset as well as from immunoblotting experiments provided evidence to support the hypothesis that the PI3K/AKT/mTOR pathway remained inhibited during chronic PI3Ki treatment, and that this pathway was reactivated upon PI3Ki removal (Fig 4.9). One interesting observation was that the remodelling underwent by PI3Ki-resistant cells after drug withdrawal did not bring the phosphoproteome of these cells to the initial state of parental cells, but rather different signalling network landscapes. This was shown by the phosphorylation motifs present in PI3Ki-resistant cells compared to those in parental cells (Fig 4.11), and the by the profile of the phosphoproteomes of PI3Ki-resistant cells compared to the phosphoproteome of parental cells (Fig 4.12A).

Analysis of predicted kinase activities reported an increased activity of CAMKII and MEK in PI3Ki-resistant cells (Fig 4.12B), and combination of compounds that target PI3K and CAMKII or MEK reduced the proliferation of PI3Ki-resistant cells to a greater extent the single treatment, suggesting that CAMKII and MEK kinases mediated the resistance to PI3K inhibition (Fig 4.13).

To summarise, MS-based proteomics and phosphoproteomics approaches were used to investigate the modulations of pathways in cells that had acquired resistance to PI3Ki, as well as the pathways changes in those cells upon removal of the selection drug (i.e. 1 μM GDC-0941). These experiments showed that PI3Ki-resistant cells increased the levels of several proteins involved in various metabolic processes compared to parental cells (Fig 4.5 and Appendix 1), and revealed that PI3Ki-resistant cells during drug holidays increased the levels of proteins associated with different metabolic process, including pentose phosphate pathway and gluconeogenesis (Fig 4.5A and Table 4.1). In addition, the phosphoproteomics dataset reveal profound signalling changes in PI3Ki-resistant cells (e.g. enrichment of substrates of MEK and CAMKII) as well as increase redox activity of PI3Ki-resistant cell during drug holidays.

The metabolic features of PI3Ki/mTORi-resistant cells during treatment and drug holidays were then investigated and presented in the next Chapter.

Chapter 5. Metabolic adaptations of models of acquired resistance to PI3K/mTOR inhibitors

5.1 Introduction and aims of the study

The results presented in Chapter 4 detailed the changes in the proteomes and signalling pathways of PI3Ki-resistant cells grown with the PI3Ki or on its absence, highlighting the molecular changes undergone by PI3Ki-resistant cells and the degree of heterogeneity between these cell lines. These data also demonstrated that proteins that have a role in metabolic processes were modulated in PI3Ki-resistant cells exposed to drug holidays.

In addition, during routine cell culture it was consistently appreciated that PI3Ki-resistant cells acidified the culture media to a greater extent than parental cells, which was considered to be an indicator of an altered metabolism in these models.

Therefore, the aim of the experiments presented in this Chapter was to characterise the bioenergetic status of parental and resistant cells that had acquired resistance to PI3K inhibition as well as the response of the metabolism of drug-resistant cells to drug withdrawal. The mechanisms underlying such metabolism were also examined. Lastly, the metabolism of seven additional pairs of parental/resistant cells with acquired resistance to PI3K/mTOR inhibition was characterised (Fig 5.1).

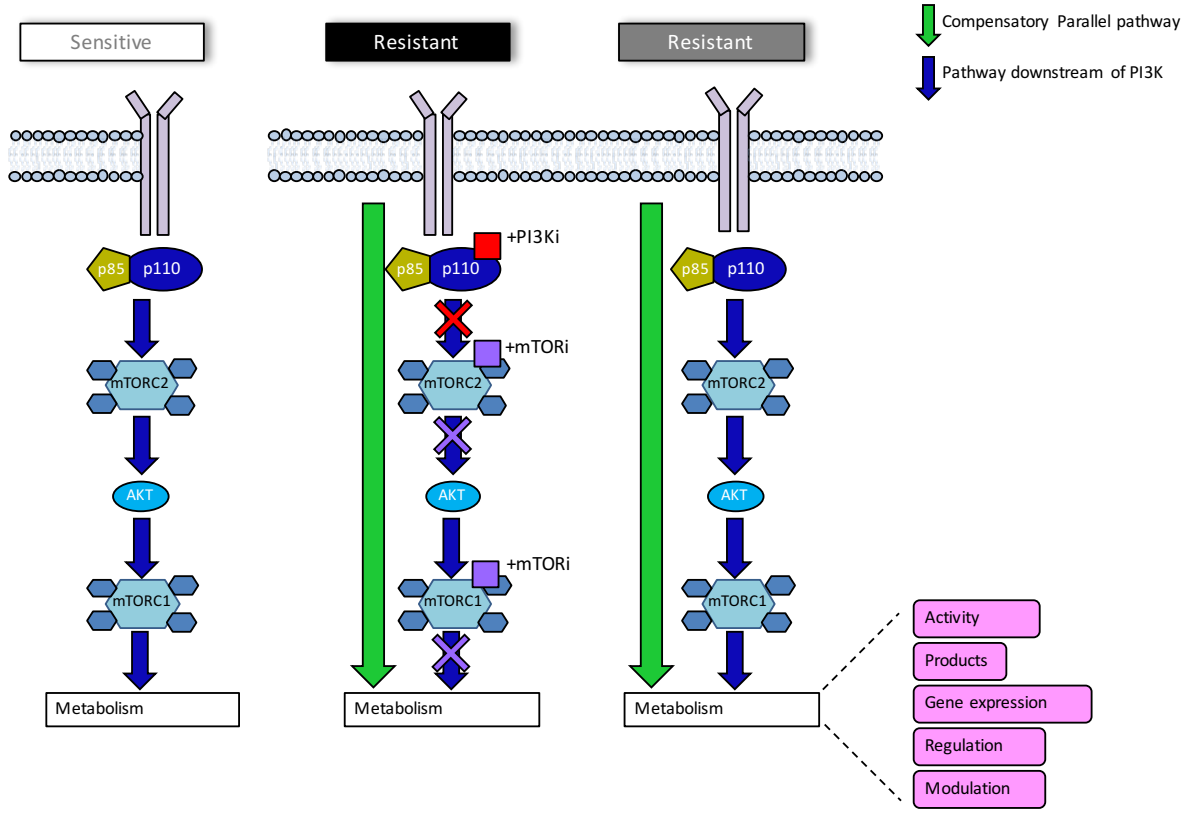

Figure 5.1 Overview of the metabolic profile investigations of models of acquired resistance to PI3Ki. Parental cells regulate their metabolism to maintain a metabolic homeostasis. During the development of resistance to kinase-targeted treatment, enhancement of alternative pathways maintains the metabolic activity of resistant cells. When selection drug (e.g. PI3Ki or mTORC1/2i) is removed, supra-physiological metabolic input levels may emerge if the signalling pathways that compensate for the absence of chronically inhibited signalling are not restored to signalling levels of parental cells. The bioenergetic activity, metabolic-derived products, expression of metabolic genes, regulation of the metabolic phenotype, and response to modulation of the metabolism of cells that had acquired resistance to PI3Ki (as presented and discussed in Chapters 3 and 4) was analysed. An additional panel of seven pairs of sensitive/resistant cells resistant to mTORC1/2 inhibition [226] and PI3Kα inhibition [305] were included to analyse the bioenergetics profile and quantify the metabolism-derived products of those models.

5.2 Defining the effects of drug holidays on metabolism

As mentioned above, during routine culture of PI3Ki-resistant cells, it became apparent that some PI3Ki-resistant cells exposed to drug holidays conditions — especially G2- resistant cells — turned the culture media yellow quicker that parental cells, indicating greater acidification rate. To examine this phenomenon more in detail, equal number of cells (0.2×10^6 per well) were seeded in 6-well plates and maintained with either 1 µM GDC-0941 or 0.1% DMSO for 5 days. The extracellular acidity of the media was measured with a pH meter, used as a proxy of the cellular proton efflux rate. The resulting data, shown in Fig 5.2A, revealed that PI3Ki-resistant cells grown in the absence of PI3Ki increased the acidification of culture media compared to the same cells grown in the presence of the compound.

The extent of this increase was different across resistant cell lines. For example, G2- cells acidified the media to pH 6.86, whereas G1- and G3- cells acidified the media to pH 7.32 and 7.37, respectively. Parental cells did not acidify the media to a great extent (pH 7.73). Treatment of PI3Ki-resistant cells with PI3Ki prevented the acidification of media: G1+ cells acidified the growth media up to pH 7.70; G2+ cells acidified the growth media up to pH 7.62 and G3+ cells acidified the growth media up to pH 7.64. The glycolytic phenotype of PI3Ki-resistant cells was proved to be reversible, since drug readministration reverted the initial phenotype (Fig 5.2B).

The oxidative capacity of parental and PI3Ki-resistant cells exposed to the absence and presence of PI3Ki was then quantified by the ability of cells to oxidise the 3-(4,5-dimethylthiazol-2-yl)-5-(3-carboxymethoxyphenyl)-2-(4-sulfophenyl)-2H-tetrazolium (MTS) reagent. Equal number of cells (0.02 x 10^6 per well) were seeded in 96-well plates and the cells were maintained with either 1 μM GDC-0941 or 0.1% DMSO for 1, 2, 3 or 5 days. The production of formazan from the MTS assay by the cellular oxidoreductase enzymes was used as a surrogate measure for the oxidative activity of cells at the given time-points. The experiment was performed in triplicate. The data shown in Fig 5.2C demonstrated that exposure of PI3Ki-resistant cells to drug holidays led to increase oxidative activity of these cells. Thus, after 5 days in drug holidays, the oxidative activity of G1- cells was 1.46-fold higher compared to that one of G1+ cells; the oxidative activity of G2- cells was 1.48-fold higher compared to that one of G2+ cells; and the oxidative activity of G3- cells was 1.43-fold higher compared to that one of G3+ cells (Fig 5.2C).

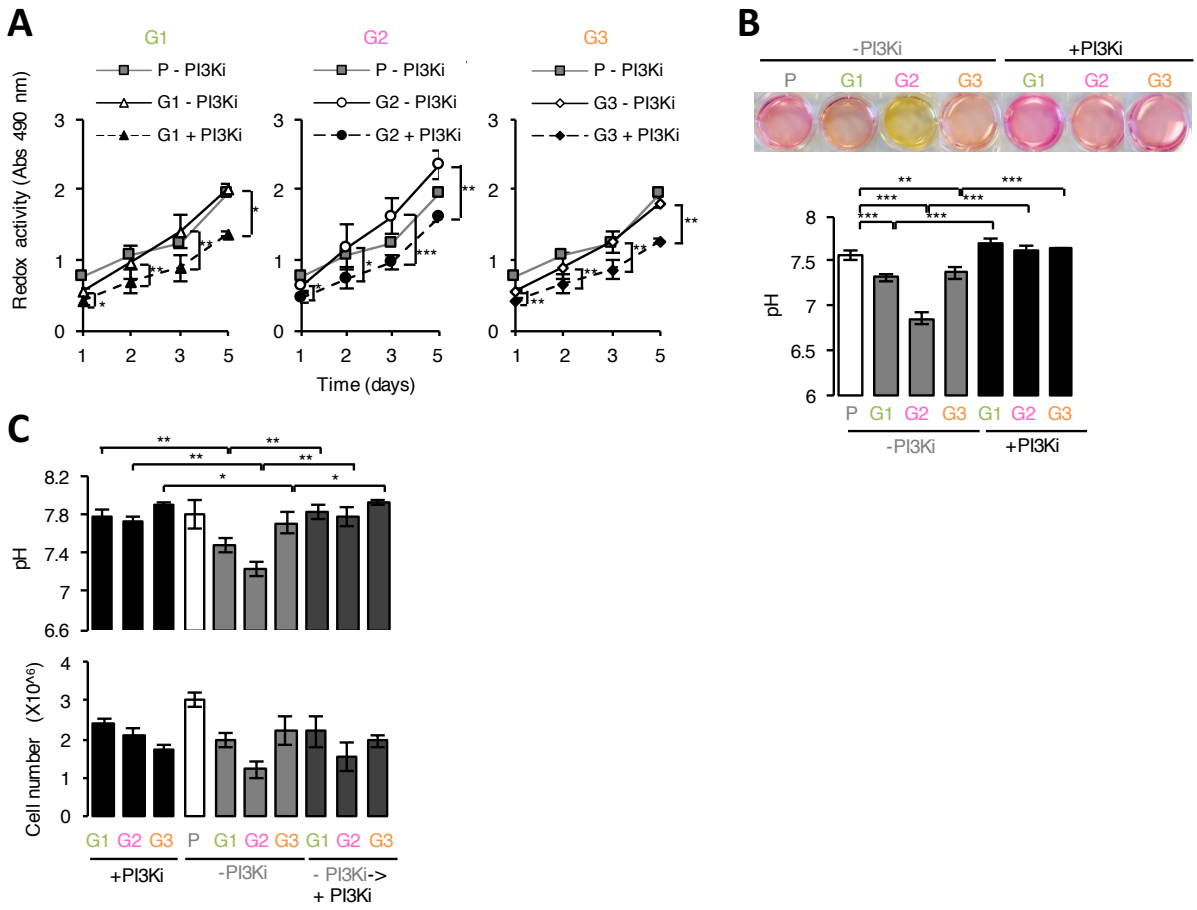

Figure 5.2 Drug removal from resistant cells results in increased cellular redox potential and media acidification (**A**) Representative media images and pH values of media where parental and resistant cells were grown for 5 days in the absence or presence of PI3Ki. (**B**) pH values and number of parental and PI3Ki-resistant cells cultured for 10 days in the presence of GDC-0941 (+PI3Ki) or in the absence of GDC-0941 (-PI3Ki) or for 5 days with vehicle control followed by 5 days with GDC-0941 (-PI3Ki -> +PI3Ki). (**C**) MTS oxidoreductases activity of parental and resistant cells maintained in the absence or presence PI3Ki measured at the indicated times. Data are represented as mean ± SD ($n \geq 3$, independent biological replicates). *P*-values were calculated using an unpaired, two-tail Student's *t*-test comparing as indicated; * $P < 0.05$; ** $P < 0.01$; *** $P < 0.001$.

5.3 Optimisation of the Seahorse methodology parameters

To conduct a more precise and sensitive analysis of the bioenergetic profile of parental and PI3Ki-resistant cells, the Seahorse bio-flux machine was used to measure fluctuations in media O_2 and pH. Given that the accuracy of the Seahorse analysis relies on the LED sensors precision to measure such oscillations, the performance of LED sensors was monitored along the experiments implemented in this machine. Accordingly, the LED status across experiments was recorded as "good", and the O_2 and pH were within the range values recommended by the manufacturer (i.e. 10,000 and 25,000 for O_2 and pH emission, respectively) (Appendix 6).

A series of optimisation steps were performed to maximise the outcome of the Seahorse experiments. Initially, given that the performance of the sensors depends on the physical chamber of media created by the cells as well as on the measuring time, the optimal cell seeding density and the instrument timing-framework measurements were determined. To achieve this, and based on published findings [306], initially 50,000 MCF7 cells per well were seeded and the instrument parameters were set to default (i.e. mixing time: 2 min; calibrating time: 2 min; and measuring time: 2 min). The result of these experiment showed that the average mitochondria activity (inferred from the oxygen consumption rate [OCR]) and capacity to acidify the media (inferred from the extracellular acidification rate [ECAR]) were 46 pMoles/min and 2 pMoles/min, respectively (Fig 5.3A). Following the Seahorse manufacturer's recommendation to set up a basal OCR within 50-400 pMoles/min and a basal ECAR within 20-120 mpH/min, the number of cells was increased to 80,000 cells/well for further testing, to increase the degree of cell confluence and the amount of oxygen consumed as well as the capacity of acidifying the extracellular milieu. The result of this initial experiment also led to the decision to increase the operational cycles length to gain consistency across measurement acquisitions (i.e. mixing time: 3 min; calibrating time: 2 min; and measuring time: 4 min). Subsequently, the concentration of mitochondrial inhibitors injected was optimised to obtain maximal effect. To this end, 2 µM and 1.5 µM of the ionophore FCCP were titrated, and 1 µM oligomycin was tested. The result of this experiment showed that 2 µM of FCCP produced highest electron transport uncoupling from the ATP synthase, providing maximal stimulation of cellular respiratory activity (Fig 5.3B). These data also showed that 1 µM oligomycin was insufficient to decrease the respiratory activity to minimum levels. Therefore, 5µM of the ATP synthase inhibitor oligomycin was selected for further experiments to maximise the ATP synthase inhibition. Moreover, and based on the literature [306, 307], 1 µM antimycin and 1 µM rotenone were selected for subsequent experiments to reduce the non-mitochondrial respiration to background levels.

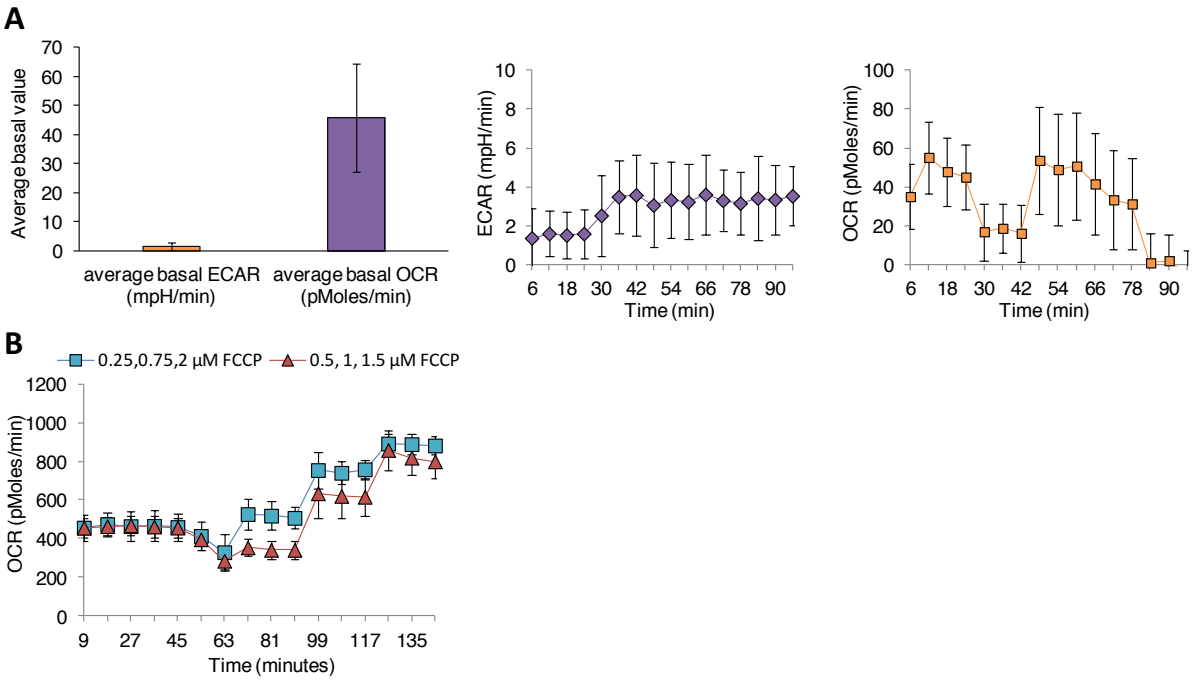

Figure 5.3 Optimisation of the number of cells, Seahorse instrument timing parameters and mitochondrial drugs concentrations. (**A**) Average basal ECAR and OCR values measured after seeding 50,000 MCF7 parental cells (left panel). Line graph of ECAR and OCR values after seeding 50,000 MCF7 parental cells (right panel). (**B**) Line graph of OCR values after treatment of cells with 1.5 µM or 2 µM FCCP. In this experiment 1 µM of oligomycin was used to inhibit the ATP synthase.

5.4 Examination of bioenergetic profile of resistant cells

Having optimised the Seahorse methodology, the bioenergetic metabolism of parental and PI3Ki-resistant cells maintained in the presence of PI3Ki or on its absence was investigated. For the aim of these experiments, a total of 80,000 cells were concentrated in 150 µL culture medium (as described in Section 2.7.2). Four consecutive measurements of each well were obtained before the addition of the mitochondrial inhibitory compounds and three measurements were recorded after those (i.e. basal respiration). Data from three wells per experiment were combined across replicates. The experiment was performed in triplicates.

These experiments demonstrated that the respiratory (Fig 5.4A) and glycolytic profile (Fig 5.4B) of PI3Ki-resistant cells changed because of PI3Ki removal from cell culture media.

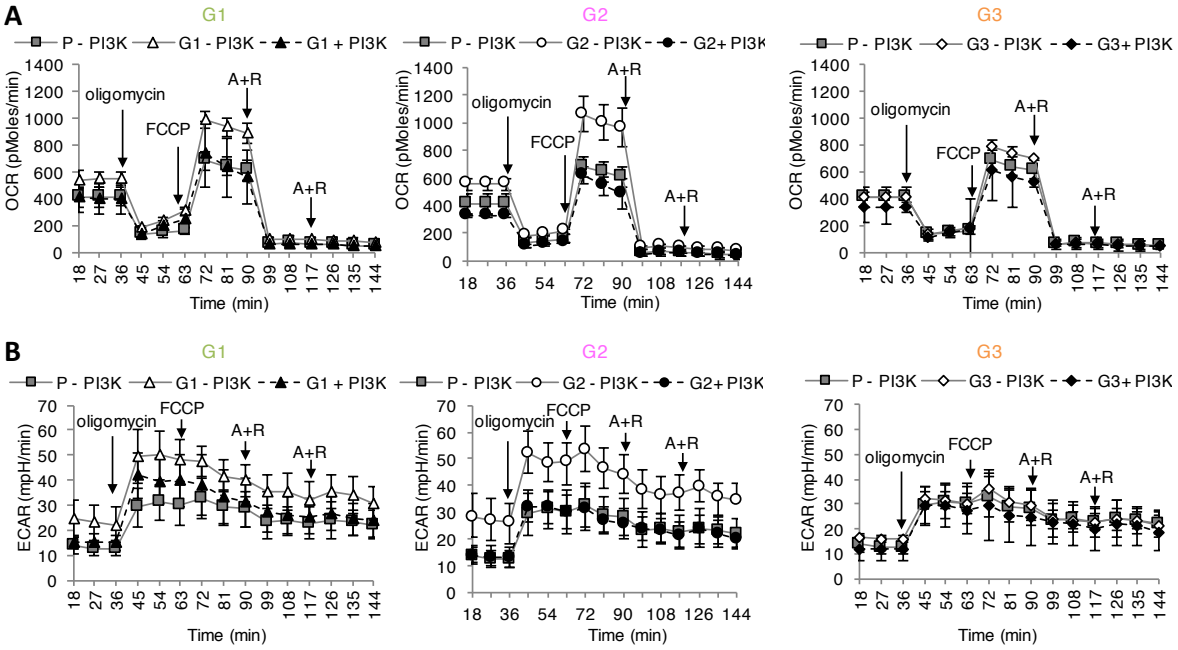

Figure 5.4 PI3Ki-resistant cells increase their mitochondrial and glycolytic activity after drug removal. (**A**) OCR profile of parental and PI3Ki-resistant cells grown in the presence or in the absence of PI3Ki. (**B**) ECAR profile measured in the same cells as in (**A**). Data are represented as mean ± SD (*n*=3, independent biological replicates). O, oligomycin; FCCP [carbonyl cyanide 4-(trifluoromethoxy) phenylhydrazone]; A, antymycin; R, rotenone.

Extraction from these data of the response of each of the components of the ETC to each modulator target (as described in Section 2.7.2; Fig 2.1) showed that the basal respiration, i.e. the amount of O_2 consumed by cells to fulfil the ATP demand, significantly increased in G1- and G2- cells as a result of PI3Ki withdrawal (Fig 5.5A). Moreover, the ATP production, i.e. the proportion of respiration used by cells to generate ATP, increased from 281 pMoles/min to 358 pMoles/min in G2- cells after removal of PI3Ki (Fig 5.5B). Maximal respiration capacity, i.e. the greatest rate of respiration achievable by cells, was significantly elevated in PI3Ki-resistant cells on drug holidays conditions: 1.5-fold greater for G1- cells (*P*= 0.007), 1.8- fold greater for G2- cells (*P*= 0.001), and 1.3-fold greater for G3- cells (*P*= 0.008) and, in these conditions, was significantly higher compared to that of parental cells (Fig 5.5C). The proton leak, a proxy of mitochondrial damage, did not increase in G1- and G2- cells and increased in G3- cells (Fig 5.5D). Non-mitochondrial respiration increased in G1- resistant cells as a result of drug holidays (Fig 5.5E). Basal glycolysis, inferred by the acidification of media caused by the glycolytic flux, increased in PI3Ki-resistant cells maintained on drug holidays compared to the same cells treated with the PI3Ki (Fig 5.5F). Blockade of the ATP synthase prompts glycolytic activity and media acidification to sustain the levels of energy produced by mitochondria. Fig 5.5G showed that the media acidification after treatment with oligomycin in PI3Ki-resistant cells withdrawn from PI3Ki was not significantly higher compared to media acidification by the same cells maintained with PI3Ki.

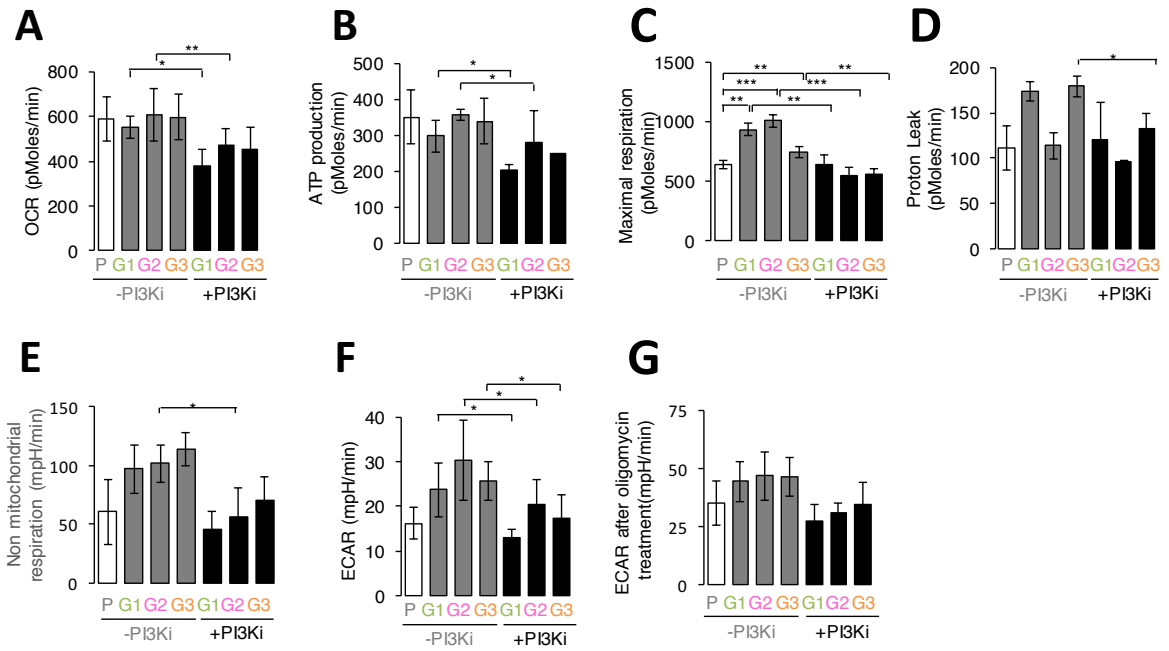

Figure 5.5 Main parameters associated to mitochondrial and glycolytic functions for parental and PI3Ki-resistant cells (**A**) Basal OCR extracted from values in Figure 5.4A. (**B**) ATP production extracted from values in Figure 5.4A. (**C**) Maximal respiration extracted from values in Figure 5.4A. (**D**) Proton Leak extracted from values in Figure 5.4A. (**E**) Non mitochondrial respiration extracted from values in Figure 5.4A. (**F**) Basal ECAR extracted from values in Figure 5.4B. (**G**) ECAR after oligomycin treatment extracted from values in Figure 5.4B. *P*-values were calculated using an unpaired, two-tail Student's *t*-test comparing as indicated; * $P < 0.05$; ** $P < 0.01$; *** $P < 0.001$.

5.5 Changes in the extracellular lactic acid upon exposure to drug holidays

The contribution of CO_2, product of the TCA, to the cellular acidification is derived from the CO_2 hydration to H_2CO_3 and further dissociation to HCO_3^- and H^+. Although this contribution is minimal compared to the glycolytic-derived acidification, it could be partially responsible for the observed ECAR values [308]. An experiment was designed to quantify the amount of lactic acid, product of the glycolytic activity, in the culture media used to grow in triplicates parental and PI3Ki-resistant cells either with 0.1% DMSO or PI3Ki for 5 days. Liquid extraction was used to extract lactic acid from the growth media. Prior to measurement of lactic acid by comparison to a lactic acid standard, quantification of lactic acid from the standard curve was performed as mentioned in Section 2.7.1 (Appendix 7). The resulting analysis demonstrated that the amount of lactic acid in the culture media where PI3Ki-resistant cells were grown increased as a function of PI3Ki removal from the media (Fig 5.6A).

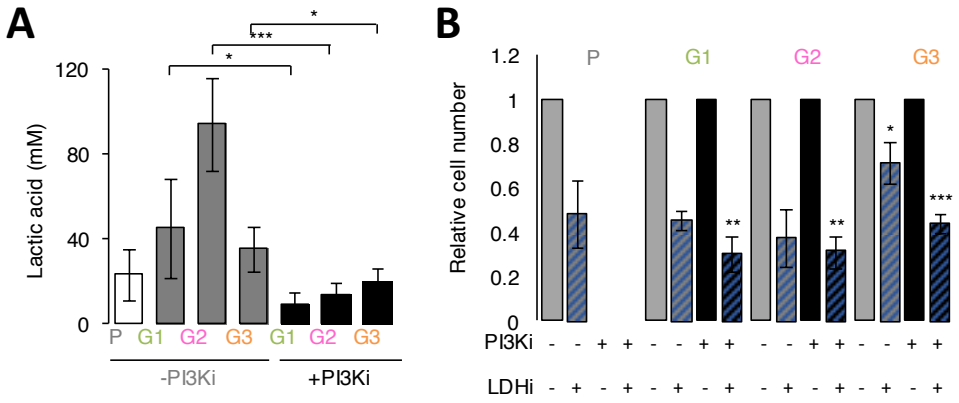

Figure 5.6 Resistant cells increase the production of lactic acid upon removal of PI3Ki and reduction of lactic acid production impairs their proliferation. (**A**) Lactic acid values of parental and resistant cells maintained in the presence or the absence of PI3Ki. (**B**) Proliferation of cells as a function of treatment with 1 µM GDC-0941 (PI3Ki), 40 mM oxamate or combination of both for 5 days. Values are mean ± SD (*n*=3, independent biological experiments). *P*-values were calculated using an unpaired, two-tail Student's *t*-test comparing each cell line against the lack of treatment. * $P < 0.05$; ** $P < 0.01$; *** $P < 0.001$.

To determine whether the produced lactic acid was detrimental for proliferation of parental and PI3Ki-resistant cells, lactic acid production was inhibited by treatment of the cells with the pyruvate analogue oxamate. For this experiment, 0.2 x 10^6 cells were seeded in 6-well plates and cells were treated with 1 µM GDC-0941, 40 mM of oxamate, 0.1% DMSO or the combination for 5 days. The resulting data, shown in Fig 5.6B, revealed that the LDH competitor oxamate reduced the viability of parental and PI3Ki-resistance cells to a similar extent.

5.6 Changes in intracellular free radicals upon drug holidays exposure

The experiments presented in Sections 5.4 and 5.5 indicated that a break from PI3Ki treatment led to an increase mitochondrial activity as well as increase glycolytic activity that yielded net increase of extracellular lactic acid measured in the culture media of PI3Ki-resistant cells. It was therefore hypothesised that the levels of ROS, which could derived from the mitochondrial respiratory activity, may increase in PI3Ki-resistant cells after a period of drug holidays.

To monitor the amount of intracellular ROS in parental and PI3Ki-resistant cells grown with or without PI3Ki, the levels of ROS were determined after 7 days culture by means of the well-established fluorescence-based probe DCFH-DA (see Section 2.7.4). The experiment was performed in triplicate and seven field images were taken per experiment. The data shown in Fig 5.7A demonstrated that PI3Ki-resistant cells increased the intracellular ROS content after removal of PI3Ki from the culture media (See Appendix 8 for all the images taken in these experiments). The ROS signal was 1.9-fold

times higher (*P*= 0.004) in G2- cells compared to G2+ cells and 1.8-fold times higher (*P*= 0.005) in G1- cells compared G1+ cells. This was consistent with the observed increased basal mitochondrial activity of these cells (Fig 5.5A). Moreover, G1- cells showed 1.6-fold times higher ROS levels (*P*= 0.005) compared to the ROS levels of parental cells and G2- cells showed 1.4 -fold times higher ROS levels (*P*= 0.004) compared to the ROS levels of parental cells, indicative of higher accumulation of free radicals in G1- and G2- resistant cells (Fig 5.7A).

To understand the impact of intracellular ROS accumulation on the proliferation of PI3Ki-resistant cells, ROS were down-regulated by the free radical quencher *N*-acetyl cysteine (NAC). Initially, the capacity of NAC to quench free radicals was assessed by measuring the DCFH-DA intensity after treatment with 1 µM of GDC-0941, 200 µM of NAC, 0.1% DMSO or combinations for 7 days, with daily culture media replacements. The number of viable cells at that time was also measured using a Vi-CELL counter. The experiment was performed in triplicate. The data shown in Fig 5.7B demonstrated that the fluorescence, derived from the oxidative activity of reactive species, was diminished after treatment with NAC, confirming that NAC reduced the levels of free radicals in parental and PI3Ki-resistant cells. The resulting data also showed that dousing ROS levels contributed to the proliferation of those cells with high ROS levels, e.g. G2- resistant cells, while reducing the proliferation of those cells with lower ROS levels (Fig 5.7B). The response of cells proliferation after longer treatment with NAC (14 days) was then explored. In agreement with the previous observations, this experiment showed that antioxidant treatment enhanced the proliferation of cells that accumulate high levels of ROS, but reduced the proliferation of cells with lower ROS levels. For example, after two weeks of treatment with NAC, the number of G1- resistant cells increased by 1.74-fold (P = 1.74E-02), the number of G2- resistant cells increased by 1.69-fold (*P* = 3.39E-04), but the number of parental cells decreased by 1.99-fold (*P* =2.94E-04).

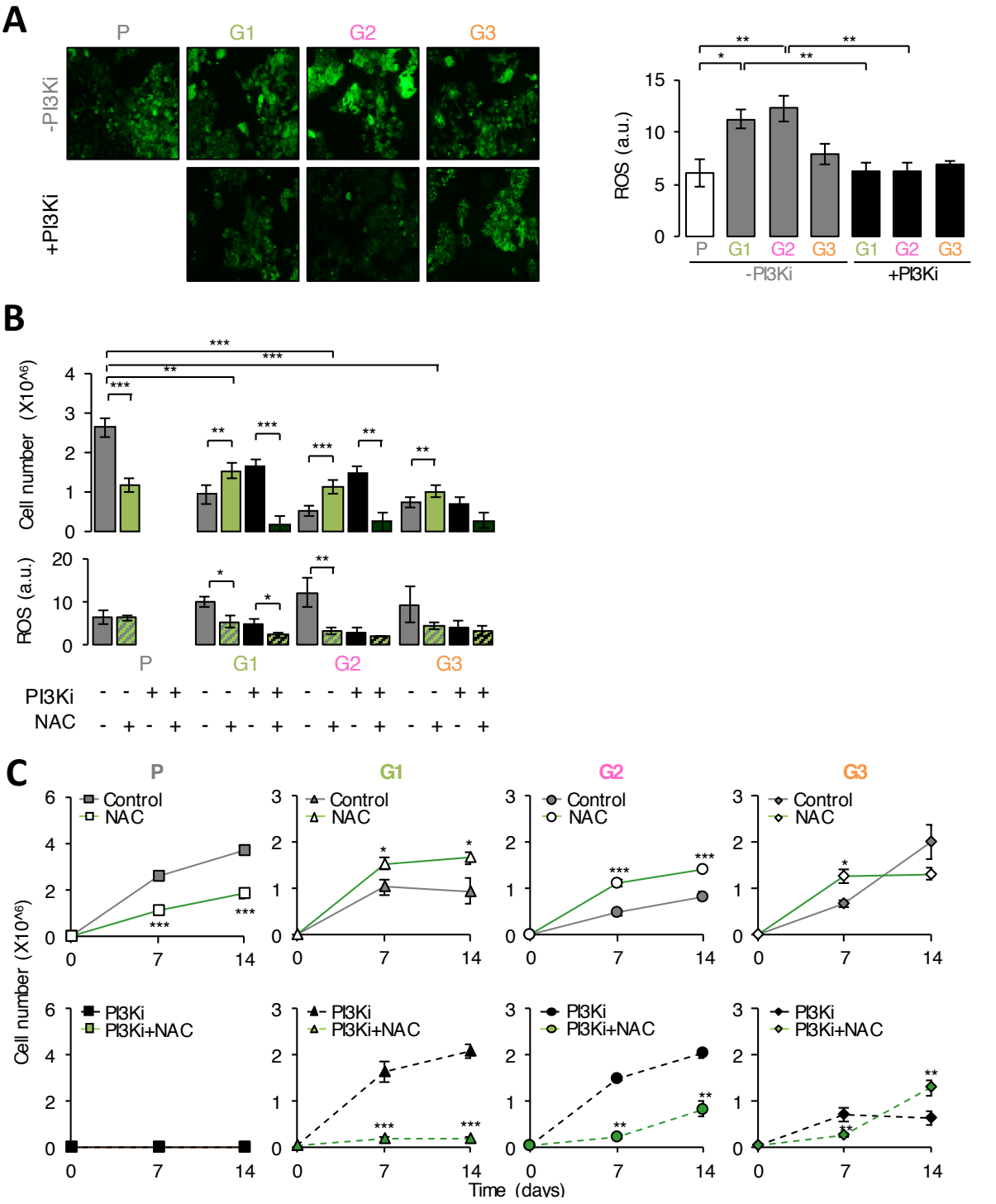

Figure 5.7 Resistant cell during drug holidays produced a toxic content of ROS that can be reduced by free radical scavengers. (**A**) Representative images and ROS levels of parental and PI3Ki-resistant cells grown with or without PI3Ki for 7 days. (**B**) Proliferation of cells and quantification of ROS after 7 days treatment with 1 µM GDC-0941 (PI3Ki), 200 µM NAC or combination. ROS values are mean ± SD (*n*=3 images). (**C**) Number of cells as a function of treatment with 1 µM GDC-0941 (PI3Ki), 200 µM NAC or combination of both for 7 and 14 days. Media were replaced daily. *P*-values were calculated using an unpaired, two-tail Student's *t*-test comparing as indicated. * $P < 0.05$; ** $P < 0.01$; *** $P < 0.001$.

The effect of a lipophilic ROS attenuator, α-tocopherol, on the proliferation of parental and PI3Ki-resistant cells was then tested. The result of these data showed that this antioxidant reduced the proliferation of parental cells (Fig 5.8). The proliferation of G2- cells was promoted by α-tocopherol, in a concentration dependent manner; thus, the proliferation rate of G2- resistant cells was higher after treatment with up to 20 µM α-tocopherol.

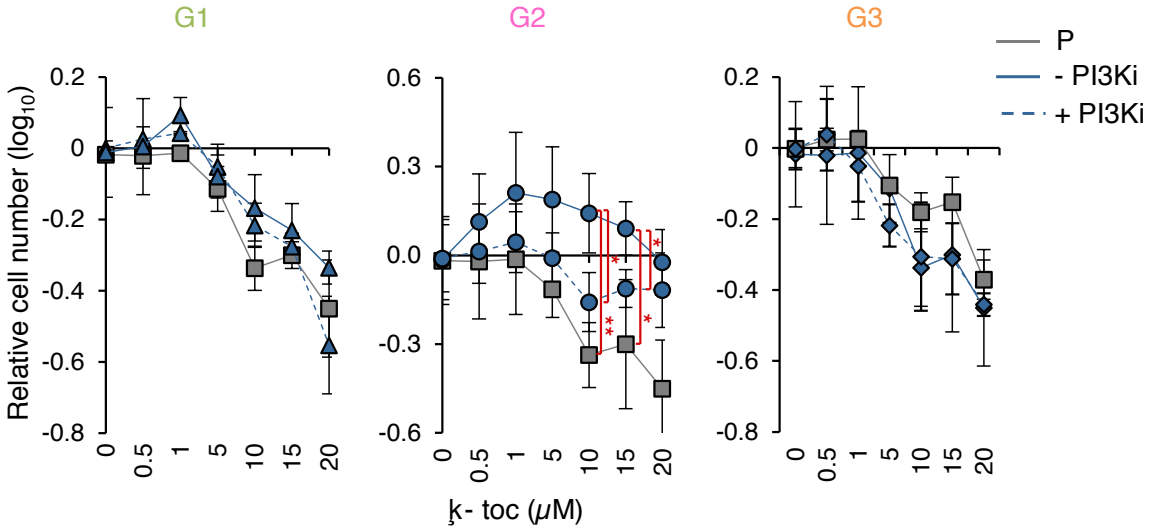

Figure 5.8 Relative cell numbers as a function of treatment with α-tocopherol. Parental cells were exposed to increasing concentrations of α-tocopherol (grey line) and resistant cells were exposed to increasing concentrations of α-tocopherol in the presence (dash line) or absence (continuous line) of GDC-0941. Before α-tocopherol treatment, resistant cells were grown for 7 days in the presence or absence of GDC-0941. Cell proliferation was assessed using the crystal violet assay. Data are represented as mean ± SD (*n*=3, three technical replicates). *P*-values were calculated using an unpaired, two-tail Student's *t*-test comparing as indicated. * $P < 0.05$; ** $P < 0.01$; *** $P < 0.001$.

5.7 Transcript levels of selected metabolic genes

To profile the changes in expression of genes usually associated to metabolic activity in PI3Ki-resistance cells, the transcription levels of 76 genes involved in 15 metabolic pathways were quantified. For this purpose, 1 x 10^6 parental and PI3Ki-resistant cells grown with and without PI3Ki were pelleted into RNA free tubes. After RNA extraction, transcripts were pre-amplified by qRT-PCR.

Differential abundance analysis highlighted the modulation of metabolic transcripts in PI3Ki-resistant cells compared to parental cells, and this modulation was conditional of the presence of PI3Ki (Fig 5.9). Thus, the number of metabolic transcripts increased in PI3Ki-resistant cells grown without PI3Ki (i.e. 37, 27, and 14 transcripts were significantly up-regulated in G1-, G2- and G3- resistant cells, respectively, compared to parental cells). However, the number of metabolic transcripts decreased in PI3Ki-resistant cells grown with PI3Ki (i.e. 51, 42, and 44 transcripts had significantly lower levels in G1+, G2+ and G3+ resistant cells, respectively, compared to those for parental cells).

The expression of genes that belong to 15 metabolic pathways in PI3Ki-resistant cells as a function of PI3Ki treatment was then analysed. Fig 5.10 showed that removal of PI3Ki led to increased expression of genes involved in multiple metabolic processes in PI3Ki-resistant cells. Interestingly, genes whose expression is modulated by the transcriptional activity of HIF [309], including HIF itself, demonstrated increased expression when PI3Ki was removed (Fig 5.10, purple arrows). This analysis also revealed a degree of heterogeneity in the expression of metabolic genes between PI3Ki-resistant cells, and captured the transcription profile proximity of G1- and G2- cells (Fig 5.10).

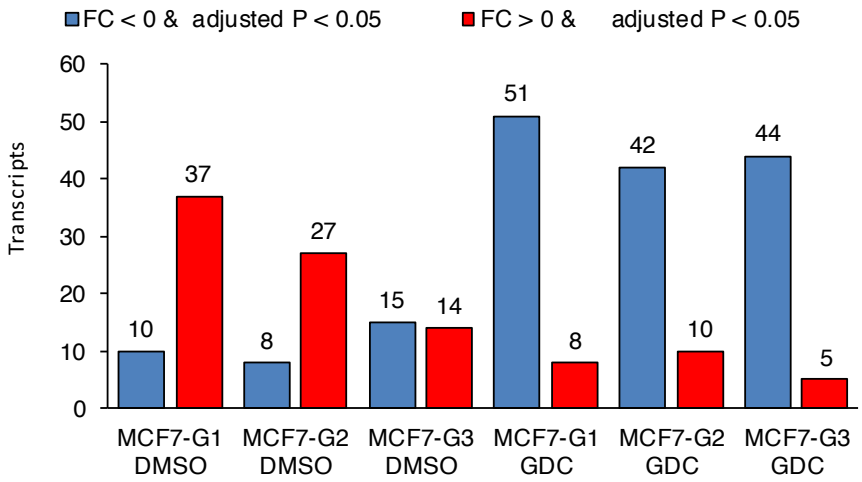

Figure 5.9 Differential abundance of transcript levels showing the number of transcripts that either significantly (FDR<0.05) decreased (blue bars) or increased (red bars) in abundance compared to parental cells. FC, $\log_2$ fold-change vs P; adjusted *P*, is the corrected *P*-value for multiple testing by the Benjamini-Hochberg method.

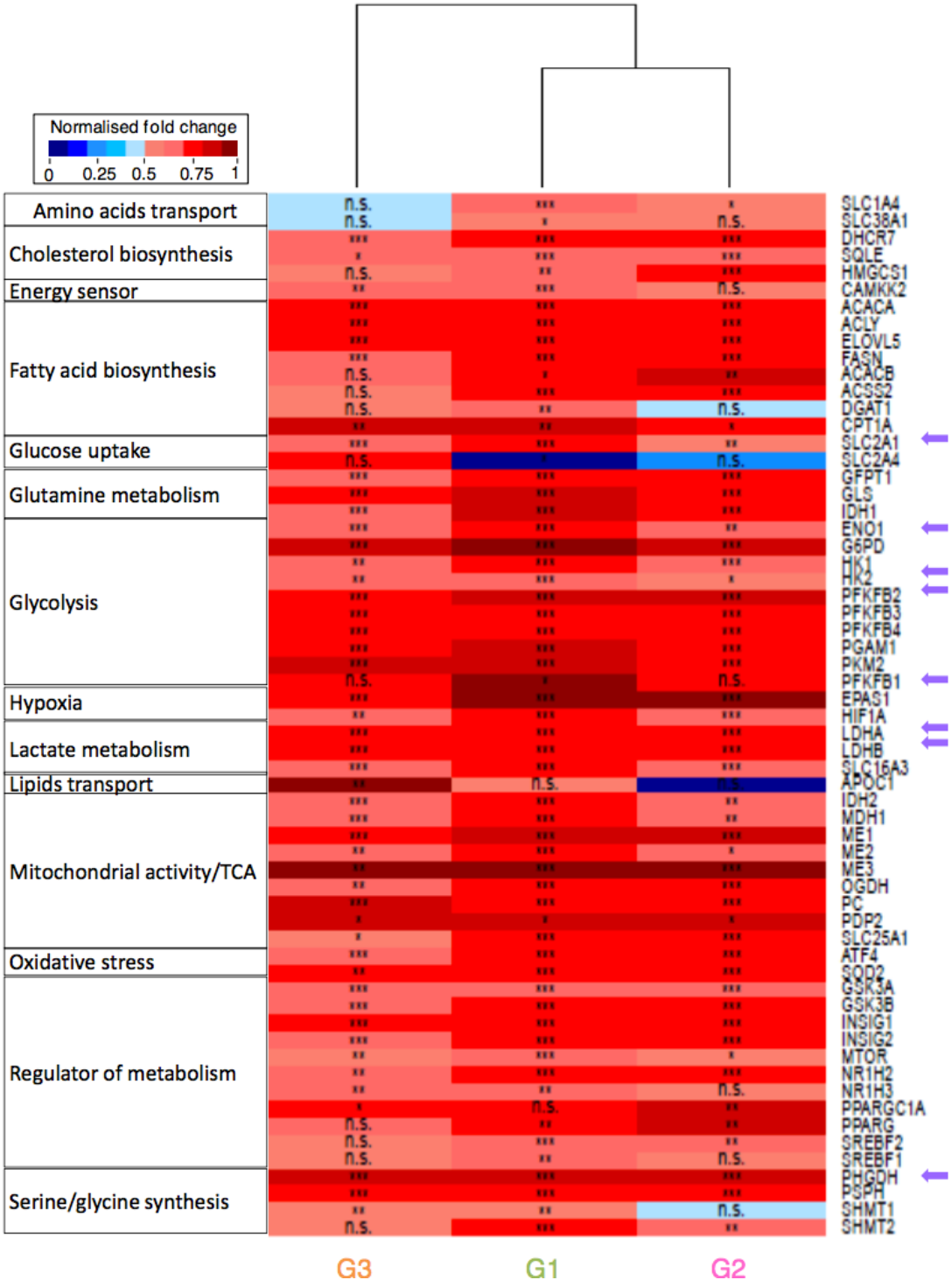

Figure 5.10 Levels of transcripts for known metabolic genes increase in PI3Ki-resistant cells upon drug removal. Heatmap showing the relative levels of transcripts of resistance cells maintained in the absence of PI3Ki compared to the same cells maintained in the presence of PI3Ki. Genes were grouped based on their known function in several metabolic pathways. Purple arrows indicate genes that belong to HIF signalling transduction pathway. n.s. non-significant, * $P < 0.05$; ** $P < 0.01$; *** $P < 0.001$.

5.8 HIF activity

The data presented in section 5.7 revealed that the expression levels of several transcripts regulated by the activity of HIF increased in PI3Ki-resistant cells as a consequence of PI3Ki removal. To determine the transcriptional activities of HIF (HIF-1α and HIF-2α) in parental and PI3Ki-resistant cells in a more direct manner, the Hypoxia Response Elements (HREs)-driven activity of the luciferase transporter was quantified (see Section 2.6.6). The results of this experiment, presented in Fig 5.11A, demonstrated that HIF's transcriptional activities in normoxic conditions increased between 3.3 to 13.6 times in PI3Ki-resistant cells grown without the PI3Ki compared to the same cells grown with the compound. Interestingly, placing parental cells in hypoxic conditions led to increased HIF's activities up to approximately 20-fold times in comparison to HIF's activities of parental cells in normoxia, whereas, on the same conditions, PI3Ki-resistant cells withdrawn from PI3Ki only increased their HIF activity an average of 3.4-fold times (Fig 5.11B). These data suggested that whilst parental cells have the capacity to greatly increase the activities of HIF when exposed to hypoxia, this capability was lost in PI3Ki-resistant cells.

To determine the total amount of HIF-1α protein (the most widely expressed HIF isoform [310]), Western blot for the levels of this protein in normoxic conditions was performed. The level of HIF-1α increased in PI3Ki-resistant cells after PI3Ki withdrawal (Fig 5.11C), mirroring the HIF activities showed in Fig 5.11A.

To investigate the functional effect of HIF activities both on the proliferation of parental and PI3Ki-resistant cells and also on the production of lactic acid in those cells, 10 nM chetomin was used as well as 0.1% DMSO, 1 μM GDC-0941, or the combination to treat cells for 5 days. The number of viable cells as well as the pH of the growth media were measured after that time using Beckman Vi-CELL counter and a pH meter, respectively. The results presented in Fig 5.11D showed that chetomin reduced the proliferation of parental cells. The proliferation of G1- and G2- cells was not significantly affected by chetomin; the combination of PI3Ki and chetomin, however, significantly reduced the proliferation of G1+ and G3+ cells. Furthermore, these data showed that treatment with chetomin diminished the media acidification of PI3Ki-resistant cells to similar levels as to those of cells treated with PI3Ki (Fig 5.11E).

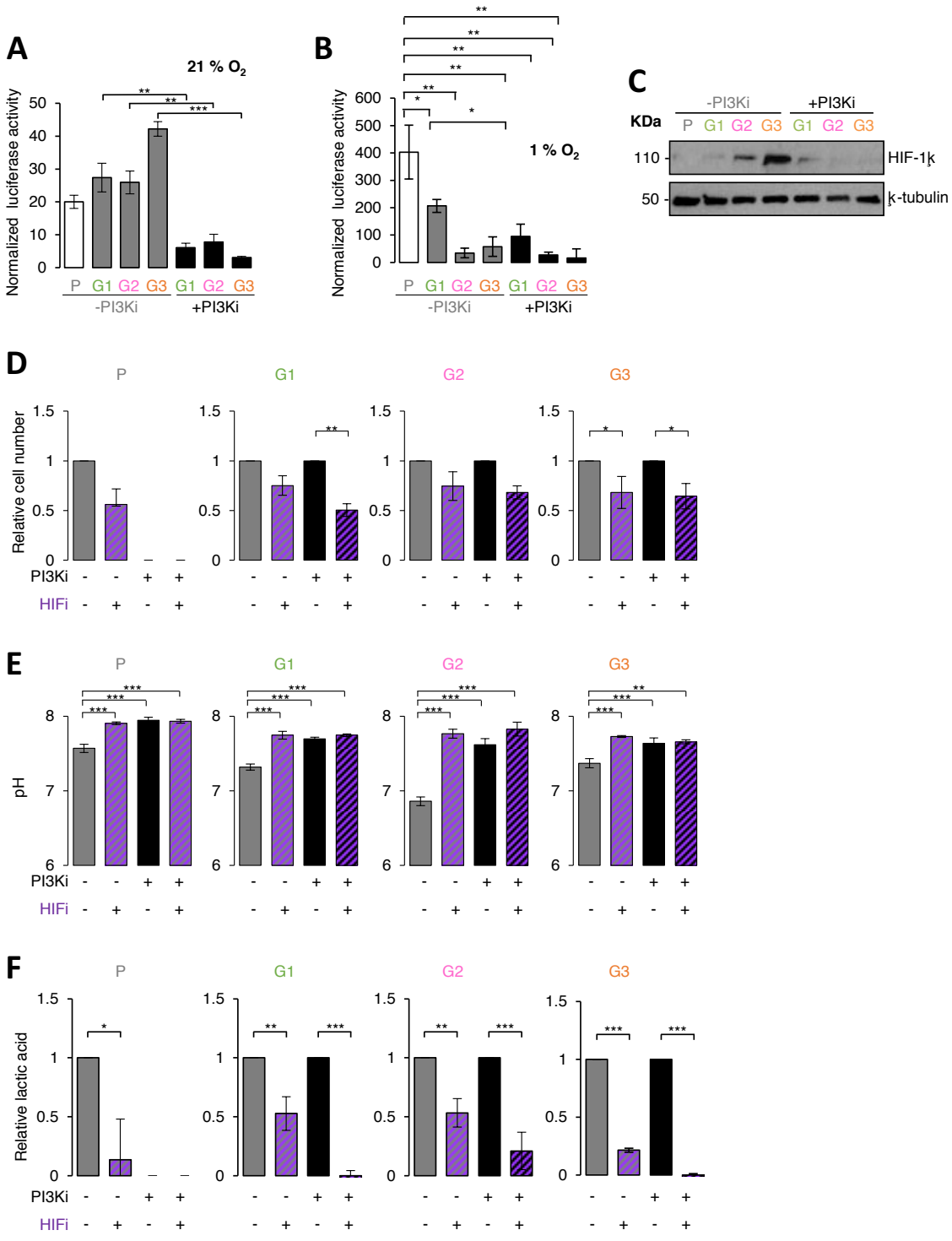

Figure 5.11 HIF controls the production of lactic acid in PI3Ki-resistant cells. (**A**) Transcriptional activity of HIF measured after exposure of parental and resistant cells to a normoxic atmosphere (21% O_2) for 2 days. Data are represented as mean ± SD (*n*=3, three independent technical replicates). *P*-values were calculated using an unpaired, two-tail Student's *t*-test comparing as indicated. * $P < 0.05$; ** $P < 0.01$; *** $P < 0.001$. (**B**) Same as in (**A**), with the difference that cells were maintained in hypoxic atmosphere (1% O_2). (**C**) Western blot for HIF-1 and α-tubulin loading control. (**D**) Relative number of cells, (**E**) values of pH of media, and (**F**) concentration of lactic acid in the media used to culture for 5 days parental and resistant cells with 1 μM GDC-0941 (PI3Ki), 10 nM chetomin (HIFi) or combination of both, as indicated. Data are represented as mean ± SD (*n*=3, three biological replicates). *P*-values were calculated using an unpaired, two-tail Student's t-test. * $P < 0.05$; ** $P < 0.01$; *** $P < 0.001$.

To measure the lactic acid concentration after treatment with chetomin, the accumulated lactic acid in media where parental and PI3Ki-resistant cells were treated with 1 µM of GDC-0941, 10 nM of chetomin, 0.1% DMSO or the combination for 5 days was quantified using the method described in Section 2.7.1. The experiment was performed in triplicates. Quality control for these experiments is shown in Appendix 9. The resulting data showed that the amount of lactic acid in the growth media significantly decreased upon HIF inhibition (Fig 5.11F). These data were consistent with the transcriptional activities of HIF controlling the expression of genes involved in the production of lactic acid [51], and with the data shown in Figs 5.10 and 4.6D showing an increase in the expression of members of the glycolytic pathway at the transcript and protein levels, respectively.

To further validate the role of HIF activities in the production of lactic acid, the expression of HIF-1α was down-regulated by specific small interfering RNA (siRNA) targeting HIF-1α. To accomplish this, parental, G2-, and G2+ resistant cells were seeded at 70% confluence and transfected either with a specific sequence against a region of HIF-1α mRNA or with a scramble sequence and cells cultured for 72 h. After that time, cell pellets were collected for Western blot analysis of HIF-1α and LDHB. The results of this experiment demonstrated that siRNA efficiently reduced HIF-1α expression (seen for parental and G2- cells) and reduced LDHB expression of G2- resistant cells (Fig 5.12).

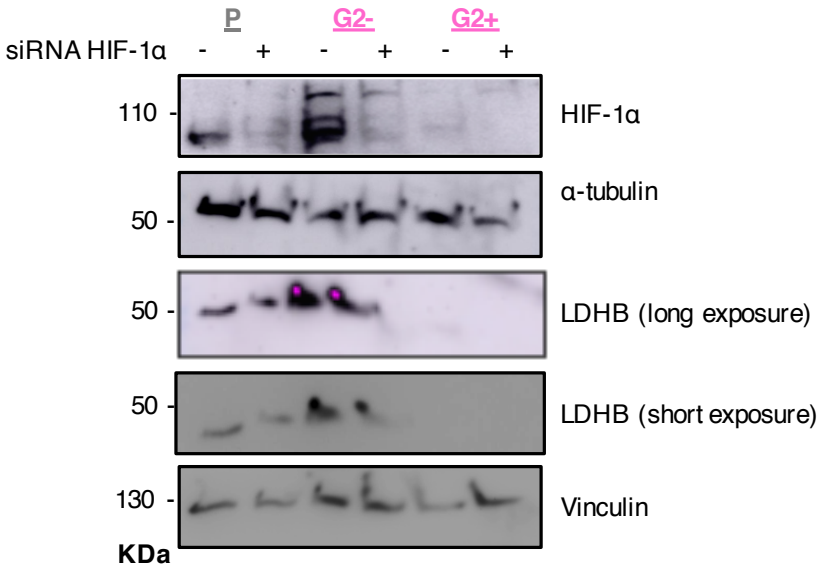

Figure 5.12 HIF and LDHB protein levels in parental and G2 resistant cells in upon siRNA treatment against HIF-1α or scrambled control. Western blot for HIF-1α and LDHB of parental, G2-, and G2+ resistant cells after transfection with siRNA against HIF-1α or scrambled for 72 h. Vinculin loading is shown as loading control.

5.9 Role of ROS on the glycolytic phenotype

The stability of HIF-1α can be regulated by ROS, through mechanisms that affect the activity of prolyl hydroxylases (PHD) and Hippel-Lindau tumour suppressor protein (VHL), proteins involved in the hydroxylation and ubiquitination of HIF-1α, respectively [311]. Based on the observations that ROS (Fig 5.7A) and HIF's transcriptional activities (Fig 5.11A) increased in PI3Ki-resistant cells during drug holidays, it was reasonable to hypothesise that the reduction of ROS by the treatment of cells with a ROS quencher may lead to the degradation of HIF-1α.

To test this hypothesis, HIF-1α was analysed by Western blot after treating parental and PI3Ki-resistant cells with the ROS quencher NAC. The resulting data clearly demonstrated that the levels of HIF-1α protein decreased after ROS scavenging, indicating that ROS contribute to the stability of HIF-1α in these models (Fig 5.13A). Given the observed role of HIF in the production of lactic acid (Fig 5.11F), it was rationalised that treatment of parental and PI3Ki-resistant cells with antioxidants may result in decreased lactic acid in the culture media. To test this hypothesis, cells were treated with 1 μM of GDC-0941, 20 μM of NAC, 0.1% DMSO or the combination for 5 days, and lactic acid was then quantified by LC-MS as outlined in the methods Section 2.7.1. The experiment was repeated three times. The standard curve used to quantify the lactic acid in these experiments is shown in Appendix 10.

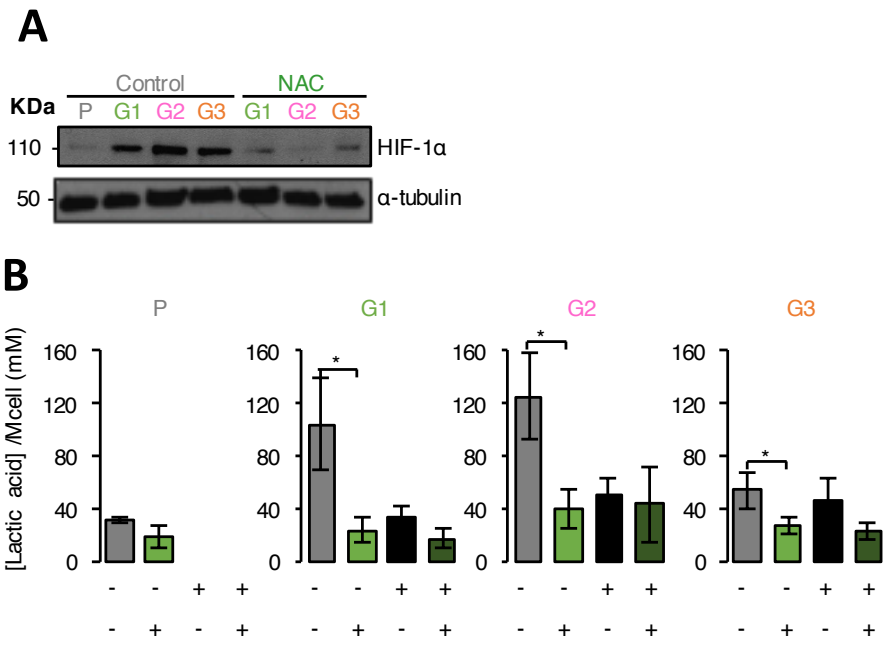

Figure 5.13 Role of ROS on the production of lactic acid. (**A**) Western blots against HIF-1α for parental and resistant cells treated with 200 μM NAC or DMSO for 5 days. α-tubulin is shown as loading control. (**B**) Lactic acid present in the culture media normalised to number of cells cultured for 5 days in the absence or presence of vehicle, PI3Ki, NAC or the combination, as indicated. Data are represented as mean ± SD (*n*=3, three biological replicates). *P*-values were calculated using an unpaired, two-tail Student's *t*-test comparing as indicated. * $P < 0.05$.

The data shown in Fig 5.13B showed a decrease in the lactic acid present in the culture media after NAC treatment: the amount of lactic acid decreased by 4.4-times for G1- cells (P = 0.02); decrease by 3.1-times for G2- cells (P = 0.02); and decrease by 2.0-times for G3- cells (P = 0.04), suggesting that ROS sustained the production of lactic acid mediated by HIF.

5.10 Contribution of c-MYC to the phenotype of PI3Ki-resistant cells

In addition to HIF, c-MYC also regulates the glycolytic activity in some systems [152]. Given the observed increased of c-MYC protein levels (Fig 4.7), and the increased c-MYC phosphorylation at Thr^{58}/Ser^{62} in PI3Ki-resistant cells (Fig 4.10), the role of c-MYC contributing to the resistance and metabolic phenotype of PI3Ki-resistant cells was then investigated. To do so, the transcriptional activity of c-MYC was prevented with compounds that compete for the formation of the c-MYC-MAX heterodimer (i.e. 10058-F4 and 10074-G5) [155, 156]. Here, it was important to stress that given that these compounds prevent the assembly of the transcriptional machinery rather than directly inhibiting c-MYC, two highly selective and structurally diverse disruptors of the c-MYC-MAX heterodimer were selected, to increase confidence in the results. The data shown in Fig 5.14A indicated that c-MYC sustained the proliferation of PI3Ki-resistant cells in conditions where PI3K was inhibited. Accordingly, the c-MYC and PI3K inhibitors had a slight effect by themselves on lowering the proliferation of PI3Ki-resistant cells, whereas the combination of c-MYC and PI3K activities-blockade decreased the number of PI3Ki-resistant cells up to 1/3 relative to the single treatment (Fig 5.14A).

The contribution of c-MYC to the glycolytic phenotype of PI3Ki-resistant cells was then examined. The result of this experiment indicated that chemical blockade of c-MYC activity did not prevent the glycolytic phenotype of PI3Ki-resistant cells growing without PI3Ki, implying that c-MYC activity was not needed for the glycolytic phenotype of PI3Ki-resistant cells (Fig 5.14B). Double treatment of PI3Ki-resistant cells with PI3Ki and c-MYCi impeded the acidification of culture media.

Overall, these results indicated that although the activity of c-MYC help resistant cells to survive in a background of chronic PI3K inhibition, the activity of this transcription factor is not required to develop the glycolytic phenotype in PI3Ki-resistant cells.

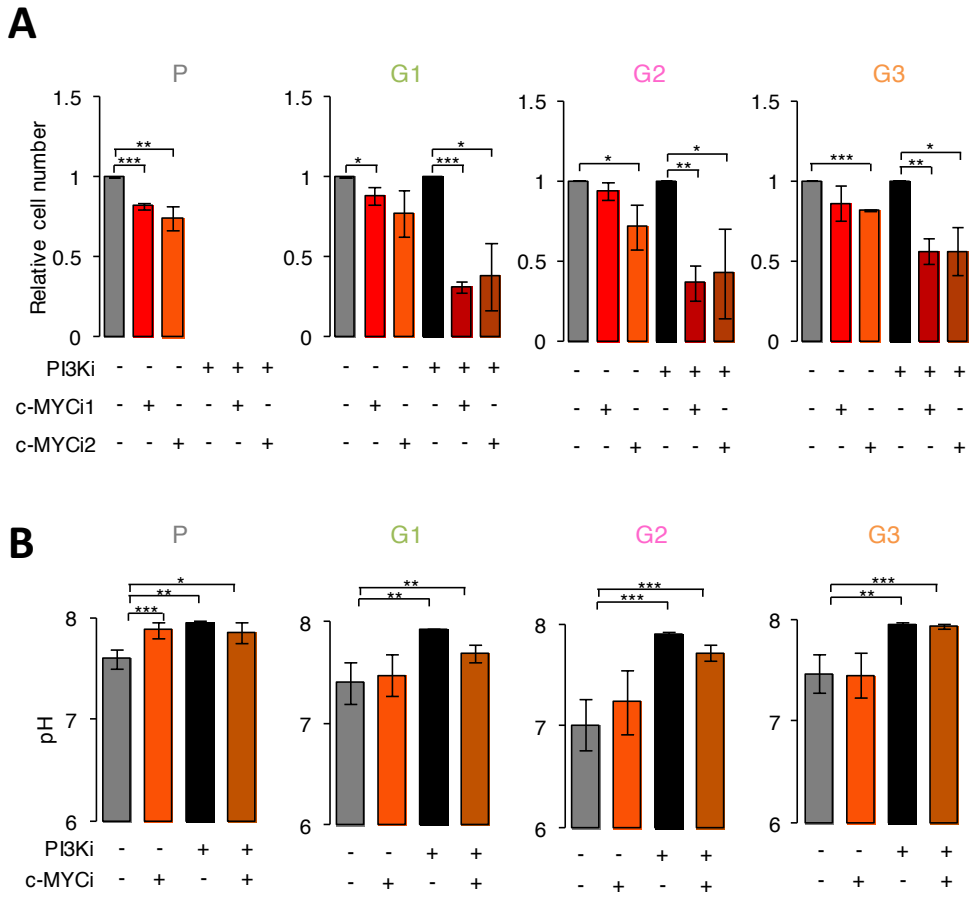

Figure 5.14 c-MYC inhibition does not prevent the metabolic phenotype of PI3Ki-resistant cells. (**A**) Relative cell number of parental and resistant cells measured after 5 days of treatment with two disruptors of c-MYC transcriptional activation (normalised to DMSO or GDC-0941). PI3Ki, GDC-0941 (1 µM); c-MYCi1, 10058-F4 (25 µM); c-MYCi2, 10074-G5 (20 µM). (**B**) Values of the pH of the culture media where parental and resistant cells grown after treatment with 1 µM GDC-0941 (PI3Ki), 20 µM 10074-G5 or combination of both for 5 days. Data are represented as mean ± SD ($n \geq 3$, independent replicates). *P*-values were calculated using an unpaired, two-tail Student's *t*-test comparing as indicated; * $P < 0.05$; ** $P < 0.01$; *** $P < 0.001$.

5.11 Regulation of the metabolic phenotype in resistant cells

To delineate the potential mechanisms involved in the increased bioenergetic activity in PI3Ki-resistant cells, the media acidification and the levels of intracellular ROS in parental and PI3Ki-resistant cells were measured as a function of treatment with inhibitors of several kinases that act downstream of PI3K. Equal number of parental and PI3Ki-resistant cells (0.02×10^6 per well) were seeded in 6-well plates containing 2 mL of growth media and treated with several kinases inhibitors. For the luminescence experiment, cells were grown on coverslip as described in Section 2.7.4. Media acidification was measured by means of a pH meter and ROS were visualised by means of a fluorescent microscope. Analysis of these results showed that inhibition of PI3K and mTOR impeded the acidification of the media used to grow PI3Ki-resistant cells (Fig 5.15A), suggesting that these kinases were involved in the control of the glycolytic metabolism of PI3Ki-resistant cells. Interestingly,

inhibition of AKT did not impede the acidification of media for PI3Ki-resistant cells. Similar results were obtained for the inhibition of SGK isoforms, since treatment with SGK inhibitor did not prevent acidification of the media by PI3Ki-resistant cells (Fig 5.15A).

ROS were reduced after treatment with PI3Ki, mTORC1/2i or mTORC1i in those PI3Ki-resistant cells that had high levels of ROS (G1- and G2- cells) (Fig 5.15B). However, ROS levels of those cells were not reduced after treatment with AKTi, SGKi or with disruptors of c-MYC or HIF transcriptional activity (Fig 5.15B).

Taken together, these data indicated that a PI3K/mTOR axis controls the metabolic phenotype of PI3Ki-resistant cells.

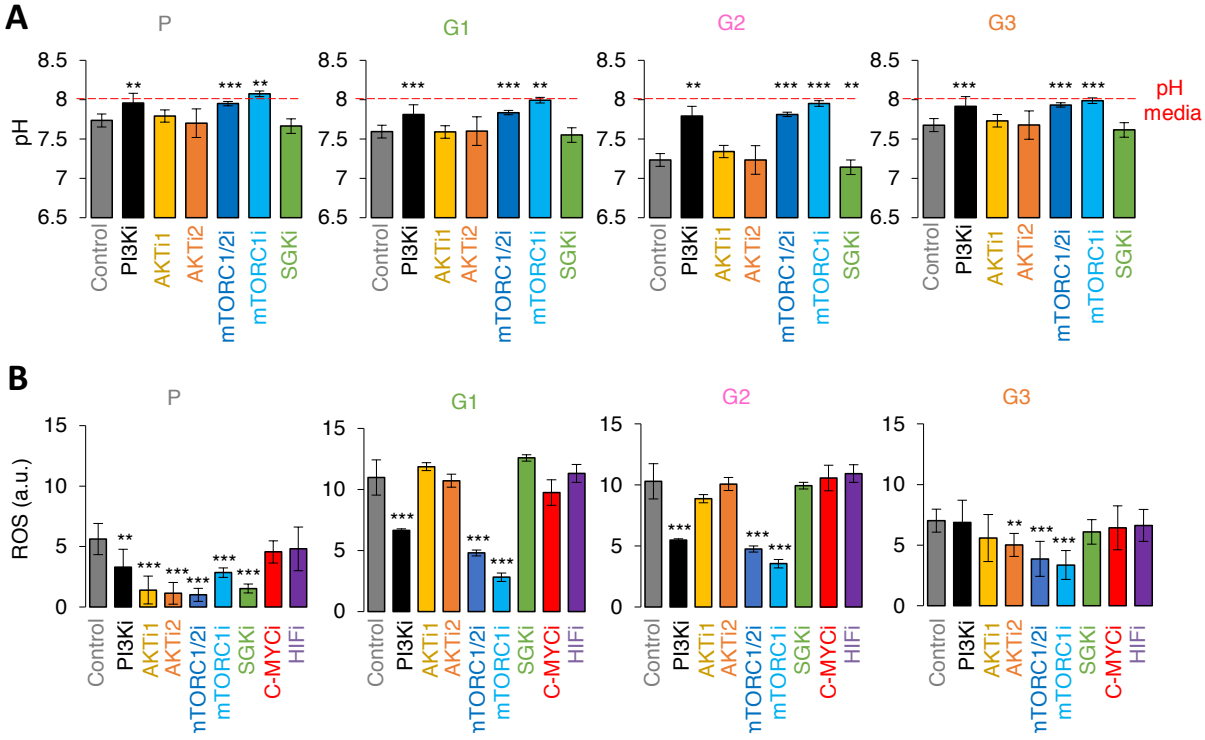

Figure 5.15 An AKT-independent PI3K/mTOR signalling pathway governs the metabolic phenotype of PI3Ki-resistant cells. (**A**) Values of the pH of media where parental and resistant cells grown after treatment with 1 μM GDC-0941 (PI3Ki), 1 μM AV-II (AKTi1), 1 μM MK-2206 (AKTi2), 1 μM KU-0063794 (mTORC1/2i), 20 nM everolimus (mTORC1i) or 0.5 μM GSK650394 (SGKi), for 5 days. Data are represented as mean ± SD (*n*=3, independent biological replicates). (**B**) ROS levels after treatment of cells with the indicated inhibitors. 7 fields per conditions were taken. *P*-values were calculated using an unpaired, two-tail Student's t-test; ** $P < 0.01$; *** $P < 0.001$.

5.12 Evaluation of a non-canonical AKT-independent PI3K/mTOR signalling in resistant cells

To determine the extent of PI3K-mTOR, but AKT-independent, signalling in PI3Ki-resistant cells, an experiment was designed to treat in duplicate G2 resistant cells with 1 μM GDC-0941 (PI3Ki), 1 μM MK-2206 (AKTi), 1 μM KU-0063794 (mTORC1/2i) or 0.1% DMSO (control) for 1 h. After cell lysis and phosphoenrichment, samples were analysed in duplicate in an LTQ-Orbitrap XL. A quality control analysis for these data is shown in Appendix 11. Of the 4,035 peptides quantified in this experiment, 3,180 were phosphorylated. The results shown in Fig 5.16A showed that, whilst PI3K and mTORC1/2 inhibitors prevented the phosphorylation of 90 and 99 sites, respectively, AKT inhibitor only reduced the phosphorylation of 24 sites (at $P<0.05$, $\log_2$-fold <-1). PI3K and mTORC1/2 inhibitors, but not the inhibitor of AKT, decreased the phosphorylation of EIF4E-BP2 at Ser^{44}/Thr^{45}, a downstream target of mTORC1 (Fig 5.16B). In contrast, the inhibitors of PI3K, AKT, and mTORC1/2 reduced the phosphorylation of the AKT substrate PRAS40 at Thr^{246}.

Hierarchical clustering of the significantly modulated phosphopeptides demonstrated a clear separation between the phosphopeptides modulated as a function of treatment of G2 resistant cells with AKTi, PI3Ki or mTORC1/2i (Fig 5.16C).

The inhibitory effect of AKT and mTORC1 inhibitors was confirmed by Western blot (Fig 5.16D). Thus, the allosteric AKT inhibitor prevented the phosphorylation of PRAS40 at Thr^{246} (an AKT target) but not of 4E-BP1 at Thr^{37}/Thr^{45} (a mTOR target). The mTORC1 inhibitor reduced the phosphorylation of 4E-BP1 at Thr^{37}/Thr^{45}. These data confirmed that inhibition of AKT does not prevent the phosphorylation of target of mTORC1 downstream targets in these cell models. Thus, these experiments provided further evidence of the existence of a PI3K-mTOR signalling pathway that was independent of AKT's activity in G2 resistant cells.

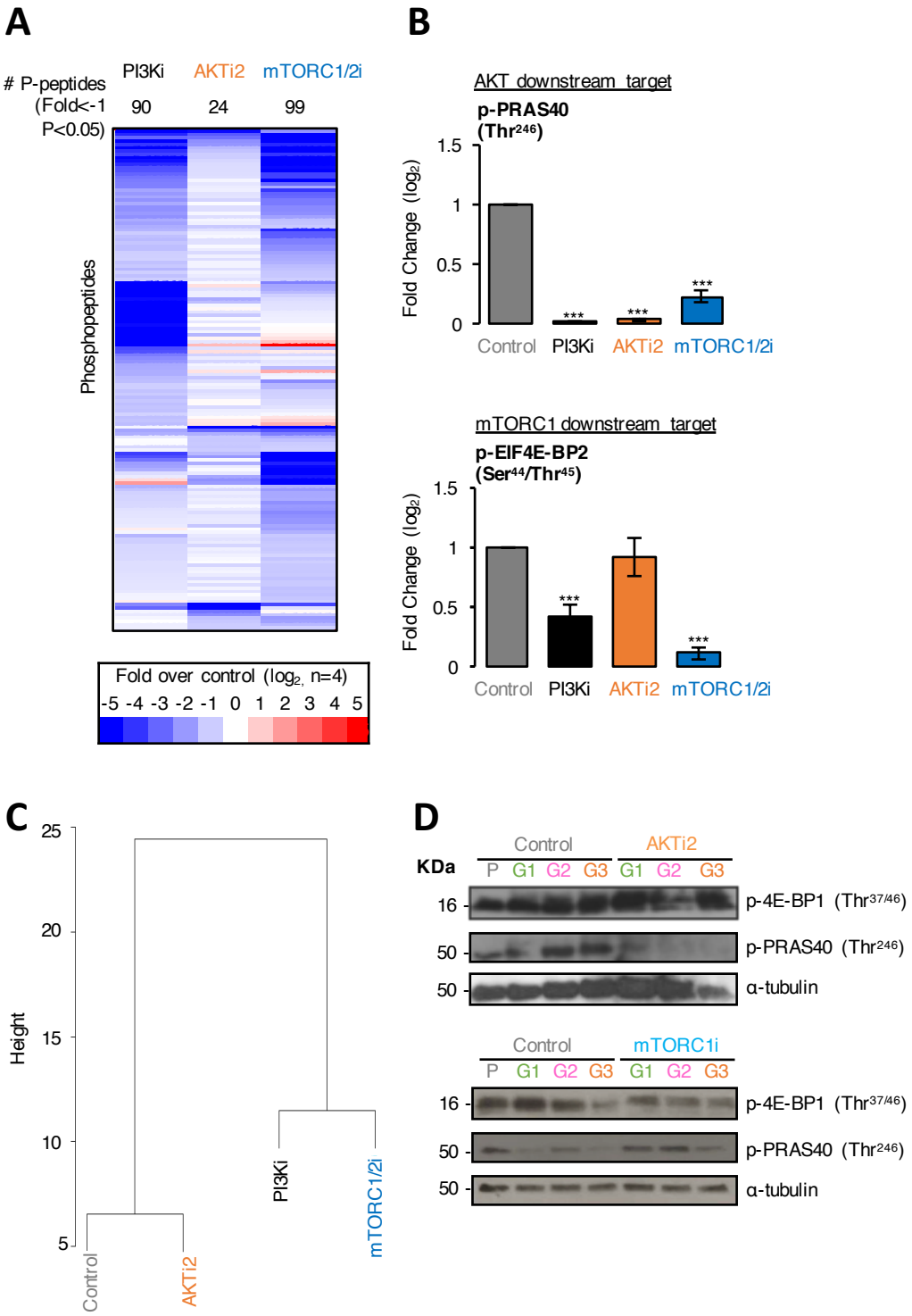

Figure 5.16 PI3Ki-resistant cells have a non-canonical AKT-independent PI3K/mTOR signalling pathway. (**A**) Heatmap showing phosphopeptides significantly modulated in G2 resistant cells treated for 1h with the indicated kinase inhibitors. (**B**) Relative intensity of selected targets downstream of AKT and mTORC1. (**C**) Unsupervised hierarchical clustering of the mean log_2 fold-ratios for the 53 filtered phosphopeptides with FDR<0.05. (**D**) Western blots for p-4E-BP1 ($Thr^{37/46}$) and p-PRAS40 (Thr^{246}), known substrates of mTORC1 and AKT, respectively, after treatment of PI3Ki-resistant cells with the indicated inhibitors. α-tubulin loading control is shown.

5.13 Response of parental and resistant cells to modulation of the bioenergetic metabolism

It was hypothesised that the enhanced metabolism of PI3Ki-resistant cells was functionally associated with a greater demand of nutrients that provide carbon sources of these cells. To test this hypothesis, parental and resistant cells were challenged to glucose or glutamine starvation, since these nutrients serve as primary sources to produce ATP [312]. For this experiment, the same number of parental and PI3Ki-resistant cells were seeded overnight and consequently starved of either glucose or glutamine for one and two days. After the indicated time, the number of viable cells was measured by means of a Vi-CELL counter. These data showed that withdrawal of PI3Ki made PI3Ki-resistant cells more sensitive to glucose starvation compared to the same cells cultured in the presence of PI3Ki (Fig 5.17A, upper panel). PI3Ki-resistant cells in drug holidays were also more sensitive to glucose deprivation than parental cells. Of note, the extent of the sensitivity was proportional to the intensity of the metabolic phenotype in that the number of G2- and G1- cells decreased more after glucose deprivation than G3- cells or parental cells. Similarly, G2- resistant cells in drug holidays also increased their sensitivity to glutamine depletion compared to the same cells maintained with PI3Ki treatment (Fig 5.17A, lower panel). These data indicated that the metabolic phenotype of PI3Ki-resistant cells led to a functional dependency on glucose and glutamine.

The effect of challenging parental and PI3Ki-resistant cells with an external source of free radicals, such as H_2O_2, was also explored. The result of this experiment demonstrated that cells that accumulated intracellular ROS responded to an oxidative challenge. For example, G1- and G2-resistant cells grown in the absence of PI3Ki reduced their proliferation after H_2O_2 treatment to a greater extent than the same cells grown with PI3Ki (Fig 5.17B).

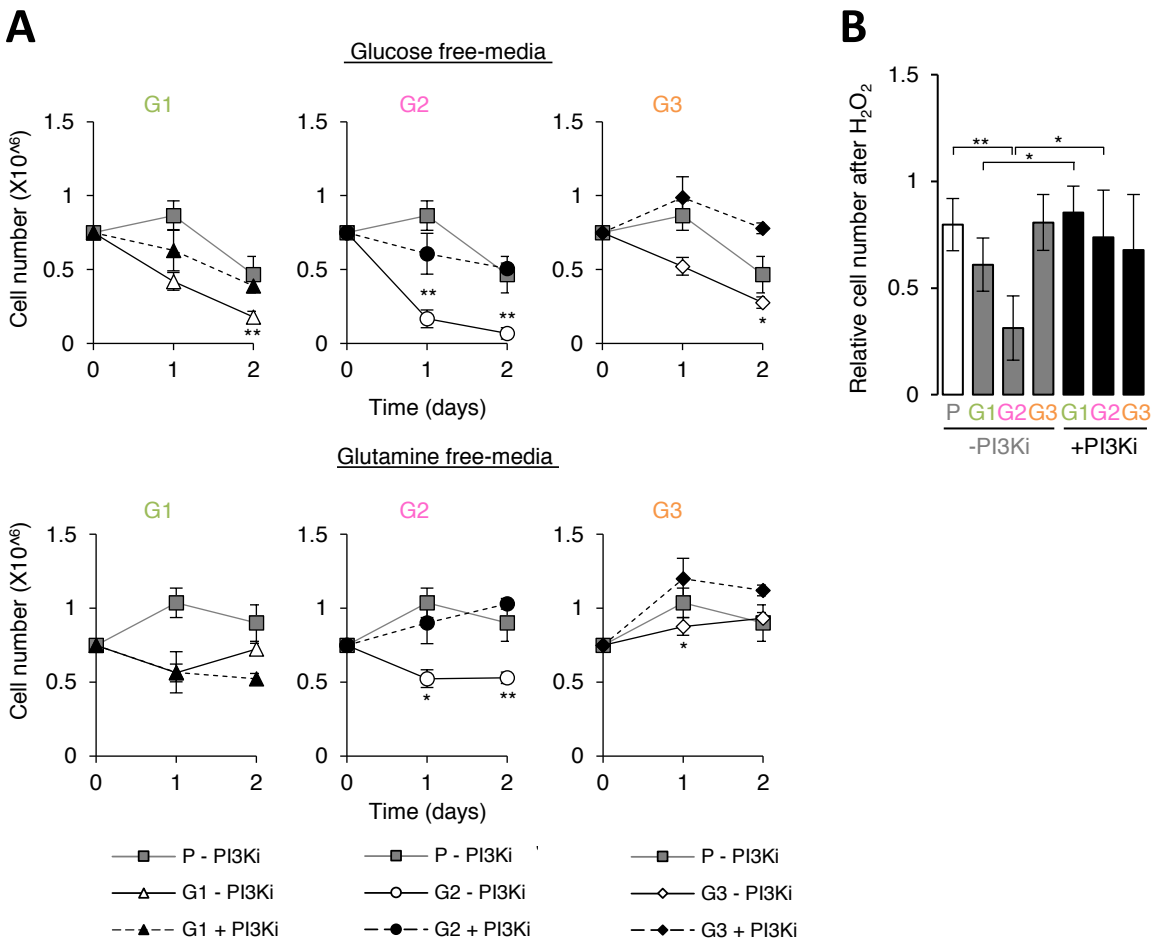

Figure 5.17 Resistant cells are sensitive to metabolic challenge during drug holidays. (**A**) Number of parental and PI3Ki-resistant cells grown either in the presence or absence of PI3Ki as a function of glucose starvation for 1 and 2 days (upper panel), or as a function of glutamine starvation for 1 and 2 days (lower panel). (**B**) Relative cell numbers of parental and PI3Ki-resistant cells either in the presence or absence of PI3Ki treated with 130 µM H_2O_2 for 5 days. Data are represented as mean ± SD (*n*=3, independent replicates). *P*-values were calculated using an unpaired, two-tail Student's t-test; * $P < 0.05$; ** $P < 0.01$.

5.14 Metabolic status in additional models of acquired resistance

To extend the observation of the metabolism being modulated in resistant cells, the bioenergetic profile of additional cell models of acquired resistance to PI3K/mTOR inhibition was examined. These included a panel of seven sensitive and resistant cell line pairs derived from breast (MCF7-K1, MCF7-K2, and MCF7-K3), oesophagus (KYSE70 and KYSE180), and head and neck cancers (LB771-HNC and CAL33). The cells lines used in this study had *PIK3CA* amplified (KYSE180, KYSE70 and LB771-HNC cells) [305] or mutated (MCF7 and CAL33 cells) [226, 305]. KYSE180, KYSE70, LB771-HNC and CAL33 cell lines were resistant to PI3Kαi, and MCF7 cells had been made resistant to survive on a background of mTORC1/2 inhibition These resistant cells reactivated the PI3K/mTOR signalling pathway in the

absence of PI3Ki/mTORi [226, 305]. The metabolic profile of these cells was characterised, and the metabolic-derived ROS as well as the cell viability were quantified.

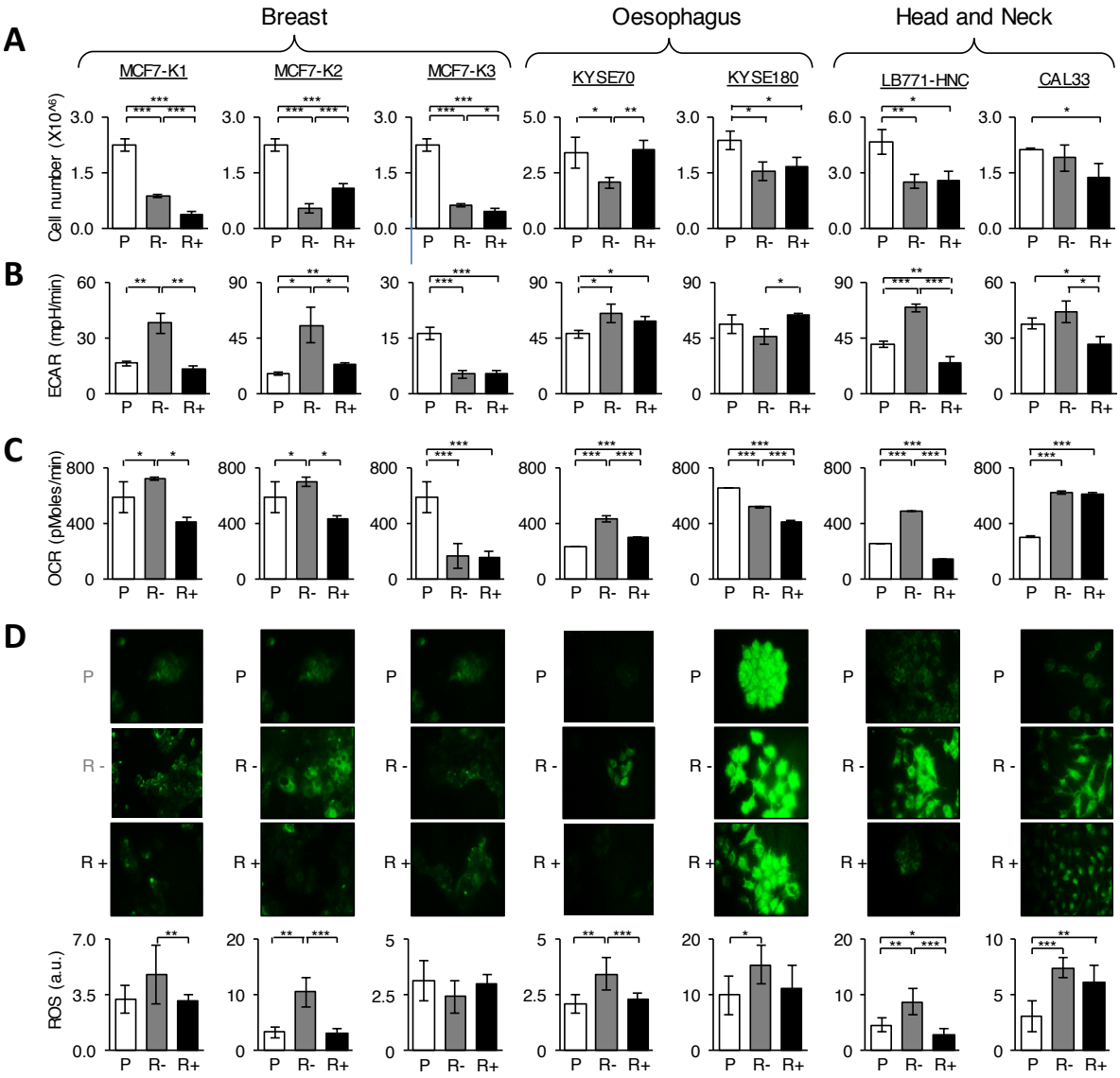

Figure 5.18 Additional models of PI3K/mTOR resistant cells show increased bioenergetic activity upon drug removal. (**A**) Number of parental and resistant cells derived from breast, oesophagus and head and neck cancers cell lines resistant to mTORC1/2 inhibitor (those derived from breast) or PI3K (those derived from oesophagus and head and neck). Cells were maintained in the presence (R+) or absence (R-) of the selection drug. Data are represented as mean ± SD (*n*=3, three independent replicates)**.** (**B**) ECAR values for the same cells as in (**A**). Data are mean ± SD (*n*=3, three independent replicates). (**C**) OCR values for the same cells as in (**A**). Data are mean ± SD (*n*=3, three independent replicates). (**D**) Representative images and ROS levels for the same cells as in (**A**). Seven image fields were taken per condition. Data are mean ± SD of 7 fields. *P*-values were calculated using an unpaired, two-tail Student's *t*-test comparing conditions as indicated; * $P < 0.05$; ** $P < 0.01$; *** $P < 0.001$.

The resulting data showed that drug holidays caused a proliferative disadvantage in two of these cell lines (i.e. K2- and KYSE70- resistant cells) (Fig 5.18A). In-line with the observation in Section 3.3.3, cells resistant to PI3K/mTOR inhibition did not recover the proliferative rate of parental cells, even when the selection drug was removed from the culture media (Fig 5.18A). ECAR increased in 4 of these cell lines (i.e. K1-, K2-, LB771-, and CAL33- resistant cells) after drug withdrawal from the culture media (Fig 5.18B). OCR increased in 5 of these cell lines (i.e. K1-, K2-, KYSE70-, KYSE180- and LB771- resistant cells) (Fig 5.18C). Consistent with an elevation of OCR, the amount of ROS increased in 5 of these cell lines, although the difference was not significant for KYSE180- cells (Fig 5.18D) (See Appendix 12 for all the images taken in this experiment). The data shown in Fig 5.18D also demonstrated distinct ROS and ECAR levels across cell lines. As an example, ROS intensity was about five times higher for KYSE180 parental cells than for KYSE70 parental cells.

From the total panel of 10 resistant cell lines analysed (i.e. G1, G2, G3, K1, K2, K3, KYSE70, KYSE180, LB771, and CAL33 cells) drug holidays significantly reduced proliferation rate of four cell lines (i.e. G1, G2, K2, and KYSE70 cells) and significantly increased in the rate of proliferation of two of those (i.e. K1 and K3 cells) (Fig 5.19A). To understand the relationship between the modulation of metabolism in resistant cells induced by withdrawal of selection drug (e.g. PI3Ki or mTORC1/2i) and cell proliferation, a correlation analysis between the ratio of proliferation upon drug withdrawal and the ratio of ECAR (considered as a pro-proliferative metabolic parameter, when in homeostasis) against ROS (considered as an anti-proliferative metabolic parameter, when homoeostasis is lost) was performed. Plotting the ratio of cell proliferation upon drug removal and the ratio of glycolytic activity to ROS concentration of resistant cells exposed to drug holidays clearly produced a high linear relation between the two (Fig 5.19B). The correlation between the proliferation of resistant cells upon drug withdrawal and the ratio of glycolytic activity to ROS concentration was notably high ($R= 0.94$, $P= 5.3 \times 10^{-05}$).

Overall, these data indicated that cells that had evolved to survive in the absence of a functional PI3K/mTOR signalling axis developed a metabolic imbalance upon drug withdrawal. The extent of the proportion between the glycolysis and ROS accumulation dictated the proliferative capacity of PI3Ki- and mTORC1/2i-resistant cells after drug removal.

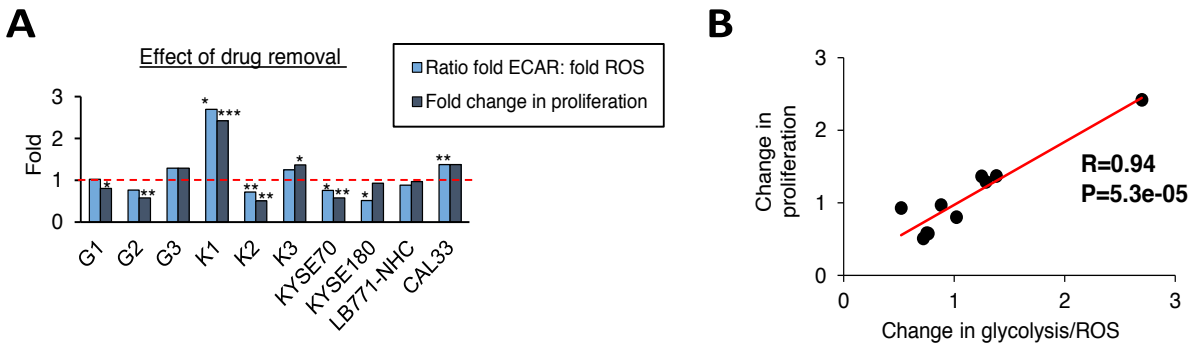

Figure 5.19 The extent of metabolic adaptation determines the proliferative capacity of drug-resistant cells (**A**) Effect of drug removal on the ratio between the ECAR and the ROS value and the proliferation of resistant cells. Values greater than 1 indicate that removal of selection drug from culture of resistant cells increase their ECAR: ROS ratio or their proliferation. (**B**) Association between the ratio ECAR: ROS and proliferation (based on Pearson Correlation coefficient, R).

5.15 Conclusions

The experiments presented in this Chapter aimed to characterise the bioenergetic profiles of cells resistant to PI3K/mTOR inhibition.

PI3Ki-resistant cells increased the acidification of the culture media, measured by a pH meter, as well as the cellular reductase activity when PI3Ki was withdrawn from the culture media, inferred by MTS assay measurements (Fig 5.2). Investigation of the metabolic activity of parental and resistant cells by means of the Seahorse analyser revealed that PI3Ki-resistant cells adapt the mitochondrial activity and the extracellular acidification rate to similar levels of parental cells, and that drug holidays promoted an overall increase of the metabolic activity of PI3Ki-resistant cells (Fig 5.4). Consistently, during drug holidays PI3Ki-resistant cells accumulated lactic acid in the media, measured by LC-MS (Fig 5.6A) as well as intracellular ROS, inferred from the DCFH-DA intensity measured by a fluorescence microscope (Fig 5.7A).

To test the hypothesis that accumulated ROS contributed to the deficient proliferation of resistant cells during drug holidays, ROS levels were quenched by two antioxidants, NAC and α-tocopherol. After confirming that NAC doused the levels of free radicals in the cells (Fig 5.7B), the effect of this compound on the proliferation of resistant cells was tested at various time points. The accumulation of excessive amount of ROS was toxic for some cells (e.g. G2- resistant cells), and the detrimental effect of free radicals was reversed by treatment with NAC (Fig 5.7C) or α-tocopherol (Fig 5.8). Contrarily, ROS scavengers hampered the proliferation of cells with lower ROS levels (Figs 5.7C and 5.8).

To further resolve which enzymes were involved in the metabolic phenotype of PI3Ki-resistant cells, the transcriptional expression levels of several metabolic genes were measured. This analysis showed that PI3Ki-resistant cells increased the expression of multiple metabolic genes upon drug removal (Fig 5.9) and HIF-1α, and HIF-1α-regulated genes were among the enzymes that increased in resistant cells during drug holidays (Fig 5.10). Because the proteomics data had previously showed that targets of HIF transcriptional activity were increased in PI3Ki-resistant cells (Fig 4.6D), the activity of HIF in resistant cells was further explored.

In normoxic conditions, HIF's activities of PI3Ki-resistant cells grown in the absence of the lipid kinase inhibitor were higher compared to the same cells maintained of the presence of PI3Ki (Fig 5.11A). However, in hypoxic conditions the activities of HIF in parental cells were higher compared with PI3Ki-resistant cells withdrawn from PI3Ki (Fig 5.11B), suggesting that resistant cells have lost the capacity to activate HIF to similar extent of parental cells when exposed to hypoxia.

Treatment of cells with the competitive inhibitor of HIF/p300 interaction chetomin led to reduced concentration of lactic acid in the culture media (Fig 5.11F), and knockdown of HIF-1α mRNA reduced the levels of LDHB protein (which expression can be controlled by HIF-1α) in PI3Ki-resistant cell (Fig 5.12). Taken together, these data suggested that the activities of HIF control the transcription of genes required for the glycolytic activity of the resistant cell models.

Because ROS can stabilise HIF in some systems [311], the role of ROS on HIF in PI3Ki-resistant cells was explored. Immunoblotting data revealed that ROS scavenging reduced the amount of HIF-1α protein of PI3Ki-resistant cells (Fig 5.13A) and the amount of lactic acid in the culture media (Fig 5.13B), suggesting that ROS maintained the glycolytic activity by stabilising HIF-1α.

c-MYC oncogene has been identified in several preclinical models as a mechanism to acquire resistance to PI3K inhibition [301, 313, 314], and it is known to coordinate the expression of metabolic genes in some biological systems [100]. Because proteins transcriptionally controlled by c-MYC increased in PI3Ki-resistant cells (Fig 4.6D), the role of c-MYC in the proliferation and metabolic phenotype of these cells was investigated. As predicted, treatment of PI3Ki-resistant cells with two structurally different competitors of c-MYC-binding partners required for its transcriptional activity potentiated the effect of PI3Ki reducing the proliferation of PI3Ki-resistant cells (Fig 5.14A). However, treatment with these compounds did not prevent the glycolytic phenotype of PI3Ki-resistant cells during drug holidays, suggesting that c-MYC activity was not essential for the glycolytic phenotype of these cells (Fig 5.14B).

Similarly, targeted inhibition of AKT permitted the acidification of culture media and the production of ROS in PI3Ki-resistant cells, but inhibition of PI3K's or mTOR's activities reversed the metabolic

phenotype of PI3Ki-resistant cells (Fig 5.15). In fact, and in contrast to the canonical view of the PI3K signalling, PI3Ki-resistant cells presented a signalling cascade mediated by PI3K/mTOR that was independent from AKT's activity, as supported by the observation that inhibition of PI3K and mTORC1/2 reduced the phosphorylation of many sites that were not modulated upon AKT blockade (Fig 5.16).

Challenging resistant cells with additional metabolic stress (i.e. either nutrient reduction or increase oxidative stress) revealed that the drug holiday condition made PI3Ki-resistant cells more susceptible to these metabolic challenges (Fig 5.14).

Examination of the bioenergetic profiles of additional models of acquired resistance to PI3K/mTOR inhibition showed that drug holidays enhanced the bioenergetic profile of most of PI3Ki- and mTORC1/2i-resistant cells (Fig 5.18 B-D). More remarkably, there was a high correlation between impaired proliferation of resistant cells during drug holidays and defective metabolic homeostasis, characterised by the accumulation of ROS relative to the glycolytic activity of these cells (Fig 5.19B).

Overall, the results presented in this Chapter highlight that the ability of drug-resistant cells to correctly adapt their metabolism determines their capacity to proliferate.

Chapter 6. Analysis of the genetic background of PI3Ki-resistant cells

6.1 Introduction and aims of the study

Tumour evolution is driven by the selection pressure from cellular and microenvironmental factors experienced by cancer cells [315, 316]. Recent studies shed light on how the nature of accumulated genomic aberrations during long term drug treatment conjointly with non-mutational changes contribute to various mechanisms to acquire drug-resistance [179, 317]. Those studies made increasingly clear that the reversibility of the resistance phenotype is conditional to the mechanism that led to the acquisition of resistance.

The aim of the work presented in this Chapter was to characterise the genomic background of cell models that had acquired resistance to PI3Ki (presented in Chapters 3-5). To accomplish this, the whole-exome profiles of parental and PI3Ki-resistant cells were investigated (Fig 6.1).

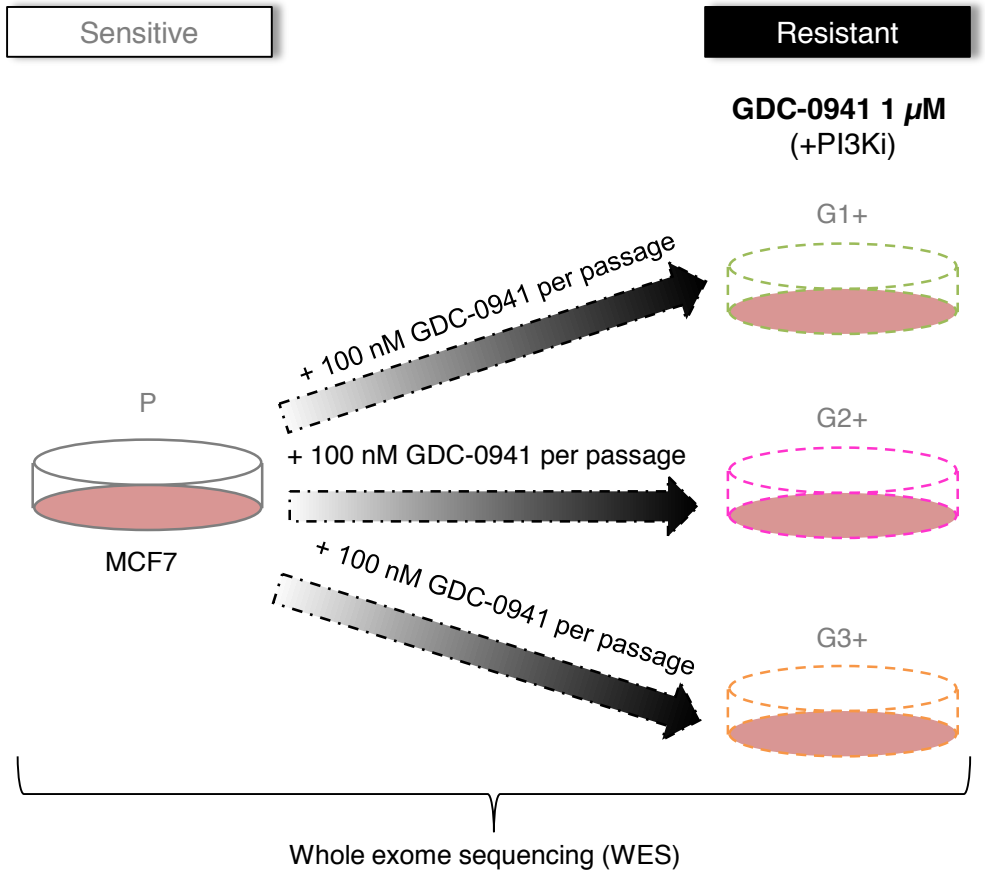

Figure 6.1 Experimental design followed to sequence the exomes of parental and PI3Ki-resistant cells. The exomes of three models of cancer cells resistant to 1 μM GDC-0941 (G1:G3) as well as the exome of parental cells were explored following the steps described in Section 2.11.

6.2 Genomic landscape of PI3Ki-resistant cells

To explore the genomic background of PI3Ki-resistant cells, DNA of these cells was extracted as described in Section 2.11. The initial quality control of the generated libraries for paired-end sequencing is shown in Appendix 13. Short sequence-reads of parental and PI3Ki-resistant cells were matched to the reference human genome, with a 89-98% span coverage at more than 20 reads sequencing depth (i.e. number of times a nucleotide base is sequenced) (Table 6.1). The mean number of reads for parental and PI3Ki-resistant cells was between 67-152 million reads (Table 6.1). The sizes of exomes of PI3Ki-resistant cells were rather heterogeneous, with the exome size of G1 and G2 resistant cells bigger (i.e. 5.8 Gb and 7.7 Gb, respectively) compared to the sequenced exome of G3 resistant cells (3.4 Gb) and the exome of parental cells (4.8 Gb) (Table 6.1).

Table 6.1 Sequencing metrics for MCF7 parental and PI3Ki-resistant cells. The number of reads per sample includes both forward and reverse strands.

	Parental	G1	G2	G3
Mean number of reads per sample (M)	95.7	115.3	151.8	67.1
Mean sequenced nucleotides (Gb)	4.8	5.8	7.7	3.4
% of targeted based covered at least by 20 reads	95.8	97.2	98.4	89.2

The number of non-synonymous mutations was also heterogeneous, being higher for G2 cells (65 non-synonymous)> G1 cells (50 non-synonymous)> G3 cells (21 non-synonymous) (Fig 6.2A). Fig 6.2B shows that the most common transversion was G>T/C>A, a mutation associated to DNA replication through 8oxoG lesion. The prevalence of this transversion was reported in other cancer types, such as lung cancer tumours [318]. Moreover, most of the point mutations of PI3Ki-resistant cells were missense mutations, indicating a potential selective advantage for those missense mutations (Fig 6.2C). The variant allele frequencies (VAFs) of PI3Ki-resistant cells showed average VAFs between 0.21-0.27 (Fig 6.2D).

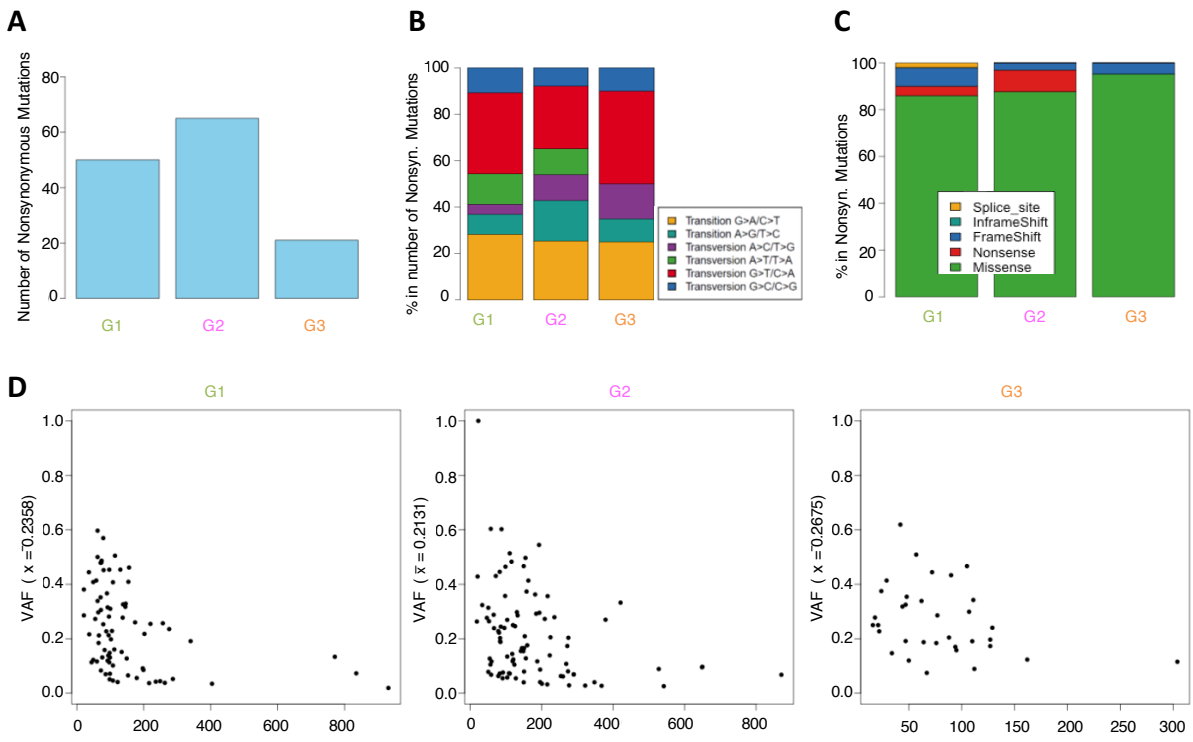

Figure 6.2 Point mutations frequencies of PI3Ki-resistant cells. (**A**) Total number of non-synonymous mutations in resistant cells. (**B**) Base substitution distribution for all SNVs identified in resistant cells. (**C**) Mutation type distribution for all SNVs identified in resistant cells. (**D**) Variant allele frequency (VAF) distribution for all the non-synonymous mutations identified by whole-exome sequencing on each PI3Ki-resistant cell lines.

6.3 Point mutations in PI3Ki-resistant cells

Analysis of the point mutations revealed that, whilst twenty point mutations were common between G1 and G2 resistant cells, none of these were shared with G3 resistant cells (Fig 6.3A). The common mutations between G1 and G2 resistant cells were predominantly missense mutations, except two stop mutations in *Erbb2* and *Map2k7* genes (the nature of the mutation at *TMEM67* gene was not certain, given that the local proximity of several mutations suggested those could be sequencing artefacts) (Table 6.2). The truncation in *Erbb2* gene was in the intracellular C-terminal region of ERBB2 protein (i.e. amino acid 1161), whereas the premature stop mutation of the gene *Map2k7* — which encodes for the stress kinase MKK7 — located within MKK7 kinase domain (i.e. amino acid 211) (Fig 6.3B). It is important to note that the truncation of the signalling domain of ERBB2 transmembrane protein deletes the Tyr^{1248} from its sequence. The phosphorylation status of this site has been associated with trastuzumab sensitivity and ERBB2 degradation [319]. MKK7, on the other hand, phosphorylates and activates c-Jun amino (N)-terminal kinases (JNK1/3); disruption of MKK7 kinase activity in G1 and G2 resistant cells may impede the MKK7-mediated phosphorylation of JNK, known to be responsive to stress stimuli [320].

Two computer programs that predict the impact of mutations in protein functionality, namely SIFT (Sorting Tolerant From Intolerant) [281] and PolyPhen-2 [282], were used to estimate the possible impact of the identified point mutations. SIFT gives a score to the effect of an amino acid substitution based on the physico-chemical similarity between the native amino acid and the alternate amino acid, designating each change as 'tolerated' or 'damaging' for the protein function. PolyPhen-2 scores the effect of amino acid alterations based on each protein's 3D structure, returning the impact of a substitution as being 'probably damaging', 'possibly damaging', 'benign' or 'unknown' for the protein functionality. Given that both prediction methods are based on different protein characteristics, disparities between both methods are expected. The summary of the nature all point mutations in PI3Ki-resistant cells are presented in Appendix 14.

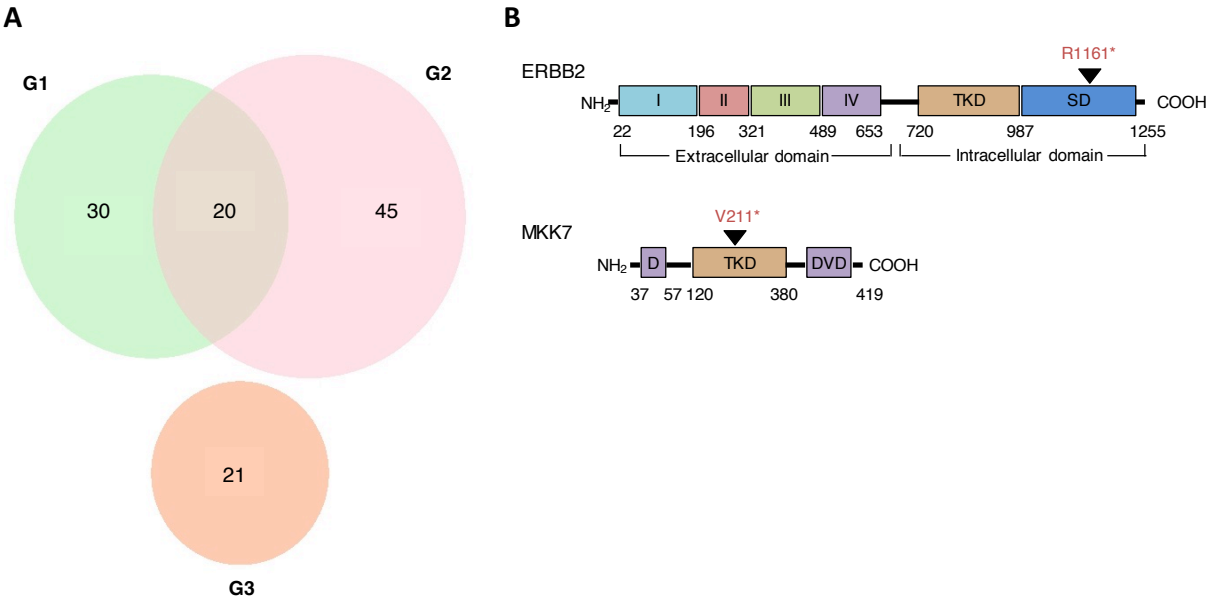

Figure 6.3 Reported common point mutations between G1 and G2 resistant cells. (**A**) Venn diagram shows the 20 point mutations shared between G1 and G2 resistant cells and the 21 point mutations exclusive of G3 resistant cells. (**B**) Location of missense mutations in ERBB2 and MKK7 proteins. TKD, Tyrosine kinase domain; SD, C-terminal signalling domain; D, D domain; DVD, Dual variable domain; * represents a stop-codon.

Table 6.2 Common point mutations for G1 and G2 resistant cells. Point mutations in ERBB2 and MAPK7 result in the truncation of these proteins.

Chr	Position	Reference	Alteration	Gene name	Amino acid position	Amino acid change	Mutation type	Sift_Prediction	Poly_Prediction
10	25273776	A	T	ENKUR	218	I>K	nonsyn	TOLERATED	PROBABLY DAMAGING
12	20787953	C	T	PDE3A	655	A>V	nonsyn	TOLERATED	BENIGN
14	105517794	T	G	GPR132	227	K>T	nonsyn	TOLERATED	POSSIBLY DAMAGING
14	59961938	C	A	**JKAMP**	166	P>T	nonsyn	DAMAGING	PROBABLY DAMAGING
14	74388787	G	A	ZNF410	400	S>N	nonsyn	DAMAGING	BENIGN
16	68156591	T	C	**NFATC3**	269	S>P	nonsyn	DAMAGING	PROBABLY DAMAGING
17	37884010	C	T	**ERBB2**	1161	R>*	nonsyn:stop-gain	Na	na
19	7975396	TG	T	**MAP2K7**	211	V>V	frameshift:stop-gain	Na	na
22	21991190	C	A	CCDC116	558	P>H	nonsyn	TOLERATED	POSSIBLY DAMAGING
3	180327887	T	A	**TTC14**	624	S>T	nonsyn	DAMAGING	PROBABLY DAMAGING
4	103682008	C	A	MANBA	15	G>V	nonsyn	TOLERATED	UNKNOWN
4	20736354	A	T	**KCNIP4**	145	F>Y	nonsyn	DAMAGING	PROBABLY DAMAGING
4	56865526	A	G	CEP135	690	K>E	nonsyn	TOLERATED	PROBABLY DAMAGING
4	6052337	G	A	**JAKMIP1**	626	L>F	nonsyn	DAMAGING	PROBABLY DAMAGING
5	78602211	C	T	JMY	632	A>V	nonsyn	TOLERATED	PROBABLY DAMAGING
8	110497292	T	A	**PKHD1L1**	3199	I>K	nonsyn	DAMAGING	PROBABLY DAMAGING
8	94767182	TG	T	TMEM67	14	W>C	frameshift:stop-gain	Na	na
8	94767184	G	T	TMEM67	14	W>C	nonsyn	TOLERATED	POSSIBLY DAMAGING
9	139735084	C	G	RABL6	409	C>W	nonsyn	DAMAGING	UNKNOWN
9	8499826	G	T	PTPRD	715	P>T	nonsyn	TOLERATED	PROBABLY DAMAGING

6.4 Chromosomal alterations in PI3Ki-resistant cells

Investigation of chromosomal alterations of PI3Ki-resistant cells, including copy number alterations (CNAs) (either gain or loss of chromosomal regions) and regions that showed loss of heterozygosity (LOH), revealed both common and cell line-exclusive chromosomal alterations across the three PI3Ki-resistant cell lines (Fig 6.4).

The most prevalent region in copy number gain was detected at the chromosomal 8 q arm (Fig 6.5A). It was interesting to observed that the three PI3Ki-resistant cell lines had gained copy number of *c-MYC*, a well-described oncogene frequently amplified in breast cancer cells [314], located in the 8q21 amplicon. *c-MYC* is a member of the NOTCH1 signalling pathway, and it has been found up-regulated in breast cancer cell models of acquired resistance to PI3Ki [313]. HEY1, another member of the NOTCH1 pathway, was amplified in the three PI3Ki-resistant cell lines (Fig 6.5A). *RAD21* and *EXT1*, located the chromosome 8 long arm, were also amplified in G1, G2, and G3 resistant cells.

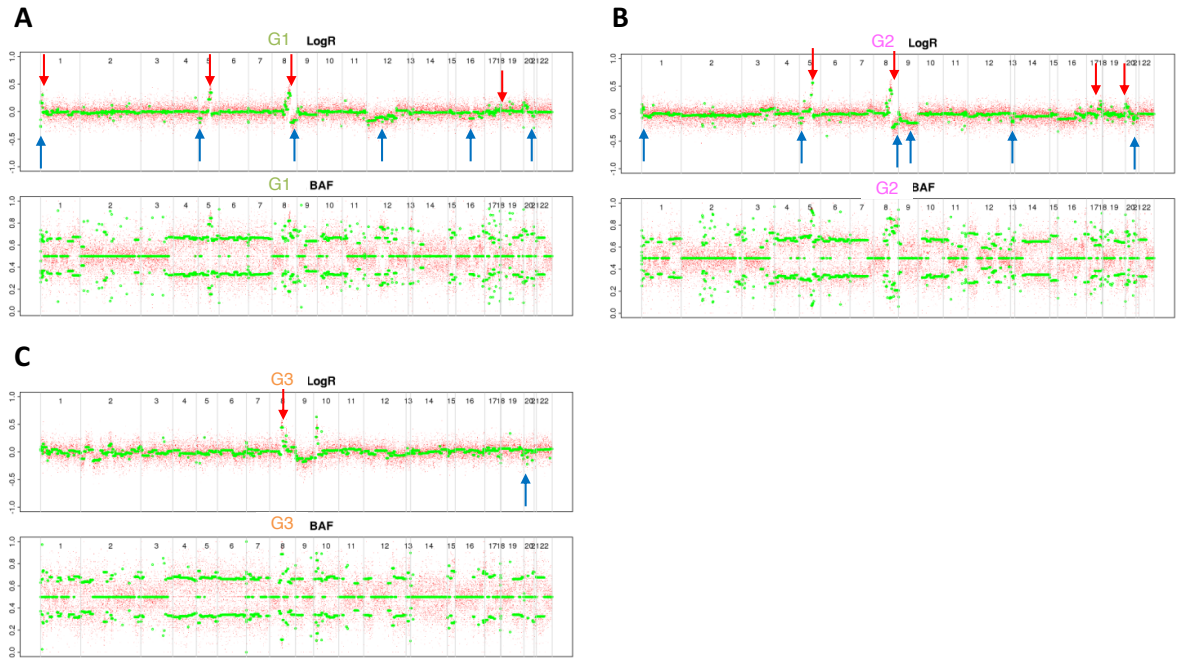

Figure 6.4 Copy number profiles show common and distinct altered areas along the genome (x axis) of the three PI3Ki-resistant cells. (**A**) (Upper panel) log ratio for G1 cells. Log Ratio is the log transform ratio of the observed probe intensity versus the expected intensity across all chromosomes. Deviations from 0 indicate copy number gain of loss. (Lower panel) the B allele frequency (BAF) for the G1 cells. BAF represents the proportion of a designated allele compared to the other allele. BAF 0.5 indicates homozygosity. (**B**) Same as in (**A**) for G2 cells. (**C**) Same as in (**A**) for G3 cells. Red arrows indicate gain in chromosomal regions and blue arrows indicate loss in chromosomal regions.

In addition to chromosomal region gains shared between the three PI3Ki-resistant cells, G1 and G2 resistant cells shared copy number gain of regions containing tumour suppressor genes that encode for APC, SMAD (and its associated protein ZN521), pro-apoptotic genes encoding for BCL2 protein and the BCL10-enhancer MALT1 and the SET-associated protein SETBP1. Overexpression of SETBP1 — a protein that binds and protects SET protein, which itself is a protease for PP2A — has proposed as a leukemogenic mechanism in elderly AML patients [321]. Two chromosomal regions — 5 q13.1-2 and 8 q24.22 — containing the *IL7R* and the *LIFR* genes respectively, were in copy number loss in G1 and G2 resistant cells, and one region — 20 q13.12 which contains the *SDC4* gene — was in copy number loss for G1 and G3 resistant cells (Fig 6.5A). *LIFR* has been identified as a tumour suppressor gene in metastatic breast cancer cells, and *in vivo* data demonstrated that restoring *LIFR* expression triggers the Hippo signalling pathway limiting tumour metastatic colonisation [322]. Interestingly, G2 and G3 resistant cells shared copy-number neutral LOH in regions of the small arm of the chromosome 12 (Fig 6.5A).

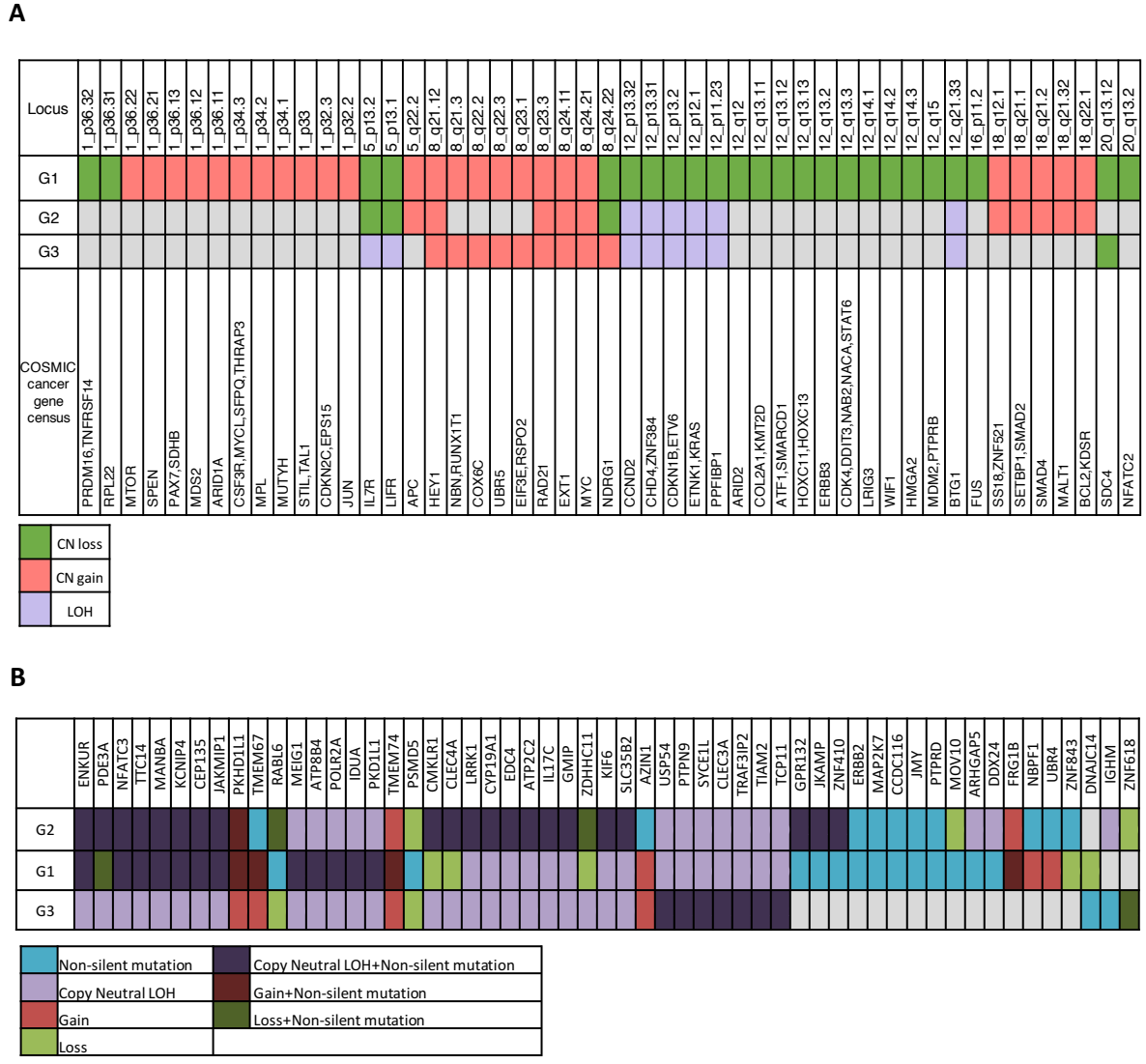

Figure 6.5 Summary of the genes mapped to the Catalogue Of Somatic Mutations In Cancer (COSMIC) database of regions that showed copy number alteration in resistant cells compared to parental. (**A**) Type of copy number variant and chromosomal location identified in the resistant cells. Genes catalogued in the database of cancer somatic mutations COSMIC [284] located in altered chromosomal regions in PI3Ki-resistant cells are shown. (**B**) Type of copy number variants and the mutational status of genes contained in altered chromosomal regions in PI3Ki-resistant cells are shown.

Copy-number neutral LOH events originate either through homologous chromosomal-recombination or by chromosomal regional-duplication and further deletion [323]. Analysis of the type of LOH in PI3Ki-resistant cells revealed that most of LOH regions did not contained non-silent mutations, despite LOH affected regions in G1 and G2 resistant cells where 7 genes presented non-silent mutations (Fig 6.5B). Moreover, whilst G1 and G2 cells amplified a chromosomal region that contained a non-silent mutation in the gene *PKHD1L1*, G3 resistant cells amplified that region but did

not have any mutation in *PKHD1L1* gene. The gene *ZDHHC11* was in copy number loss for G1 and G2 resistant cells, but was in copy neutral LOH for G3 resistant cells.

6.5 Conclusions

A comprehensive characterisation of the exome landscapes of three cell lines that had acquired resistance to GDC-0941 (G1:G3) and the parental MCF7 cells (P) was performed using whole-exome sequencing. This analysis recapitulated the higher similarity between G1 and G2 resistant cells in terms of the number and type of non-synonymous point mutations (Fig 6.2A and 6.2C). The VAF density (VAF range of 0.21-0.27) indicated that not all cells within the population of each resistant cell lines had the mutational allele, evidencing the heterozygosity of the PI3Ki-resistant cells (Fig 6.2D).

G1 and G2 resistant cells carried common missense point mutations in *Erbb2* and *Mapk7* genes that will result in the premature translation termination of the proteins encoded by those genes (Fig 6.3 and Table 6.2). The orphan receptor ERBB2 serves as a partner to form heterodimers with other receptors of the ERBB family (e.g. ERBB3 or EGFR), or constitute ERBB2 homodimers, and its expression is low in MCF7 cells compared to other breast cancer cell lines [324]. The precipitated termination of ERBB2 protein at amino acid 1161 located within the protein intracellular domain eliminates protein C-terminal phosphorylation sites Tyr^{1169}, $Tyr^{1221/1222}$ and the autocatalytic phosphorylation Tyr^{1248}. However, ERBB2 C-terminal phosphorylation site Tyr^{1139} and site Tyr^{877} at the kinase domain may remain intact in PI3Ki-resistant cells. ERBB2's phosphosite Tyr^{1139} is known to be a docking site for Grb2, and can mediate signalling by phosphorylation of p38 MAPK at Thr^{180}/Tyr^{182}, possibly promoting cell survival [325]. Phosphorylation of ERBB2 at Tyr^{877} by protein kinase c-SRC has been associated with engagement of MAPK and AKT signalling activity [326]. Thus, and despite the premature termination of ERBB2 protein in G1 and G2 resistant cells, these cells might retain some signalling activity through this receptor, and understanding ERBB2-mediated downstream signalling in PI3Ki-resistant cells would require further analysis. On the other hand, activity disruption of the stress kinase MKK7 in resistant cells might alter their genotoxic stress responses, as suggested by the data of Schramek *et al*. that showed that MKK7 inactivation enhanced the malignant progression of mice tumours [320]. Finally, it was interesting to see that G1 and G2 resistant cells also underwent point mutations predicted to be damaging for the function of JKAMP, NFATC3, TTC14, KCNIP4, JAKMIP1, and PKHD1L1 proteins (Table 6.2). Further work is required to understand the functional role of these mutations in PI3Ki-resistant cells.

Analysis of copy number variations in PI3Ki-resistant cells revealed a range of chromosomal loci that have gained or lost allelic copy number or have lost heterozygosity (Fig 6.4). In line with the observations made in previous *in vivo* studies [301, 313, 314], this study indicated that PI3Ki-resistant cell lines had copy number gain of *c-MYC* gene (Fig 6.5A). In addition, the three PI3Ki-resistant cells had an increased copy number of *RAD21* gene, which was previously found to be correlated with poor prognosis and chemotherapy resistance in various breast carcinoma types [327]. In addition, the present analysis identified recurrent mutations that have not been previously associated to PI3Ki resistance mechanisms, such as mutations in the *EXT1* gene that encodes for a glycosyltransferase involved in the biosynthesis of heparan-sulphate.

Chapter 7. Exploration of cellular responses to lactic acid treatment of a luminal breast cancer cell line

7.1 Introduction and aims of the study

Chapter 5 detailed the metabolic alterations of cancer cells that had acquired resistance to PI3K and mTORC1/2 inhibition. Among the metabolic changes of these cells, it was observed that metabolism-derived products accumulated either intracellularly (e.g. ROS) or in the extracellular milieu (e.g. lactic acid). Having explored the metabolic alterations that occur in PI3Ki-resistant cells during drug holidays, it was interesting to explore what effect lactic acid, one of the products of such metabolic imbalance, may have on the biochemistry of cancer cells.

It was hypothesised that cells that express transporters for lactate (MCTs) and lactate cognate receptor (GPR81) could be affected by extracellular or intracellular changes of this monocarboxylate (as alluded in Section 1.2.2). The acidosis derived from the deprotonation of lactic acid into lactate and proton (H^+) could impact the functionalities of cancer cells, and is regulated by a wide range of cellular mechanisms (as also alluded in Section 1.2.2).

The aim of the experiments presented in this Chapter was to determine the signalling properties of lactic acid with a marked focus on MCF7 cells (Fig 7.1). In this *in vitro* study the impact of lactic acid within the range of physiological concentrations and the contribution of acidosis was examined.

MCF7 cells were selected as a model because the lactic acid production of this cell line was previously quantified and changes in the lactic acid production in drug-resistant cells derived from MCF7 cells were detected (these results were presented in Chapter 5). Several experiments were performed to understand the lactic acid-mediated changes in the proteome and phosphoproteome of these cells as well as functional impact of exposing these cells to lactic acid. Initially, the protein expression of MCT1, MCT2, and MCT4 transporters was assessed. The effect of pharmacologically blocking MCT1 was also explored. The level of the lactate receptor GPR81 in these cells was then measured. It was hypothesised that lactic acid could serve as a nutrient for cells exposed to glucose starvation. To test this hypothesis, the proliferative effect of lactic acid on cells exposed to glucose depletion was examined. The signalling and protein expression changes upon treating the cells with lactic acid and acidosis were monitored by LC-MS/MS. Finally, the functional impact of a range of lactic acid and acidosis concentrations on cellular features including proliferation, apoptosis and cell morphology and cytoskeletal structure was examined.

Overall, it was postulated that if lactic acid affects the functionality of MCF7 cells, this cell line would represent a model to understand the impact of lactic acid exposure in cancer cells. It is important to note that the effect of lactic acid, or other metabolites, could ultimately depend on the levels of metabolite-specific transporters and receptor present in each cell type, as suggested by Birsoy *et al*. [112].

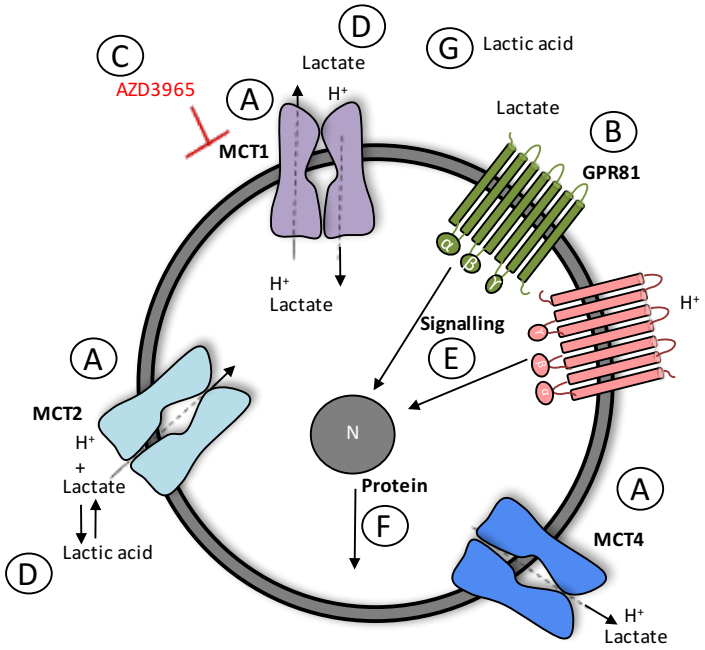

Figure 7.1 Schematic representation of experiments performed to assess the impact of lactic acid in MCF7 cells. (A) Lactate transport is modulated via MCTs. The MCT family includes 14 members and MCT1-4 mediate proton-mediated transport. Cells that express these transporters can potentially regulate the traffic of monocarboxylates including lactate, pyruvate, and ketone bodies across cellular membranes. The expression of these transporters in MCF7 parental and PI3Ki-resistant cells was initially examined. (**B**) The protein levels of lactate receptor GPR81 (also known as HCA1 or HCAR1) in MCF7 cells was examined. (**C**) The impact on MCF7 cells proliferation of treatment with a chemical inhibitor against MCT1 was examined. (**D**) The capacity of lactic acid to promote resistance to glucose-starvation in these cells was examined. (**E**) The signalling cascades modulated upon treatment of MCF7 cells with lactic acid or hydrochloric acid (this treatment was used to account for acidosis) were analysed. (**F**) The modulation of the proteome of cells upon exposure to lactic acid or HCl was characterised. (**G**) The effect of lactic acid and acidosis exposure on cellular apoptosis and cell morphology was explored.

7.2 Determination of lactate transporters in a panel of cell lines

The presence of proton-coupled monocarboxylate transporters required for lactate flux across cellular membranes (i.e. MCT1, MCT2, and MCT4) in MCF7 parental and PI3Ki-resistant cells was investigated by Western blotting. The data shown in Fig 7.2 demonstrated that MCF7 parental and PI3Ki-resistant cells express these transporters, albeit their amounts were different across cell lines. For example, MCT4 transporter was expressed at highest levels in G2- resistant cells. This result was in accordance with the observation made in Chapter 5 that G2- cells had an enhanced glycolytic phenotype, since

MCT4 is often greatly expressed in highly glycolytic tissues [328]. MCF7 parental cells showed expression of the three MCTs transporters, although the expression of MCT4 in these cells was lower compared to the expression of MCT1 and MCT2 (Fig 7.2).

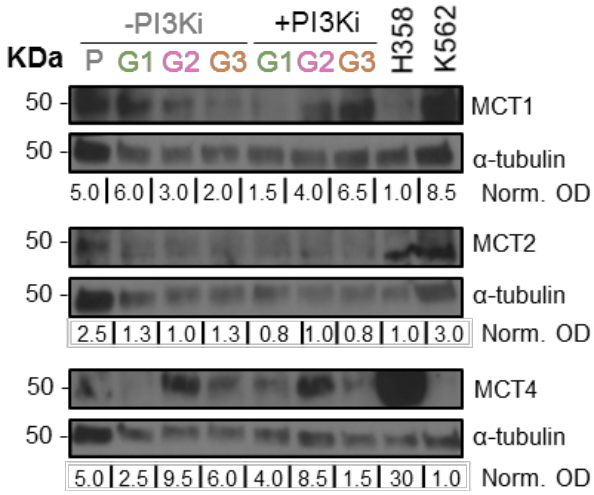

Figure 7.2 MCF7 parental and PI3Ki-resistant cells express lactate membrane transporters. Western blots against MCT1, MCT2, and MCT4 in MCF7 parental and PI3Ki-resistant cells maintained in the presence or absence of PI3Ki. H358 cell line (non-small cell lung cancer) and K562 cell line (myelogenous leukaemia) were used as positive control for MCT4 and MCT1, respectively. H358 and K562 cell lines were positive control for MCT2. α-tubulin loading controls are shown for each case.

7.3 Determination of lactate receptor in MCF7 cells

The expression of the lactate receptor GPR81 in MCF7 cells was determined. The result of this experiment demonstrated that GPR81 was expressed in MCF7 cells (Fig 7.3), in accordance with the mRNA expression of GPR81 in this cell line reported by Kapushesky *et al*. [329]. This experiment also showed that the siRNA treatment used against GPR81 failed to knock down the expression of GPR81 in a consistent manner (Fig 7.3).

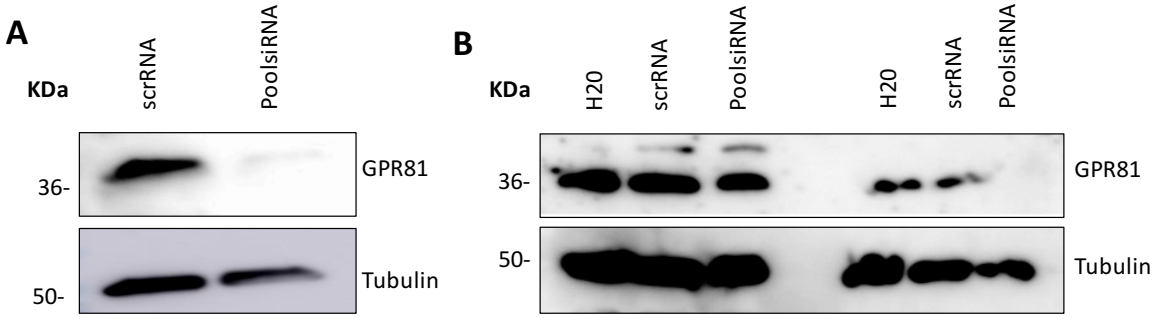

Figure 7.3 MCF7 cells express the receptor for lactate. (**A**) Western blots against GPR81 protein levels on MCF7 cells and after 72 h treatment with 35 nM pool-siRNA against GPR81. Tubulin loading control is shown. (**B**) Same as (**A**) for cells pellets extracted with RIPA buffer (first three lanes) or Laemmli buffer (last three lanes).

7.4 Response to a MCT1 transporter inhibitor

AR-C155858 is a specific inhibitor that binds to an intracellular site of the MCT1 transporter and has recently entered phase I for gastric and prostate cancer and diffuse large B-cell lymphoma in the United Kingdom [141]. Given that it was observed that MCF7 cells express MCT1 lactate transporter (Fig 7.2), the response of these cells upon treatment with an MCT1 inhibitor (MCT1i) was examined. To implement this, MCF7 cells were seeded in 6-well plated and treated with either 5 nM or 10 nM MCT1i for 72 h. The number of cells and pH of the culture media was measured after that time. Each experiment was performed in triplicate. The results of these experiments showed that MCTi reduced the number of viable MCF7 cells in a concentration dependent manner (Fig 7.4A). After 72 h, 10 nM MCT1i reduced approximately 50% of MCF7 cells (P = 0.03), and 5 nM approximately reduced a 25% number of cells. Moreover, the pH of culture media was slightly less acidic (ΔpH= 0.07 after treatment with 10 nM MCT1i), although the results did not reach statistical significance (Fig 7.4B).

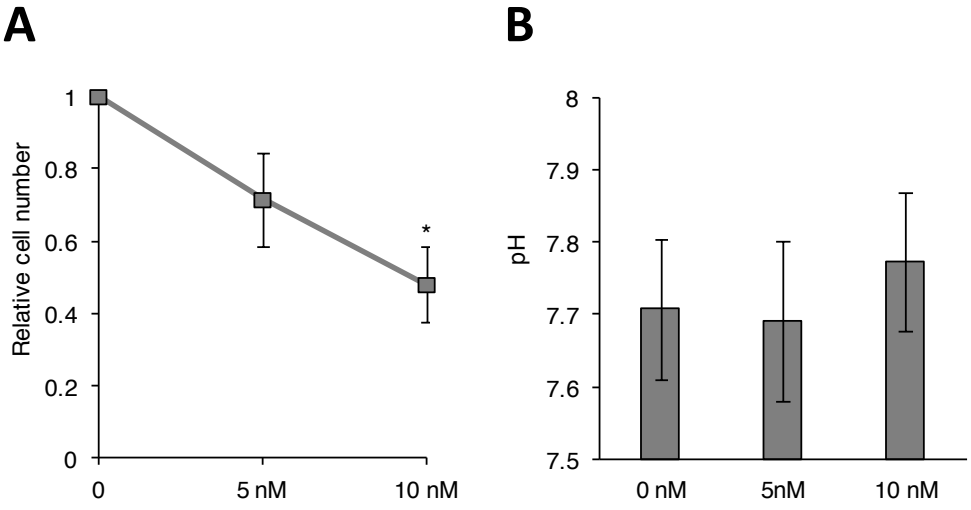

Figure 7.4 Treatment with a MCT1 inhibitor causes cell death and decreased acidification of the media. (**A**) Normalised number of MCF7 cells (relative to control DMSO) upon treatment with 5 nM or 10 nM of MCT1i for 72 h. (**B**) pH values of culture media of (**A**). Data are mean ± SD (n=3, three independent replicates). P -values calculated using an unpaired, two-tail Student's t-test for each treatment concentration against control. * P < 0.05.

7.5 Nutrient properties of lactic acid

As previously discussed in Section 5.10, MCF7 cells are sensitive to glucose depletion. It was proposed that lactic acid could contribute to cell survival under glucose starvation. To determine whether these cells could employ lactic acid as the main energy source, in other words, whether lactic acid could be the carbon-source of glucose-depleted cultures, cells were plated in triplicate in full-nutrients media for overnight attachment. The next day (t=0), complete DMEM without glucose and containing increasing concentrations of lactic acid — 10 mM, 20 mM, 30 mM or no lactic acid — was replaced

and cells were grown for 72 h. Cell viability was measured after that time. The analysis shown in Fig 7.5 suggested that lactic acid contributed to the proliferation of cell deprived of glucose, since there were between 2.5-2.7 times more cells upon treatment with 10-30 mM lactic acid, although the increase in cell viability was not significant compared to cells grown in media without glucose and lactic acid.

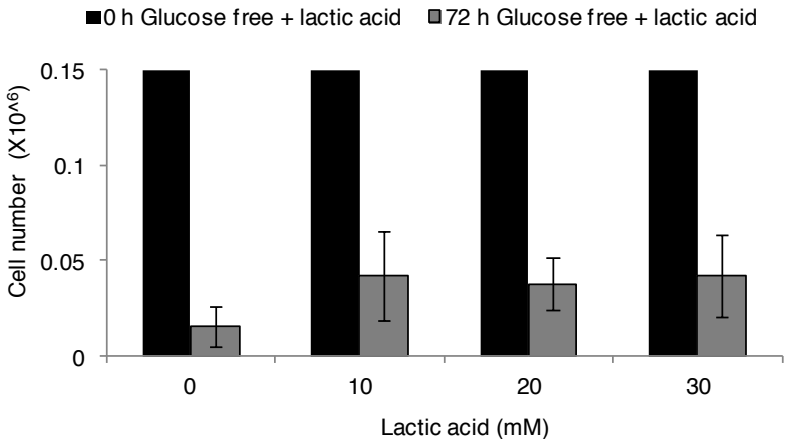

Figure 7.5 Lactic acid does not fully substitute glucose to sustain the proliferation of MCF7 cells. Numbers of MCF7 cells grown in full media depleted from glucose supplemented or not with lactate measured after 72 h. Data are represented as mean ± SD (*n*=3, three independent replicates).

7.6 Media acidification by lactic acid and hydrochloric acid

The acidic milieu can affect the cellular behaviour [113]. To resemble the acidity resulting from exposure of cells to lactic acid (which dissociated in lactate and protons [H^+]) an acidic environment was mimicked using HCl (which dissociates in protons [H^+] and the chloride ion [Cl^-]). To obtain the equivalence point for lactic acid and HCl, pH values were measured as a function of increasing concentrations of these acids in media. More specifically, range of 0-50 mM lactic acid was added to 10 mL of DMEM media. The results shown in Fig 7.6 demonstrated that 0.97 mM HCl produced a similar pH to 5 mM of lactic acid and that addition of 9.7 mM HCl produced a similar pH to 20 mM lactic acid. These values were taken further for following experiments.

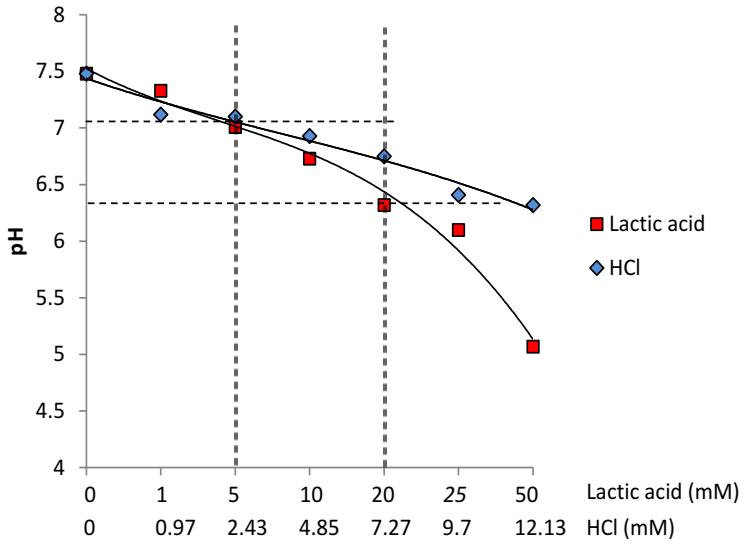

Figure 7.6 pH curves as a function of addition of lactic acid and HCl to media. pH values obtained as a function of lactic acid and HCl addition to DMEM media at the indicated concentrations.

7.7 Signalling capacity of lactic acid

Cells regularly require mitogenic factors to grow and proliferate. Foetal bovine serum (FBS) is a cocktail used to supplement growth media with the components required for cellular proliferation. The undefined and variable nature of FBS composition has motivated the implementation of alternative formulation for *in vitro* mammalian cell culture [330].

Given the expression of lactate receptor in MCF7 cells (as shown in Section 7.3) and given the know ability of lactic acid to trigger signalling events [168, 331], it was hypothesised that lactic acid may compensate the proliferative action of FBS-contained factors. An experiment was designed to explore this hypothesis, whereby MCF7 cells were grown in DMEM media depleted from FBS and supplemented with increasing concentrations of lactic acid — 1 mM, 5 mM, and 10 mM —, supplemented with the respectively concentration of HCl control, or not supplemented. Cell proliferation was measured after 24 h, 48 h or 72 h of treatment by means of a Vi-CELL counter. Lactic acid was not able to promote the growth rate of MCF7 cells cultured without FBS as shown in Fig 7.7.

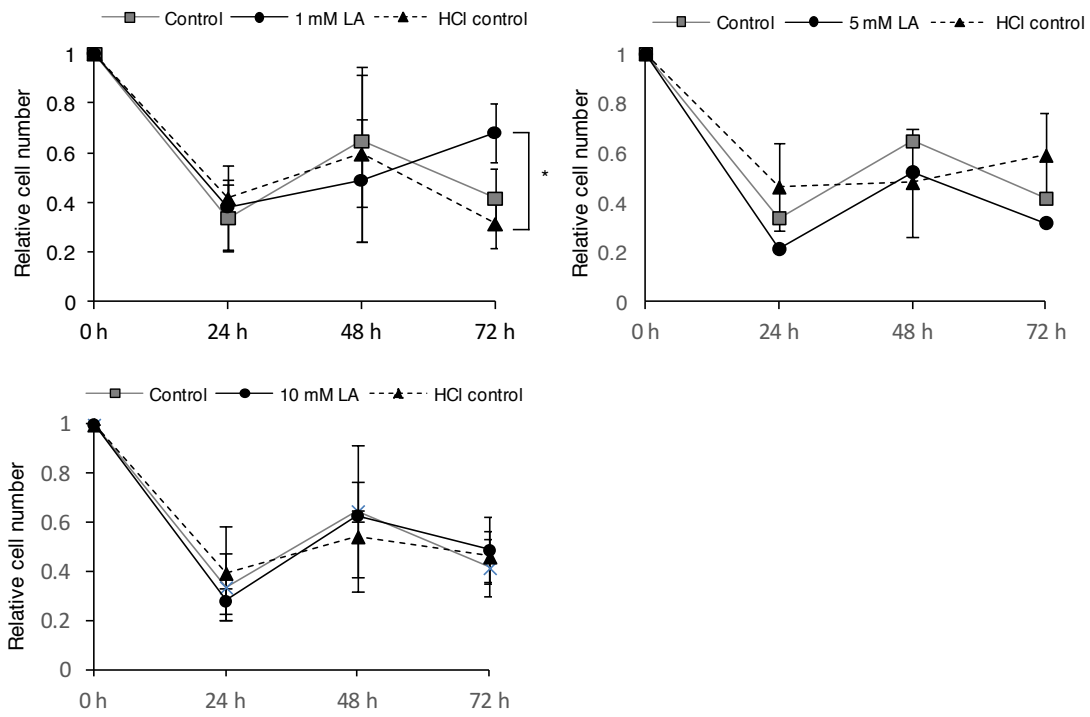

Figure 7.7 Lactic acid per se does not replace the proliferation outcome of FBS. Number of MCF7 cells grown in FBS-free media supplemented with 1 mM, 5 mM, 10 mM lactic acid, the corresponding HCl control that provide an analogous acidic microenvironment, or supplement with H_2O (control) measured after 1, 2, and 3 days. Data are represented as mean ± SD (*n*=3, three independent replicates). *P*-values were calculated using an unpaired, two-tail Student's *t*-test of the lactic acid condition against H_20 or against HCl. * $P < 0.05$.

7.8 Network plasticity in response to lactic and hydrochloric acid treatment

The previous experiments suggested that: (i) MCT1, MCT2, and MCT4 transporters are expressed in the MCF7 cell line; (ii) chemical inhibition of the MCT1 transporter reduces the proliferation of MCF7 cells; (iii) the lactate receptor GPR81 is expressed in MCF7 cells; (iv) lactic acid may contribute to the proliferation of glucose-starved cells; and (v) lactic acid was not sufficient to provide the mitogenic signals required to maintain the proliferation of MCF7 cells. Taking these results into consideration, and to shed light into the biological functions of lactate, the signalling pathways triggered by treating these cells to low and high concentrations of lactic acid and HCl were analysed. To this end, an experiment was designed using MCF7 cells maintained for 24 h with 0.5 % FBS DMEM and then treated with either 5 mM lactic acid or 0.97 mM HCl (low acidic concentrations) and 20 mM lactic acid or 9.7 mM HCl (high acidic concentrations) for 5, 15, 30, or 60 minutes, or not treated (*t*=0, control). The experiment was performed in biological duplicates and the phosphoproteomes of the cells at each time point were run in the LC-MS/MS in technical duplicates. The analysis of the quality control for these datasets is shown in Appendix 15.

7.8.1 Overview of the results

The normalised phosphoproteomics data was compared against the non-treated control. The resulting analysis of the abundance of statistically significant modulated phosphopeptides for each time-point and condition is shown in Fig 7.8. These data serve as an overview of the effect of lactic acid or HCl treatment on the cellular phosphoproteome of MCF7 cells. The number of phosphopeptides that significantly increased upon treatment with high concentration of lactic acid was greater than those that changed upon treatment with low lactic acid concentration. Moreover, the number of phosphopeptides that significantly decreased was higher at longer time-points, which highlights the differential de-phosphorylation kinetics of cells treated with lactic acid or HCl.

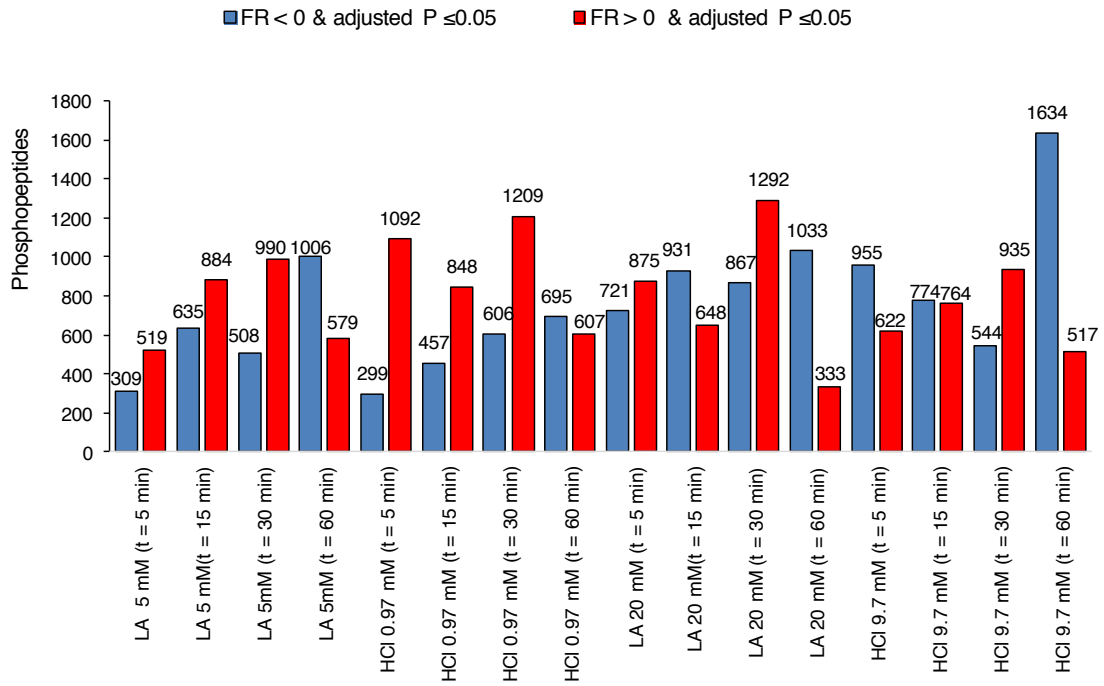

Figure 7.8 Analysis of differential abundance of phosphopeptides. The number of significantly (FDR<0.05) decreased (blue bars) or increased (red bars) phosphopeptides compared to *t* = 0 min is shown (*n*= 9,611). FR, $\log_2$ fold-ratio vs H_2O control; adjusted *P*, is the corrected *P*-value for multiple testing by the Benjamini-Hochberg method.

7.8.2 Evaluation of positive controls and validation of MS analyses

Previous studies showed that lactate promotes the activation of MAPK [115, 331] and AKT signalling [168], in a concentration- and time-dependent manner. For example, AKT signalling reached maximum activity after 10-30 min of lactate treatment [168]. Moreover, acidosis is known to induce the activity of AKT and MAPK [332, 333].

To initially investigate the MS-derived phosphoproteomics data, a number of phosphorylation sites involved in MAPK and PI3K signalling pathways were extracted from the data, and their temporal modulation profiles upon lactic acid and HCl treatment analysed. These data showed that upon treatment with high concentrations of lactic acid and HCl, members downstream of the MAPK signalling axis underwent substantial increase in phosphorylation. For instance, the phosphorylation of ERK1/2 (MAPK1 at Tyr^{187} and MAPK1 seq 173-191 phosphorylation at Ser or Thr; MAPK3 at Tyr^{204} and MAPK3 at Thr^{202} and Tyr^{204}), p90RSK (RPS6KA1 seq 729-735 phosphorylation at Ser or Thr) and p70S6K (RPS6KB1 Ser^{447} and RPS6KB1 Ser^{452}) increased upon treatment of cells with high concentrations of lactic acid or HCl (Fig 7.9A).

Similarly, phosphorylation sites associated to the PI3K/AKT/mTOR signalling axis also demonstrated differential temporal kinetics upon treatment with lactic acid or HCl. Consistent with an activation of PI3K signalling, a site on AKT1S1 (most probably at Thr^{246}), also known as PRAS40, increased its phosphorylation, and the magnitude of this activation was greater after treatment with higher concentrations of lactic acid or hydrochloric acid (Fig 7.9A). In-line with AKT's activation, the phosphorylation of peptide derived from GSK3β seq 7-27 (most probably Ser^{9}, a direct AKT's substrate) increased upon treatment with high concentrations of lactic acid or HCl. This site had a later kinetics than the phosphorylation of AKT1S1. Phosphorylation of ACLY at Ser^{455}, another substrate target of AKT that engages the activity of ACLY [334], also increased under lactic acid or HCl treatments.

Additional downstream markers related to the PI3K pathway, such as phosphorylation sites substrates of mTOR, including EIF4, RICTOR, RPS6KB1, EEF2K, and ULK1 were modified in abundance under treatment with different concentrations of acids. For example, low concentrations of acids induced an increase in the phosphorylation of the RICTOR on a phosphopeptide seq 1217-1235 (most likely at Ser^{1235}), but the abundance of this phosphorylation inhibitory site was reduced upon treatment with high levels of acids (Fig 7.9A). The RICTOR site Ser^{1235} is a substrate of GSK3β that prevents the interaction between AKT and mTORC2 [335]; blockade of activity of GSK3β associated with an increased phosphorylation at Ser^{9} might enable the activation of mTORC2-AKT signalling. Conversely, the phosphorylation of RAPTOR at Ser^{863} and Ser^{877}, which are markers of mTORC1 activity [336], decreased upon treatment with high concentration of acids (Fig 7.9A). The phosphorylation of ULK1 at Ser^{556}, a well-known substrate of AMPK and a marker of autophagy, increased in abundance upon treatment of cells with high concentrations of acids, but was not altered when the cells were treated with lower acids concentrations (Fig 7.9A). Other marks linked to AMPK activity included increased phosphorylation of SAFB at $Ser^{601/604}$ and reduced phosphorylation of eukaryotic elongation factor 2 kinase (eEF2K) at $Ser^{72/74}$ (Fig 7.9A).

Western blotting against ERK1/2 at Thr^{202}/Tyr^{204}, related to the canonical MAPK signalling activation, was performed to confirm the LC-MS/MS-derived data shown in Fig 7.9A. The resulting data confirmed that treatment with high concentrations of lactic acid or HCl led to a fast activation of MAPK signalling pathway after 5 min treatment (Fig 7.9B). In addition to this observation, and in concordance with the phosphoproteomics data, the activation of MAPK signalling was of higher magnitude upon treatment with lactic acid compared to HCl (Fig 7.9B).

Overall, these results support the notion that treatment with different concentrations of lactic acid and HCl induces the modulation of signalling activity downstream of AKT and MAPK, and in addition reveal potential novel effects of these stimuli on AMPK, mTORC1, protein translation, and autophagy.

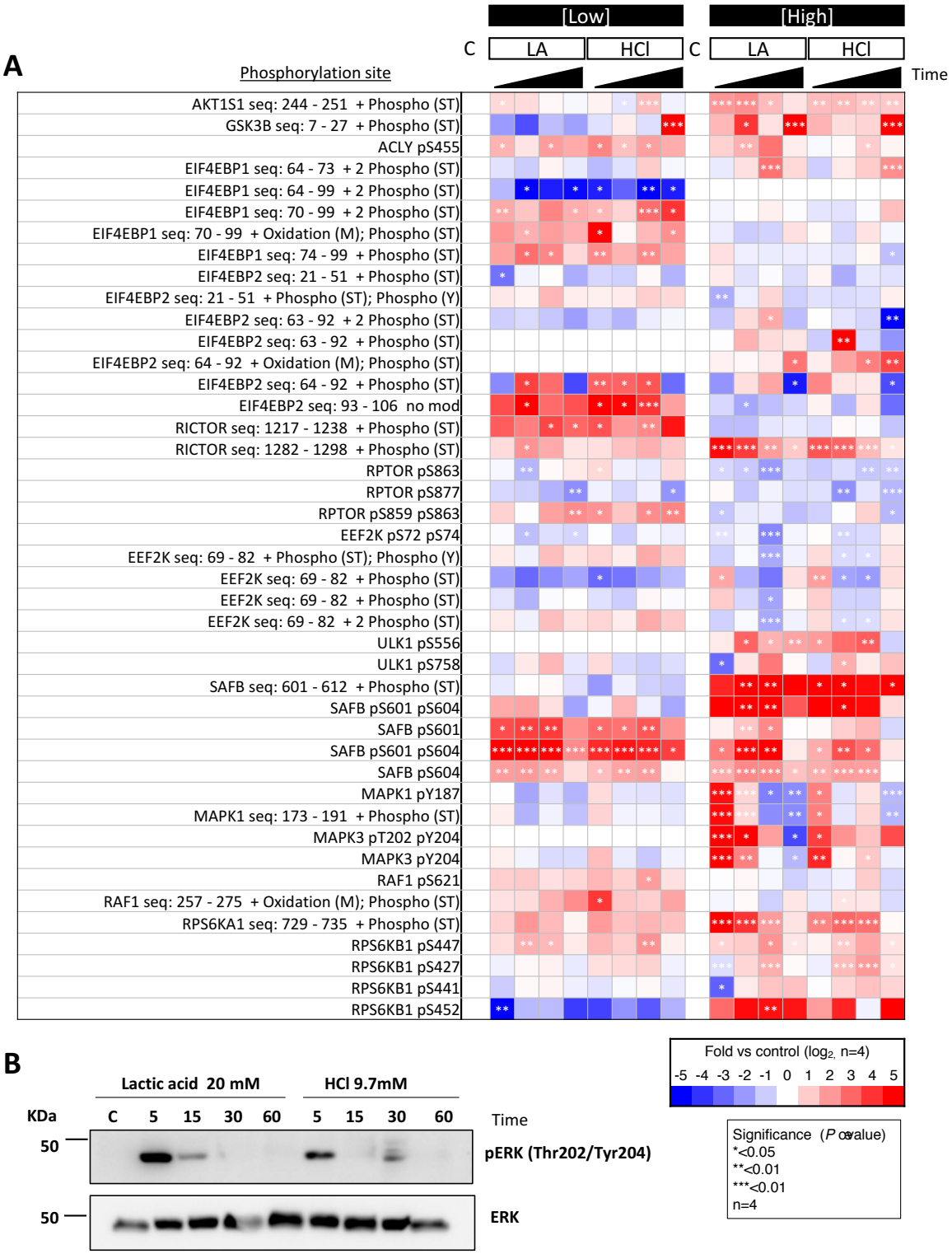

Figure 7.9 Phosphorylation sites members of the PI3K/AKT/mTOR and MAPK signalling cascades are modulated upon lactic acid and HCl treatments. (**A**) Heatmap of the $\log_2$ fold-change (vs control, C) over a time course for selected phosphorylation sites of the PI3K/AKT/mTOR and MAPK signalling axis. Uniprot gene name and phosphorylation sites are shown. If Mascot *δ*-score the peptide is < 10, peptide is shown as Uniprot gene name followed by sequence residues and phosphorylation. (**B**) Westerns blot for ERK at Thr^{202}/Tyr^{204}, marker of activity of the MAPK signalling axis. Abundance of the unmodified protein ERK loading control is shown.

7.8.3 Temporal behaviour of defined signalling branches

The dynamics of the global kinase-driven network of MCF7 cells have been previously defined [226]. The empirical characterisation of the signalling modulation of this cell line was performed based on the associations of kinases-driven signalling activity in response to external stimulation (i.e. EGF or IGF-1 stimulation). To define this signalling network, cells were treated with a panel of kinase inhibitors and sites that change their phosphorylation status were considered readouts of the kinase affected by the inhibitor, the so called CTAM network analysis, from Compound targets activity markers [226]. Concretely, this network included the relationship of 24 network branches up-regulated upon EGF stimulation of and 23 signalling axes up-regulated upon IGF-1 stimulation. This defined network represents a useful resource to perform unbiased analyses of signalling changes that occur in MCF7 cells in response to any given perturbation.

The modulation of the kinases-mediated signalling network in response to lactic acid or HCl treatment was then explored. Similarly to Fig 7.9, the analysis of signalling cascades revealed a high similarity in the behaviour of signalling branches on cells treated with similar concentrations of lactic acid or HCl, and differences in the signalling events after treatment with high and low concentrations of acids (Fig 7.10 and 7.11).

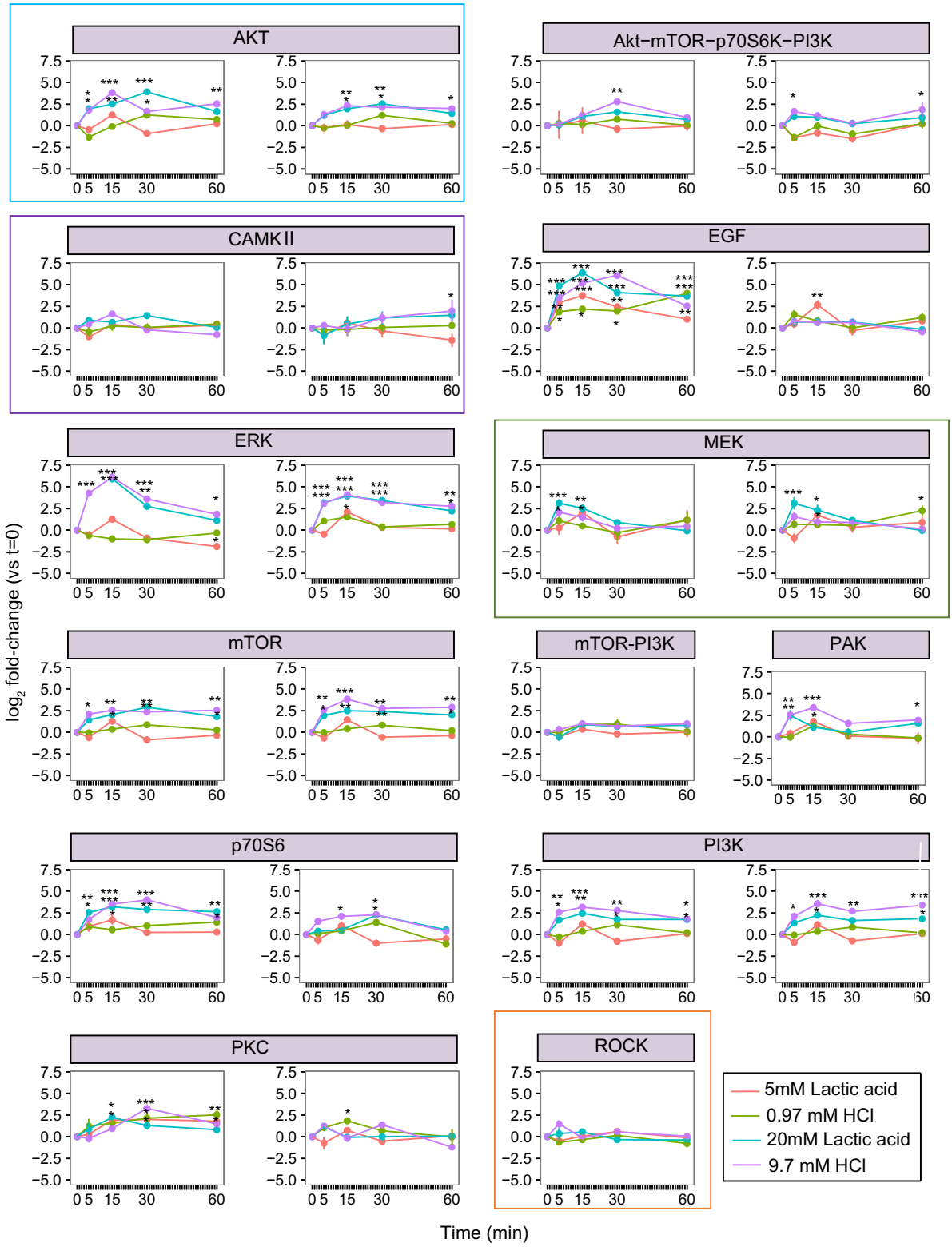

Figure 7.10 MCF7 signalling branches triggered with EGF stimulation are activated upon lactic acid and HCl treatment. MCF7 signalling branches activated upon EGF stimulation significantly modulated upon treatment with low and high concentrations of lactic acid and HCl. Data are represented as mean ± SD (n=4, four independent replicates). *P*-values were calculated from a *Z*-score between each time point and t= 0 min; * $P < 0.05$; ** $P < 0.01$; *** $P < 0.001$.

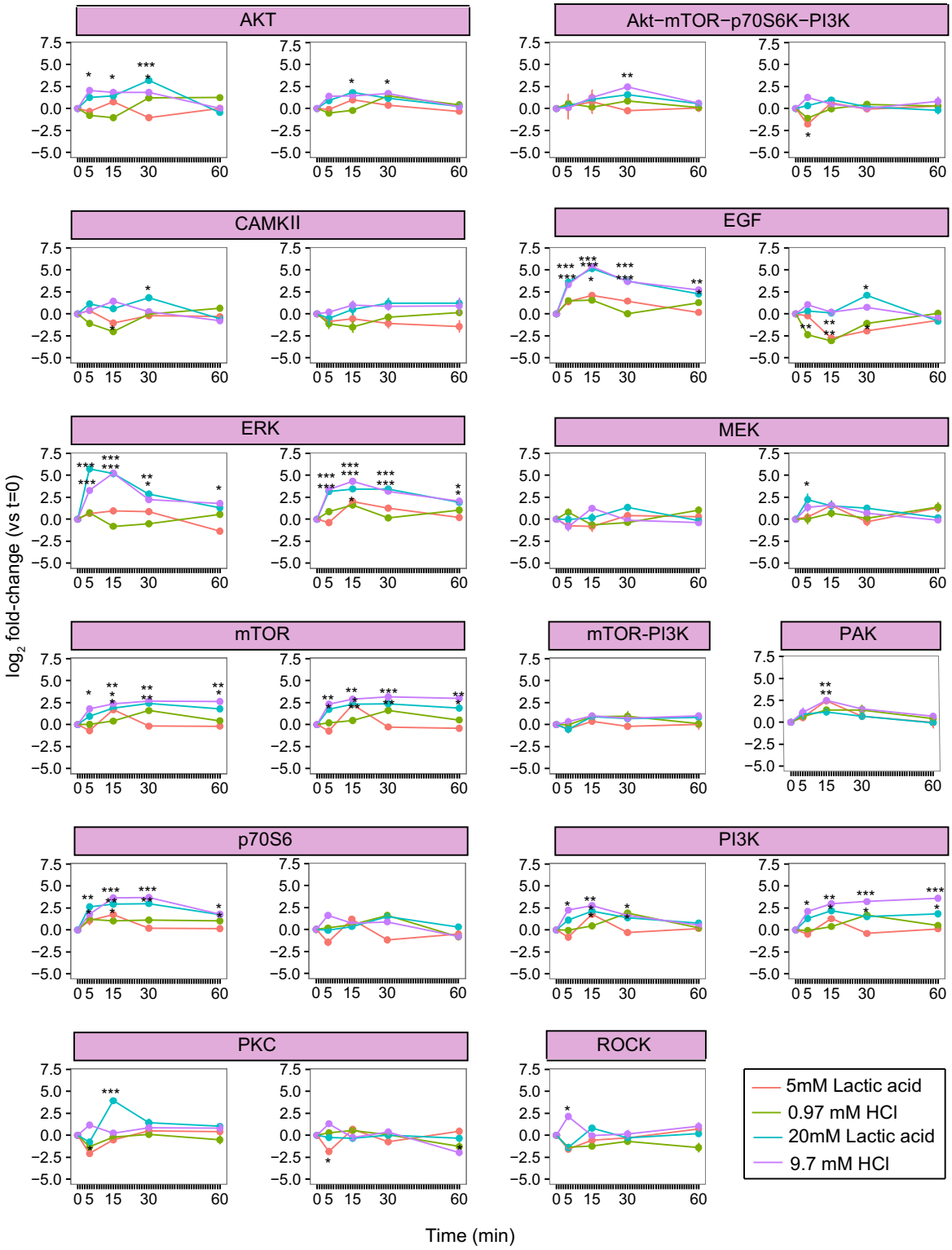

Figure 7.11 MCF7 signalling branches triggered with IGF-1 stimulation are activated upon lactic acid and HCl treatment. (**A**) MCF7 signalling branches activated upon IGF-1 treatment significantly modulated upon treatment with low and high concentrations of lactic acid and HCl. Data are represented as mean ± SD (n=4, four independent replicates). P-values were calculated from a Z-score between each time point and t= 0 min; * P < 0.05; ** P < 0.01; *** P < 0.001.

Further analysis of these data revealed that those pathways that are both up-regulated upon EGF/IGF-1 stimulation and down-regulated when MEK and PI3K are inhibited were activated upon treatment with lactic acid or HCl, being the magnitude of activation greater and more acute for EGF/IGF-1-MEK signalling branches compared to that one of EGF/IGF-1-PI3K signalling branches (Figs 7.10 and 7.11).

For example, the EGF-MEK branch underwent an average 3.1-fold change and a 1.8-fold change after 5 min treatment with 20 mM lactic acid or with 9.7 mM HCl, respectively (Fig 7.10, green square), whereas the EGF-AKT branch underwent an average 1.57-fold change and a 1.55-fold change after 5 min treatment with 20 mM lactic acid or with 9.7 mM HCl, respectively (Fig 7.10, blue square). Alongside, the extent of modifications of EGF/IGF-1-ROCK and EGF/IGF-1-CAMKII branches was lower than those involving MEK and PI3K signalling branches. More specifically, the EGF-ROCK branch underwent 0.34-fold change and 1.46-fold change after 5 min treatment with 20 mM lactic acid or with 9.7 mM HCl, respectively (Fig 7.10, orange square), and the EGF-CAMKII did not change upon treatment with 20 mM lactic acid, and underwent an average 0.48-fold change after 5 min treatment with 9.7 mM HCl (Fig 7.10, purple square).

To systematically assess the differences in temporal behaviour upon treatment with low or high concentration of lactic acid or HCl on the whole pre-defined MCF7 signalling network, a multivariate analysis of the 47 signalling cascades was performed. The resulting data demonstrated that whilst the modulation of the defined signalling branches was very similar between treatment with analogous concentrations of lactic acid and HCl (Fig 7.12B, left panel: treatment with low concentration of both acids; right panel: treatment with high concentration of acids), these signalling axes were differently modulated upon the acute exposure of cells to low or high concentration of each acid (Fig 7.12A, left image: treatment with lactic acid; right image: treatment with HCl). These analyses also revealed that this network as a whole was most different to the basal state after 15 min treatment with acids, and that the signalling activity started returning back to the original state after 60 min (Fig 7.12).

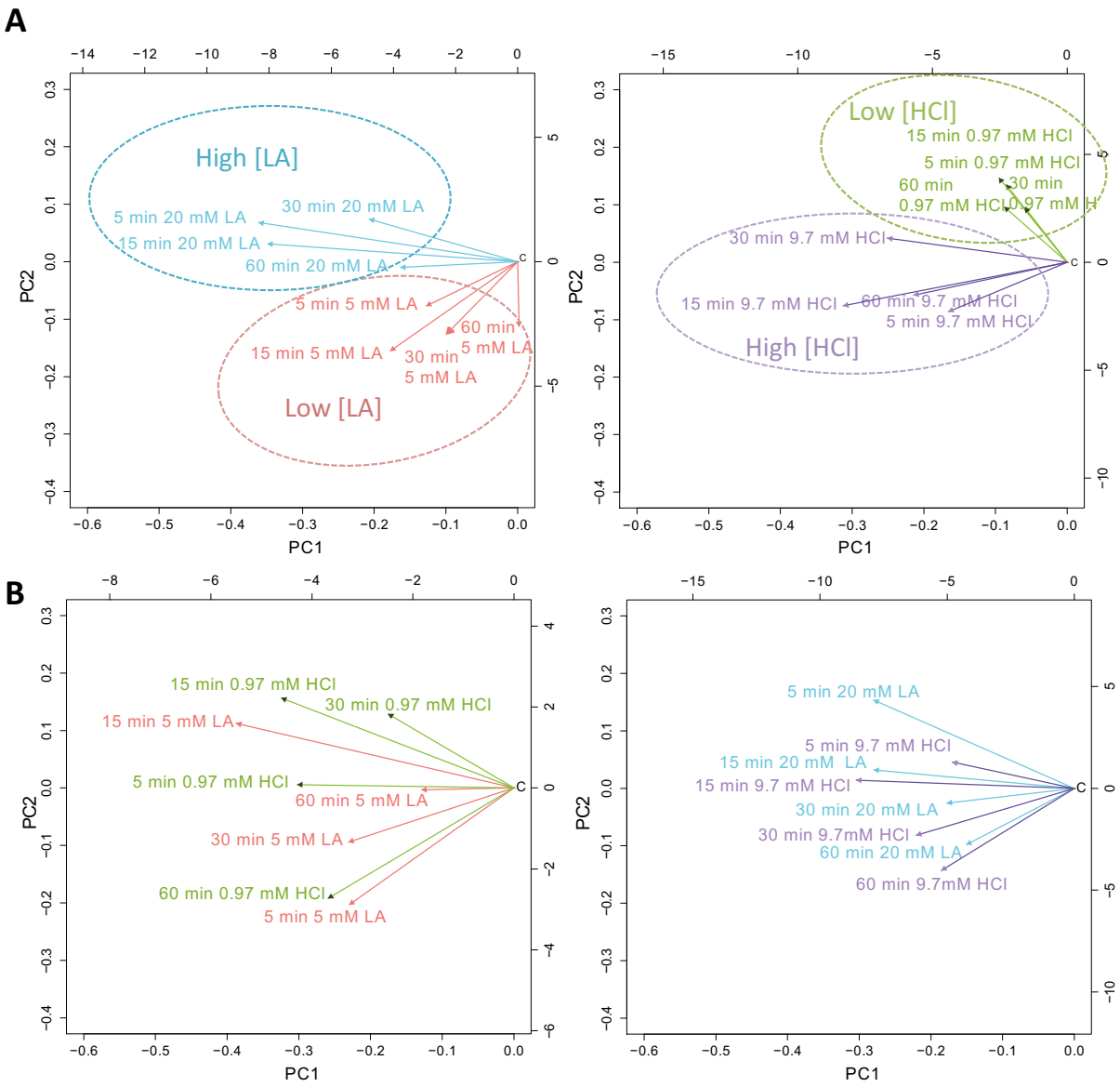

Figure 7.12 Multivariate analysis of the 47 signalling branches resolves differences upon treatment of cells with different concentrations of lactic acid or HCl. (**A**) PCA analysis of defined signalling branches of MCF7 cells over the time-course treatment with 5 mM or 20 mM lactic acid (left panel) or over the time-course treatment with 0.97 mM or 9.7 mM HCl (right panel). (**B**) PCA analysis of defined signalling branches of MCF7 cells over the time-course treatment with low concentrations of lactic acid or HCl (left panel) or over the time-course treatment with high concentrations of lactic acid or HCl (right panel).

7.8.4 Systematic analysis of the network plasticity in response to lactic acid and HCl treatment

In order to systematically analyse the biochemical modulations triggered by treating the cells with lactic acid or hydrochloric acid and in this manner complement the multivariate analysis presented in Fig 7.12, the phosphoproteomics dataset was filtered and clustered using *k*-means to include only those peptides that were significantly modulated in at least one condition compared to *t*=0. Of the 6,319 peptides quantified in this experiment, 5,155 were phosphorylated. Peptides were grouped into

9 clusters using the method described in Section 2.10.3. The data shown in Fig 7.13A showed the high similarity in the phosphorylation kinetics upon treatment with lactic acid and HCl for both low and high concentrations of the acids and the distinct phosphorylation kinetics upon treatment of cells with different concentration of acids, which was previously appreciated in the PCA analysis of signalling branches (Fig 7.12).

Phosphopeptides that increased when cells were exposed to high concentration of acids and decreased upon treatment with low acidic concentrations located in cluster 2 (160 peptides) and cluster 5 (752 peptides), whereas phosphopeptides that increased when cells were exposed to with low concentration of acids and decreased when cells were exposed to high acidic concentrations located in cluster 6 (1,273 peptides) and cluster 7 (364 peptides) (Fig 7.13A). Analysis of the biological processes associated to cluster 2 and cluster 5 revealed an enrichment of the activity of proteins related to the signalling mediated by p38α/β (Fig 7.13B). Moreover, there was an enrichment of processes associated to glucose metabolism and structural function in phosphopeptides contained in cluster 5 and an enrichment of processes associated to rRNA processing for phosphopeptides contained in cluster 2 (Fig 7.13B).

Cytoskeleton-involving processes were enriched upon treatment of cells with low concentration of acids, as suggested by the enrichment of Arf6 trafficking (in cluster 6), regulation of Rho GTPase activity (in cluster 6), regulation of RAC1 (in cluster 7), and Rho GTPase regulation activity (in cluster 7) (Fig 7.14). Appendix 16 contains the peptides associated to structural constituents of the cytoskeleton and RAC1 and Rho GTPases activity.

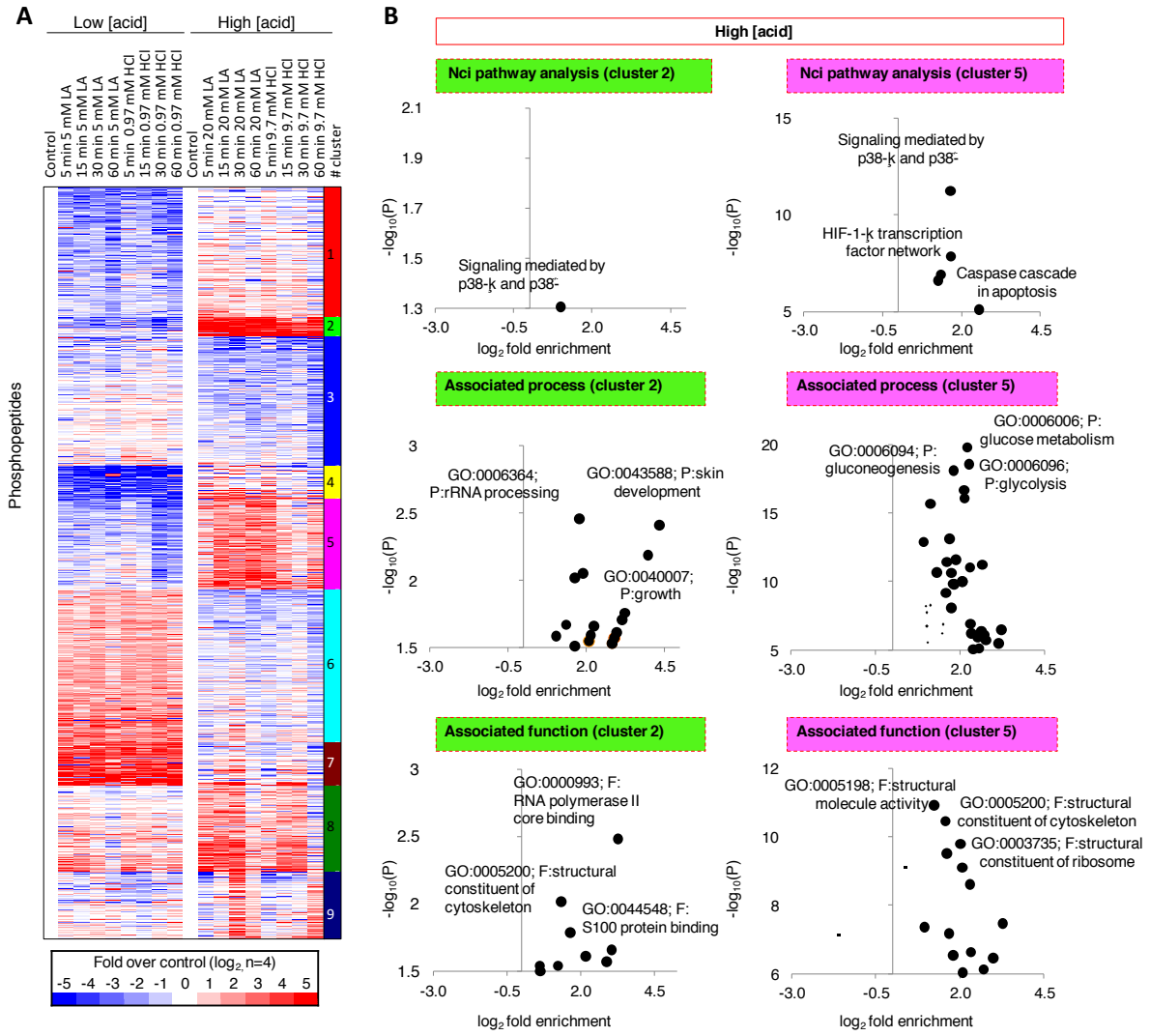

Figure 7.13 *K*-means clustering for the phosphopeptides modulated as a result of treatment of MCF7 cells with low and high concentration of lactic acid and HCl. (**A**) *k*-means algorithm grouped phosphopeptides that increased or decreased upon treatment with low or high concentrations of lactic acid and HCl for 5, 15, 30, and 60 min. (**B**) Biological processes associated to cluster 2 and cluster 5 (phosphorylation events that increased upon treatment with high concentration of lactic acid and HCl).

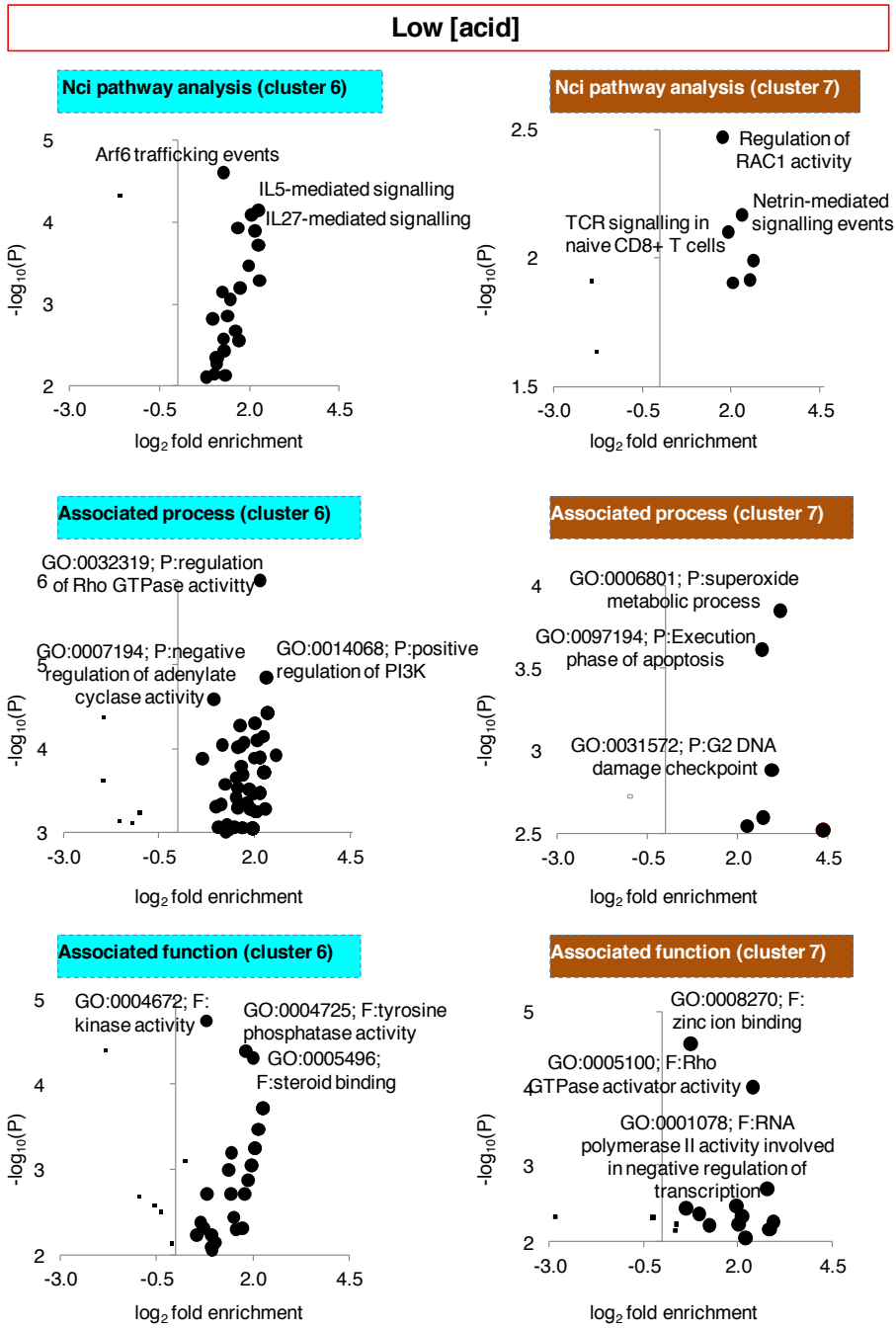

Figure 7.14 Biological processes associated to phosphopeptides contained in cluster 6 and cluster 7 of Figure 7.13. Cluster 6 and cluster 7 comprise phosphopeptides which levels increased upon treatment of cells with low concentrations of lactic acid and HCl.

7.8.5 Analysis of cell morphology upon acid treatment

To determine whether exposure to acids cause morphological changes, cells treated with lactic acid, HCl or H_2O were initially observed under the microscope. Cells treated with lactic acid and HCl slightly reduced the diameter size compared to cells maintained without treatment, but the shrinkage in cell size was not significant for any of the treatments (Fig 7.15).

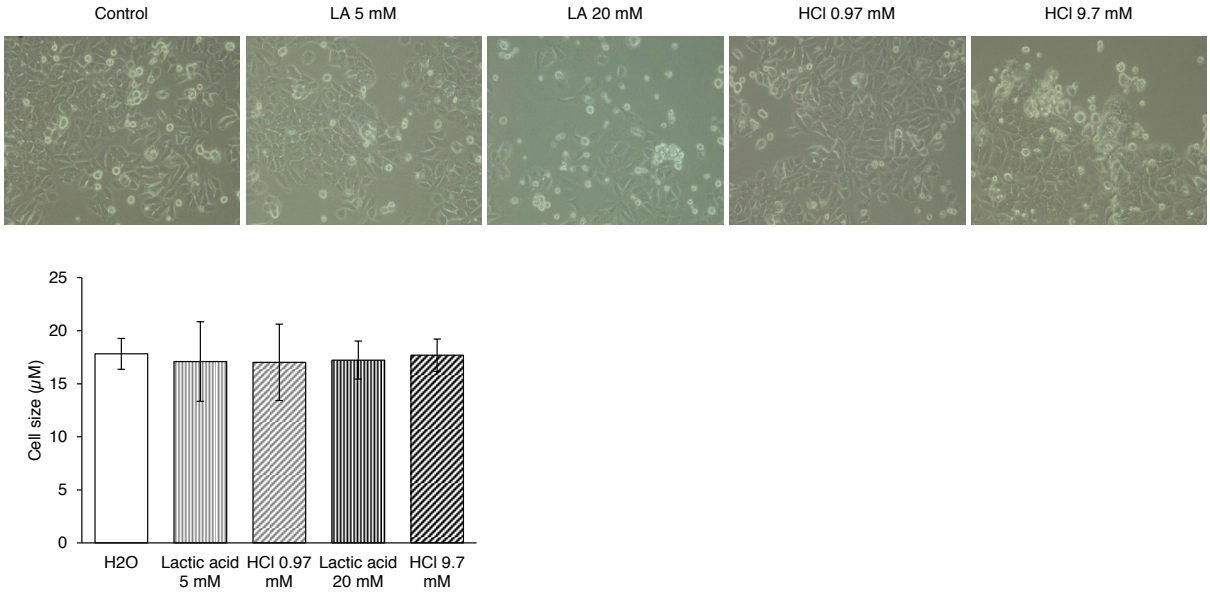

Figure 7.15 Treatment with lactic acid or HCl does not alter the morphology of MCF7 cells. Representative images and diameter size of cells treated with lactic acid, HCl or H_2O for 72 h (upper panel). Quantification of the diameter size of cells (lower panel). Data are represented as mean ± SD (*n*=3, independent technical replicates). *P*-values were calculated using an unpaired, two-tail Student's *t*-test comparing treatment with lactic acid or HCl against H_2O treatment (control).

Given that one of the main cellular responses to active Rho-kinase is the generation of actin stress fibres [337], the characteristic of actin in cells stimulated with lactic acid, HCl, or non-stimulated (H_2O) were observed under fluorescence microscope. The immunofluorescence data presented in Fig 7.16 showed that treatment with lactic acid and HCl reduced the intensity of actin staining and that this reduction was significant upon treatment with HCl.

Overall, these results suggested that lactic acid and HCl treatments change the cytoskeletal features of MCF7 cells.

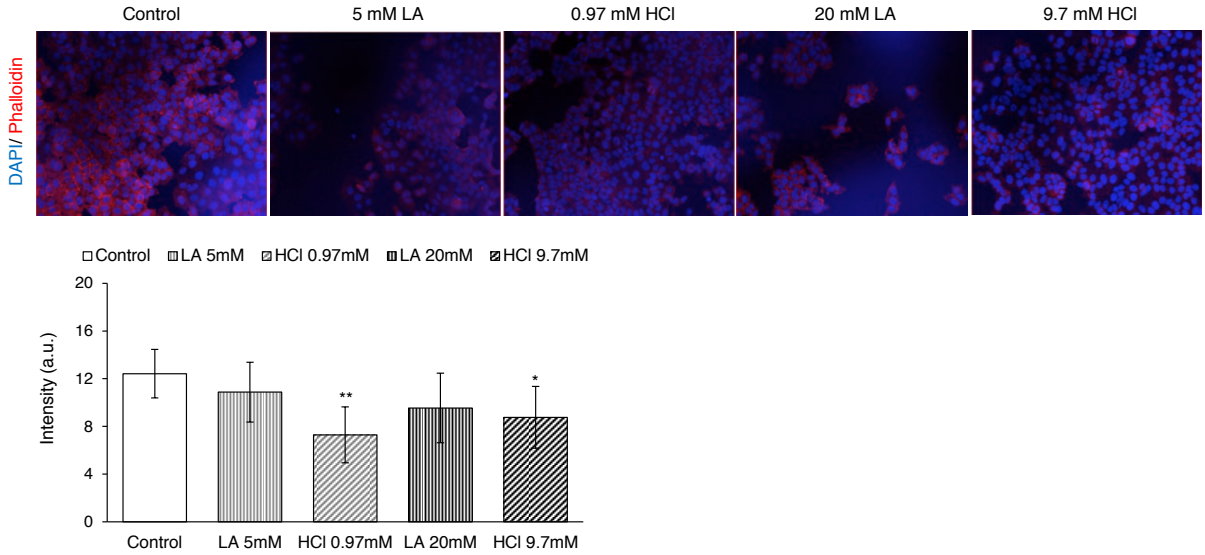

Figure 7.16 Actin intensity decreases in response to treatment with HCl. Fluorescence images of stress fibres in cells being stimulated with lactic acid, HCl or non-stimulated (H2O) over 72 h. Cells were stained with Alexa Fluor phalloidin to selectively stain for F-actin (red) and DAPI (4',6-diamidino-2-phenylindole) was used to stain DNA (blue) (upper image). Quantification of the actin staining intensity for seven field images acquired in the experiment. Data are represented as mean ± SD (*n*=7 fields images per condition). *P*-values were calculated using an unpaired, two-tail Student's *t*-test for each treatment against untreated; * $P < 0.05$; ** $P < 0.01$.

7.9 Protein expression in response to lactic acid or HCl treatment

To explore the potential effect that lactic acid and HCl on protein expression of MCF7 cells, an experiment was designed to use MCF7 cells starved with 0.5% FBS for 24 h and performed a treatment in duplicate with either 20 mM lactic acid, HCl or H_2O (control) for 4 h, 8 h or 24 h. The proteomes of the cells at each time point was run in duplicate in the LC-MS/MS. After quality control (Appendix 17), the normalised data for each treatment was compared against the treatment control at each time point.

7.9.1 Differential abundance analysis

A summary of the proteins that decreased or increased in at least one time point (from the total of 747 proteins that were found significantly modified $P<0.05$) is shown in Fig 7.17. The result of this analysis showed that a similar number of proteins were modulated in response to treatment with of 20 mM lactic acid or 9.7 mM HCl (Fig 7.17). For example, there was an increased in abundance of 545 proteins after treatment with 20 mM lactic acid and 486 proteins after treatment with 9.7 mM HCl after 4 h (compared to the number of proteins on non-treated cells). A total of 555 proteins were significantly more abundant after 24 h treatment with 20 mM lactic acid and 541 after 24 h treatment with 9.7 mM HCl.

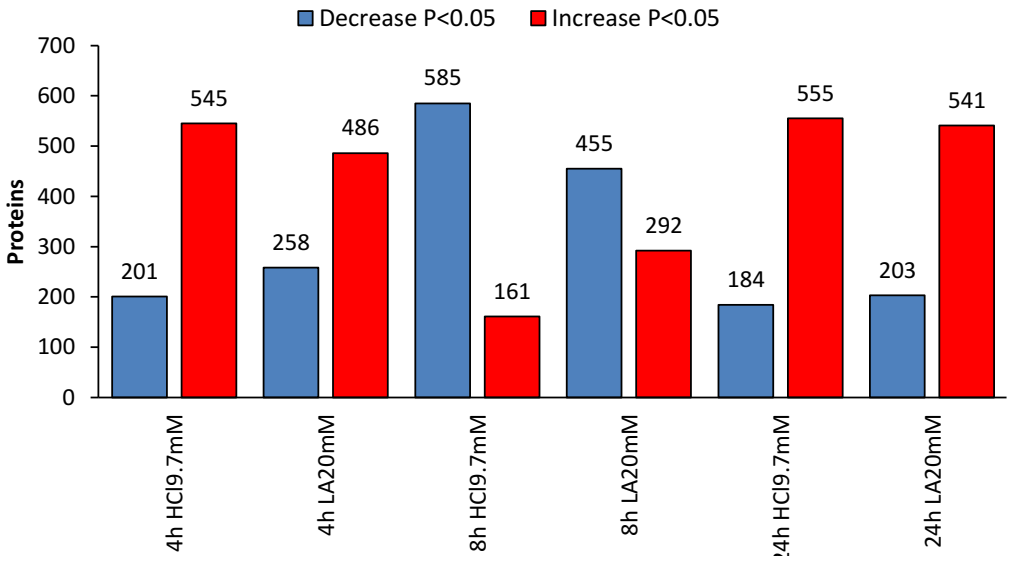

Figure 7.17 Analysis of the differential abundance over time proteomics data. Number of proteins that significantly decreased (blue bars) or increased (red bars) in abundance compared to untreated condition (H_2O) over time (*ntotal* = 747).

7.9.2 Temporal behaviour of proteins as a function of lactic acid or HCl treatments

To determine the temporal behaviour of the proteome of MCF7 cells in response to the exposure to 20 mM lactic acid or 9.7 mM HCl, a multivariate analysis was used to separate the proteomes of these cells over the period of treatment. This analysis revealed the differences in the temporal modulation of the proteomes of these cells as a consequence of treatment with lactic acid, HCl or H_2O (Fig 7.18).

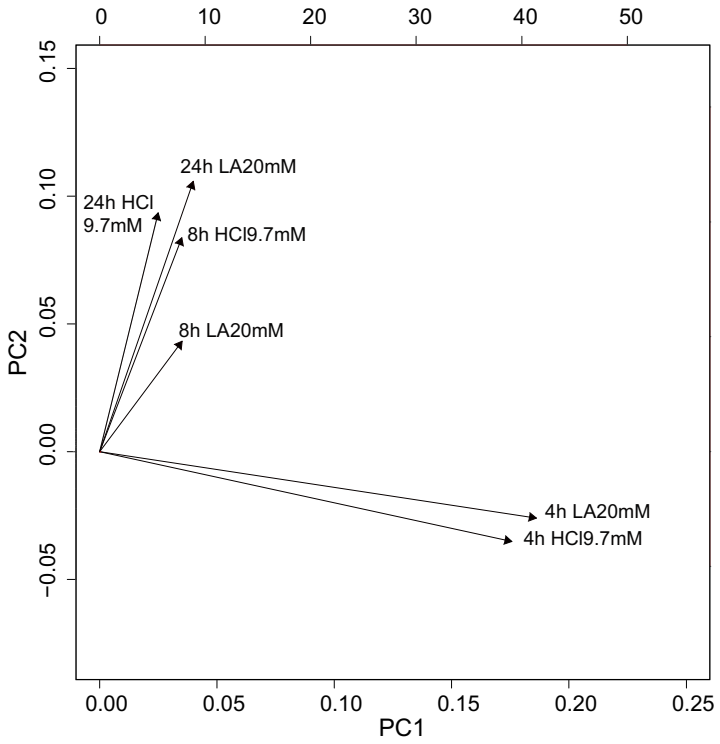

Figure 7.18 PCA of the temporal modulation of proteins upon treatment with HCl or lactic acid. PCA analysis of $\log_2$ fold-change protein modulation upon cell exposure to 20 mM lactic acid or 9.7 mM HCl compared control (H_2O) over 4, 8 or 24 h. PC1, principal component 1; PC2, principal component 2.

To understand further the associations between the proteomes of cells treated with lactic acid or HCl, a systematic analysis across those four time points grouped proteins which expression increased after short time (4 h) treatments in cluster 2 – which contains 368 proteins – and proteins which levels decreased at short times and increase at long time (24 h) treatments in cluster 6 – which contains 327 proteins (Fig 7.19A). The complete data is shown in Appendix 18. Analysis of the biological processes associated to proteins contained in these two clusters revealed that proteins involved in "cellular components organization or biogenesis" were enriched as a result of the exposure of MCF7 cells to lactic acid or HCl (Fig 7.19B). Extraction of some proteins contained in this ontology is shown in Fig 7.19C. These data revealed that the levels of several proteins involved in the cytoskeletal organization, such as α-actinin 1 and Cadherin 1, significantly decreased upon 8 h treatment with 9.7 mM HCl (Fig 7.19C).

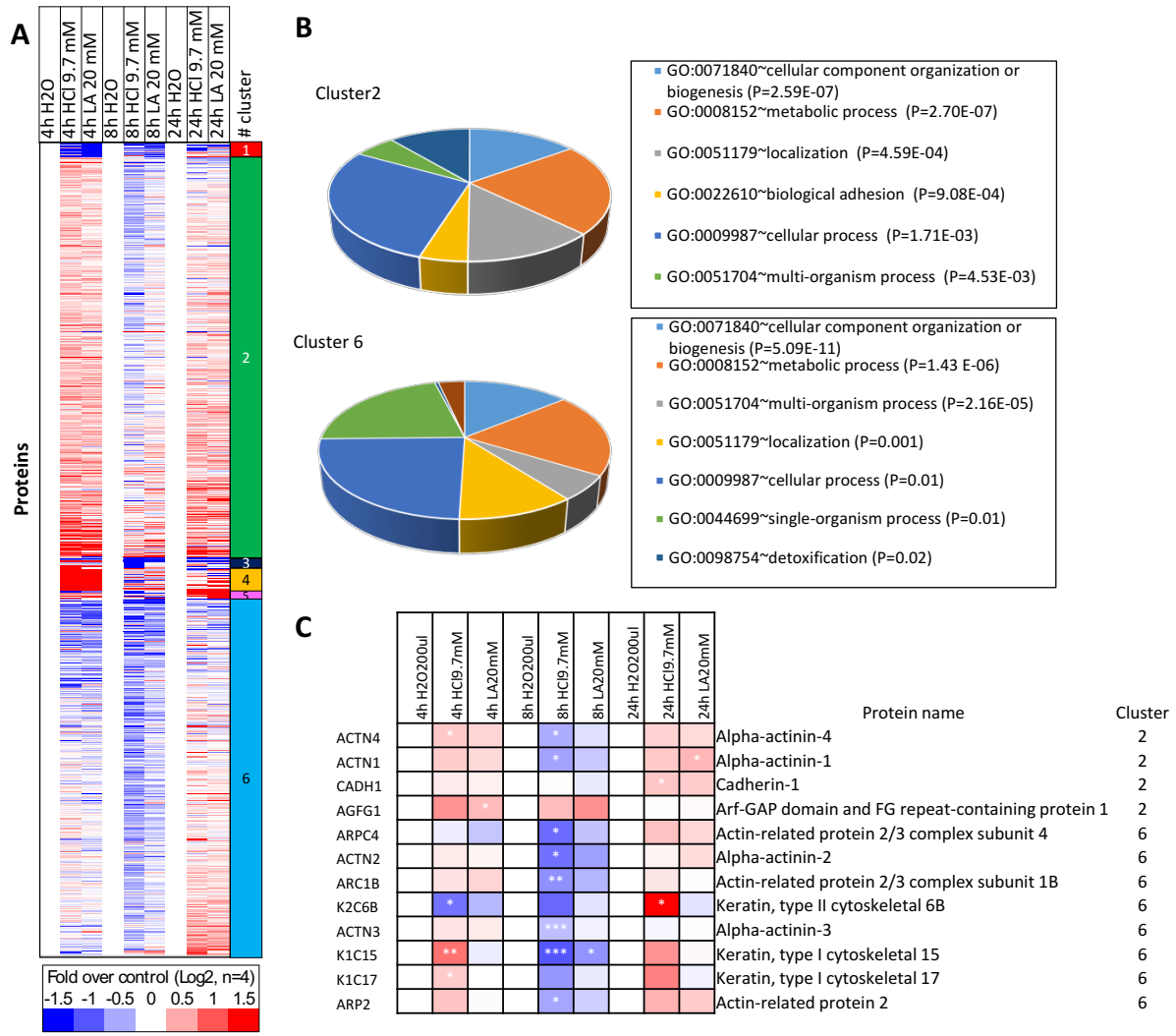

Figure 7.19 *K*-means clustering for the proteins modulated as a result of treatment with 20 mM lactic acid or HCl over time. (**A**) *k*-means algorithm grouped proteins that increased or decreased upon treatment with 20 mM lactic acid or HCl for 4, 8 or 24 h relative to control (H_2O). (**B**) Biological processes associated to cluster 2 (upper panel) and cluster 6 (lower panel). (**C**) Representative proteins associated to GO: 0071840; cellular component organization or biogenesis, contained in cluster 2 and cluster 6.

7.10 Apoptotic response of cells exposed to lactic acid or acidosis

To assess the impact of lactic acid and acidosis on cellular apoptosis, equal number of cells (0.02×10^6 per well) was cultured in 96-well plates and cells were exposed to lactic acid, HCl or H_2O for 72 h. The results presented in Fig 7.20 indicated that treatment with high concentration of lactic acid and HCl increased the number of cells in early apoptosis, inferred from binding of Annexin V to phosphatidylserine in apoptotic cells.

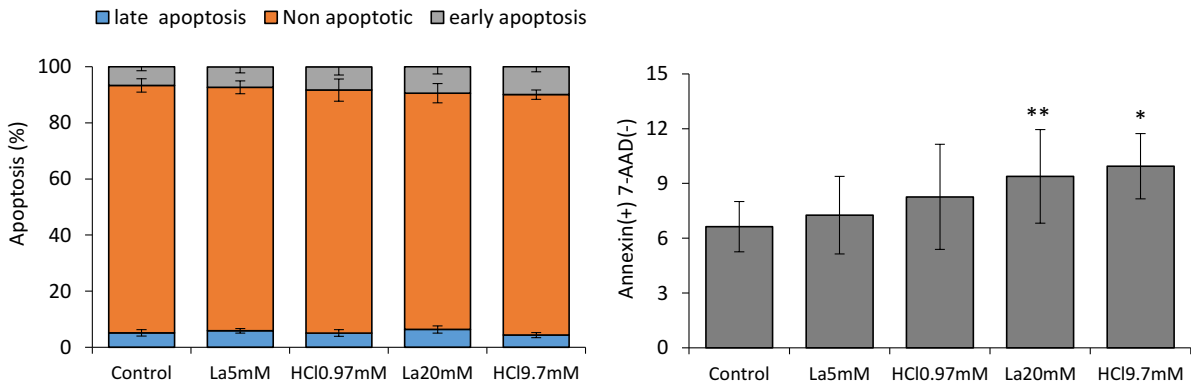

Figure 7.20 The percentage of cells in early apoptosis increases in cells exposed to high concentrations of acids. Percentage of non-apoptotic and apoptotic cells (left panel). Percentage of cells in early apoptosis as a readout of cells labelled with Annexin V maintained in media containing 25 mM glucose and 10% FBS and treated with lactic acid, HCl or H_2O for 3 days (right panel). Data are mean ± SD (*n*=3, three independent technical replicates). *P*-values were calculated through an unpaired, two-tail Student's *t*-test for each treatment with lactic acid or HCl against untreated; * P <0.05; ** P <0.01.

7.11 Proliferative capacity of lactic acid

The effect of different concentrations of lactic acid on the proliferation of MCF7 cells grown with standard 25 mM glucose was then examined. To do this, cells were allowed to attach with 10% FBS media overnight and media was supplemented with 0.5 % FBS and 1 mM, 5 mM, 10 mM or 20 mM lactic acid in triplicate. The number of cells was measured after 1, 2, and 3 days by means of the Vi-CELL counter. To assess the effect of acidosis in the proliferation of these cells, those were treated with an equivalent concentration of HCl. The data presented in Fig 7.21 showed that the proliferative capacity of lactic acid was similar to that one of HCl. Moreover, these data revealed that, on cells grown with standard glucose concentration, high concentration of lactic acid — 10 mM and 20 mM — tended to limit cell proliferation.

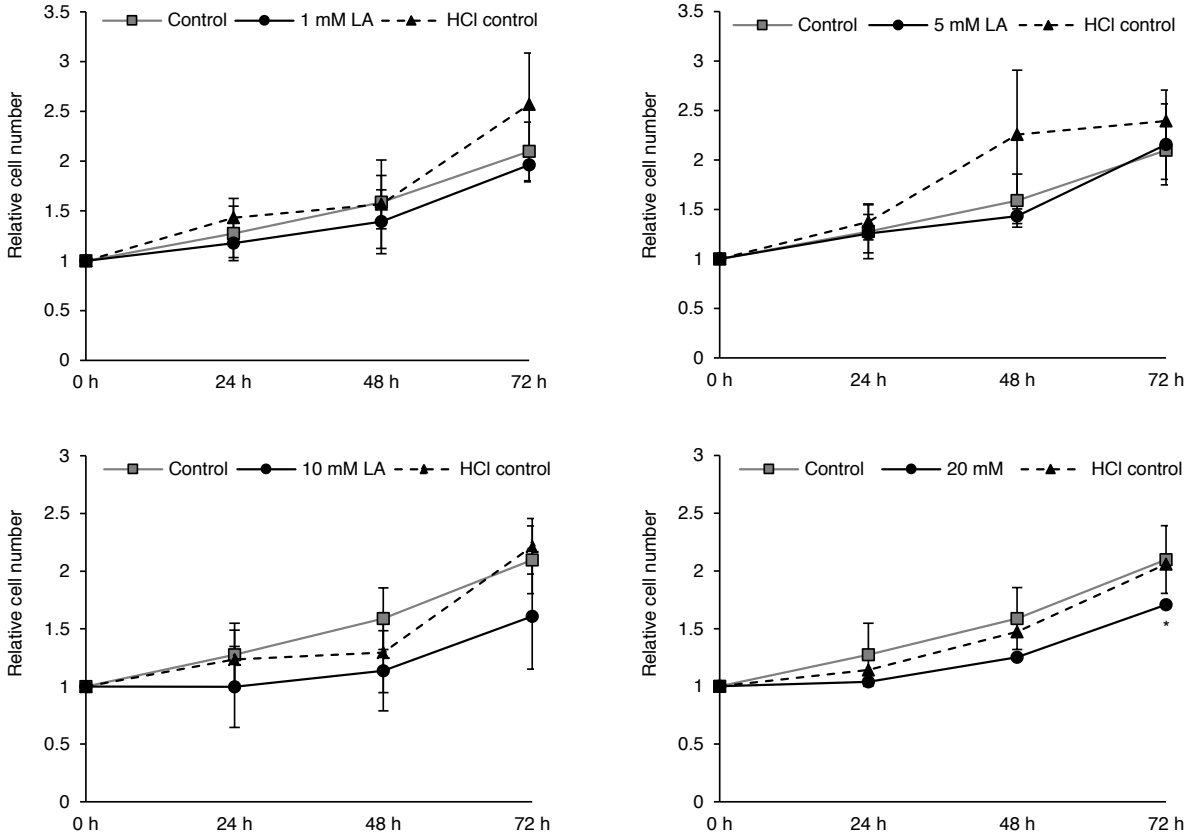

Figure 7.21 High concentration of lactic acid limits cell proliferation. Numbers of MCF7 cells grown in media supplemented with 1 mM, 5 mM, 10 mM or 20 mM lactic acid, the respective HCl control that provide a similar acidic microenvironment or supplement with H_2O (control) measured after 1, 2, and 3 days. Data are represented as mean ± SD (*n*=3, three independent replicates). *P*-values were calculated using an unpaired, two-tail Student's *t*-test of the lactic acid condition against H_2O or against HCl. * $P < 0.05$.

7.12 Conclusions

A characteristic of the tumour microenvironment is local metabolic acidosis, mainly caused by an increased production of lactic acid in cancer cells [338]. In this study, a strategy was designed to extensively characterise the impact of extracellular lactic acid perturbations on MCF7 breast cancer cells (Fig 7.1). Initially, Western blots analyses determined that transporters of lactate/H^+ — MCT1, MCT2 and MCT4 — as well as the lactate cognate receptor GPR81 were expressed in MCF7 cells (Figs 7.2 and 7.3). Treatment with a MCT1 chemical inhibitor reduced the number of viable cells after 72 h (Fig 7.4). This result suggested that MCT1 transporter was functional in MCF7 cells and, in accordance with other studies [142, 339], inhibition of MCT1 reduced the viability of these cells possibly through the intracellular accumulation of lactic acid. Nevertheless, the modest increase of media pH observed upon treatment with the MCT1i (Fig 7.4B) could be due to a decrease in lactic acid export or alternatively, this increase could be simply a result of reduced number of metabolically active viable cells. This last question was not further addressed in this study.

Low glucose is another characteristic of the microenvironment of many solid tumours [338]. To determine the nutrient capacity of lactic acid during glucose starvation, glucose was withdrawal from cell culture media and supplemented with lactic acid. This experiment revealed that lactic acid reduced by more than two-fold the death of MCF7 cells (Fig 7.5).

A minimal concentration of FBS is needed to provide the signalling molecules that MCF7 cells require to proliferate [340]. Given the expression of the lactate-specific receptor GPR81 in these cells (Fig 7.3), and the known properties of lactate to activate some signalling cascades, such as PI3K/AKT/mTOR and MAPK signalling pathways, it was hypothesised that lactic acid could substitute the signalling properties of FBS. However, the data presented in Fig 7.7 demonstrated that lactic acid alone could not substitute the signalling properties of FBS required to maintain a positive proliferation of MCF7 cells.

The signalling changes of MCF7 cells triggered by lactic acid and HCl were assessed via label-free shotgun phosphoproteomics. Extraction and Western blot validation of phosphorylation sites from the phosphoproteomics data showed that members of the MAPK signalling cascade — e.g. MAPK3 at Thr^{202}/Tyr^{204} — were activated after treatment of cells with high concentration of both acids, and that the magnitude of the change was greater in response to lactic acid treatment (Fig 7.9). In addition, the phosphoproteomics data showed that both lactic acid and HCl treatments induced the phosphorylation of several sites known to be substrates of AKT — e.g. ATK1S1 at Thr^{246}, GSK3β Ser^{9} and ACLY at Ser^{455} —, and the intensity of these change was higher for the treatment with 20 mM lactic acid compared 5 mM lactic acid treatments and similar between equivalent concentrations of lactic acid and HCl (Fig 7.9A). It was interesting to observe that the phosphorylation of known substrates of AMPK — including ULK1 at Ser^{556} and SAFB $Ser^{601/604}$ — was induced upon treatments with lactic acid and HCl (Fig 7.9A).

The activity of signalling branches of MCF7 defined to be up-regulated following EGF or IGF-1 stimulation and mediated by the activity of AKT and MAPK was up-regulated upon treatment with lactic acid and HCl (Figs 7.10 and 7.11). Multivariate analysis of the modulation of the defined MCF7 signalling network across all time points clearly resolved differences in signalling response between perturbation with low and high concentration of lactic acid and HCl (Fig 7.12A), and it resolved slight differences between acids at equivalent concentrations (Fig 7.12B). Altogether, these analyses demonstrated that the amount of acidic perturbation impact very differently the phosphoproteome of MCF7 cells and that analogous concentrations of lactic acid and HCl modulate the phosphoproteome of these cells similarly.

Proteins associated to p38α and p38β MAPK signalling and structural components of the cytoskeleton were enriched upon treatment of cells with high concentrations of lactic acid and HCl (Fig 7.13B). Proteins associated with Rho/Rac signalling activity were enriched upon treatment with low concentration of acids (Fig 7.14). Given that one of the main pH-sensitive systems in the cell is the actin cytoskeleton [341], the morphology of polymerised actin fibres after treatments with lactic acid and HCl was investigated. Acidosis produced a dose-dependent reduction in F-actin staining intensity (Fig 7.16).

The proteome of MCF7 cells was similarly modulated over time upon treatment of cells with either lactic acid or HCl (Figs 7.17 and 7.18). Analysis of the biological processes associated to proteins modulated in response to treatment with 20 mM lactic acid or 9.7 mM HCl revealed a significant decrease after 8 h treatment with HCl of proteins associated to “cellular component organization or biogenesis”, such as actin-related protein 2/3 complex subunit 1B (ARC1B) (Figs 7.19B-C).

Analysis of markers of apoptosis including Annexin A5 indicated that high concentration of acids triggered apoptosis in MCF7 cells (Fig 7.20). Furthermore, high concentration of lactic acid (20 mM) hampered the proliferation of MCF7 cells cultured in the presence of glucose (Fig 7.21).

Overall, the results presented in this Chapter revealed global changes in signalling cascades, protein levels, and functional processes in a model breast cancer cell line treated with two different concentration of lactic acid and HCl.

Chapter 8

Discussion

The PI3K/AKT/mTOR pathway responds to external and internal stimuli and has an essential role modulating key cellular functions [85]. Targeting kinases of this signalling pathway is relevant in cancer biology, as their activities are frequently altered during carcinogenesis [6]. Nevertheless, acquired resistance to anti-cancer compounds almost invariably results in treatment failure. Cessation of inhibitor treatment (i.e. drug holidays) has proved to exploit the dependency of drug-resistant cancer cells to targeted inhibitors and in this manner regain sensitivity [342].

The project presented in this thesis focused on three major areas of investigation to examine the biochemical adaptations occurring in cancer cells exposed to differential selection pressures: (i) the genomic, transcriptomic, proteomic and signalling characterization of cellular models of acquired resistance to PI3K blockade, and the functional implications of those modifications; (ii) the metabolic status of cancer cells that had acquired resistance to PI3K and mTORC1/2 inhibition; and (iii) the response to lactic acid, a metabolic product, of a predefined signalling network of the MCF7 breast cancer cell line.

Understanding the mechanisms used by cancer cells that have evolved to survive the chronic inhibition of kinase-driven signalling pathways is fundamental to optimise therapeutic strategies to eliminate cancer cells. Nevertheless, the biochemical changes of drug-resistant cancer cells exposed to differential selection pressures have not been comprehensively investigated. Therefore, the phenotypes as well as the proteomes and phosphoproteomes of PI3Ki-resistant cells exposed to the PI3Ki, or its withdrawal, were investigated (Chapter 3 and Chapter 4). Cell signalling pathways and metabolic pathways are not separate entities but they regulate each other. Aiming to understand the metabolic adaptations of PI3Ki-resistant cells, and after characterising the changes in pathways and signalling activity of these cells, their metabolic profiles were characterised, and the amount of some metabolism-derived products quantified (Chapter 5). To then provide insights into the genomic changes driving the resistance phenotype, the exomes of parental and PI3Ki-resistant cells were sequenced and compared (Chapter 6).

The niche of tumours mediates the biology of both cancer cells and neighbouring untransformed cells [343]. Having demonstrated profound changes in the production of metabolites in drug-resistant cells, the capacity of lactic acid to modulate the proteome and phosphoproteome of a breast cancer cell line was investigated. These results revealed that the signalling response to lactic acid is high, and

highlighted that there is a functional association between exposure to lactic acid and the biochemistry of these cells (Chapter 7).

8.1 Phenotype of models of acquired resistance to PI3Ki in presence absence of selection drug

8.1.1 Introduction

Experience with successful small molecule inhibitors that target kinases indicates that the evolution of cancer cells frequently limits the efficacy of targeted agents to limiting tumour growth [163, 164, 344]. Cancer is a product of somatic cell evolution; analogously, acquired drug-resistance is a product of additional mutations and epigenetic adaptations of cancer cells, whereby the proliferation of resistant cells is strengthened upon transformations aside from inbuilt programs of cancer cells behaviour.

Given the central role of PI3K in cell biology and cancer [2, 345], characterising phenotypic changes of PI3Ki-resistant cancer cells upon drug administration and withdrawal is essential to assess the dependency drug-resistant cells to PI3K inhibitors. In this study, the phenotypic modifications of MCF7 parental cells and three models of MCF7-derived cells resistant to the PI3Kα/δ inhibitor GDC-0941 — G1, G2, and G3 resistant cells described in Wilkes *et al.* [226] — were investigated upon the exposure of these cells to the selection drug or its withdrawal, as well as to other kinase inhibitors.

8.1.2 Main findings

The PI3Ki-resistant cell models used in this study showed a degree of heterogeneity between each other, as the response of these cells to PI3Ki was non-identical. This confirmed previous reports [226] and highlights the observation that resistant cells derived from an original parental cell population exposed to the same selecting pressure evolved into drug-resistant cell lines of different nature. The infeasibility to predict evolutionary routes of cancer cells is a conclusion made in other laboratories [317, 346], in the context of precision medicine [347], and is a fundamental characteristic of cell populations [348].

PI3Ki-resistant cells were cross-resistant to inhibitors of kinases downstream of PI3K, whilst MCF7 parental cells were not intrinsically resistant to those inhibitors. This observation suggested that cells that acquired resistance to PI3Ki do not reactivate PI3K-downstream pathways to survive, and was in line with the partial cross-resistance described for other models of acquired resistance to targeted

kinases inhibitors [349]. It should be noted that potential off-target effects of inhibitors (i.e. non-specific effects of the compound) can affect their outcome [350]. While this study does not eliminate the contribution of potential off-target effects, the usage of two inhibitors against some kinases (i.e. AKT and mTORC1), alongside with the reported specificity of these inhibitors [136, 351-355], provide confidence in the results. In fact, the potential off-targets effects of targeted inhibitors do not explain the capacity PI3Ki-resistant cells to proliferate after treatment. Nevertheless, to fully assess whether possible non-specific effects of the small-molecule inhibitors used in this study have any effect on cell proliferation, these compounds could be used in an orthogonal study to treat additional cells that had acquired resistance to inhibitors of the kinase targeted. Positive proliferation of those drug-resistant cells would indicate that the potential unspecific effects of the inhibitors do not impact cell viability. In addition, immunoblotting of substrates of the targeted kinases would have determined the inhibitory effects of the small molecule inhibitors panel used in this study.

PI3Ki-resistant cells proliferated at lower rate compared to the parental cells from which they originated, and this proliferative deficiency was not reverted after removal of PI3Ki treatment. It was very interesting to observe that the growth rate of two out of three resistant cells, i.e. G1 and G2 resistant cells, was lower when these cells were not exposed to the selection drug, which indicated that the PI3Ki confers a selective advantage to these cells. Lower proliferation of drug-resistant cells as a consequence of drug holidays has been previously observed [183, 356, 357], and here the effects of drug holidays on several phenotypic features of PI3Ki-resistant cells were characterised for the first time.

PI3Ki-resistant cells increased their protein content and enlarged their cell size during drug holidays, and G1- and G2- resistant cells halted their cell cycle progression upon PI3Ki removal from culture media. Together, these observations suggest that G1- and G2- resistant cells reduce their capacity to proliferate during drug holidays, even though they increase their biomass and cell size in those conditions.

PI3Ki withdrawal did not induce apoptosis of PI3Ki-resistant cells. This contrasts with previous reports that indicated that drug holidays led to signalling overdose and apoptosis of TKI-resistant cells *in vivo* [358], suggesting that drug holidays prompt apoptosis of some cell models.

8.1.3 Implications of the study and directions for future research

Collectively, the experiments presented in Chapter 3 demonstrate the emergence of diverse resistant phenotypes of cells that derived from a single cell line (i.e. MCF7 cells) and evolved under identical

selective pressure (i.e. treatment with a PI3K inhibitor). To date the cellular features of drug-resistant cells after drug deprivation have not been extensively characterised. This study represents a step forward in this direction. Yet, it is important to note that, although alternative dosing schemes were not explored in this study, testing additional timescales of intermittent treatments would help this and previous efforts to get a better understanding of the drug holidays phenomenon [181, 190, 191].

The discovery that cessation of PI3K inhibitor treatment changes various phenotypic features of PI3Ki-resistant cells could have major implications for cancer treatment given that several agents that target nodes of this pathway often reach clinical trials [359]. The mechanisms that mediate the resistance phenotype were explored in subsequent experiments.

8.2 Characterisation of the proteome and phosphoproteome of PI3Ki-resistant cells

8.2.1 Introduction

It is becoming increasingly clear that understanding the plasticity of protein and signalling networks helps to elucidate the mechanisms that drive cellular phenotypes [360-362]. Knowledge of the levels and activation status of proteins expressed in drug-resistant cells could facilitate designing alternative therapies or combinations between available treatments to effectively reduce tumour cell populations [363]. Even though a previous study demonstrated that the signalling plasticity of cells that had acquired PI3Ki resistance is high [226], the global pathways rewiring of those PI3Ki-resistant cells prompted by PI3Ki withdrawal remained unexplored. From a therapeutic standpoint, understanding the molecular remodelling occurring in drug-resistant cells during drug holidays may help to identify druggable molecular targets and guide the selection of effective treatment schemes during dose intermittent regimes, often implemented to overcome therapy toxicities [178].

The proteomes and phosphoproteomes of PI3Ki-resistant cells under treatment with the PI3Ki or on its absence were characterised by means of LC-MS/MS. The ultimate goal of this study was to determine the molecular events underlying the previously observed heterogeneous phenotypes of PI3Ki-resistant cells.

8.2.2 Main findings

The proteomes of PI3Ki-resistant cells were markedly different to the proteome of parental cells from which they derived, and were heterogeneous between each other. Heterogeneity across proteomes

of cell lines and primary cancer cells has been reported [360, 364], and this study presents for the first time a deep proteome characterisation of PI3Ki-resistant cells exposed to drug holidays.

The amount of several proteins involved in diverse metabolic processes changed in PI3Ki-resistant cells compared with parental cells. Given the known role of PI3K-downstream effectors regulating the metabolism [365], modulations of metabolic mediators on cancer cells that had evolved to survive PI3K blockade could have been expected.

Ontology analysis of the proteomics data revealed that proteins involved in translational activity increased in PI3Ki-resistant cells and that proteins transcriptionally controlled by c-MYC as well as members of the HIF-1α transcription factor network increased in PI3Ki-resistant cells. It is interesting to note that, although previous studies described that PI3K signalling mediates the regulation and activation of HIF in certain tumours [366, 367], no data have underlined the relevance of HIF's activity in PI3Ki-resistant cells to the best of this author's knowledge.

In PI3Ki-resistant cells, c-MYC increased its phosphorylation at Thr^{58}/Ser^{62}, sites associated with c-MYC's transactivation activity [302], as revealed by the phosphoproteomics data; these changes were probably mediated by higher c-MYC at the protein level, as revealed by immunoblotting of c-MYC. Thus, the results presented in this study expand previous knowledge from the literature that indicated that highly expressed or amplified c-MYC is crucial to mediate the resistance to PI3K inhibition of breast cancer cells [301, 313, 314].

Similarly to the changes in the proteomes, the phosphoproteomes of PI3Ki-resistant cells showed differences compared to parental cells. PI3K/AKT/mTOR signalling activity of PI3Ki-resistant cells was blocked during PI3Ki treatment, which suggested that resistance to PI3Ki was not acquired through a drug-efflux pumping system or reactivation of the PI3K signalling during PI3Ki treatment. Conversely, reactivation of the signalling activity downstream of PI3K upon drug withdrawal confirmed the conservation of this signalling cascade's activity in this context. This was similar to the functional reactivation of kinases downstream of PI3K upon drug removal observed in other models of PI3Ki resistance [305].

PI3Ki removal led to signalling rewiring of PI3Ki-resistant cells, and the network of G1- and G2-resistant cells was markedly distinct to that one of G3- resistant cells. The antioxidant activity of PI3Ki-resistant cells was engaged as a consequence of drug holidays, as deduced from the phosphoproteomics data. Previous *in vivo* and *in vitro* studies have reported that antioxidant agents can enhance the progression and migration of malignant cells [368], and the PI3Ki-resistant cells analysed in this research may increase their antioxidant activity to deal with higher oxidative stress in these conditions.

The inferred activity of CAMKII and MEK was higher in PI3Ki-resistant cells than in parental cells. The proliferation of PI3Ki-resistant cells decreased by interfering with the activities of PI3K and CAMKII or MEK, which suggested that these kinases promoted the resistance phenotype of these models. The coordination between MAPK and PI3K signalling activity to maintain cell proliferation was in accordance with the well-known extensive cross-talk across these signalling pathways and the known mechanism through MAPK kinase pathway activity used by cancer cells to acquired resistance to PI3K inhibitors [171, 369]. In addition, these data reproduced the association between CAMKII's activity and the PI3Ki-resistance phenotype previously uncovered by Wilkes *et al*. [226]; before the latter study, CAMKII activity was not associated with PI3Ki resistant mechanism, highlighting that other drug-resistant mechanism may be discover in future explorations.

8.2.3 Limitations of the (phospho)-proteomics experiments

It is important to note that the (phospho)-proteomics experiments presented in this Chapter were performed in populations of cells, and the conclusions derived from these analyses are the average of signalling intensities across each resistant cell lines. Several methodologies, including mass cytometry [370] and single-cell barcode chips [371] allow single-cell analyses; however, given that these methods rely on antibodies, they do not utterly serve as untargeted discovery tools. Therefore, given the untargeted nature of the MS-based approaches, the methodology used in this study provides a rich characterisation of the molecular events occurring in drug-resistant cells without prior knowledge of their biochemistry.

It could also be argued that the observed changes in signalling activity are contingent to the timescale of analysis. Indeed, the generated data represent the signalling state at the timeframe cells were treated with different inhibitors, and it is of limited value in predicting any signalling changes that could take place at other timescales. Examination of the signalling state of drug-resistant cancer cells at additional time points would increase the information of their signalling dynamics.

Moreover, and in the view of recent comparisons between substrate-based methods to infer changes in kinase regulation [271], it could be argued that the predictions of kinase activities may be influenced by the number of substrates considered and by the source of supported substrates. This motivates future investigations of kinase activity inference strategies using differential constrains.

8.2.4 Implications of the study and directions for future research

The experiments presented in Chapter 4 uncover the biochemical mechanisms by which cancer cells

survive the inhibition of PI3K. This study highlights that the pathways activities of drug-resistant cells upon drug withdrawal are not reverted back to the parental signalling state but to very different conditions (e.g. high antioxidant activity).

Integration of the phosphoproteomic datasets with additional annotation resources, such as kinase-mediated epigenetics modulation of histones and chromatin remodelling factors [372] will potentially contribute to shed light in the status of epigenetic modulations in PI3Ki-resistant cells.

Further exploration of the synergistic capacity of compounds that target PI3K and MEK or CAMKII to limit the viability of PI3Ki-resistant cells (i.e. calculation of the drugs combination index [CI] [373]) will reveal which combination treatment confers the greater synergistic toxicity to PI3Ki-resistant cells.

8.3 Bioenergetic remodelling in models of acquired resistance to PI3K/mTOR inhibition

8.3.1 Introduction

The metabolism of cancer cells is reprogrammed to maintain highly proliferative phenotypes [95]. The results presented in Chapter 4 demonstrated that cancer cells able to survive the absence of PI3K signalling rewire several pathways, including metabolic pathways. Subsequent experiments aimed to explore the mechanistic insights of that metabolic reprogramming, and were presented in Chapter 5. It was also sought to determine whether metabolic adaptations yield vulnerabilities in drug-resistant cancer cells that could be exploited therapeutically, as shown for other models of resistance to targeted therapies [344, 374].

Finally, it was reasoned that delineation of cellular metabolic profiles could assist designing experiments to investigate, by means of LC-MS, the signalling changes that occur in cancer cells in response to metabolic perturbations. This aspect was crucial to profile the lactic acid-mediated changes in signalling activity and cellular proteomes performed afterwards and presented in Chapter 7.

8.3.2 Main findings

Drug holidays caused an increase in the acidification of culture media and the redox activity of PI3Ki-resistant cells. This metabolic phenotype is not driven by mutation events, but rather by non-genetic changes, as indicated by the reversible capacity of resistant cells to acidify the culture media. Metabolic plasticity in response to specific stress was recently found in metformin-resistant cancer cells that preserve stemness features [375], supporting the observation that changes aside from genetic hardwiring may control the metabolism drug-resistant cells.

PI3Ki-resistant cells adapted their glycolytic activity and mitochondrial respiration rate (inferred by the extracellular media acidification and O_2 consumption of cells, respectively) to that one of parental cells. This suggests that metabolic adaptations are required to maintain the viability of drug-resistant cells. This is the first characterisation of the metabolic profiles of cancer cells that had acquired resistance to a class I PI3K inhibitor, and implies that altered cellular metabolism is not only a hallmark of oncogenesis, but also happens during the process of acquiring resistance to targeted therapy. During drug holidays, however, PI3Ki-resistant cells enhanced their metabolic activity. Given the central role of the PI3K signalling pathway coordinating the metabolism [376], restoration of PI3K signalling activity possibly aggregated to the metabolic activity gained by PI3Ki-resistant cells over the course of acquisition of resistance.

The amount of metabolic products (i.e. lactic acid as a product of the glycolytic activity and the intracellular ROS as product of the mitochondrial respiration) increased in PI3Ki-resistant cells during drug holidays, mirroring their enhanced metabolic activity. ROS overproduction limited the proliferation of resistant cells, and such deficient proliferative capacity was reverted upon treatment with antioxidants. This observation suggests that despite the increased antioxidant activity of PI3Ki-resistant cells during drug holidays (as presented in Section 4.4.6), those adaptations were not sufficient to counteract the toxic effects of ROS accumulation derived from an augmented metabolism.

The expression of multiple genes controlled by HIF's transcriptional activity increased in PI3Ki-resistant cells during drug holidays. This was in line with recent work that reported that certain stress conditions lead to HIF-1α up-regulation and transactivation of HIF-downstream genes on normoxia [377]. In fact, the levels and activity of HIF isoforms increased in PI3Ki-resistant during drug holidays, as determined by HIF-1α immunoblotting and by the activity of HRE-luciferase reporter, respectively. Treatment with chetomin, which is a chemical competitor of HIF adaptors, hampered the proliferation of PI3Ki-resistant cells and reduced their glycolytic activity. This suggests that HIF's activities control the proliferation and the glycolytic rate of resistant cells. This was further supported by the lower amount of LHDB protein in response to siRNA treatment against HIF-1α. Nevertheless, the ability of chetomin to prevent HIF's transcriptional activity could be analyses in follow up studies. On another note, the levels of HIF-2α (encode by the endothelial PAS protein 1 [*EPAS1*] in the human genome), which in conjunction with HIF-1α accounts for the main effect mediated by HIF, remained to be elucidated for these cells. In this study it was showed that the stability of HIF-1α was promoted by ROS, since ROS scavenging reduced the levels of HIF-1α and the lactic acid production of PI3Ki-resistant cells.

Alongside with HIF, the transcription factor c-MYC regulates the transcription of genes involved in glycolytic and glutaminolytic pathways [100, 378]. It was previously appreciated, and presented in Chapter 4 of this thesis, that: (i) proteins transcriptionally controlled by c-MYC increased in PI3Ki-resistant cells compared to parental cells; (ii) the phosphorylation status of sites associated with the stability of c-MYC was higher in resistant cells relative to parental cells; and (iii) PI3Ki-resistant cells express higher c-MYC protein compared to parental cells. The efficiency of the molecules that disrupt c-MYC transcription machinery has proven in other studies [379]. The data presented in Chapter 5 indicated that the activity of c-MYC contributed to the proliferation of PI3Ki-resistant cells in a background of PI3K inhibition, since treatment with competitors of c-MYC's transcriptional machinery reverted the sensitive phenotype of resistant cells treated with the PI3Ki but had a small effect on reducing their proliferation and the proliferation of parental cells when used as a single agent. This result was similar to the synergistic cytotoxic effect of the combination treatment with inhibitors against PI3K and c-MYC reported by Sheperd and colleagues [172]. Several links between c-MYC and PI3K — e.g. ATM-mediated engagement of DNA replication checkpoint by c-MYC [380] — and between c-MCY and mTOR — e.g. convergence of c-MYC and mTOR in 4-EBP1 phosphorylation [381] — may explain the coordination between these proteins to sustain cell proliferation. However, treatment with a c-MYC competitor did not prevent the glycolytic phenotype of PI3Ki-resistant cells, implying that c-MYC is not involved in their glycolytic phenotype. Future studies could address the potential role of c-MYC in the glutamine metabolism of PI3Ki-resistant cells.

The activities of PI3K and mTOR, but not the activity of AKT, control the glycolytic and mitochondrial phenotype of PI3Ki-resistant cells, as suggested by the lack of metabolic phenotype of these cells after treatment with compounds that target these kinases. Phosphoproteomics data provided evidence to suggest that a PI3K-mTORC1 signalling cascade is functional in PI3Ki-resistant cells. Although the compounds used in this study might have potential off-target effects, considering their high specificity (as described in refs [136, 351, 353]) and that the phosphorylation of certain sites (e.g. EIF4E-BP2 at Ser^{44}/Thr^{45}) was reduced upon treatment with PI3Ki and mTORi but not by the AKTi treatment support the hypothesis of the presence of a PI3K-mTOR signalling axis in PI3Ki-resistant cells.

The involvement of proteins that act in between PI3K-mTORC1 in PI3Ki-resistant cells remains to be addressed. A recent study described the role of PDK1-SGK1 signalling axis mediating mTORC1 activation in PI3Ki-resistant cells [382]; treatment of PI3Ki-resistant cells with a PDK1 inhibitor (e.g. GSK2334470 or BX-912) would help to determine the role of this kinase in the metabolic phenotype of drug-resistant cell lines.

Overall, these data are in agreement with several studies that implicated various kinases — including RAC, mTORC2 and PDK1 — in the AKT-independent PI3K signalling activity of cancer cells [383], and with recent observations of mTOR signalling independent of AKT in models of acquired resistance to PI3K inhibition [305, 382].

Finally, the enhanced metabolic phenotype of drug-resistant cancer cells suggested that strategies based on metabolism challenging could intensify the capacity of the drug holiday strategy to remove resistant cells. Indeed, drug holidays made resistant cells more sensitive to carbon sources starvation and to further oxidative stress. Interfering with cellular mechanisms that scavenge free radicals [368] or interfering with the carbon metabolism [384] could synergise with the drug holiday strategy to delay resistance to PI3K inhibition.

8.3.3 Exploring the recurrence of metabolic adaptations in drug-resistant cells

The metabolic features of seven independent models resistant to PI3K/mTOR inhibition were examined. PI3Ki/mTORi-resistant cells did not recover the proliferative rate of parental cells even after treatment break, similarly to previous observations made for models of acquired resistance to PI3Ki (and presented in Chapter 3 of this thesis). The metabolism of resistant cells tended to increase during drug holidays, as deduced from measurements of glycolytic and mitochondrial activity as well as by the metabolites produced by these cells. The correlation of cell proliferation with the ratio between glycolysis/ROS demonstrated a direct, strong correlation between a correct metabolic adaptation and enhanced cell proliferation of drug-resistant cells during drug holidays. This led to propose a model where the overall contribution of the pro-proliferative glycolytic activity and the anti-proliferative ROS accumulation dictate cell proliferation.

The ability to measure the metabolic adaptations of drug-resistant cancer cells during drug holidays could predict their proliferative outcome and could be an indicator of the potential efficacy of switching from a kinase-targeted treatment to a therapy based on metabolic vulnerabilities. It is important to note that this study has being performed *in vitro* and xenograft models would help to determine whether the findings presented here have any implications in an *in vivo* setting.

Furthermore, this study does not ascertain that increased metabolic activity during drug holidays would occur in other models of drug-resistance. For example, in *in-vivo* models of adaptation to RTK therapies, drug withdrawal led to decreased glycolytic rate and enhanced lipid synthesis; blockade of lipid synthesis prevents metastatic dissemination of those models [385]. Alternatively, the balance between c-MYC/PGC-1α expression conditioned the metabolic phenotype and vulnerability to metformin in undifferentiated resistant cancer-stem cells [375]. This highlights that diverse metabolic

adaptations may take place in drug-resistant cells, and only experimental data will define the nature of metabolic adaptations of a given tumour.

8.3.4 Implications of the study and directions for future research

The metabolic features of cancer cells resistant to PI3K/mTOR signalling blockade was analysed and presented in Chapter 5. The enrichment in metabolic proteins/pathways in PI3Ki-resistant cells during drug holidays inferred from the LC-MS-derived datasets (described in Chapter 4) was supported by functional metabolic assays.

Defective proliferation has been attributed to some drug-resistant cancer cells during drug holidays [187, 386], and was observed for some of the cell models of this study. It is worth noting that this study reveals that PI3Ki-resistant cells exposed to drug holidays are sensitive to metabolic manipulation. The therapeutic window of agents that target the metabolism during drug holidays might be of easier application in the clinic than combinatorial approaches. As for any other therapies, the pharmacokinetics, pharmacodynamics, safety, and efficiency of these treatments entail close monitoring during therapy [140].

This research introduces the concept that targeting metabolic dependencies of cancer cells may be an effective therapeutic strategy to potentiate the ability of the drug holiday strategy to forestall resistance to drugs that target the PI3K/mTOR pathway.

The work in this study could be enlarged by analysing the metabolome of PI3Ki/mTORi-resistant cells. This will exceed the understanding of the pathobiology of acquisition of resistance, and could uncover metabolite biomarkers of acquired resistance.

Lastly, the hypothesis that MCF7 parental cells have a transduction cascade that by-passes the activity of AKT to connect PI3K and mTOR is yet to be determined. To test this, the phosphoproteomes of these cells treated with inhibitors against PI3K, AKT and mTOR would need to be analysed. The hypothesis would be confirmed if inhibition of PI3K and mTOR, but not AKT, prevents the phosphorylation of common substrates, similar to what observed in MCF7-derived PI3Ki-resistant cells.

8.4 Whole-exome sequencing of sensitive and resistant cells

8.4.1 Introduction

Characterisation of genomic alterations in cancer cells provides information about the genetic background underlying tumour progression, and therefore there is great interest in sequencing cancer

genomes. Large scale genomic sequencing initiatives, such as COSMIC have unveiled thousands of genetic mutations in cancer cells [284], contributing to discover gene biomarkers for therapeutic monitoring and treatment [387]. Some of the recurring mutations drive the malignant phenotype and are useful disease biomarkers; less frequent mutations may also be conductive to tumour growth, and much research effort to estimate their predictive value is currently in progress [388].

Next-generation sequencing has been proved useful to identify recurrent mutations in breast cancer cells that acquired resistance to GDC-0941 treatment, including increased c-MYC copy number [301] or mutation in *PIK3CB* [389].

The exomes of parental and three PI3Ki-resistant cell models (previously characterised in Chapters 3-5) were sequenced to portray the genetic status of all known protein-coding regions of those models.

8.4.2 Point mutations in PI3Ki-resistant cells

The nature and number of point mutations in PI3Ki-resistant were heterogeneous, and the exome profiles of G1 and G2 resistant cells were more similar relatively to the exome of G3 resistant cells. Concretely, G1 and G2 cells evolved 20 identical point mutations whereas G3 cells have 21 exclusive point mutations. G1 and G2 resistant cells have point mutations that will result in truncated ERBB2 and MKK7 proteins; although previous studies indicated that over-expression of ERBB2 mediates the migration and survival of breast luminal epithelial cells [390], the recurrent point mutations in *Erbb2* and *Map2k7* genes identified in this study in PI3Ki-resistant cells were not covered in the literature. The functional effects of each of these mutations — for example, the ability of mutated ERBB2 to dimerise with other members of the ErbB family — were not evaluated in this study.

The lack of secondary mutations in PI3K supports the hypothesis that the targeted inhibitor GDC-0941 effectively binds to the kinase, suggesting that the mechanism by which PI3Ki-resistant cells overcome the inhibition of the PI3K pathway is not mediated by secondary mutations in PI3K. It is interesting to note that neither loss-of-function mutation nor loss of PTEN was not found in any of the three PI3Ki-resistant cell lines. This observation contrast the convergent PTEN loss found in other tumour models [168]. Further validation of the identified genomic alterations by methods such as Sanger sequencing or tagged amplicon sequencing would be necessary to confirm their value. In addition, the contribution of other non-synonymous mutations to the resistant phenotypes could be analysed in future studies with computer programs meant to ease the interpretation of genomic variants [283].

8.4.3 Chromosomal variations of PI3Ki-resistant cells

Similarities between G1 and G2 resistant cells, and divergence from G3 resistant cells, were also detected at the chromosomal loci copy number level. It was interesting to observe, however, copy number gain of genetic regions that contain genes members of the NOTCH pathway (i.e. *c-MYC* and *HEY1*) in the three PI3Ki-resistant cells. The c-MYC oncoprotein locates downstream of PI3K and MAPK signalling pathways, and several studies showed that c-MYC helps to gain resistance to PI3K inhibition in various tumour types, including breast cancer cells [301, 313, 314] and acute lymphoblastic leukaemia (ALL) [172]. In addition to this documented mechanism of acquired resistance to PI3K inhibitors, copy number analysis showed that the three PI3Ki-resistant cell lines carry amplifications of regions that contain the loci for *RAD21* and *ETX1* oncogenes. More research is needed to understand the functional consequences, if any, of these mutations.

8.5 Overall implications of the study and directions for future research

The research work of this study yields several substantial insights about the nature of PI3Ki/mTORi-resistant cells that may have potential implications in cancer therapeutics (Fig 8.1). First, drug-sensitive cancer cells exposed to identical drug selecting pressure evolve into heterogeneous drug-resistant cells. This observation mirrors the notion that *the sequence of antecedent states determines the outcome* proposed by Stephen Jay Gould to explain the diversity of life forms in the Cambrian world [391], and the observations made in some laboratories that acquired resistance to targeted treatments can emerge through multiple molecular mechanisms in cancer cells [317, 346].

Second, the heterogeneous nature of PI3Ki-resistant cells translates into diverse signalling pathways modulations as well as diverse viability of PI3Ki-resistant cells during drug holidays. Thus, this study reveals that the viability of PI3Ki-resistant cells can either increase or decrease upon PI3Ki treatment removal depending on the extent of their metabolic adaptation.

Third, this study makes evident that drug responses can be difficult to infer from genomic data. For instance, the cross-resistance of PI3Ki-resistant cells to AKT inhibitors was unnoticed in the genetic landscapes of PI3Ki-resistant cells.

Finally, this study did not focus on characterising the genetic landscape of cells during the occurrence of resistance, and it is therefore of limited value to reconstruct the evolutionary patterns that shaped the diversity of resistant cells. A previous study involved the collection of PI3Ki-resistant cells at different time points during chronic treatment with the PI3Ki [226]. Such collection of cell lines with different extends of resistance could be characterised by genomic, proteomic,

phosphoproteomic, and metabolic analyses. This would contribute to understand the effect of contingency (i.e. the dependency on the history of cellular features) during the evolution of resistance to targeted drug therapies, analogously to other studies [348, 387].

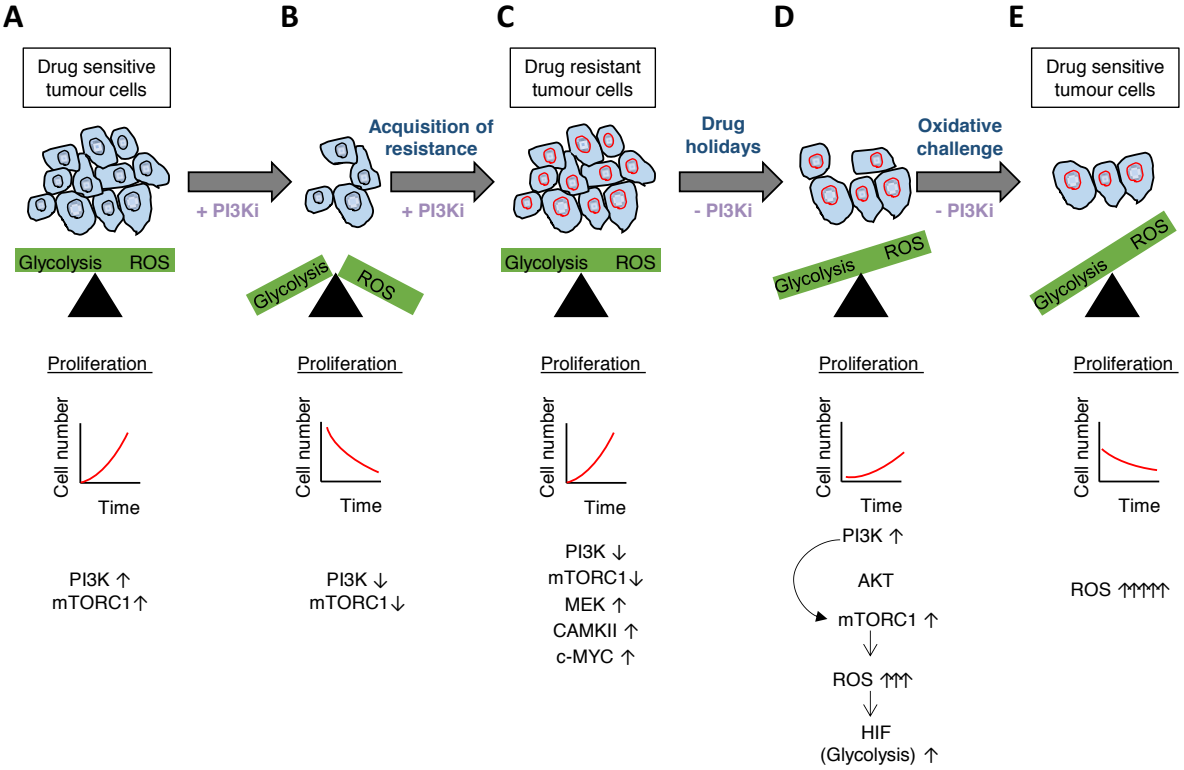

Figure 8.1 Model of metabolic adaptations of sensitive cells and cells that acquired resistance to the inhibition of PI3K signalling. (**A**) Parental cells in basal conditions: the glycolytic and respiratory activities are in homeostasis, sustained by the activity of signalling pathways to maintain a positive cell proliferation of drug-sensitive cancer cells. (**B**) Parental cells treated with a PI3K inhibitor (represented in purple): inhibition of PI3K signalling induces cell death and loss of metabolic activity. (**C**) Resistant cells treated with a PI3K inhibitor: resistant cells develop genomic mutations (represented in red), modulate the activity of several proteins and recover the metabolic balance by activating compensatory signalling pathways that enable cell proliferation. (**D**) Resistant cells during drug holidays: reactivation of the suppressed signalling pathway causes a defective metabolic activity that hinders the proliferation of drug-resistant cells. (**E**) Oxidative challenge in resistant cells withdrawn from PI3Ki: additional metabolic stress potentiates the metabolic imbalance and reverses the sensitive phenotype of drug-resistant cancer cells.

8.6 Role of lactic acid in cancer cells

8.6.1 Introduction

A common characteristic of tumours is the accumulation of lactic acid in the microenvironment, ascribed to an enhanced glycolic activity of cancer cells [392]. Published studies have demonstrated that metabolism-derived lactate can directly stimulate the activity of some signalling networks in an autocrine manner [108]. However, the plasticity of signalling networks and the remodelling of the proteomes of cells in response to lactic acid have not been comprehensively investigated to date.

The effect of lactic acid treatment on a defined signalling network and several phenotypic features were investigated. MCF7 cells were selected as a model to understand the cellular changes promoted by lactic acid because: (i) a kinase-mediated signalling network of the MCF7 cell line was defined previously in the Cutillas laboratory [226]; (ii) the lactic acid production of this cell line was quantified and presented in Chapter 5 of this thesis; and (iii) MCF7 cells are an easy-to-manipulate experimental system.

8.6.2 Main findings

MCF7 cells co-expressed the three lactate transporters MCT1/2/4 and the lactate receptor GPR81, as indicated by Western blot data of these proteins. The expression pattern of MCTs in these cells was similar to observations made by others [393]: MCF7 cells have higher levels of MCT1 and MCT2 compared to the MCT4 transporter. Together, these experiments provided the bases to reason that lactic acid could have an impact on the biology of MCF7 cells.

MCT1i treatment reduced the viability of MCF7 cells in a concentration dependent manner, further supporting the anti-cancer therapeutic usage of chemical inhibitors that target MCT1 [141]. The observed effect of MCT1i in these cells was agreement with other studies that revealed that targeting MCT1's activity impaired the proliferation of breast cancer cells *in vitro* and *in vivo* [142, 394]. Analysis of the proteome and phosphoproteome of cells upon treatment with the MCT1 inhibitor would contribute to shed light into the mechanisms of action of this compound to trigger cell death.

Lactic acid alone does not fully replace glucose as the carbon source of MCF7 cells, as revealed by the cell death upon glucose starvation and supplementation with lactic acid. Similar results have been reported for other *PIK3CA*-mutant cell lines, which could not compensate the glucose withdrawal when the nutrient source was replaced [98]. Nevertheless, here it was observed that lactic acid reduced death of MCF7 cells, suggesting that these cells were adept at utilising lactic acid to diminish glucose deprivation-induced cell death. Further investigations are required to determine whether, at shorter incubation times (e.g. 24 h or 48 h), lactic acid can fully rescue cells from glucose-starvation death, or whether, alternatively, the acidosis derived from lactic acid promotes the viability of MCF7 cells. Given that glucose deficiency is a common characteristic of solid tumours, those experiments would aid in the understanding of the functional relevance of interfering with lactic acid metabolism as a strategy to reduce the viability of cancer cells. The results of previous studies demonstrated *in vivo* that lactic acid and GPR81 are critical for the expression of MCTs and for the viability of pancreatic adenocarcinoma cells exposed to glucose-free conditions, but not in conditions where glucose is abundant [395].

Although neither lactic acid nor acidosis *per se* are sufficient to maintain the proliferation of MCF7 cells, treatment with high concentration of lactic acid increased the phosphorylation of various peptides, and the observed number of differentially modulated phosphopeptides by treatment with high concentration of lactic acid was greater compared to that one after treatment with either low lactic acid concentration or HCl, as unveiled by MS-based phosphoproteomics experiments. It is known that short-time treatment with lactic acid [115] or acidosis [396] stimulates the activity of PI3K/AKT/mTOR and MAPK signalling pathways. Supervised extraction from the phosphoproteomics data revealed an increase in the phosphorylation of several nodes of these pathways after short-time treatment with either lactic acid or HCl. The phosphorylation of MAPK3 at Thr^{202}/Tyr^{204} observed in the phosphoproteomics data was confirmed by immunoblotting, and it was noted that lactic acid treatment phosphorylated nodes of the MAPK pathway to a greater extent compared to HCl. Several substrates of AKT (PRAS40 at Thr^{246}, GSK3β Ser^{9}, and ACLY at Ser^{455}) increased their phosphorylation as a result of acute treatment with high concentration of lactic acid and HCl.

Treatment with high concentrations of lactic acid and acidosis reduced phosphorylation of eEF2K at Ser^{72}/Ser^{74}, which is an indicative marker of lower protein synthesis at the stage of translation elongation [397], and reduced phosphorylation of Raptor at Ser^{863} and Ser^{877}, which are associated with mTORC1's activity [336]. On the other hand, the phosphorylation of several substrates linked to AMPK activity — including SAFB $Ser^{601/604}$ and ULK1 at Ser^{556} — increased after exposure of cells to lactic acid and acidosis. It is tempting to speculate that potential modulation of protein translation and autophagy triggered by excessive extracellular lactic acid and acidosis could protect cells from responses similar to glucose starvation as reported in other studies [398].

Autophagy contributes to recycling intracellular components to promote cell survival, and is triggered in non-malignant and cancer cells in response to stress conditions, including acidosis [55]. The hypothesis that lactic acid and acidosis induce autophagy in these cells could be tested by measuring well-known autophagic markers such as the conjugate LC3-phosphatidylethanolamine protein (LC3-II) and Sequestosome 1 (SQSTM1, also known as p62) protein cargo for autophagy of poliubiquitinated proteins [399]. These experiments would help to determine whether cells undergo autophagy when exposed to either lactic acid or acidosis.

The phosphoproteomics data uncovered that lactic acid and HCl mediate the activation of various signalling branches (e.g. EGF-ERK axis, IGF-1-ERK axis, EGF-AKT axis, and IGF-1-AKT axis). This was previously uncharacterised. Indeed, this study provides the first large scale analysis of how the signalling networks of MCF7 respond to lactic acid and HCl, and was in agreement with other observations that demonstrated a dose-dependent, lactate-mediated phosphorylation of some

kinases, such as p38 MAPK at Thr^{180}/Tyr^{182} [400]. This study also evidences that the signalling activity of HCl may have been overlooked; actually, experiments conducted to understand the signalling activity of lactate through GPR81 did not control for acidosis [108].

Ontology analysis of the phosphoproteomics dataset revealed that processes associated with signalling mediated by p38α and p38β kinases and structural components of the cytoskeleton were enriched upon treatment of cells with high concentrations of lactic and hydrochloric acid. Conversely, processes associated with the regulation of Rho/Rac GTPases activity were enriched upon treatment with low concentration of acids. Data from previous studies associated glycolytic rates with cytoskeletal remodelling [401]; however, a direct role of lactic acid in the regulation of Rho/Rac kinases activity has not reported to date. The impact of lactic acid on Rho/Rac activities could be analysed in future experiments by exploring the activation markers of some of their targets — e.g. Myosin light chain (MLC) at Ser^{19} or focal adhesion kinase (FAK) at Ser^{910} — by immunoblotting.

F-actin staining intensity of MCF7 cells was reduced by acidosis treatment: the polymerisation of actin filaments, essential for the migration of cells, could be affected in these cells by the response to acidosis of proteins containing pH-sensing domains, such as cofilin and talin [341]. The interplay and response of actin-binding proteins and Rho proteins to lactic acid and acidosis treatments warrants further investigation.

Overall, these data serve to demonstrate that lactic acid is a signalling molecule in a breast cancer cell line (i.e. MCF7 cells), and that acidosis (derived from HCl) also promotes signalling activity in this cell line. The capacity of acidosis to trigger signalling responses through GPR81 remains to be proven. That finding would expand the growing knowledge of pH-sensing G protein-coupled receptor family [402]. Ultimately, it remains to be explored whether the signalling effects mediated by lactic acid and acidosis observed *in vitro* study occur *in vivo*.

8.6.3 Limitations of the analysis of the impact of lactic acid in cell signalling

A major limitation of the investigations of the role of lactic acid in the signalling activity of MCF7 cells was that it was not possible to discern the lactate-specific, GPR81-mediated signalling responses of these cells. Given that lactic acid deprotonates into lactate and protons on culture media conditions, the acidosis-derived signalling response to lactic acid treatment could not be eliminated. In fact, a similar signalling response to treatment with similar lactic acid and HCl concentrations was observed. Considering the low expression of the proton-sensor receptors OGR1 and GPR4 in MCF7 cells [403], it was hypothesised that protons could trigger signalling activity in these cells through other proton

sensors, such as NHE1 or NBCn1 [404]. The LC-MS-based proteomics methods employed in this study were not optimised to enrich for membrane proteins and alternative fractionation methods [405] could help in this regard.

A substantial improvement in this study would have been to use a method to selectively inhibit the GPR81 cognate receptor for lactate. However, several attempts using siRNA targeting GPR81 transcripts were disappointing, and did not consistently reduce the expression levels of GPR81 (Fig 7.3 as a representative example). Optimisation of siRNA transfection conditions or usage of inhibitors against GPR81 (such as pertussis toxin) or analogues of lactic acid (such as 3-hydroxybutyrate) would contribute to characterise the signalling pathways mediated by lactate. In addition, and as previously mentioned, given that limited glucose is common in the tumour microenvironment, the signalling response to lactic acid of cells exposed to glucose limiting conditions could be explored in future experiments.

In this study, the effect of lactic acid and HCl on the intensity of F-actin fibres was analysed. Exploration of the response of additional cytoskeletal features, e.g. focal adhesions, to treatment with these acids will contribute to reveal their role on the biology of the cell cytoskeleton. Boyden Chamber assays could be used as a proxy to investigate the role of lactic acid and acidosis in cell invasion and migration.

8.6.4 Proteome changes in response to treatment with lactic acid or HCl

The proteomes of MCF7 cells were modulated after 4 h, 8 h, or 24 h treatments with either 20 mM lactic acid or 9.7 mM HCl: this was characterised by an increase of proteins upon 4 h, a decrease after 8 h and an increased after 24 h treatments. Ontology analyses revealed that several biological processes changed in response to treatment with lactic acid or HCl. For instance, essential cytoskeletal proteins, such as α-actinins 1-4, known to be actin-crosslinking proteins [406], were significantly reduced after 8 h treatment with 9.7 mM HCl.

Albeit the intracellular pH or the lactate uptake were not measured in these experiments, the cellular location and pH-sensing domains of proteins could impact their response to intracellular pH and might explain some of the observed changes; indeed, changes in protein protonation has shown experimentally to change the function and subcellular location of some proteins [407]. Further analysis of the location and structural properties of the proteins modulated by acidosis and lactate might help to explain the observed changes in the proteomes of cells in response to lactic acid and

HCl treatments. Nonetheless, this is the first experimental evidence of a temporal modulation of protein expression upon treatment with acidosis or lactic acid in a holistic manner.

8.6.5 Apoptotic response and proliferation of cells treated with lactic acid or HCl

Cells grown on glucose-plentiful conditions and treated with high concentrations of lactic acid or HCl engaged cellular apoptosis. However, treatment with lower concentration of acids did not increase the higher number of apoptotic cells. Although enhanced cellular apoptosis and reduced cytokine production of T-cells exposed to high concentration of lactic acid has been documented before [116], the mechanisms that induce early apoptosis in MCF7 cells promoted by lactic acid and acidosis remained to be elucidated.

High concentration of lactic acid (20 mM) hampered the proliferation of cells cultured on glucose-rich media. The hypothesis that treatment with high lactic acidosis hamper glucose uptake, similar to what observed in other studies [398], remained to be tested.

8.6.6 Biological outcome mediated by a metabolite

This study is a proof-of-concept of the role of the metabolite lactic acid on the *in vitro* behaviour of a cellular model. A lesson learnt from this study is that the response of a breast cancer cell line greatly depends on the extent of the metabolite concentration: high concentration of lactic acid (20 mM), but not low concentration of lactic acid (5 mM), limits the proliferation of MCF7 cells. Anabolic pathways — involving AKT, mTOR, ERK and MEK signalling nodes — and catabolic pathways — including eEF2K and the activity of AMPK — may be modulated upon treatment of these cells with lactic acid and acidosis, as indicated by time-resolved phosphoproteomics experiments.

Functional experiments suggested that the presence or absence of glucose is critical for the response of cells to lactic acid. Thus, when glucose is absent as a carbon source, MCF7 cells benefit from the presence of lactic acid; contrarily, extracellular lactic acid limits the proliferative capacity of cells exposed to abundant glucose. The results presented in this study expand upon growing literature regarding the therapeutic relevance of interfering with the transport of lactic acid to limit tumour growth [408].

Ultimately, functional metabolic assays could be instrumental to determine the effect of lactic acid and acidosis treatments on metabolism (e.g. glycolytic activity and oxidative phosphorylation). In addition, exploration of the biochemical responses to compounds that interfere with lactic acid metabolism (e.g. the MCT1 inhibitor AZD3965) using untargeted approaches will potentially help to

provide the rational to design treatment strategies to enhance the response to these compounds, and stratify patients for clinical trials using these compounds.

8.7 Concluding remarks

The signalling activities mediated by PI3K and mTOR kinases are important to control the biology of non-malignant and cancer cells. Signalling cascades are highly interconnected, and global analysis of signalling pathways facilitates a comprehensive understanding of the molecular mechanisms that control cellular systems. Signalling networks evolve during treatment, and adapt in response to stimuli. Mass spectrometry-based (phospho)-proteomics allows the quantification of proteins and phosphate-mediated post-translational modification of proteins in an extensive manner.

The aim of this thesis was to understand the biochemical adaptations that allow cancer cells to compensate for the chronic PI3K signalling inhibition, with the ultimate objective to identify vulnerabilities in those cells when exposed to differential selection pressures.

The results presented in this thesis revealed exciting associations between metabolic modulations and kinase-mediated signalling pathways, and characterise how these modulations impact the functionalities of cancer cells resistant to targeted therapies. In particular, exploiting the loss of metabolic homeostasis of drug-resistant cells is proposed as an effective adjuvant therapy to the drug holidays approach to delay drug-resistance of cancer cells treated with targeted drugs. Future research in this topic should focus on pre-clinical studies in *in vivo* systems.

Furthermore, the impact of lactic acid on the signalling activity of a luminal epithelial breast cancer cell line was characterised in this thesis. These experiments demonstrated a dose-response in the plasticity of signalling cascades upon treatment of cells with lactic acid or hydrochloric acid, and suggested that these acids modify the activity of pathways related to catabolic and anabolic processes and cytoskeletal features. These results provide the bases to hypothesise that acidosis, which is high in the tumour microenvironment, may disrupt cancer cell's biochemistry.

Appendix 1

Summary of first 10 terms over-represented pathways containing proteins modulated in PI3Ki-resistant cells inferred by DAVID online application (Chapter 4).

Term	PValue	Proteins
GO:0006006~glucose metabolic process	7.93E-09	AK1A1, ODP2, UGDH, G6PD, ENOG, DCXR, 6PGD, PYGB, G3P, DHSO, AKT1, ENOB, LDHB, LDHA, K6PL, DHTK1, PCKGM, PYC, ENOA
GO:0005996~monosaccharide metabolic process	2.28E-08	AK1A1, ODP2, UGDH, G6PD, HEXB, ENOG, DCXR, 6PGD, PYGB, NAGK, G3P, DHSO, AKT1, ENOB, LDHB, FCL, LDHA, K6PL, DHTK1, PCKGM, PYC, ENOA
GO:0055114~oxidation reduction	2.72E-08	IDHC, DECR, AL4A1, IMDH2, QOR, MAOX, C1TC, SERA, DCXR, 6PGD, G3P, TXD12, PRDX2, CX6B1, FAS, PRDX1, AK1A1, RIR2B, UGDH, G6PD, BLVRB, PRDX4, FDFT, GSHR, IDH3A, DHB4, ETFB, AL7A1, IDHP, ARK72, DHSO, RIR2, FCL, LDHB, LDHA, UCRI, DHTK1, ACAD9
GO:0019318~hexose metabolic process	5.28E-08	AK1A1, ODP2, UGDH, G6PD, ENOG, DCXR, 6PGD, PYGB, G3P, DHSO, AKT1, ENOB, LDHB, FCL, LDHA, K6PL, DHTK1, PCKGM, PYC, ENOA
GO:0016052~carbohydrate catabolic process	1.24E-07	AK1A1, ODP2, G6PD, HEXB, ENOG, PYGB, 6PGD, G3P, DHSO, ENOB, LDHB, LDHA, K6PL, DHTK1, ENOA
GO:0046164~alcohol catabolic process	2.05E-07	6PGD, ODP2, G3P, DHSO, ENOB, LDHB, LDHA, G6PD, COMT, K6PL, DHTK1, ENOG, ENOA
GO:0044271~nitrogen compound biosynthetic process	2.56E-07	ATPA, PYRG1, NDKA, RIR2B, PYR1, AL4A1, PURA2, MAOX, IMDH2, C1TC, NADC, SERA, PUR2, KCY, PUR6, PUR9, AKT1, RIR2, SPEE, SERB, ASSY, ASNS, PAPS1, PNPH, MSH2
GO:0044275~cellular carbohydrate catabolic process	3.52E-07	6PGD, PYGB, ODP2, G3P, DHSO, ENOB, LDHB, LDHA, G6PD, K6PL, DHTK1, ENOG, ENOA
GO:0006412~translation	3.62E-07	SYWC, RL22L, EIF3C, SYAC, RL10, RL22, SYHM, RM12, EIF3K, PABP4, LRC47, SYYC, RL7, RL1D1, IF5, EIF3B, RS4X, SYTC, SYG, DHYS, RS17, SYLC, EF1D, EFTU
GO:0006007~glucose catabolic process	5.04E-07	ODP2, 6PGD, G3P, ENOB, LDHB, LDHA, G6PD, K6PL, DHTK1, ENOG, ENOA

Appendix 2

Summary of the complete proteomics dataset contained in the *K*-means clustering analysis for proteins (Chapter 4).

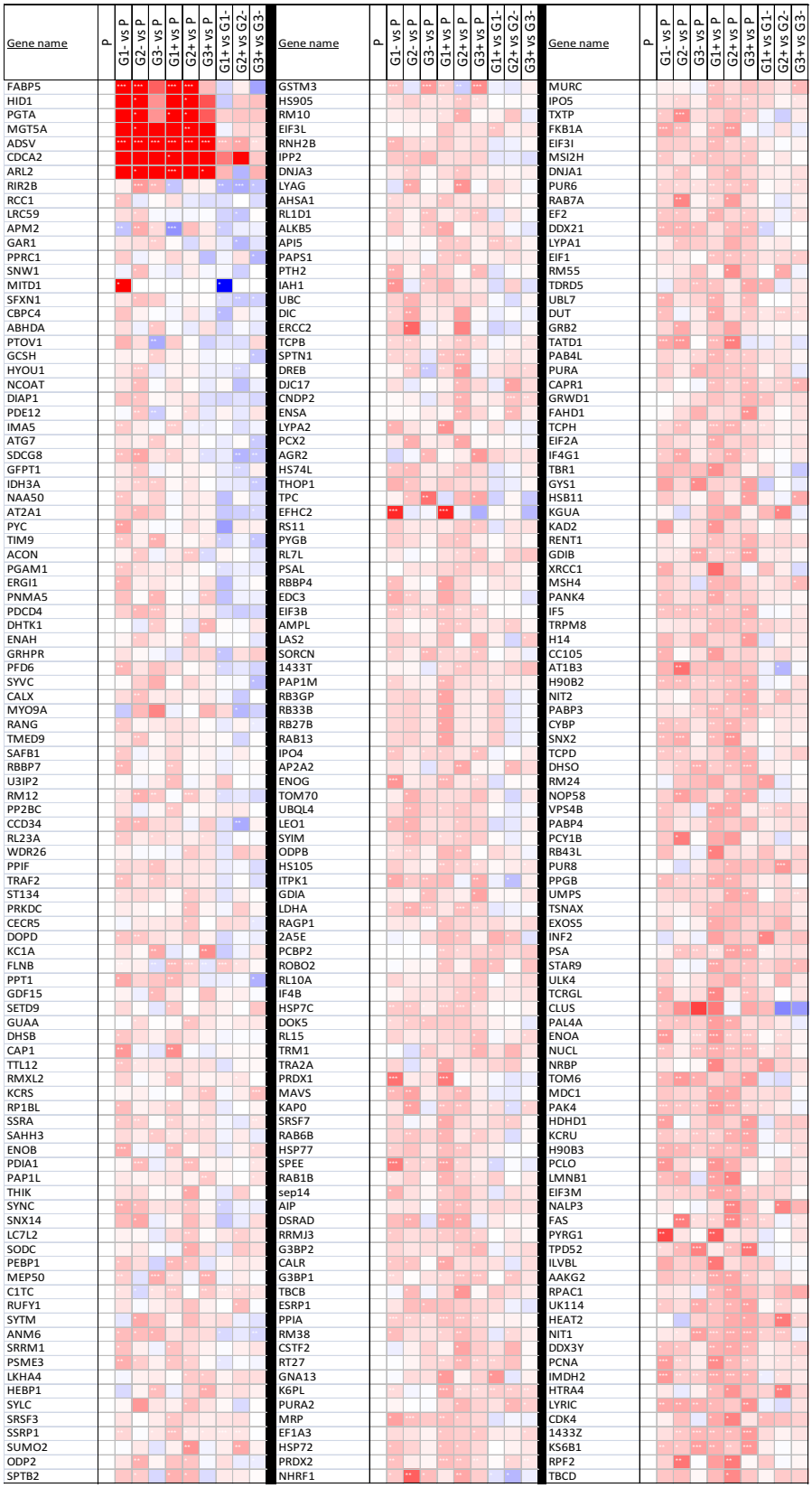

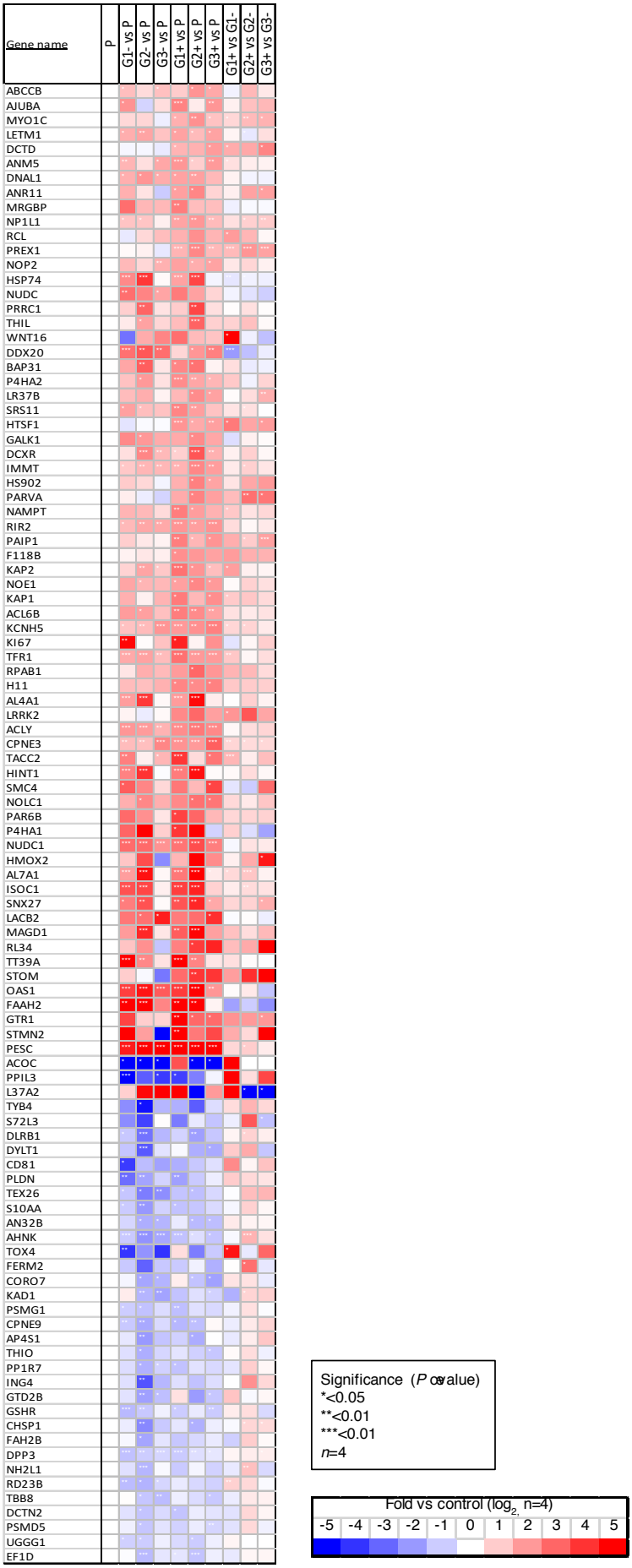
Gene name
P
G1- vs P
G2- vs P
G3- vs P
G1+ vs P
G2+ vs P
G3+ vs P
G1+ vs G1-
G2+ vs G2-
G3+ vs G3-
ABCCB
AJUBA
MYO1C
LETM1
DCTD
ANM5
DNAL1
ANR11
MRGBP
NP1L1
RCL
PREX1
NOP2
HSP74
NUDC
PRRC1
THIL
WNT16
DDX20
BAP31
P4HA2
LR37B
SRS11
HTSF1
GALK1
DCXR
IMMT
HS902
PARVA
NAMPT
RIR2
PAIP1
F118B
KAP2
NOE1
KAP1
ACL6B
KCNH5
KI67
TFR1
RPAB1
H11
AL4A1
LRRK2
ACLY
CPNE3
TACC2
HINT1
SMC4
NOLC1
PAR6B
P4HA1
NUDC1
HMOX2
AL7A1
ISOC1
SNX27
LACB2
MAGD1
RL34
TT39A
STOM
OAS1
FAAH2
GTR1
STMN2
PESC
ACOC
PPIL3
L37A2
TYB4
S72L3
DLRB1
DYLT1
CD81
PLDN
TEX26
S10AA
AN32B
AHNK
TOX4
FERM2
CORO7
KAD1
PSMG1
CPNE9
AP4S1
THIO
PP1R7
ING4
GTD2B
GSHR
CHSP1
FAH2B
DPP3
NH2L1
RD23B
TBB8
DCTN2
PSMD5
UGGG1
EF1D
Significance (P value)
*<0.05
**<0.01
***<0.01
n=4
Fold vs control (log2, n=4)
-5
-4
-3
-2
-1
0
1
2
3
4
5

Appendix 3

Quality control of phosphoproteomics MS data of MCF7 parental and GDC-0941 resistant cells grown in the presence or in the absence of PI3Ki (Chapter 4).

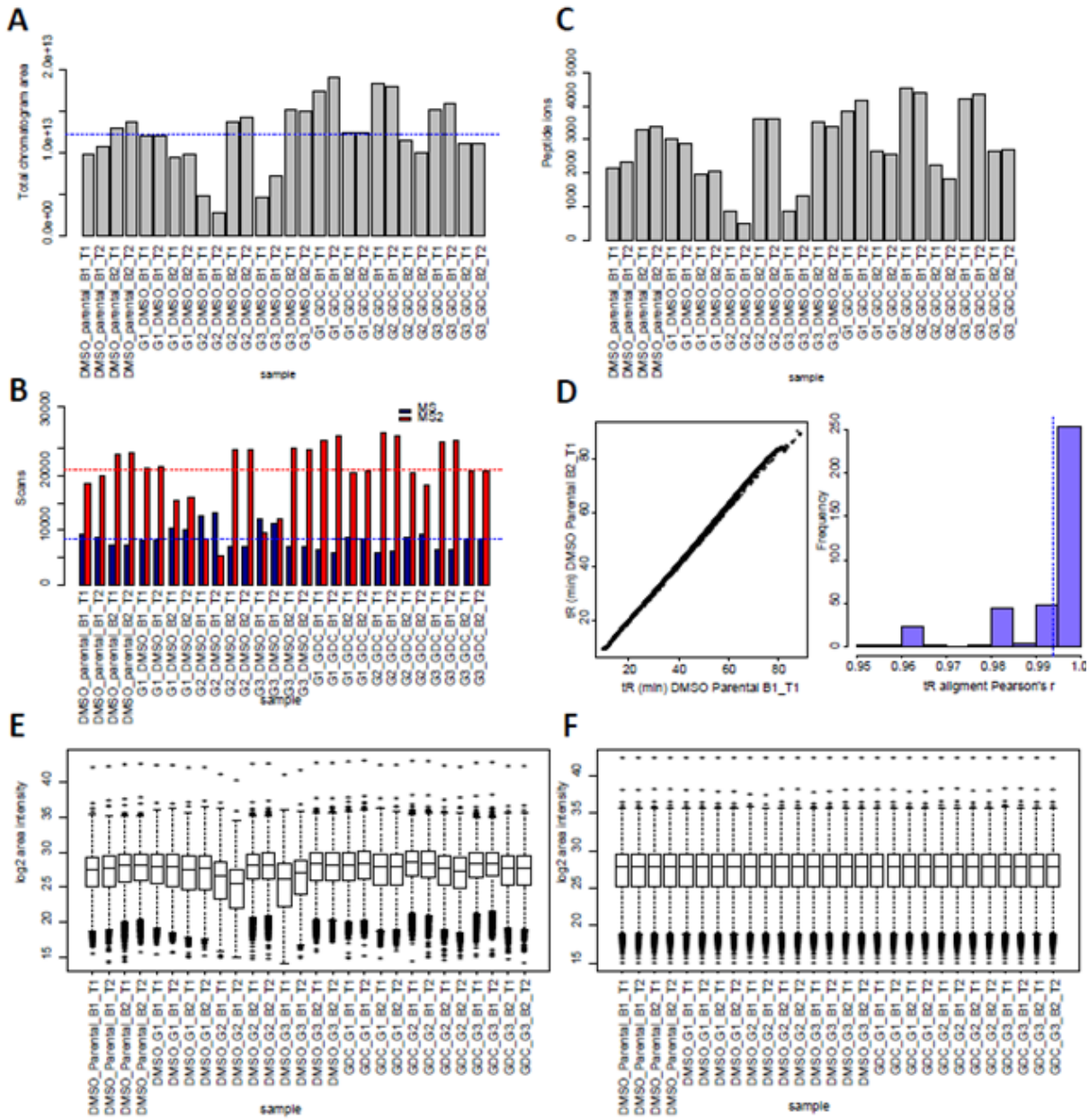

Appendix 3. (**A**) Quantification of total area under the chromatographic peaks contained in 28 phosphoproteomics MS runs. (**B**) Number of MS and MS2 scans quantified by RawMeat. (**C**) Number of identified peptide ions (FDR<0.05) that generate the database created from the 28 MS runs. (**D**) Representative alignment between retention times of two experimental samples (left panel) and histogram distribution of the correlation between the alignment of retention times of all experimental samples (right panel). (**E**) Box plots demonstrating the distribution of log_2-transformed phosphopeptide peak intensities pre-normalisation. (**F**) log_2 distribution of phosphopeptides peak intensities post-quantile normalisation.

Appendix 4

Summary of the complete phosphoproteomics dataset contained in the *K*-means clustering analysis (Chapter 4).

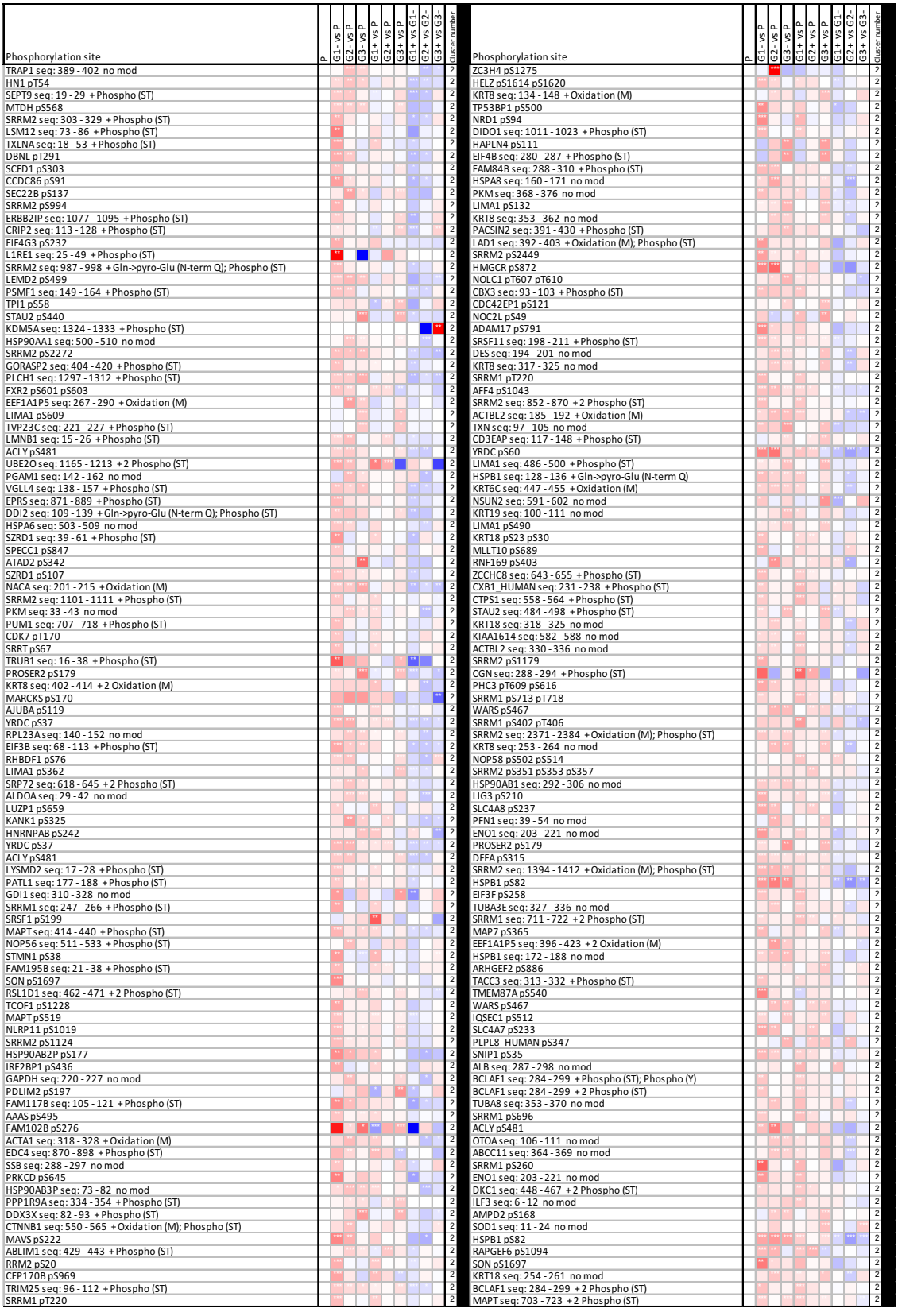
Phosphorylation site
P
G1- vs P
G2- vs P
G3- vs P
G1+ vs P
G2+ vs P
G3+ vs P
G1+ vs G1-
G2+ vs G2-
G3+ vs G3-
Cluster number
TRAP1 seq: 389 - 402 no mod
HN1 pT54
SEPT9 seq: 19 - 29 +Phospho (ST)
MTDH pS568
SRRM2 seq: 303 - 329 +Phospho (ST)
LSM12 seq: 73 - 86 +Phospho (ST)
TXLNA seq: 18 - 53 +Phospho (ST)
DBNL pT291
SCFD1 pS303
CCDC86 pS91
SEC22B pS137
SRRM2 pS994
ERBB2IP seq: 1077 - 1095 +Phospho (ST)
CRIP2 seq: 113 - 128 +Phospho (ST)
EIF4G3 pS232
L1RE1 seq: 25 - 49 +Phospho (ST)
SRRM2 seq: 987 - 998 +Gln->pyro-Glu (N-term Q); Phospho (ST)
LEMD2 pS499
PSMF1 seq: 149 - 164 +Phospho (ST)
TPI1 pS58
STAU2 pS440
KDM5A seq: 1324 - 1333 +Phospho (ST)
HSP90AA1 seq: 500 - 510 no mod
SRRM2 pS2272
GORASP2 seq: 404 - 420 +Phospho (ST)
PLCH1 seq: 1297 - 1312 +Phospho (ST)
FXR2 pS601 pS603
EEF1A1P5 seq: 267 - 290 +Oxidation (M)
LIMA1 pS609
TVP23C seq: 221 - 227 +Phospho (ST)
LMNB1 seq: 15 - 26 +Phospho (ST)
ACLY pS481
UBE2O seq: 1165 - 1213 +2 Phospho (ST)
PGAM1 seq: 142 - 162 no mod
VGLL4 seq: 138 - 157 +Phospho (ST)
EPRS seq: 871 - 889 +Phospho (ST)
DDI2 seq: 109 - 139 +Gln->pyro-Glu (N-term Q); Phospho (ST)
HSPA6 seq: 503 - 509 no mod
SZRD1 seq: 39 - 61 +Phospho (ST)
SPECC1 pS847
ATAD2 pS342
SZRD1 pS107
NACA seq: 201 - 215 +Oxidation (M)
SRRM2 seq: 1101 - 1111 +Phospho (ST)
PKM seq: 33 - 43 no mod
PUM1 seq: 707 - 718 +Phospho (ST)
CDK7 pT170
SRRT pS67
TRUB1 seq: 16 - 38 +Phospho (ST)
PROSER2 pS179
KRT8 seq: 402 - 414 +2 Oxidation (M)
MARCKS pS170
AJUBA pS119
YRDC pS37
RPL23A seq: 140 - 152 no mod
EIF3B seq: 68 - 113 +Phospho (ST)
RHBDF1 pS76
LIMA1 pS362
SRP72 seq: 618 - 645 +2 Phospho (ST)
ALDOA seq: 29 - 42 no mod
LUZP1 pS659
KANK1 pS325
HNRNPAB pS242
YRDC pS37
ACLY pS481
LYSMD2 seq: 17 - 28 +Phospho (ST)
PATL1 seq: 177 - 188 +Phospho (ST)
GDI1 seq: 310 - 328 no mod
SRRM1 seq: 247 - 266 +Phospho (ST)
SRSF1 pS199
MAPT seq: 414 - 440 +Phospho (ST)
NOP56 seq: 511 - 533 +Phospho (ST)
STMN1 pS38
FAM195B seq: 21 - 38 +Phospho (ST)
SON pS1697
RSL1D1 seq: 462 - 471 +2 Phospho (ST)
TCOF1 pS1228
MAPT pS519
NLRP11 pS1019
SRRM2 pS1124
HSP90AB2P pS177
IRF2BP1 pS436
GAPDH seq: 220 - 227 no mod
PDLIM2 pS197
FAM117B seq: 105 - 121 +Phospho (ST)
AAAS pS495
FAM102B pS276
ACTA1 seq: 318 - 328 +Oxidation (M)
EDC4 seq: 870 - 898 +Phospho (ST)
SSB seq: 288 - 297 no mod
PRKCD pS645
HSP90AB3P seq: 73 - 82 no mod
PPP1R9A seq: 334 - 354 +Phospho (ST)
DDX3X seq: 82 - 93 +Phospho (ST)
CTNNB1 seq: 550 - 565 +Oxidation (M); Phospho (ST)
MAVS pS222
ABLIM1 seq: 429 - 443 +Phospho (ST)
RRM2 pS20
CEP170B pS969
TRIM25 seq: 96 - 112 +Phospho (ST)
SRRM1 pT220
ZC3H4 pS1275
HELZ pS1614 pS1620
KRT8 seq: 134 - 148 +Oxidation (M)
TP53BP1 pS500
NRD1 pS94
DIDO1 seq: 1011 - 1023 +Phospho (ST)
HAPLN4 pS111
EIF4B seq: 280 - 287 +Phospho (ST)
FAM84B seq: 288 - 310 +Phospho (ST)
HSPA8 seq: 160 - 171 no mod
PKM seq: 368 - 376 no mod
LIMA1 pS132
KRT8 seq: 353 - 362 no mod
PACSIN2 seq: 391 - 430 +Phospho (ST)
LAD1 seq: 392 - 403 +Oxidation (M); Phospho (ST)
SRRM2 pS2449
HMGCR pS872
NOLC1 pT607 pT610
CBX3 seq: 93 - 103 +Phospho (ST)
CDC42EP1 pS121
NOC2L pS49
ADAM17 pS791
SRSF11 seq: 198 - 211 +Phospho (ST)
DES seq: 194 - 201 no mod
KRT8 seq: 317 - 325 no mod
SRRM1 pT220
AFF4 pS1043
SRRM2 seq: 852 - 870 +2 Phospho (ST)
ACTBL2 seq: 185 - 192 +Oxidation (M)
TXN seq: 97 - 105 no mod
CD3EAP seq: 117 - 148 +Phospho (ST)
YRDC pS60
LIMA1 seq: 486 - 500 +Phospho (ST)
HSPB1 seq: 128 - 136 +Gln->pyro-Glu (N-term Q)
KRT6C seq: 447 - 455 +Oxidation (M)
NSUN2 seq: 591 - 602 no mod
KRT19 seq: 100 - 111 no mod
LIMA1 pS490
KRT18 pS23 pS30
MLLT10 pS689
RNF169 pS403
ZCCHC8 seq: 643 - 655 +Phospho (ST)
CXB1_HUMAN seq: 231 - 238 +Phospho (ST)
CTPS1 seq: 558 - 564 +Phospho (ST)
STAU2 seq: 484 - 498 +Phospho (ST)
KRT18 seq: 318 - 325 no mod
KIAA1614 seq: 582 - 588 no mod
ACTBL2 seq: 330 - 336 no mod
SRRM2 pS1179
CGN seq: 288 - 294 +Phospho (ST)
PHC3 pT609 pS616
SRRM1 pS713 pT718
WARS pS467
SRRM1 pS402 pT406
SRRM2 seq: 2371 - 2384 +Oxidation (M); Phospho (ST)
KRT8 seq: 253 - 264 no mod
NOP58 pS502 pS514
SRRM2 pS351 pS353 pS357
HSP90AB1 seq: 292 - 306 no mod
LIG3 pS210
SLC4A8 pS237
PFN1 seq: 39 - 54 no mod
ENO1 seq: 203 - 221 no mod
PROSER2 pS179
DFFA pS315
SRRM2 seq: 1394 - 1412 +Oxidation (M); Phospho (ST)
HSPB1 pS82
EIF3F pS258
TUBA3E seq: 327 - 336 no mod
SRRM1 seq: 711 - 722 +2 Phospho (ST)
MAP7 pS365
EEF1A1P5 seq: 396 - 423 +2 Oxidation (M)
HSPB1 seq: 172 - 188 no mod
ARHGEF2 pS886
TACC3 seq: 313 - 332 +Phospho (ST)
TMEM87A pS540
WARS pS467
IQSEC1 pS512
SLC4A7 pS233
PLPL8_HUMAN pS347
SNIP1 pS35
ALB seq: 287 - 298 no mod
BCLAF1 seq: 284 - 299 +Phospho (ST); Phospho (Y)
BCLAF1 seq: 284 - 299 +2 Phospho (ST)
TUBA8 seq: 353 - 370 no mod
SRRM1 pS696
ACLY pS481
OTOA seq: 106 - 111 no mod
ABCC11 seq: 364 - 369 no mod
SRRM1 pS260
ENO1 seq: 203 - 221 no mod
DKC1 seq: 448 - 467 +2 Phospho (ST)
ILF3 seq: 6 - 12 no mod
AMPD2 pS168
SOD1 seq: 11 - 24 no mod
HSPB1 pS82
RAPGEF6 pS1094
SON pS1697
KRT18 seq: 254 - 261 no mod
BCLAF1 seq: 284 - 299 +2 Phospho (ST)
MAPT seq: 703 - 723 +2 Phospho (ST)


Phosphorylation site
P
G1- vs P
G2- vs P
G3- vs P
G1+ vs P
G2+ vs P
G3+ vs P
G1+ vs G1-
G2+ vs G2-
G3+ vs G3-
Cluster number
SLC9A3R1 seq: 41 - 50 no mod
SRRM2 pS2132
NRD1 seq: 92 - 105 + Phospho (ST)
KRT18 seq: 302 - 314 + Oxidation (M)
TPD52 pS176
SRRM1 pS738
SRRM2 seq: 1539 - 1556 + Phospho (ST)
STK10 seq: 447 - 464 + 2 Phospho (ST)
TPI1 seq: 180 - 186 no mod
KRT8 seq: 473 - 483 no mod
MAPT seq: 713 - 723 + Phospho (ST)
ENO1 seq: 72 - 80 no mod
TUBGCP4 seq: 48 - 54 no mod
KRT18 seq: 91 - 97 no mod
FAM195B seq: 21 - 38 + Phospho (ST)
MTFR1L pS103
ABLIM1 pS655
HMGCR pS872
SHROOM3 pS439 pS443
PRDX2 seq: 140 - 150 no mod
HSPA2 seq: 104 - 109 no mod
NOS1AP seq: 255 - 268 + Phospho (ST)
HSPB1 seq: 172 - 188 no mod
PRPF4B seq: 427 - 440 + 2 Phospho (ST)
SNIP1 pS35
ASPSCR1 pS502
SRRM2 pS2272
HSPB1 seq: 80 - 89 no mod
MYCBP2 seq: 2831 - 2844 + Phospho (ST)
RCC1 pS11
SNW1 pS224
SRRM2 pS1124
KNOP1 pS42
NPM1 seq: 33 - 45 no mod
SHROOM2 seq: 919 - 937 + 2 Phospho (ST)
ENO1 seq: 344 - 358 no mod
ENO3 seq: 344 - 358 no mod
CUL4A pS10
TBC1D9B seq: 409 - 440 + Phospho (ST)
SRRM2 seq: 871 - 882 + Phospho (ST)
RBBP8 seq: 325 - 337 + Phospho (ST)
STK10 pS438
IRF2BP1 pS66
HSPA2 seq: 173 - 189 no mod
HSP90AB3P seq: 56 - 69 no mod
FNBP4 pS116
SRRM2 pS1132
SRSF10 pS131 pS133
PRCC seq: 259 - 282 + Phospho (ST)
SRRM1 pS769 pS773 pS781
RPLP1 pS101
LAD1 seq: 392 - 403 + Phospho (ST)
TRAM1 pS365
TBC1D4 seq: 747 - 768 + 2 Phospho (ST)
ABI2 seq: 220 - 230 + Phospho (ST)
BTF3 seq: 95 - 122 no mod
PRDX2 seq: 17 - 26 no mod
EEF1A1P5 seq: 173 - 179 no mod
MTA1 seq: 516 - 527 + Phospho (ST)
HNRNPA2B1 seq: 204 - 213 no mod
RAN seq: 13 - 23 no mod
SRSF10 pS133
TAF2_HUMAN pS790
HSPA1A seq: 160 - 171 no mod
SRRM2 pS1179
NPM1 seq: 240 - 248 no mod
KRT9 seq: 164 - 170 no mod
LATS1 pS464
SRRM1 pT614 pS616
NOP58 pS502 pS514
HSP90AB2P pS177
SORBS3 seq: 520 - 532 + Phospho (ST)
SRRM1 pS769 pS775
KRT2 seq: 189 - 195 no mod
MKI67 seq: 1806 - 1818 + Phospho (ST)
NHS_HUMAN seq: 504 - 509 + Phospho (ST)
SRRM2 seq: 1589 - 1594 + Phospho (ST)
PRPF38B pS268
TRAF3IP3 seq: 108 - 113 + Phospho (ST)
DHX9 pS321
HSPB1 seq: 189 - 198 no mod
SRSF11 seq: 198 - 211 + Phospho (ST)
SRRM2 pS2272
SNIP1 pS35
SRSF11 seq: 443 - 451 + Phospho (ST)
SNIP1 pS35
SRRM1 pS769 pS775
KRT8 seq: 226 - 233 no mod
HSPB1 seq: 80 - 89 + Gln->pyro-Glu (N-term Q); Phospho (ST)
USP24 pS2047
KRT8 seq: 134 - 148 + Oxidation (M)
FIP1L1 pS492
NOLC1 pT607 pT610
ATXN2L seq: 400 - 411 + Oxidation (M); Phospho (ST)
KRT19 seq: 266 - 274 no mod
CGN pS149
CUX1 pS1270
MED1 seq: 1475 - 1496 + 2 Phospho (ST)
PPIG pS356 pT358
MARCKSL1 seq: 26 - 43 + Phospho (ST)
PRKAR1B pT85
PRRC2A pS456
PNN pS100
MCM2 pS108
ATXN2L seq: 333 - 345 + Gln->pyro-Glu (N-term Q); Phospho (ST)
SRRM1 pS653
CHAMP1 pS427
SRRM1 pS605 pS607
EEF1A1P5 seq: 167 - 172 no mod
HSP90AA1 seq: 339 - 345 no mod
XPNPEP3 seq: 149 - 155 no mod
KRT18 seq: 7 - 14 no mod
BCLAF1 pS385
SRRM1 pS402 pT406
RPS25 seq: 86 - 94 no mod
PSMD2 pS361
HSPD1 seq: 134 - 141 no mod
RPS28 seq: 52 - 63 no mod
SRSF5 seq: 110 - 118 no mod
PRKCD seq: 505 - 524 + Phospho (ST)
GNL1 seq: 45 - 61 + Phospho (ST)
WRNIP1 pS153
JUN seq: 57 - 70 + Phospho (ST)
ACTA1 seq: 318 - 328 no mod
SIPA1L1 seq: 254 - 269 + Phospho (ST)
ENO1 seq: 270 - 281 no mod
HOMEZ pT451
RANBP2 pS955
PSMF1 seq: 51 - 62 no mod
PRKCH pS675
PREX1 seq: 800 - 832 + Phospho (ST)
SRRM1 pT614 pS616
PROSER2 seq: 283 - 315 + Phospho (ST)
HSP90AA2 seq: 283 - 291 no mod
HDGF pS165
SRRM2 pS2132
FIP1L1 seq: 490 - 504 + Phospho (ST)
MAPT seq: 701 - 723 + 3 Phospho (ST)
TACC1 seq: 262 - 283 + Phospho (ST)
SRRM1 pS769
HSPA8 seq: 129 - 137 no mod
NCL seq: 64 - 70 + Phospho (ST)
FRPD1_HUMAN seq: 1095 - 1101 + Phospho (ST)
ILF3 pT592
PSMA5 pS56
TERF2IP seq: 154 - 165 + Phospho (ST)
HNRNPK seq: 208 - 219 no mod
ACIN1 pS825
HSPB1 seq: 115 - 123 no mod
RCOR1 pS257
PDE5A pS86
CLMN pS419
HSPD1 seq: 397 - 405 no mod
RIPK2 seq: 529 - 538 + Phospho (ST)
SRRM2 pS1179
CHD4 seq: 1529 - 1539 + Phospho (ST)
PRDX6 seq: 42 - 53 no mod
SRRM2 pS1329
FKBP4 seq: 359 - 373 no mod
YWHAE seq: 143 - 153 no mod
ALB seq: 438 - 452 no mod
DSG2 seq: 262 - 275 no mod
EPB41L3 pS409
SRRM1 pS560 pS562
EEF1A2 seq: 248 - 255 no mod
AHSG seq: 312 - 317 no mod
RPL27A seq: 95 - 105 no mod
NCL seq: 334 - 342 no mod
DKC1 pS451 pS453
SRRM1 pT581 pS583
PRCC pS157 pS159
CTPS1 pS571 pS573
PRDX4 seq: 201 - 208 no mod
ANKS1A pS663
CTPS1 seq: 565 - 591 + Phospho (ST); Phospho (Y)
NPM1 seq: 268 - 273 no mod
CCNL2 pS369
RXRA seq: 5 - 25 + Phospho (ST)
TPR seq: 367 - 387 + Phospho (ST)
ALB seq: 500 - 508 no mod
RPS6 seq: 120 - 131 no mod
EBAG9 pS36
ZNF687 pS1057
ESF1 pS663
SRRM1 pS549 pS551
DOCK7 pS1432
EBAG9 pS36
CIT seq: 1937 - 1951 + Phospho (ST)
AHNAK pT5824
KRT12 seq: 343 - 349 no mod
EFHD2 seq: 63 - 78 + Phospho (ST)
BCLAF1 seq: 256 - 271 + 2 Phospho (ST)
SMTN seq: 271 - 287 + Phospho (ST)
NCL seq: 325 - 333 no mod
ATF2 pS112
ESF1 pS657 pS663
KIAA1671 seq: 1224 - 1234 + Phospho (ST)
NCK1 seq: 82 - 103 + Phospho (ST)
CLDN3 pS209
OSBP seq: 186 - 212 + Phospho (ST)
TPD52 pS176
SRRM1 pT572 pT574


Phosphorylation site
P
G1- vs P
G2- vs P
G3- vs P
G1+ vs P
G2+ vs P
G3+ vs P
G1+ vs G1-
G2+ vs G2-
G3+ vs G3-
Cluster number
HSPA4 seq: 737 - 748 +Oxidation (M) 2
SRRM1 pS560 pS562 2
FASN seq: 317 - 326 no mod 2
PDE5A pS86 2
FLNB seq: 2476 - 2495 +Phospho (ST) 2
ALB seq: 258 - 264 no mod 2
SOX13 seq: 301 - 314 +Phospho (ST) 2
CAPZA1 seq: 20 - 37 no mod 2
RPL27 seq: 85 - 93 no mod 2
FARP1 seq: 417 - 438 +2 Phospho (ST) 2
NCL seq: 363 - 370 no mod 2
ATP5A1 seq: 134 - 149 no mod 2
PRDX1 seq: 159 - 168 no mod 2
CLK1 pS140 2
CD2AP pS224 2
NME1 seq: 7 - 18 no mod 2
CIAO1 seq: 128 - 154 no mod 2
KRT18 seq: 371 - 381 no mod 2
SRP72 seq: 618 - 645 +3 Phospho (ST) 2
FOXK1 seq: 416 - 430 +Oxidation (M); 2 Phospho (ST) 2
PRDX2 seq: 128 - 135 no mod 2
SMAP2 seq: 210 - 226 +Phospho (ST) 2
MAP4K5 seq: 431 - 454 +Phospho (ST) 2
CTU2 pS419 2
MDH2 seq: 92 - 104 no mod 2
ARFGAP2 pS432 2
SRRM2 seq: 1856 - 1862 +Phospho (ST) 2
PRKD2 seq: 195 - 208 +Phospho (ST) 2
SVIL seq: 850 - 867 +Phospho (ST) 2
MAP4 pS507 2
EEF1D pT147 pS162 2
PDCD4 pS457 2
MAP3K2 seq: 329 - 348 +Phospho (ST) 2
ZNRF2 pS135 2
ENO1 seq: 222 - 228 no mod 2
TAGAP_HUMAN seq: 56 - 65 +Oxidation (M) 2
SVIL pS221 2
AMPD2 pS100 2
EIF3E pS399 2
PA2G4 seq: 34 - 62 no mod 2
PCBP1 seq: 178 - 200 +Phospho (ST) 2
RPS6 seq: 233 - 243 +2 Phospho (ST) 2
PRDX2 seq: 111 - 119 no mod 2
FOXK1 pS416 pS420 2
MMACHC pS275 pS279 2
ETV5 pS425 2
SPDEF pS308 2
SFRP2 seq: 286 - 291 +Phospho (ST) 2
POLH pS380 2
NCL seq: 411 - 420 no mod 2
AHCTF1 seq: 1209 - 1225 +Phospho (ST) 2
MDH2 seq: 177 - 185 no mod 2
CHERP seq: 817 - 838 +2 Phospho (ST) 2
FOXK1 pS416 pS420 2
FAM103A1 pS36 2
HSPB1 pS15 2
PRDX1 seq: 111 - 120 no mod 2
CTPS1 seq: 571 - 591 +2 Phospho (ST) 2
AHNAK pS570 2
ARPP19 seq: 102 - 109 +Phospho (ST) 2
SRRM2 pS1320 2
AHNAK pS511 2
CHD4 seq: 306 - 338 +2 Phospho (ST) 2
USP14 pS143 2
TKT seq: 556 - 594 no mod 2
TBC1D22A pS132 2
SRRM2 pS2702 pS2706 3
CN159_HUMAN pS9 pS13 3
DPYSL2 pS522 3
CCSER1 seq: 8 - 14 +Phospho (ST) 3
ZC3H13 pT263 pS265 3
HSPA9 seq: 469 - 485 no mod 3
NDRG2 pS338 3
NUCKS1 pS181 3
CHMP3 pS200 3
TLE1 seq: 282 - 300 +Phospho (ST) 3
GPATCH8 seq: 721 - 745 +Phospho (ST) 3
FAM83H pS936 3
MSL2 seq: 343 - 362 +Phospho (ST) 3
CDK13 pS437 pS439 3
RPS6 seq: 234 - 243 +2 Phospho (ST) 3
RBBP6 pS1179 3
PCBP1 seq: 244 - 268 +Gln->pyro-Glu (N-term Q); Pho 3
RAB11FIP1 seq: 498 - 520 +Phospho (ST) 3
ADD3 seq: 664 - 684 +Phospho (ST) 3
AHNAK pS5841 3
FLNA pS1459 3
LZTS2 pS570 3
HSPA5 seq: 47 - 60 no mod 3
NOP56 seq: 511 - 534 +Phospho (ST) 3
MAP4K5 seq: 333 - 350 +Phospho (ST) 3
SEC16A seq: 1872 - 1879 +Phospho (ST) 3
NUCKS1 pS181 3
SNRNP70 pS226 3
AHNAK seq: 5726 - 5744 +2 Phospho (ST) 3
SHANK2 seq: 41 - 64 +Phospho (ST) 3
ARHGEF16 pS107 3
H1FX pS31 3
MATR3 pS188 3
ZNF185 seq: 463 - 482 +Phospho (ST) 3
NDRG2 pT330 pS332 3
TBX2 pS401 3
WDHD1 pS868 3
NUMA1 pS1862 3
SENP3 pS188 3
NUCKS1 pS181 3
SRRM1 pT872 pS874 3
GTF2I seq: 674 - 702 +Phospho (ST) 3
TMPO pS66 pS67 3
AHNAK seq: 5724 - 5744 +Phospho (ST) 3
CTNND1 pS268 3
AHNAK seq: 5724 - 5744 +2 Phospho (ST) 3
GTF2I seq: 674 - 702 +Phospho (ST) 3
NUMA1 pS2077 3
TPM4 seq: 56 - 69 no mod 3
ANP32A seq: 21 - 28 no mod 3
OCIAD1 pS108 3
SMC4 seq: 13 - 38 +Phospho (ST) 3
FAM21B seq: 448 - 467 +Phospho (ST) 3
PRC1 pT481 3
SIPA1L1 seq: 1248 - 1259 +Phospho (ST) 3
NUCKS1 pT179 pS181 3
SMC4 pS28 3
SNX1 pS188 3
CAP2 seq: 294 - 314 +Phospho (ST) 3
AHNAK pS5731 3
BCL11B seq: 369 - 390 +2 Phospho (ST) 3
POTEI seq: 729 - 739 no mod 3
SNRPD3 seq: 9 - 29 no mod 3
LMO7 seq: 1591 - 1604 +Phospho (ST) 3
AHNAK pS216 3
TRPV3 pS374 3
NSFL1C seq: 137 - 156 +Phospho (ST) 3
LRRFIP1 seq: 118 - 134 +Phospho (ST) 3
HERC2 pS2928 3
TRIP11 pS1891 3
SRRM1 seq: 870 - 888 +Phospho (ST) 3
PHLDB1 pS419 3
NSRP1 seq: 15 - 47 +Phospho (ST) 3
RPS3 seq: 202 - 227 +Phospho (ST) 3
CDC42EP4 seq: 269 - 297 +Phospho (ST) 3
STMN1 pS25 3
TMPO seq: 345 - 356 +Phospho (ST) 3
EIF4EBP1 seq: 20 - 56 +2 Phospho (ST) 3
AHNAK pS511 3
PPP1R12A pS445 3
NUCKS1 pS181 3
BUD13 pS271 3
UBXN7 pS288 3
MTMR4 seq: 627 - 641 +Phospho (ST) 3
CHAMP1 seq: 457 - 470 +Phospho (ST) 3
ZFP36L2 pS490 3
HDAC2 pS394 3
AHNAK seq: 5726 - 5744 +Phospho (ST) 3
NUF2 pS247 3
NFATC2IP pS204 3
RBM23 pS149 3
SHROOM2 pS413 3
IRS1 pS1078 3
BCLAF1 pS512 3
PPP1R12A seq: 442 - 456 +Phospho (ST) 3
ZBTB17 seq: 113 - 136 +Phospho (ST) 3
SIPA1L1 seq: 174 - 197 +Phospho (ST) 3
ATAD2B seq: 73 - 91 +Phospho (ST) 3
RALBP1 seq: 27 - 43 +Phospho (ST) 3
MCM2 pS139 3
WDR46 pS41 3
AHNAK seq: 5780 - 5812 +2 Phospho (ST) 3
ZC3H13 pS242 3
SRSF9 pS211 3
EEF1D pS162 3
HDAC2 pS394 3
NFATC2IP seq: 231 - 263 +Phospho (ST) 3
KRT18 pS18 3
NUMA1 pS1991 pT2000 3
HSP90AA1 seq: 300 - 314 no mod 3
MSH6 seq: 4 - 22 +Phospho (ST) 3
ZNF652 seq: 54 - 66 +Phospho (Y) 3
STMN1 pS63 3
BCLAF1 pS512 3
SRSF9 pS211 3
FAM91A1 seq: 826 - 838 +Phospho (ST) 3
BCLAF1 pS658 3
STMN2 seq: 120 - 129 no mod 3
STMN1 seq: 86 - 95 no mod 3
NAP1L4 seq: 108 - 138 +Phospho (ST) 3
IQGAP3 seq: 1424 - 1436 +Phospho (ST) 3
SRSF3 seq: 12 - 28 no mod 3
USP1 pS327 3
MYH14 pS1969 3
NCL pT76 3
MAGI3 seq: 835 - 859 +Phospho (ST) 3
MCM4 seq: 114 - 149 +Phospho (ST) 3
MCM2 pS139 3
SRRM2 pS2702 pS2706 3
C9orf142 pS152 3
AHNAK seq: 5748 - 5765 +Phospho (ST) 3
FIP1L1 seq: 488 - 506 +Phospho (ST) 3
MYOF pS174 3
DENND4C seq: 1040 - 1059 +Phospho (ST) 3
PRRC2C pT2673 3
SHROOM2 pS1036 3


Phosphorylation site
P
G1 - vs P
G2 - vs P
G3 - vs P
G1+ vs P
G2+ vs P
G3+ vs P
G1+ vs G1-
G2+ vs G2-
G3+ vs G3-
Cluster number
BRIP1 seq: 988 - 995 +Phospho (ST)
RGPD3 pS1535
AHNAK seq: 172 - 181 +Phospho (ST)
TMPO seq: 151 - 173 +2 Phospho (ST)
NUCKS1 pS19
NUCKS1 pS19
C9orf142 pS148
AGFG1 pS181
THRAP3 seq: 678 - 688 +Phospho (ST)
MSH6 seq: 129 - 140 +Phospho (ST)
STMN1 pS16
LMNB1 seq: 398 - 407 +Phospho (ST)
PPP1R12A seq: 443 - 456 +Phospho (Y)
REPS1 seq: 270 - 286 +Phospho (ST)
SLC9A3R1 seq: 288 - 331 +Oxidation (M); Phospho (ST)
PPP1R12A seq: 443 - 456 +Phospho (ST)
SIPA1L1 pS1433
FIP1L1 pS492 pS500
LARP1 seq: 620 - 642 +Phospho (ST)
XRCC1 pS241
NCAPH2 pS284
KIAA1598 seq: 485 - 505 +Phospho (ST)
TNKS1BP1 seq: 492 - 520 +2 Phospho (ST)
CDK13 seq: 861 - 873 +Phospho (ST)
STMN1 pS16
CPNE3 seq: 126 - 139 no mod
NPM1 pS70
SHROOM2 seq: 644 - 662 +Phospho (ST)
AHNAK pS4986
ZNF652 seq: 54 - 66 +Phospho (ST)
EML3 pS176
MYOM2 seq: 1157 - 1162 +Phospho (ST)
H2AFZ seq: 86 - 92 no mod
EEF1B2 pS106
CCDC88C pS1887
PHLDB1 pS563
WDHD1 pS383
PRPF31 seq: 445 - 471 +2 Phospho (ST)
SIPA1L1 seq: 205 - 227 +Phospho (ST)
TRAM1 seq: 349 - 367 +Phospho (ST)
NUCKS1 seq: 176 - 186 +2 Phospho (ST)
NFYA pS326
SRRM2 seq: 2114 - 2129 +Oxidation (M); 2 Phospho (ST)
SF3B2 pT780
CHAMP1 pS308 pS319
RPS6KB1 seq: 444 - 459 +Phospho (ST)
CHAMP1 pS308 pS319
C11orf84 seq: 239 - 263 +Phospho (ST)
EEF1B2 pS106
CHD3 pS1601 pS1605
TPI1 seq: 213 - 225 no mod
SMARCC1 pS328 pS330
NUCKS1 pS19
NUCKS1 pS19
ZCRB1 pS155
ANKRD34A pS247
PPP2R5D pS573
CLNS1A pS102
HIST3H2BB seq: 59 - 73 +2 Oxidation (M)
ARGLU1 pS77
CDK1 pT14 pY15
CTR9 pT925
ZC3HC1 pS359 pS370
ANKRD34A pS461
SRRM2 pS508 pS510
MCM2 pS139
NCOA3 pS214
CDK18 pS12
KRT19 seq: 254 - 265 no mod
TNKS1BP1 pS1029
PPP6R3 pS617
UNG pS23
SCRIB seq: 1575 - 1615 +Phospho (ST)
PLEC seq: 4361 - 4383 +Phospho (ST)
HNRNPK pS216
ZC3H4 seq: 1265 - 1292 +2 Phospho (ST)
UBL4A pS90
CEP170B pS1179
SRRM2 seq: 1078 - 1089 +Gln->pyro-Glu (N-term Q); Phospho (ST)
ZC3H4 seq: 1265 - 1292 +2 Phospho (ST)
CENPT pS397
C9orf142 pS148
SVIL pS221
TPI1 pS58
KRT8 seq: 317 - 328 no mod
TBC1D30 seq: 111 - 131 +Phospho (ST)
CDK18 pT152
CDK3 pT14
KRT8 seq: 317 - 328 no mod
STMN1 pS16 pS25
HNRNPK pS216
CHAMP1 seq: 280 - 301 +Phospho (ST)
RB1CC1 seq: 641 - 655 +Phospho (ST)
LAMTOR1 seq: 48 - 60 +Phospho (ST)
CPNE3 seq: 126 - 139 no mod
ZFYVE20 seq: 208 - 227 +2 Phospho (ST)
SRRM2 seq: 1878 - 1885 +2 Phospho (ST)
STC2 seq: 274 - 301 +Phospho (ST)
CABL1_HUMAN seq: 284 - 289 +Phospho (ST)
ZC3H13 seq: 316 - 330 +2 Phospho (ST)
STMN1 pS16 pS25
ERBB2IP seq: 1077 - 1095 +Gln->pyro-Glu (N-term Q); Phospho (ST)
DOCK7 seq: 896 - 916 +Phospho (ST)
PUM2 pS587
ATAD2 seq: 335 - 346 +Phospho (ST)
MCM3 seq: 701 - 724 +Oxidation (M); Phospho (ST); Phospho (Y)
RBM15 pT32
CHAMP1 seq: 441 - 456 +2 Phospho (ST)
RNF20 seq: 126 - 142 +Phospho (ST)
UNG seq: 51 - 73 +2 Phospho (ST)
CGN pS332
IRS1 seq: 328 - 353 +Phospho (ST)
MYL6 seq: 80 - 94 no mod
POGZ seq: 1322 - 1341 +Phospho (ST)
CDK11A pS271
SRRM2 seq: 2114 - 2129 +Phospho (ST)
PLEC pS1732
PRPF4B seq: 427 - 440 +3 Phospho (ST)
SLC9A3R1 seq: 288 - 331 +Oxidation (M); 2 Phospho (ST)
NOLC1 pS698
RANBP2 pS1456
TNS3 seq: 774 - 792 +Phospho (ST)
LASP1 seq: 131 - 153 +Phospho (ST)
PDHA2 seq: 287 - 300 +2 Phospho (ST)
RBM15 seq: 666 - 681 +2 Phospho (ST)
HEATR6 seq: 630 - 645 +Phospho (ST)
DOCK7 seq: 896 - 916 +Phospho (ST)
SVIL pT852
OSBPL11 pS189
MCM3 seq: 701 - 724 +Oxidation (M); 2 Phospho (ST)
MYL9 seq: 18 - 35 +Phospho (ST)
CHAMP1 pS476
KIAA1598 pS506
SF3B1 seq: 214 - 231 +2 Phospho (ST)
PPP1R12A pS862 pS871
NCL seq: 611 - 624 no mod
LMNB1 pS391 pS393
SRRM2 seq: 286 - 303 +2 Phospho (ST)
STRN pS245
PKP3 pS180
C9orf40 pS69
HIRIP3 seq: 94 - 117 +2 Phospho (ST)
CGN seq: 129 - 146 +2 Phospho (ST)
NELFE pS131
NCOR2 seq: 2048 - 2080 +2 Phospho (ST)
ZC3H4 seq: 157 - 179 +Phospho (Y)
PTPN21 pS637
XRCC1 pS241
ZBTB7A seq: 505 - 530 +Phospho (ST)
FTSJ3 seq: 568 - 579 +Phospho (ST)
SRSF9 pS211 pS216
MYH10 seq: 1945 - 1976 +Gln->pyro-Glu (N-term Q); Phospho (ST)
LDB1 seq: 300 - 320 +Phospho (ST)
NUCKS1 pS19
NCOA3 seq: 562 - 590 +Phospho (Y)
NOTCH2 seq: 1801 - 1824 +Phospho (ST)
AHNAK pS5400
CGN seq: 129 - 146 +2 Phospho (ST)
EIF3H seq: 341 - 352 no mod
NUCKS1 pS19
SIPA1L1 seq: 1430 - 1471 +3 Phospho (ST)
TBC1D5 seq: 41 - 57 +Phospho (ST)
TIMELESS seq: 1082 - 1092 +Phospho (ST)
UBE2O seq: 423 - 466 +2 Phospho (ST)
PXN seq: 111 - 123 +Phospho (Y)
MAP3K2 pS153
TBC1D10B seq: 649 - 666 +2 Phospho (ST)
AMPD2 pS168
HNRNPA2B1 seq: 4 - 12 no mod
OSBP pS190 pS193
PGM3 pS64
GATAD2B seq: 117 - 137 +2 Phospho (ST)
LDB1 seq: 300 - 320 +Oxidation (M); Phospho (ST)
SRRM2 seq: 777 - 787 +Phospho (ST)
EEF2K pS74
BCL9L pS1017
SRRM2 pT2738 pS2740
NPM1 pS70
KRT19 seq: 371 - 381 no mod
FLNB pS2465
KRT38 seq: 395 - 405 no mod
KRT18 pS7
UBL7 pS230
MAGED2 seq: 241 - 249 +Phospho (ST)
ANKRD34A pS392
RB1 seq: 788 - 798 +2 Phospho (ST)
SRRM2 pT2738 pS2740
RABL6 pS596 pT599
KRT19 seq: 126 - 138 no mod
HAT1 seq: 358 - 364 +Phospho (ST)
TJP3 pS164 pS169
PPIAL4G seq: 119 - 125 no mod
DCDC2 seq: 261 - 276 +Phospho (ST)
BCKDHA pS347
CALM1 seq: 92 - 107 no mod
CNKSR3 seq: 380 - 393 +Phospho (ST)
SORBS3 seq: 542 - 550 +Phospho (ST)
KRT18 seq: 166 - 175 no mod
KIF1B pS1057
DDX55 pS544
CCDC88C seq: 1815 - 1838 +Phospho (ST)
SIPA1L1 seq: 205 - 227 +2 Phospho (ST)
MTDH seq: 492 - 504 +Phospho (ST)
TMEM54 seq: 84 - 91 +Phospho (ST)
ANK3 pS1459
EPHB4_HUMAN seq: 499 - 508 +Phospho (ST)


Phosphorylation site
P
G1 vs P
G2 vs P
G3 vs P
G1+ vs P
G2+ vs P
G3+ vs P
G1+ vs G1
G2+ vs G2
G3+ vs G3
Number of matches
KRT18 seq: 371 - 381 no mod 3
SRRM1 seq: 387 - 396 +2 Phospho (ST) 3
MCM2 pS108 3
SH3KBP1 pS230 3
AHNAK seq: 208 - 225 +2 Phospho (ST) 3
PDHA2 seq: 287 - 300 +2 Phospho (ST) 3
LARP1 seq: 620 - 642 +2 Phospho (ST) 3
SIPA1L1 seq: 153 - 164 +Phospho (ST) 3
NDE1 seq: 304 - 315 +Phospho (ST) 3
MLPH seq: 550 - 556 +Phospho (ST) 3
EIF5B pS135 pS137 3
KIF13B pS1410 3
PLEKHF2 pS16 3
CDK3 pT14 pY15 3
CDK18 seq: 148 - 158 +Phospho (ST); Phospho (Y) 3
PPP1R12A seq: 908 - 917 +Phospho (ST) 3
NASP seq: 610 - 617 no mod 3
ZC3H4 seq: 1094 - 1124 +3 Phospho (ST) 3
HMGN2 pS25 pS29 3
NGDN seq: 130 - 162 +2 Phospho (ST) 3
PCBP1 pS173 3
MRE11A pS649 3
HCFC1 seq: 2016 - 2024 +Phospho (ST) 3
CHD3 pS1601 pS1605 3
SRRM2 seq: 852 - 870 +Gln->pyro-Glu (N-term Q); Phospho (ST) 3
SEZ6_HUMAN seq: 782 - 788 +Phospho (ST) 3
PARK7 seq: 149 - 156 no mod 3
SRRM1 seq: 603 - 611 +2 Phospho (ST) 3
TPM3 seq: 79 - 91 no mod 3
AHNAK seq: 5745 - 5765 +2 Phospho (ST) 3
PREX1 seq: 1188 - 1209 +Oxidation (M); Phospho (ST) 3
VCL seq: 340 - 352 +Phospho (ST) 3
HASP_HUMAN pT624 3
VCL pS290 3
PARD3 seq: 692 - 712 +Phospho (ST) 3
GIGYF2 pS236 3
MISP seq: 154 - 171 +Phospho (ST) 3
TBC1D15 pS70 3
ZNF687 pS1057 3
EIF4B seq: 445 - 472 +Phospho (ST) 3
HIST2H2BD seq: 36 - 44 no mod 3
MAP7D1 seq: 273 - 283 +Phospho (ST) 3
PKP4 pS221 3
FAM83B pS664 3
NELFB pS557 3
VCL seq: 340 - 352 +Phospho (ST) 3
TNS3 seq: 774 - 792 +Phospho (ST) 3
WDR70 pS638 3
MISP seq: 154 - 171 +Phospho (ST) 3
MLPH seq: 300 - 320 +Phospho (ST) 3
PKD1L1 seq: 2276 - 2281 +Phospho (ST) 3
FNBP4 seq: 448 - 453 +Oxidation (M); Phospho (ST) 3
MKI67 pS2002 3
TRIM33 seq: 1085 - 1113 +Phospho (ST) 3
FAM53C pS232 pS234 3
FLNB seq: 2198 - 2205 no mod 3
FAM110B pS301 3
MINK1 seq: 699 - 709 +Phospho (ST) 3
ANXA2P2 seq: 120 - 135 no mod 3
SMN1 pS28 pS31 3
FBXO4 pS12 3
ZNF74 seq: 635 - 643 +Phospho (ST) 3
PREX1 pS1200 3
PKP4 seq: 325 - 339 +Phospho (ST) 3
UBR4 seq: 2712 - 2721 +Phospho (ST) 3
PREX1 pS1200 3
DECR1 seq: 189 - 214 no mod 3
PREX1 pS1200 3
RBMXL3 seq: 50 - 63 +Phospho (ST) 3
WDR77 seq: 93 - 118 no mod 3
SRSF2 pS189 pS191 3
PREX1 pS319 3
SRRM1 pS260 3
CDK1 seq: 7 - 20 +Phospho (Y) 3
STC2 seq: 276 - 301 +Phospho (ST) 3
RPLP1 pS101 pS104 3
PROSER2 seq: 283 - 315 +Phospho (ST) 3
TBC1D15 seq: 68 - 81 +Phospho (ST) 3
CDV3 pS30 3
KRT2 pS191 3
ROCK1 seq: 1094 - 1120 +2 Phospho (ST) 3
PRPF31 seq: 445 - 470 +2 Phospho (ST) 3
PRPF4B seq: 385 - 391 +Phospho (ST) 3
PDHA2 seq: 287 - 300 +Phospho (ST) 3
FOSL2 pS200 4
MACF1 pS4521 4
MTA2 seq: 50 - 64 +Phospho (ST) 4
VGLL4 seq: 46 - 56 +Phospho (ST) 4
GPRIN1 seq: 606 - 621 +Phospho (ST) 4
PDYN_HUMAN seq: 98 - 104 +Phospho (ST) 4
WIPI2 seq: 407 - 416 +Phospho (ST) 4
EPB41L5 seq: 413 - 445 +Phospho (ST) 4
UBA1 pS816 4
EHMT2 pS232 4
ACIN1 seq: 384 - 396 +2 Phospho (ST) 4
TRIM33 pS1119 4
KRT8 seq: 234 - 252 +Oxidation (M) 4
TUBA3E seq: 41 - 60 no mod 4
CDCA5 seq: 19 - 28 +Phospho (ST) 4
CALR seq: 56 - 73 no mod 4
IER3 seq: 29 - 56 +Phospho (ST) 4
ETV6 seq: 15 - 39 +2 Phospho (ST) 4
KRT8 pS478 4
PATL1 seq: 176 - 188 +2 Phospho (ST) 4
Phosphorylation site
P
G1 vs P
G2 vs P
G3 vs P
G1+ vs P
G2+ vs P
G3+ vs P
G1+ vs G1
G2+ vs G2
G3+ vs G3
Number of matches
SNTB2 pS110 4
LDHAL6B pT358 4
PLEC pS4386 pS4389 4
SLC9A1 seq: 680 - 698 +Phospho (ST) 4
BAD seq: 73 - 94 +Phospho (ST) 4
BAD seq: 97 - 109 +Phospho (ST) 4
WDR77 seq: 122 - 145 no mod 4
MAP4 seq: 600 - 634 +Phospho (ST) 4
CLASP2 seq: 323 - 338 +Phospho (ST) 4
ARID1A pS696 4
BAD pS99 4
RBM14 pS618 4
TPI1 seq: 187 - 193 no mod 4
FRMD6 seq: 520 - 532 +Phospho (ST) 4
ACLY seq: 453 - 469 +Phospho (ST) 4
TMPO pS306 4
DPYSL2 seq: 512 - 532 +3 Phospho (ST) 4
RTN4 seq: 178 - 201 +2 Phospho (ST) 4
DPYSL2 seq: 512 - 525 +Phospho (ST) 4
LIMD2 pS29 4
ZCCHC8 pT479 4
HMGCS1 pS495 4
NOP2 seq: 773 - 789 +Phospho (ST) 4
DGCR8 seq: 365 - 384 +Phospho (ST) 4
TP53I11 pS14 4
BAZ1B seq: 345 - 354 +Phospho (ST) 4
NPY1R pS368 4
FARP1 seq: 14 - 27 +Phospho (ST) 4
PLEC pS1435 4
SLC9A1 seq: 766 - 790 +Phospho (ST) 4
PRRC2B seq: 216 - 233 +Phospho (ST) 4
TRIM16 seq: 54 - 85 +Phospho (ST) 4
SNRPD3 seq: 32 - 51 no mod 4
PLEC seq: 4384 - 4401 +Phospho (ST) 4
SYNRG pS1075 4
KRT8 pS475 4
DMXL2 pS1857 4
NOP2 pS67 4
PACR_HUMAN seq: 415 - 419 no mod 4
YWHAZ seq: 140 - 158 no mod 4
BAG3 seq: 366 - 388 +Phospho (ST) 4
DNMT1 seq: 952 - 960 +Phospho (ST) 4
EIF3A pS584 4
YA023_HUMAN pT54 4
LMNB2 pS296 4
EAF1 seq: 157 - 175 +Phospho (ST) 4
TUBA4A seq: 340 - 352 no mod 4
XBP1 pS47 4
FAM129B pS665 4
ZC3H13 seq: 204 - 214 +2 Phospho (ST) 4
ELMSAN1 pS461 4
PLEC seq: 4610 - 4627 +Phospho (ST) 4
PGRMC1 seq: 45 - 67 +Phospho (ST) 4
TNKS1BP1 pS178 4
ELMSAN1 seq: 698 - 722 +Phospho (ST) 4
RANBP3 seq: 124 - 138 +Phospho (ST) 4
GNB2L1 seq: 140 - 155 no mod 4
AEBP1 seq: 402 - 407 +Phospho (ST) 4
BRSK2 pS489 4
GSK3B seq: 7 - 27 +Phospho (ST) 4
GSK3A seq: 17 - 50 +Phospho (ST) 4
YBX1 seq: 205 - 234 +Phospho (ST) 4
ABI1 pS183 4
BAG3 pS386 4
FAM129B seq: 686 - 705 +Phospho (ST) 4
CREBBP pS2063 4
ACLY seq: 453 - 469 +Phospho (ST) 4
LMNA pT19 4
TRIP10 pS296 4
TJP3 pS591 4
RELA seq: 134 - 149 no mod 4
SMTNL2 pS344 4
SEC31A pS799 4
TJP3 seq: 164 - 182 +Phospho (ST) 4
KIF21A pS1212 4
EPPK1 seq: 2713 - 2732 +Phospho (ST) 4
TBC1D4 seq: 584 - 594 +Phospho (ST) 4
NOP2 pS786 4
CASZ1 seq: 735 - 771 +Phospho (ST) 4
ELMSAN1 pS461 4
CTAGE5 pS536 4
FARP1 seq: 417 - 431 +Phospho (ST) 4
DLG5 seq: 1248 - 1260 +Phospho (ST) 4
STX17 seq: 286 - 300 +Phospho (ST) 4
SPICE1 seq: 228 - 250 +Phospho (ST) 4
BAG3 seq: 194 - 203 +Phospho (ST) 4
ZBTB7A seq: 505 - 531 +Phospho (ST) 4
RAD51C pS20 4
EEF1D seq: 112 - 123 +Phospho (ST) 4
BAG3 seq: 194 - 203 +Phospho (ST) 4
BET1L pS9 4
NCOR2 seq: 1975 - 2004 +Phospho (ST) 4
FAM129B pS665 pS681 4
ARID3A seq: 67 - 95 +Phospho (ST) 4
ULK1 pS450 4
ZNF560 seq: 585 - 592 +Phospho (ST); Phospho (Y) 4
CHD7 pS2559 4
EPPK1 pS2716 4
TJP2 seq: 702 - 715 +Phospho (ST) 4
NCOR2 seq: 2398 - 2410 +Phospho (ST) 4
DSP seq: 163 - 185 +2 Phospho (ST) 4
PAK4 pS181 4
TMPO pS306 4
TP53I11 pS14 4


Phosphorylation site
P
G1- vs P
G2- vs P
G3- vs P
G1+ vs P
G2+ vs P
G3+ vs P
G1+ vs G1-
G2+ vs G2-
G3+ vs G3-
Cluster number
FARP1 pS427 4
TPI1 seq: 138 - 150 no mod 4
pS91 4
STK10 pS438 4
PCBP1 seq: 244 - 268 +Gln->pyro-Glu (N-term Q); Oxidation (M); Phospho 4
ACD seq: 422 - 437 +Phospho (ST) 4
KIF21A pS1212 4
GTF3C3 seq: 40 - 63 +Phospho (ST) 4
ZDHHC5 seq: 375 - 392 +Phospho (ST) 4
PKM seq: 189 - 206 no mod 4
BAD pS118 4
ANLN seq: 293 - 307 +Phospho (ST) 4
RPS6KB1 pT444 pS447 4
ZYX seq: 273 - 295 +Phospho (ST) 4
FAM129B pS665 4
GAB2 seq: 403 - 414 +Phospho (ST) 4
KRT8 seq: 134 - 148 +2 Oxidation (M) 4
KIAA1522 pS404 4
EPPK1 pS2716 4
CRTC3 seq: 366 - 384 +Phospho (ST) 4
SLC35C2 seq: 332 - 344 +Phospho (ST) 4
ARHGAP39 seq: 278 - 293 +Phospho (ST) 4
LARP4B pS718 4
PRKAR1B seq: 69 - 92 +Phospho (ST) 4
MAP4 seq: 634 - 651 +Phospho (ST) 4
UBR5 pS1549 4
RAB12 pS21 4
SQSTM1 seq: 22 - 46 +Phospho (ST) 4
NCOR2 pS956 4
PATL1 seq: 176 - 188 +2 Phospho (ST) 4
BAG3 pS289 4
MACF1 seq: 7328 - 7360 +Phospho (ST) 4
TNKS1BP1 pS1138 4
PLEKHA5 seq: 853 - 870 +Phospho (ST) 4
GSK3A seq: 19 - 50 +Phospho (ST) 4
CHMP3 seq: 184 - 216 +Oxidation (M); Phospho (ST) 4
HDGFRP2 pS454 4
NCOR2 pS956 4
TMCC1 pS382 4
BAZ2A seq: 132 - 143 +Phospho (ST) 4
NCOR2 seq: 981 - 1020 +Phospho (ST) 4
ZBTB7A seq: 503 - 530 +Phospho (ST) 4
PGRMC1 seq: 45 - 67 +Phospho (ST) 4
ZMYND8 pS547 4
BAG3 seq: 171 - 193 +Phospho (ST) 4
PPFIBP1 seq: 538 - 565 +Phospho (ST) 4
SRRM2 seq: 979 - 998 +2 Phospho (ST) 4
TJP2 pS130 4
PPP1R3D seq: 40 - 63 +Phospho (ST) 4
ANKLE2 pS662 4
TOMM34 pS186 4
ZNF217 seq: 792 - 819 +Phospho (ST) 4
SCRIB seq: 1536 - 1574 +Phospho (ST) 4
ATXN2L seq: 400 - 411 +Phospho (ST) 4
EEF1D seq: 112 - 123 +Phospho (ST) 4
TNKS1BP1 seq: 859 - 879 +Phospho (ST) 4
BAG3 pT285 4
DBN1 seq: 328 - 354 +Oxidation (M); Phospho (ST) 4
NOP2 seq: 773 - 789 +Phospho (ST) 4
TNKS1BP1 pS691 4
MBD3 seq: 81 - 90 +Phospho (ST) 4
KIF23 seq: 910 - 932 +Phospho (ST) 4
TJP2 pS702 4
EPPK1 pS2716 4
ANKLE2 pS662 4
FNBP1L seq: 293 - 308 +Phospho (ST) 4
COMT seq: 129 - 135 +Phospho (ST) 4
DDX42 pS185 4
GSE1 pS909 4
RPS6KB1 pT444 pS447 4
BAZ2A seq: 1388 - 1405 +Phospho (ST) 4
ACLY pS455 4
VDAC2 pS115 4
EPPK1 seq: 2714 - 2732 +Phospho (ST) 4
MPRIP seq: 346 - 368 +Phospho (ST) 4
BTF3 pS30 4
KRT18 seq: 56 - 90 +3 Oxidation (M) 4
BAG3 seq: 171 - 193 +Phospho (ST) 4
PTK2 pS840 4
NOP56 seq: 511 - 534 +Oxidation (M); Phospho (ST) 4
MORC2 seq: 722 - 736 +Phospho (ST) 4
CARHSP1 seq: 28 - 35 +Phospho (ST) 4
TRIP12 seq: 310 - 321 +Phospho (ST) 4
MBD1 pS297 4
CARHSP1 seq: 36 - 47 +Phospho (ST) 4
DBN1 pS142 4
RREB1 pS1653 4
MKI67 pS1131 4
NCOR2 seq: 1254 - 1265 +Phospho (ST) 4
TOP2B seq: 1574 - 1599 +Phospho (ST) 4
PDIA6 seq: 38 - 60 no mod 4
PEBP1 pS52 4
MAP7 pS209 4
ZNF687 seq: 422 - 435 +Phospho (ST) 4
SAMD4B seq: 260 - 291 +Phospho (ST) 4
FAM64A pS131 4
IBTK pS1045 4
LPHN2 seq: 1428 - 1439 +Phospho (ST) 4
EDC3 pS131 4
PVRL4 pS444 4
BRAF seq: 444 - 462 +Phospho (ST) 4
HMGXB4 pS497 4
APC pT1438 4
Phosphorylation site
P
G1- vs P
G2- vs P
G3- vs P
G1+ vs P
G2+ vs P
G3+ vs P
G1+ vs G1-
G2+ vs G2-
G3+ vs G3-
Cluster number
GALNT6 seq: 503 - 517 no mod 4
SLTM seq: 989 - 1006 +Phospho (ST) 4
FAM129B seq: 686 - 705 +2 Phospho (ST) 4
UBAP2L seq: 601 - 618 +Phospho (ST) 4
MAP4 seq: 277 - 290 +Oxidation (M); Phospho (ST) 4
TRPS1 seq: 84 - 108 +Phospho (ST) 4
TBC1D10B pS687 4
UBR5 pS1549 4
ZC3H11A seq: 100 - 124 +Phospho (ST) 4
PLEKHG3 pS76 4
TRPS1 pS178 4
LARP4 seq: 643 - 671 +Phospho (ST) 4
MEF2D pS251 4
KRT18 seq: 56 - 90 +3 Oxidation (M) 4
TJP2 pS1159 4
DBN1 seq: 328 - 354 +Phospho (ST) 4
HDAC1 seq: 405 - 413 +Phospho (ST) 4
CAMSAP3 seq: 812 - 823 +Phospho (ST) 4
PI4KB seq: 253 - 270 +Phospho (ST) 4
GTF2I seq: 681 - 702 no mod 4
TNKS1BP1 pS893 4
PAN3 seq: 349 - 358 +Phospho (ST) 4
PXN seq: 76 - 93 +Phospho (ST) 4
TP53BP1 pS1430 4
ZFC3H1 pS655 4
BAG3 seq: 366 - 388 +2 Phospho (ST) 4
EEF1D pS133 4
KIAA1522 seq: 856 - 876 +Phospho (ST) 4
FAM208B pS1025 4
CCDC88C seq: 1578 - 1598 +Phospho (ST) 4
AAK1 seq: 9 - 37 +Phospho (ST) 4
RAF1 seq: 283 - 309 +Phospho (ST) 4
KIF21A pS1239 4
CEP170B pS829 4
TOP2B pT1575 4
CASKIN2 seq: 390 - 414 +Phospho (ST) 4
PARD3 seq: 713 - 731 +Phospho (ST) 4
MAP4 pS1073 4
EIF4G3 pS495 4
CCT3 seq: 249 - 266 no mod 4
CIAPIN1 seq: 181 - 196 +Phospho (ST) 4
FKBP15 seq: 1096 - 1124 +Phospho (ST) 4
LARP1 pS766 pS774 4
CAST seq: 213 - 249 +Phospho (ST) 4
PYGL seq: 12 - 17 +Phospho (ST) 4
MAP4 seq: 937 - 946 +Phospho (ST) 4
NCOR2 pT1391 4
FAM102B seq: 282 - 294 +Phospho (ST) 4
ZMYND8 pS406 4
TNK1 seq: 502 - 524 +2 Phospho (ST) 4
TBC1D10B pS22 4
METTL3 pS43 4
KLC2 pS445 4
PAGR1 pS237 4
MAST4 pS206 4
EEF1D pS133 4
SMARCA5 seq: 98 - 119 +Gln->pyro-Glu (N-term Q); 2 Phospho (ST) 4
LRRC47 seq: 508 - 542 +Phospho (ST) 4
C7orf43 seq: 515 - 525 +Phospho (ST) 4
MYH9 seq: 1731 - 1751 no mod 4
CTTN seq: 397 - 428 +2 Phospho (ST) 4
WIZ pS1151 4
MKL2 seq: 535 - 561 +Phospho (ST) 4
SYTL2 pS535 4
MAP4 seq: 353 - 368 +Phospho (ST) 4
FAM102B seq: 191 - 205 +Phospho (ST) 4
LMNA seq: 281 - 296 no mod 4
TJP2 seq: 1155 - 1176 +Phospho (Y) 4
TJP2 seq: 1155 - 1176 +Phospho (ST) 4
MEF2D pS180 4
FAM83H pS881 4
ABCF1 pS109 4
NUMA1 pT2000 4
MAP4 pS1073 4
DIP2B seq: 98 - 113 +Phospho (ST) 4
ELF1 seq: 160 - 174 +Phospho (ST) 4
STIM1 pS512 4
NOP2 seq: 722 - 743 +Phospho (ST) 4
EIF4EBP1 seq: 64 - 99 +2 Phospho (ST) 4
HABP4 seq: 96 - 119 +Phospho (ST) 4
NUP210 pS1874 4
AHNAK seq: 5834 - 5858 +Phospho (ST) 4
ZC3H11A pS132 4
CAMSAP3 pS814 4
LAMTOR1 pS27 4
CBX8 seq: 253 - 274 +Phospho (ST) 4
NUP35 seq: 270 - 282 +Phospho (ST) 4
BAZ2A seq: 132 - 143 +Phospho (ST) 4
HMGA1 pT53 4
BAZ1A pS1413 4
FAM83H seq: 923 - 933 +Phospho (ST) 4
RPTOR pS877 4
MAP7D1 seq: 111 - 133 +Phospho (ST) 4
FAM83H pS647 4
FAM83H seq: 923 - 934 +Phospho (ST) 4
FAM102B pS350 4
DIDO1 seq: 1231 - 1274 +2 Phospho (ST) 4
BTF3 pS30 4
RBMXL1 pS208 4
HIST3H2A seq: 101 - 119 no mod 4
TBX2 seq: 379 - 395 +Phospho (ST) 4
ZFP36L1 seq: 52 - 61 +Phospho (ST) 4
MAP4 pS280 4


Phosphorylation site
P
G1- vs P
G2- vs P
G3- vs P
G1+ vs P
G2+ vs P
G3+ vs P
G1+ vs G1-
G2+ vs G2-
G3+ vs G3-
Cluster number
TNRC18 pS1857
ZMYND8 pS490
COPB2 seq: 847 - 875 +Phospho (ST)
TRAM1 pS365
MARK2 seq: 607 - 627 +Phospho (ST)
TMX1 pS247
ACTN4 seq: 217 - 233 no mod
NUMB seq: 292 - 297 +Phospho (ST)
CLIC1 seq: 120 - 131 no mod
CEP55 pS436
LARP1 pS143
TJP3 pS164
CAD pS1859
LMNA seq: 628 - 644 +Phospho (ST)
MARCKS pS159
RRBP1 seq: 1263 - 1291 +Phospho (ST)
CAMSAP3 seq: 429 - 444 +Phospho (ST)
PUM2 pS82
SUV39H1 pS391
BTF3 pS30
CTTN seq: 399 - 428 +Phospho (ST)
KIF23 pS902
SLC9A3R1 pS280
TMPO seq: 49 - 86 +Phospho (ST)
MLF2 seq: 230 - 241 +Phospho (ST)
LMNA pS392
EMSY pS209
TOM1 seq: 453 - 478 +Phospho (ST)
NOTCH2 pS2081
MARCKS pS170
BCL7C seq: 110 - 142 +Phospho (ST)
TOR1AIP1 seq: 149 - 174 +2 Phospho (ST)
YWHAB seq: 130 - 140 no mod
RBM15 seq: 763 - 783 +Phospho (ST)
LSR pS643
LRRC47 seq: 508 - 542 +Phospho (ST)
KIAA1522 seq: 969 - 984 +Phospho (ST)
AIF1L pS134
BCL2L11 seq: 85 - 91 +Phospho (ST)
HNRNPK seq: 222 - 247 no mod
EIF2AK3 pS715
AHNAK seq: 5834 - 5858 +Phospho (ST)
BAG6 seq: 1073 - 1087 +Phospho (ST)
GORASP2 seq: 421 - 452 +Phospho (ST)
YWHAQ seq: 128 - 138 no mod
LARP1 pS90
FAM83H pS1003
USP15 seq: 241 - 256 +Phospho (ST)
FAM83H pS936
CTTN seq: 397 - 428 +2 Phospho (ST)
C10orf12 seq: 288 - 297 +Phospho (ST)
LMNA seq: 29 - 41 no mod
BAG3 seq: 283 - 294 +2 Phospho (ST)
ACIN1 pS657
PPP1R37 seq: 557 - 564 +Phospho (ST)
NUFIP2 pS629
MISP pS575
SCRIB pS1348
SLC9A3R1 pS280
IRS1 pS1101
LMNA pS390
KRT80 pS45
LMNA seq: 387 - 397 +Phospho (ST)
NDRG3 pS331
TP53BP1 seq: 1459 - 1490 +Phospho (ST)
ADD3 pS693
FOXA1 pS307
PPP1R10 pS313
CTNND1 pS349
UBAP2L seq: 602 - 618 +Phospho (ST)
RBM7 seq: 134 - 143 +Phospho (ST)
SCRIB pS1348
RBMXL1 seq: 204 - 217 +Phospho (ST)
CEP170 seq: 836 - 858 +Phospho (ST)
PRRC2C pT2673
MTDH pS568
ALDOA seq: 29 - 43 +Phospho (ST)
EEF1D pS162
EEF1D pS162
FAM134C seq: 433 - 464 +Phospho (ST)
TCOF1 seq: 571 - 591 +Phospho (ST)
TRIM28 seq: 592 - 629 +Phospho (ST)
ANLN pS182
GIGYF2 seq: 17 - 35 +Phospho (ST)
ABCF1 seq: 103 - 121 +Phospho (ST)
MAPK3 pY204
RBBP6 pS1179
NIPBL seq: 290 - 308 +Phospho (ST)
AFAP1 seq: 661 - 672 +Phospho (ST)
SLC9A3R1 seq: 113 - 138 no mod
COPB2 seq: 847 - 872 +Phospho (ST)
OCIAD1 pS108
CCDC86 seq: 30 - 53 +Phospho (ST)
AHNAK pS5731
AHNAK pS5731
FXR2 pS601
ZBTB7A seq: 330 - 354 +Phospho (ST)
AKAP11 pS422 pS433
TP53BP1 pS552
USP6NL pS680
EIF4B pS406
CCNYL1 pS344
DDX21 pS89
PPM1H pS221
ATXN2 pS784
CHD1 seq: 89 - 98 +Phospho (ST)
NUMA1 seq: 1990 - 2004 +Phospho (ST)
AKAP11 seq: 419 - 438 +Phospho (ST); Phospho (Y)
DVL3 seq: 106 - 143 +Phospho (ST)
MARK3 seq: 387 - 404 +Phospho (ST)
H1FX pS31
MAP7D1 pS460
TIAM1 pS231
MARCKS seq: 157 - 161 +Phospho (ST)
RPB4_HUMAN seq: 71 - 75 +Phospho (ST)
NOP2 pS786
VDAC1 pS104
LRRC16A seq: 966 - 980 +Phospho (ST)
SDE2 seq: 269 - 291 +Phospho (ST)
LARP4 pS583
KLHDC4 seq: 400 - 432 +Phospho (ST)
GAL pS116
RBM33 pS41
LDHB seq: 8 - 23 no mod
C12orf45 pS178
MTDH pS568
ANKRD13D pS465 pT469
CLASP1 pS600
KLC1 seq: 521 - 531 +Phospho (ST)
DBN1 seq: 589 - 615 +Phospho (ST)
ATXN2L pS111
MTMR12 pS564
CTTN seq: 415 - 428 +Phospho (ST)
MARCKSL1 pS93
NCOA3 pS857
ANKRD17 seq: 4 - 44 +Phospho (ST)
NAA30 pS89
PKN2 seq: 524 - 550 +Phospho (ST)
BICD2 pS582
GAPVD1 pS902
KIAA1522 pS862
ERBB3 pS982
SCRIB pS1486
CTNND1 pS349
CSRP1 pS192
KRT8 seq: 134 - 148 +2 Oxidation (M)
JPH1 pS185
ILF3 seq: 475 - 523 +Phospho (ST)
FAM91A1 seq: 340 - 376 +Phospho (ST)
UTP3 pS37
NOP56 seq: 561 - 578 +Phospho (ST)
ARFGAP2 pS146
CCDC86 seq: 30 - 53 +Phospho (ST)
KRT8 seq: 274 - 295 no mod
URI1 seq: 370 - 386 +Phospho (ST)
KRT18 seq: 383 - 407 +Oxidation (M)
ABCF1 pS140
PDAP1 seq: 76 - 88 no mod
FAM102B seq: 226 - 235 +Phospho (ST)
RPL19 seq: 22 - 38 no mod
ABCF1 pS109
NUMB seq: 4 - 9 +Phospho (ST)
EIF3G seq: 33 - 65 +Phospho (ST)
MAPKAP1 seq: 508 - 515 +Phospho (ST)
IGF2R pS2409
ROCK2 seq: 977 - 995 no mod
KRT19 seq: 254 - 264 +Oxidation (M)
CTNND1 seq: 847 - 858 no mod
SSMM1_HUMAN seq: 240 - 244 +Phospho (ST)
MARCKSL1 seq: 91 - 95 +Phospho (ST)
AHNAK pS5110
RGL4 seq: 418 - 423 +Phospho (ST)
TOP2A seq: 1239 - 1259 +Phospho (ST)
FASN pS207
HSPD1 seq: 97 - 121 no mod
KPNA2 seq: 52 - 68 +Phospho (ST)
MYH9 pS1943
RSL1D1 pS361
HSPD1 seq: 97 - 121 no mod
FAM102B pS228
PPM1H seq: 122 - 134 +Phospho (ST)
KIAA1522 pS862
HSP90B1 seq: 435 - 448 no mod
UBQLN4 seq: 88 - 136 +Phospho (ST)
FLNB pS2478
MYBBP1A seq: 1156 - 1167 +Phospho (ST)
CTTN seq: 399 - 428 +2 Phospho (ST)
BAIAP2 pT360
KPNA2 seq: 52 - 68 no mod
SLTM seq: 549 - 564 +Phospho (ST)
CAMSAP3 pS368
PPM1H seq: 122 - 134 +Phospho (ST)
CLCC1 pS438
CDCA5 pS21
AKT1S1 seq: 202 - 223 +Phospho (ST)
LAD1 seq: 266 - 282 +Phospho (ST)
RAD23B pS160
KRT8 seq: 19 - 32 +2 Phospho (ST)
EIF2A seq: 503 - 520 +Phospho (ST)
TMPO pS424
EPB41L4A seq: 309 - 316 +Phospho (ST)
MARCKSL1 pS104
RPS3 seq: 202 - 227 +Phospho (ST)
MAPK8IP3 seq: 362 - 373 +Phospho (ST)
LARP1 pS90
GATA3 pS162

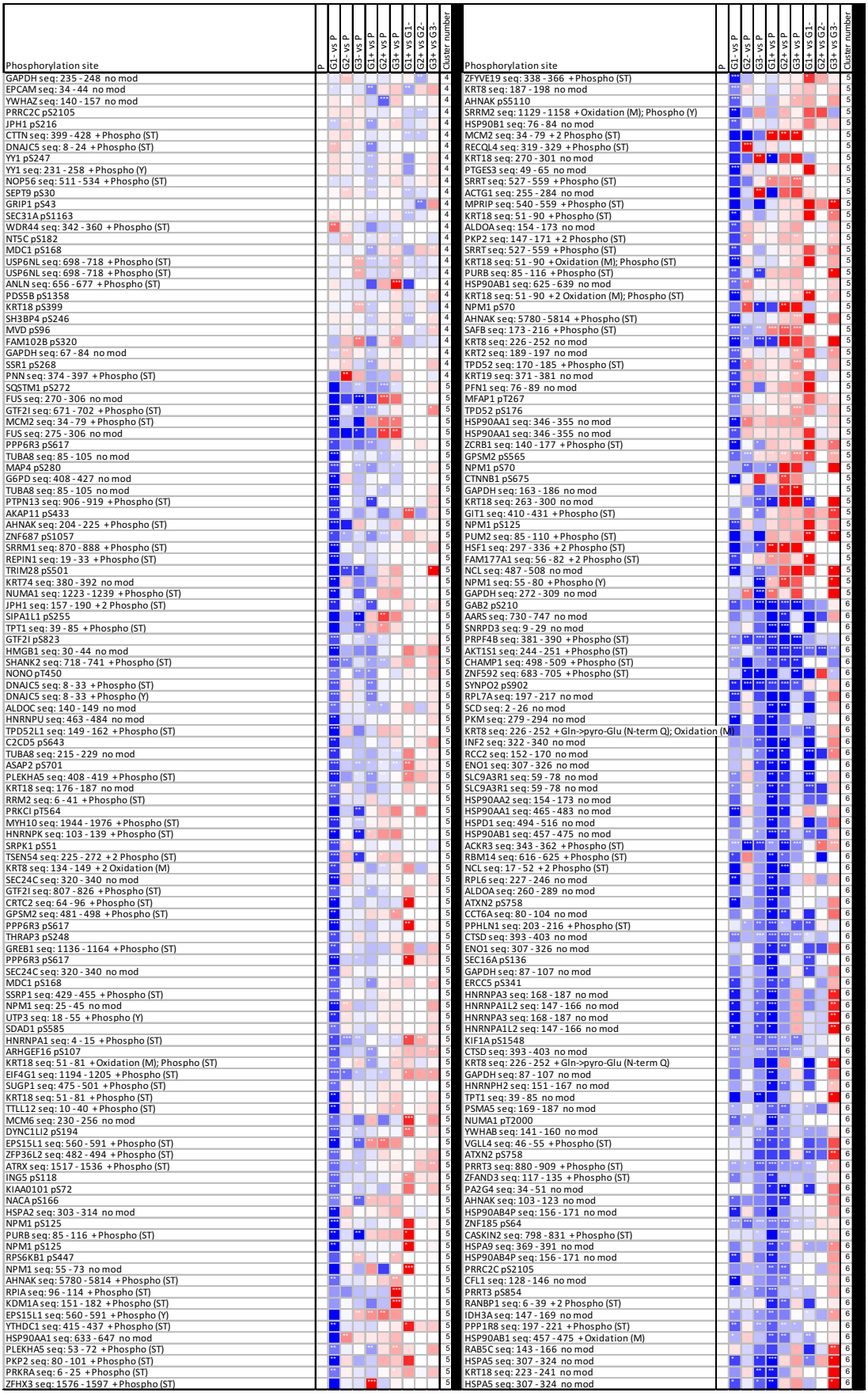
Phosphorylation site
P
G1- vs P
G2- vs P
G3- vs P
G1+ vs P
G2+ vs P
G3+ vs P
G1+ vs G1-
G2+ vs G2-
G3+ vs G3-
Cluster number
GAPDH seq: 235 - 248 no mod
EPCAM seq: 34 - 44 no mod
YWHAZ seq: 140 - 157 no mod
PRRC2C pS2105
JPH1 pS216
CTTN seq: 399 - 428 +Phospho (ST)
DNAJC5 seq: 8 - 24 +Phospho (ST)
YY1 pS247
YY1 seq: 231 - 258 +Phospho (Y)
NOP56 seq: 511 - 534 +Phospho (ST)
SEPT9 pS30
GRIP1 pS43
SEC31A pS1163
WDR44 seq: 342 - 360 +Phospho (ST)
NT5C pS182
MDC1 pS168
USP6NL seq: 698 - 718 +Phospho (ST)
USP6NL seq: 698 - 718 +Phospho (ST)
ANLN seq: 656 - 677 +Phospho (ST)
PDS5B pS1358
KRT18 pS399
SH3BP4 pS246
MVD pS96
FAM102B pS320
GAPDH seq: 67 - 84 no mod
SSR1 pS268
PNN seq: 374 - 397 +Phospho (ST)
SQSTM1 pS272
FUS seq: 270 - 306 no mod
GTF2I seq: 671 - 702 +Phospho (ST)
MCM2 seq: 34 - 79 +Phospho (ST)
FUS seq: 275 - 306 no mod
PPP6R3 pS617
TUBA8 seq: 85 - 105 no mod
MAP4 pS280
G6PD seq: 408 - 427 no mod
TUBA8 seq: 85 - 105 no mod
PTPN13 seq: 906 - 919 +Phospho (ST)
AKAP11 pS433
AHNAK seq: 204 - 225 +Phospho (ST)
ZNF687 pS1057
SRRM1 seq: 870 - 888 +Phospho (ST)
REPIN1 seq: 19 - 33 +Phospho (ST)
TRIM28 pS501
KRT74 seq: 380 - 392 no mod
NUMA1 seq: 1223 - 1239 +Phospho (ST)
JPH1 seq: 157 - 190 +2 Phospho (ST)
SIPA1L1 pS255
TPT1 seq: 39 - 85 +Phospho (ST)
GTF2I pS823
HMGB1 seq: 30 - 44 no mod
SHANK2 seq: 718 - 741 +Phospho (ST)
NONO pT450
DNAJC5 seq: 8 - 33 +Phospho (ST)
DNAJC5 seq: 8 - 33 +Phospho (Y)
ALDOC seq: 140 - 149 no mod
HNRNPU seq: 463 - 484 no mod
TPD52L1 seq: 149 - 162 +Phospho (ST)
C2CD5 pS643
TUBA8 seq: 215 - 229 no mod
ASAP2 pS701
PLEKHA5 seq: 408 - 419 +Phospho (ST)
KRT18 seq: 176 - 187 no mod
RRM2 seq: 6 - 41 +Phospho (ST)
PRKCI pT564
MYH10 seq: 1944 - 1976 +Phospho (ST)
HNRNPK seq: 103 - 139 +Phospho (ST)
SRPK1 pS51
TSEN54 seq: 225 - 272 +2 Phospho (ST)
KRT8 seq: 134 - 149 +2 Oxidation (M)
SEC24C seq: 320 - 340 no mod
GTF2I seq: 807 - 826 +Phospho (ST)
CRTC2 seq: 64 - 96 +Phospho (ST)
GPSM2 seq: 481 - 498 +Phospho (ST)
PPP6R3 pS617
THRAP3 pS248
GREB1 seq: 1136 - 1164 +Phospho (ST)
PPP6R3 pS617
SEC24C seq: 320 - 340 no mod
MDC1 pS168
SSRP1 seq: 429 - 455 +Phospho (ST)
NPM1 seq: 25 - 45 no mod
UTP3 seq: 18 - 55 +Phospho (Y)
SDAD1 pS585
HNRNPA1 seq: 4 - 15 +Phospho (ST)
ARHGEF16 pS107
KRT18 seq: 51 - 81 +Oxidation (M); Phospho (ST)
EIF4G1 seq: 1194 - 1205 +Phospho (ST)
SUGP1 seq: 475 - 501 +Phospho (ST)
KRT18 seq: 51 - 81 +Phospho (ST)
TTLL12 seq: 10 - 40 +Phospho (ST)
MCM6 seq: 230 - 256 no mod
DYNC1LI2 pS194
EPS15L1 seq: 560 - 591 +Phospho (ST)
ZFP36L2 seq: 482 - 494 +Phospho (ST)
ATRX seq: 1517 - 1536 +Phospho (ST)
ING5 pS118
KIAA0101 pS72
NACA pS166
HSPA2 seq: 303 - 314 no mod
NPM1 pS125
PURB seq: 85 - 116 +Phospho (ST)
NPM1 pS125
RPS6KB1 pS447
NPM1 seq: 55 - 73 no mod
AHNAK seq: 5780 - 5814 +Phospho (ST)
RPIA seq: 96 - 114 +Phospho (ST)
KDM1A seq: 151 - 182 +Phospho (ST)
EPS15L1 seq: 560 - 591 +Phospho (Y)
YTHDC1 seq: 415 - 437 +Phospho (ST)
HSP90AA1 seq: 633 - 647 no mod
PLEKHA5 seq: 53 - 72 +Phospho (ST)
PKP2 seq: 80 - 101 +Phospho (ST)
PRKRA seq: 6 - 25 +Phospho (ST)
ZFHX3 seq: 1576 - 1597 +Phospho (ST)
Phosphorylation site
P
G1- vs P
G2- vs P
G3- vs P
G1+ vs P
G2+ vs P
G3+ vs P
G1+ vs G1-
G2+ vs G2-
G3+ vs G3-
Cluster number
ZFYVE19 seq: 338 - 366 +Phospho (ST)
KRT8 seq: 187 - 198 no mod
AHNAK pS5110
SRRM2 seq: 1129 - 1158 +Oxidation (M); Phospho (Y)
HSP90B1 seq: 76 - 84 no mod
MCM2 seq: 34 - 79 +2 Phospho (ST)
RECQL4 seq: 319 - 329 +Phospho (ST)
KRT18 seq: 270 - 301 no mod
PTGES3 seq: 49 - 65 no mod
SRRT seq: 527 - 559 +Phospho (ST)
ACTG1 seq: 255 - 284 no mod
MPRIP seq: 540 - 559 +Phospho (ST)
KRT18 seq: 51 - 90 +Phospho (ST)
ALDOA seq: 154 - 173 no mod
PKP2 seq: 147 - 171 +2 Phospho (ST)
SRRT seq: 527 - 559 +Phospho (ST)
KRT18 seq: 51 - 90 +Oxidation (M); Phospho (ST)
PURB seq: 85 - 116 +Phospho (ST)
HSP90AB1 seq: 625 - 639 no mod
KRT18 seq: 51 - 90 +2 Oxidation (M); Phospho (ST)
NPM1 pS70
AHNAK seq: 5780 - 5814 +Phospho (ST)
SAFB seq: 173 - 216 +Phospho (ST)
KRT8 seq: 226 - 252 no mod
KRT2 seq: 189 - 197 no mod
TPD52 seq: 170 - 185 +Phospho (ST)
KRT19 seq: 371 - 381 no mod
PFN1 seq: 76 - 89 no mod
MFAP1 pT267
TPD52 pS176
HSP90AA1 seq: 346 - 355 no mod
HSP90AA1 seq: 346 - 355 no mod
ZCRB1 seq: 140 - 177 +Phospho (ST)
GPSM2 pS565
NPM1 pS70
CTNNB1 pS675
GAPDH seq: 163 - 186 no mod
KRT18 seq: 263 - 300 no mod
GIT1 seq: 410 - 431 +Phospho (ST)
NPM1 pS125
PUM2 seq: 85 - 110 +Phospho (ST)
HSF1 seq: 297 - 336 +2 Phospho (ST)
FAM177A1 seq: 56 - 82 +2 Phospho (ST)
NCL seq: 487 - 508 no mod
NPM1 seq: 55 - 80 +Phospho (Y)
GAPDH seq: 272 - 309 no mod
GAB2 pS210
AARS seq: 730 - 747 no mod
SNRPD3 seq: 9 - 29 no mod
PRPF4B seq: 381 - 390 +Phospho (ST)
AKT1S1 seq: 244 - 251 +Phospho (ST)
CHAMP1 seq: 498 - 509 +Phospho (ST)
ZNF592 seq: 683 - 705 +Phospho (ST)
SYNPO2 pS902
RPL7A seq: 197 - 217 no mod
SCD seq: 2 - 26 no mod
PKM seq: 279 - 294 no mod
KRT8 seq: 226 - 252 +Gln->pyro-Glu (N-term Q); Oxidation (M)
INF2 seq: 322 - 340 no mod
RCC2 seq: 152 - 170 no mod
ENO1 seq: 307 - 326 no mod
SLC9A3R1 seq: 59 - 78 no mod
SLC9A3R1 seq: 59 - 78 no mod
HSP90AA2 seq: 154 - 173 no mod
HSP90AA1 seq: 465 - 483 no mod
HSPD1 seq: 494 - 516 no mod
HSP90AB1 seq: 457 - 475 no mod
ACKR3 seq: 343 - 362 +Phospho (ST)
RBM14 seq: 616 - 625 +Phospho (ST)
NCL seq: 17 - 52 +2 Phospho (ST)
RPL6 seq: 227 - 246 no mod
ALDOA seq: 260 - 289 no mod
ATXN2 pS758
CCT6A seq: 80 - 104 no mod
PPHLN1 seq: 203 - 216 +Phospho (ST)
CTSD seq: 393 - 403 no mod
ENO1 seq: 307 - 326 no mod
SEC16A pS136
GAPDH seq: 87 - 107 no mod
ERCC5 pS341
HNRNPA3 seq: 168 - 187 no mod
HNRNPA1L2 seq: 147 - 166 no mod
HNRNPA3 seq: 168 - 187 no mod
HNRNPA1L2 seq: 147 - 166 no mod
KIF1A pS1548
CTSD seq: 393 - 403 no mod
KRT8 seq: 226 - 252 +Gln->pyro-Glu (N-term Q)
GAPDH seq: 87 - 107 no mod
HNRNPH2 seq: 151 - 167 no mod
TPT1 seq: 39 - 85 no mod
PSMA5 seq: 169 - 187 no mod
NUMA1 pT2000
YWHAB seq: 141 - 160 no mod
VGLL4 seq: 46 - 55 +Phospho (ST)
ATXN2 pS758
PRRT3 seq: 880 - 909 +Phospho (ST)
ZFAND3 seq: 117 - 135 +Phospho (ST)
PA2G4 seq: 34 - 51 no mod
AHNAK seq: 103 - 123 no mod
HSP90AB4P seq: 156 - 171 no mod
ZNF185 pS64
CASKIN2 seq: 798 - 831 +Phospho (ST)
HSPA9 seq: 369 - 391 no mod
HSP90AB4P seq: 156 - 171 no mod
PRRC2C pS2105
CFL1 seq: 128 - 146 no mod
PRRT3 pS854
RANBP1 seq: 6 - 39 +2 Phospho (ST)
IDH3A seq: 147 - 169 no mod
PPP1R8 seq: 197 - 221 +Phospho (ST)
HSP90AB1 seq: 457 - 475 +Oxidation (M)
RAB5C seq: 143 - 166 no mod
HSPA5 seq: 307 - 324 no mod
KRT18 seq: 223 - 241 no mod
HSPA5 seq: 307 - 324 no mod

Appendix 5

Proteins contained in the molecular functions antioxidant activity (GO:0016209) and copper ion binding (GO:0005507) (Chapter 4).

GO:0016209; F:antioxidant activity	GO:0005507; F:copper ion binding
ALB seq: 500 - 508 no mod	ALB seq: 500 - 508 no mod
ALB seq: 438 - 452 no mod	ALB seq: 438 - 452 no mod
ALB seq: 258 - 264 no mod	ALB seq: 258 - 264 no mod
ALB seq: 287 - 298 no mod	ALB seq: 287 - 298 no mod
ALB seq: 162 - 168 no mod	ALB seq: 162 - 168 no mod
PRDX2 seq: 17 - 26 no mod	TP53 seq: 307 - 319 + Phospho (ST)
PRDX6 pT44	SOD1 seq: 11 - 24 no mod
PRDX6 seq: 42 - 53 no mod	SOD1 seq: 81 - 116 no mod
PRDX3 seq: 84 - 91 no mod	S100A13 seq: 30 - 39 + Phospho (ST)
PRDX2 seq: 128 - 135 no mod	ATOX1 seq: 2 - 21 no mod
PRDX2 seq: 92 - 109 no mod	
PRDX2 seq: 67 - 91 no mod	
PRDX2 seq: 67 - 91 no mod	
VIMP pS140	
PRDX2 seq: 68 - 91 no mod	
PRDX2 seq: 111 - 119 no mod	
PRDX6 seq: 156 - 162 no mod	
PRDX2 seq: 140 - 150 no mod	
PRDX2 seq: 151 - 157 no mod	

Appendix 6

Quality control for the O_2 and pH calibration emission for all the Seahorse experiments presented in Chapter 5.

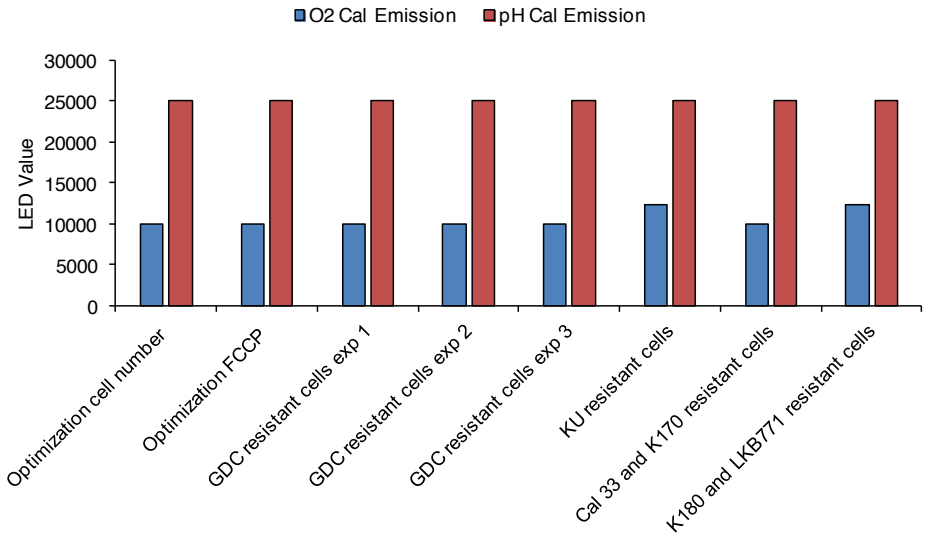

Appendix 7

External standard calibration curve of lactic acid for the measurement of lactic acid in the media of parental and PI3Ki-resistant cells grown in the presence or in the absence of PI3Ki (Chapter 5).

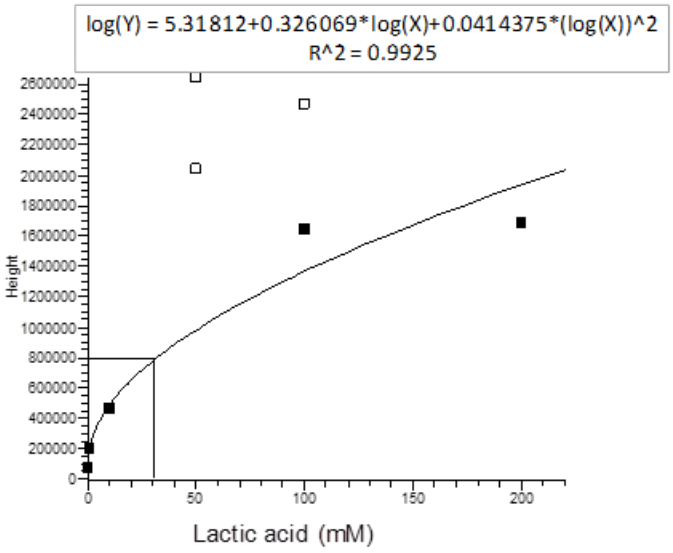

Appendix 8

Images of ROS measured by fluorescence emission of DCFH-DA on parental and resistant cells grown in culture media in the presence or in the absence of PI3Ki (Chapter 5).

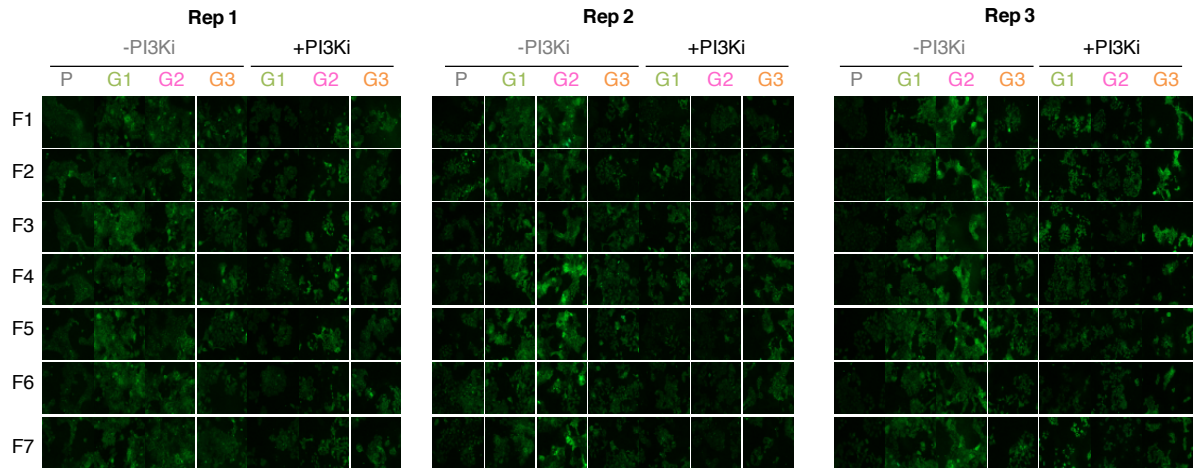

Appendix 8. Seven fields images acquired in three replicates of ROS values of parental and resistant cells grown in culture media in the presence or in the absence of PI3Ki for 7 days.

Appendix 9

External standard calibration curve of lactic acid for the measurement of lactic acid in the media upon treatment with 10 nM chetomin of parental and PI3Ki-resistant cells, grown in the presence or in the absence of PI3Ki (Chapter 5).

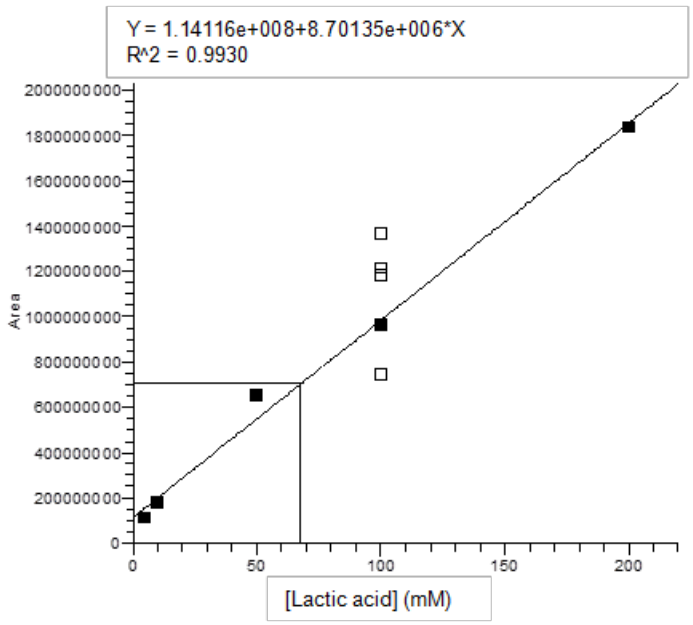

Appendix 10

External standard calibration curve of lactic acid for the measurement of lactic acid in the media upon treatment with 200 µM NAC of parental and PI3Ki-resistant cells, grown in the presence or in the absence of PI3Ki (Chapter 5).

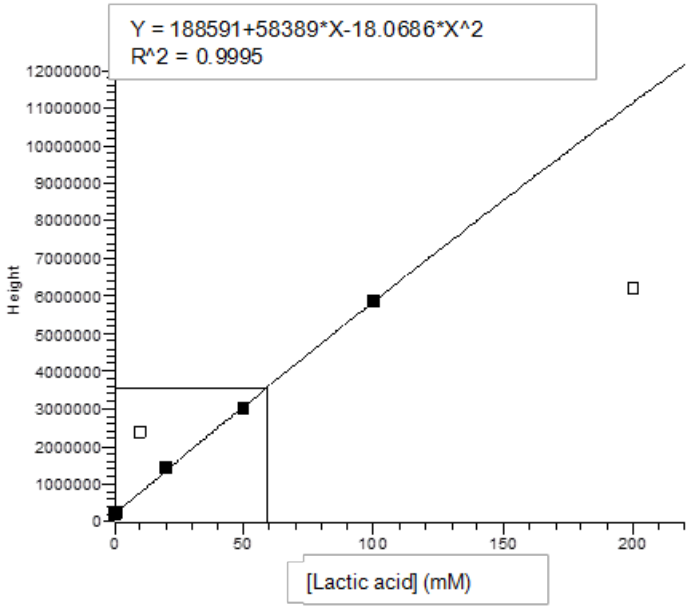

Appendix 11

Quality control of phosphoproteomics MS data of G2 resistant cells treated with control DMSO, PI3Ki, AKTi or mTORC1/2 inhibitor (Chapter 5).

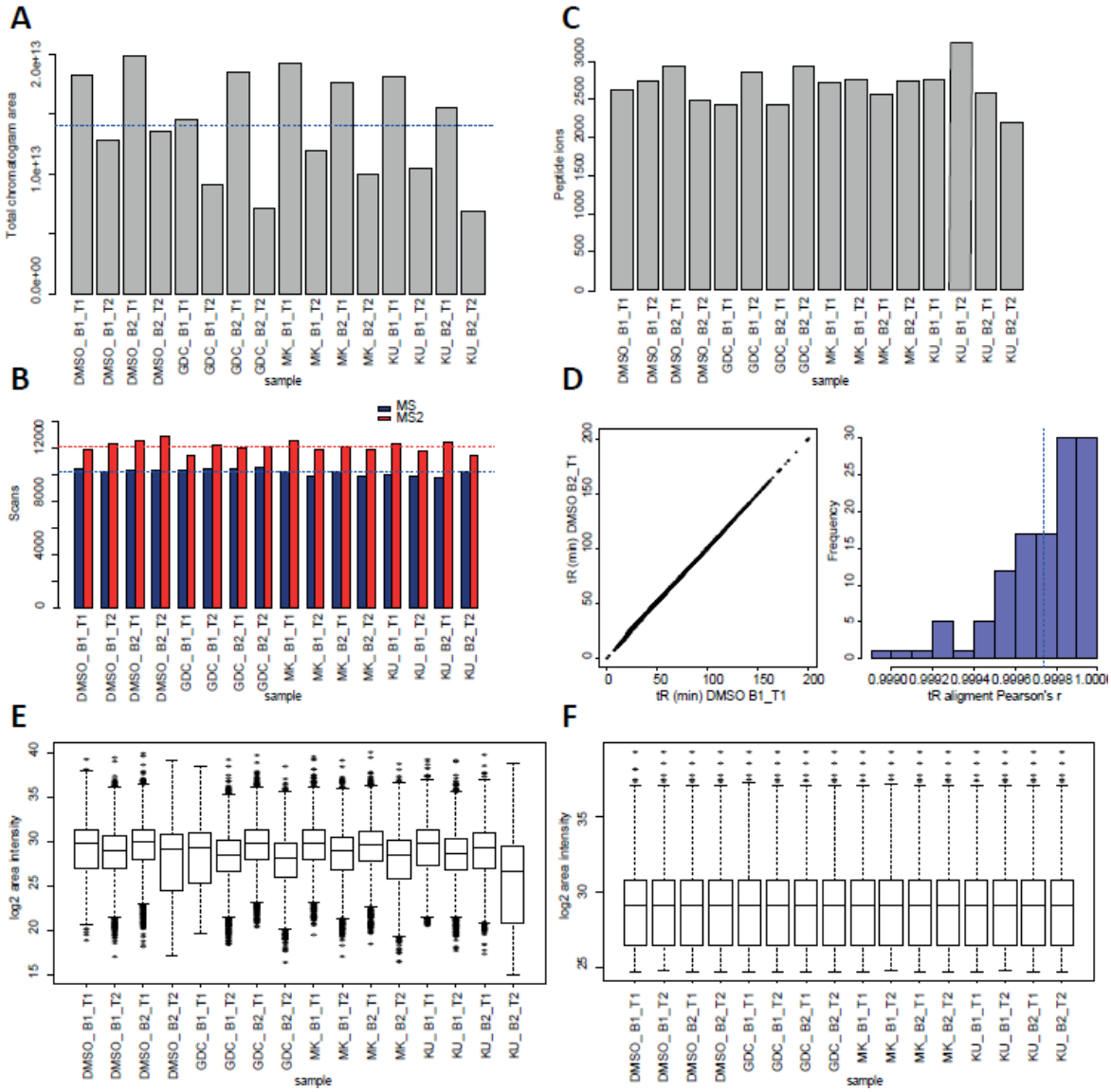

Appendix 11. (**A**) Quantification of total area under the chromatographic peaks contained in 16 phosphoproteomics MS runs. (**B**) Number of MS and MS2 scans quantified by RawMeat. (**C**) Number of identified peptide ions (FDR<0.05) that generate the database created from the 16 MS runs. (**D**) Representative alignment between retention times of two experimental samples (left panel) and histogram distribution of the correlation between the alignment of retention times of all experimental samples (right panel). (**E**) Box plots demonstrating the distribution of log_2-transformed phosphopeptide peak intensities pre-normalisation. (**F**) log_2 distribution of phosphopeptides peak intensities post-quantile normalisation.

Appendix 12

Images of ROS measured by fluorescence emission of DCFH-DA on pairs of parental and PI3K/mTOR resistant cells derived from MCF7, KYSE180, KYSE70, LB771-HNC and CAL-33 grown in culture media in the presence or in the absence of the selection drug (Chapter 5).

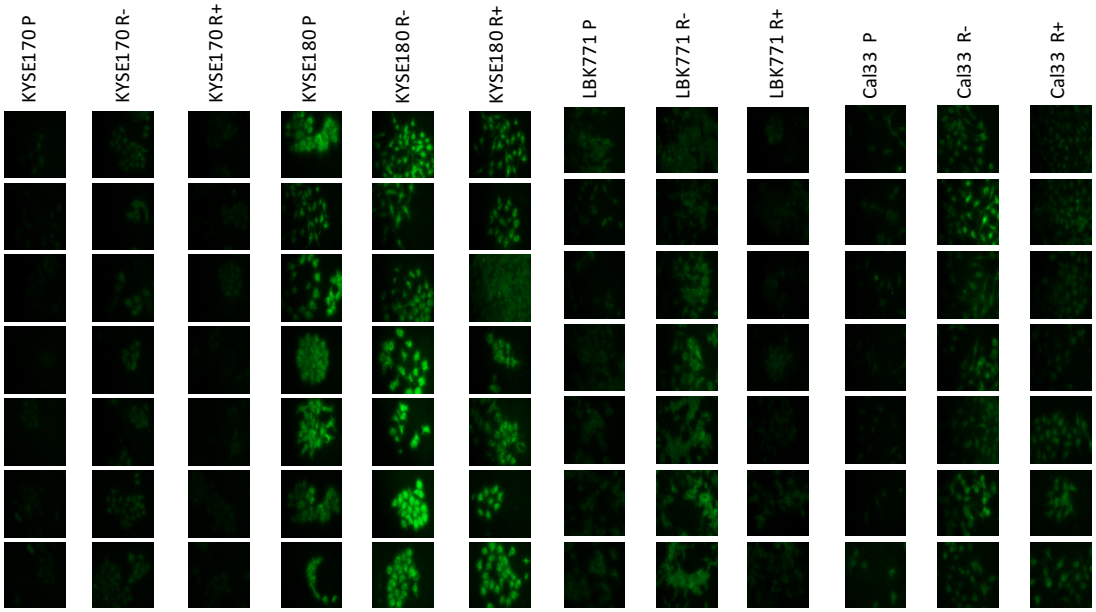

Appendix 12. Seven fields images acquired in three replicates of ROS values of parental and PI3Ki/mTOR resistant cells grown in culture media in the presence or in the absence of the drug for selection for 7 days.

Appendix 13

Electropherogram of the purified sheared DNA used in whole-exome sequencing experiment (Chapter 6).

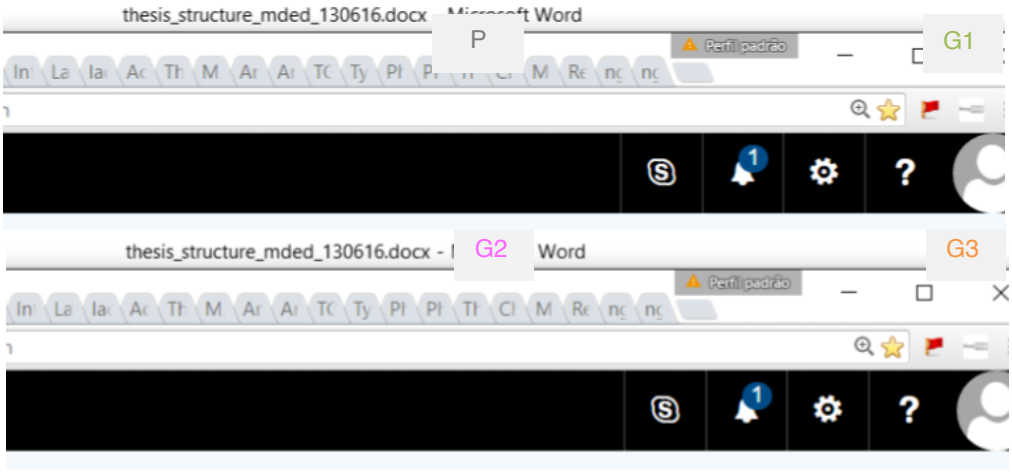

Appendix 13. Fragment distribution following PCR amplification of input DNA. The peak occurs approximately at 400 bp and this pattern of fragmentation ensures a broad range library size selection, optimal for paired-end multiplex sequencing.

Appendix 14

Summary of all point mutations identified in PI3Ki-resistant cells (Chapter 6).

G1 resistant cells

Chr	Position	Reference	Alteration	Gene name	Location on transcript structure	Amino acid position	Amino acid change	Mutation type	Sift_Score	Sift_Prediction	Poly_Score	Poly_Prediction
1	113237484	G	A	MOV10	coding	529	G>D	nonsyn	0	DAMAGING	1	PROBABLY DAMAGING
1	152328809	C	G	FLG2	coding	485	G>R	nonsyn	0.07	TOLERATED	0	UNKNOWN
1	153909116	C	A	DENND4B	coding	792	A>S	*nonsyn	0.23	TOLERATED	0	BENIGN
1	185931672	G	T	HMCN1	coding	617	M>I	nonsyn	0.18	TOLERATED	0	BENIGN
1	242511431	T	A	PLD5	coding	101	E>D	nonsyn	0.41	TOLERATED	0.002	BENIGN
10	15008531	G	C	MEIG1	coding	22	E>Q	nonsyn	0.01	DAMAGING	0.404	POSSIBLY DAMAGING
10	25273776	A	T	ENKUR	coding	218	I>K	nonsyn	0.4	TOLERATED	0.862	PROBABLY DAMAGING
11	6898572	G	A	OR10A4	coding	232	A>T	nonsyn	0.28	TOLERATED	0.062	BENIGN
12	20787953	C	T	PDE3A	coding	655	A>V	nonsyn	0.34	TOLERATED	0	BENIGN
14	105517794	T	G	GPR132	coding	227	K>T	nonsyn	0.47	TOLERATED	0.703	POSSIBLY DAMAGING
14	32561316	G	T	ARHGAP5	coding	481	E>*	nonsyn:stop-gain	na	na	na	na
14	59961938	C	A	JKAMP	coding	166	P>T	nonsyn	0	DAMAGING	0.999	PROBABLY DAMAGING
14	74388787	G	A	ZNF410	coding	400	S>N	nonsyn	0.01	DAMAGING	0.07	BENIGN
14	94528701	C	A	DDX24	coding	329	A>S	nonsyn	0.76	TOLERATED	0.004	BENIGN
15	50303116	T	G	ATP8B4	intronic (splice_site)	na			na	na	na	na
16	68156591	T	C	NFATC3	coding	269	S>P	nonsyn	0	DAMAGING	0.996	PROBABLY DAMAGING
17	37884010	C	T	ERBB2	coding	1161	R>*	nonsyn:stop-gain	na	na	na	na
17	7412449	C	T	POLR2A	coding	1218	R>W	nonsyn	0	DAMAGING	1	PROBABLY DAMAGING
19	56155962	C	A	ZNF581	coding	9	P>T	nonsyn	0.38	TOLERATED	0.265	POSSIBLY DAMAGING
19	7975396	TG	T	MAP2K7	coding	211	V>V	frameshift:stop-gain	na	na	na	na
2	168114614	G	A	XIRP2	coding	553	E>K	nonsyn	1	TOLERATED	0.003	BENIGN
2	179623854	G	T	TTN	coding	3387	S>Y	nonsyn	0.01	DAMAGING	0.998	PROBABLY DAMAGING
2	219204617	C	A	PNKD	coding	116	F>L	nonsyn	0.51	TOLERATED	0	BENIGN
20	29628233	A	G	FRG1B	coding	84	M>V	*nonsyn	0.64	TOLERATED	0.223	POSSIBLY DAMAGING
22	21991190	C	A	CCDC116	coding	558	P>H	nonsyn	0.08	TOLERATED	0.553	POSSIBLY DAMAGING
22	32215016	G	C	DEPDC5	coding	559	E>Q	nonsyn	0.44	TOLERATED	0.953	PROBABLY DAMAGING
3	118621782	G	A	IGSF11	coding	294	S>F	nonsyn	0.05	DAMAGING	0.996	PROBABLY DAMAGING
3	180327887	T	A	TTC14	coding	624	S>T	nonsyn	0.01	DAMAGING	0.993	PROBABLY DAMAGING
3	7188352	G	T	GRM7	coding	245	A>S	nonsyn	0.77	TOLERATED	0.136	BENIGN
4	103682008	C	A	MANBA	coding	15	G>V	nonsyn	0.07	TOLERATED	0	UNKNOWN
4	20736354	A	T	KCNIP4	coding	145	F>Y	nonsyn	0	DAMAGING	0.957	PROBABLY DAMAGING
4	56865526	A	G	CEP135	coding	690	K>E	nonsyn	0.98	TOLERATED	0.92	PROBABLY DAMAGING
4	6052337	G	A	JAKMIP1	coding	626	L>F	nonsyn	0.04	DAMAGING	0.889	PROBABLY DAMAGING
4	995878	G	T	IDUA	coding	301	D>Y	nonsyn	0.1	TOLERATED	1	PROBABLY DAMAGING
5	178392214	A	G	ZNF454	coding	270	K>R	nonsyn	0.07	TOLERATED	0.63	POSSIBLY DAMAGING
5	78602211	C	T	JMY	coding	632	A>V	nonsyn	0.24	TOLERATED	0.953	PROBABLY DAMAGING
7	47945538	A	T	PKD1L1	coding	475	F>Y	nonsyn	0.09	TOLERATED	0.203	POSSIBLY DAMAGING
8	109796491	G	C	TMEM74	coding	279	N>K	nonsyn	0.01	DAMAGING	0.832	POSSIBLY DAMAGING
8	110497292	T	A	PKHD1L1	coding	3199	I>K	nonsyn	0	DAMAGING	0.979	PROBABLY DAMAGING
8	22273343	AG	A	SLC39A14	coding	271	E>E	frameshift:stop-gain	na	na	na	na
8	65493351	G	A	BHLHE22	coding	2	E>K	nonsyn	0.01	DAMAGING	0.953	PROBABLY DAMAGING
8	94767182	TG	T	TMEM67	coding	14	W>C	frameshift:stop-gain	na	na	na	na
8	94767184	G	T	TMEM67	coding	14	W>C	nonsyn	0.08	TOLERATED	0.33	POSSIBLY DAMAGING
9	123591456	C	T	PSMD5	coding	198	E>K	nonsyn	0.4	TOLERATED	0.071	BENIGN
9	12702410	TACAA	T	TYRP1	coding	351	STN>STV	frameshift:stop-gain	na	na	na	na
9	13188797	C	A	MPDZ	coding	784	A>S	nonsyn	0.19	TOLERATED	0.994	PROBABLY DAMAGING
9	139735084	C	G	RABL6	coding	409	C>W	nonsyn	0	DAMAGING	0	UNKNOWN
9	8499826	G	T	PTPRD	coding	715	P>T	nonsyn	0.07	TOLERATED	1	PROBABLY DAMAGING
X	122551485	C	T	GRIA3	coding	578	P>L	nonsyn	0	DAMAGING	0.955	PROBABLY DAMAGING
X	21871561	C	A	MBTPS2	coding	204	L>M	nonsyn	0.23	TOLERATED	0.999	PROBABLY DAMAGING

G2 resistant cells

Chr	Position	Reference	Alteration	Gene name	Location on transcript structure	Amino acid position	Amino acid change	Mutation type	Sift_Score	Sift_Prediction	Poly_Score	Poly_Prediction
1	114340234	G	T	RSBN1	coding	376	Y>*	nonsyn:stop-gain	na	na	na	na
1	114340235	T	G	RSBN1	coding	376	Y>S	nonsyn	0.04	DAMAGING	0.978	PROBABLY DAMAGING
1	16891340	T	A	NBPF1	coding	1046	R>S	nonsyn	na	na	na	na
1	171121155	G	T	FMO6P	coding	312	V>L	nonsyn	0.5	TOLERATED	0.002	BENIGN
1	19513935	C	A	UBR4	coding	498	K>N	nonsyn	0.25	TOLERATED	0.021	BENIGN
10	25273776	A	T	ENKUR	coding	218	I>K	nonsyn	0.4	TOLERATED	0.862	PROBABLY DAMAGING
11	34156760	G	T	NAT10	coding	650	M>I	nonsyn	0.06	TOLERATED	0.003	BENIGN
11	4903392	G	A	OR51T1	coding	115	W>*	nonsyn:stop-gain	na	na	na	na
12	108686583	G	A	CMKLR1	coding	53	L>F	nonsyn	0.1	TOLERATED	0.983	PROBABLY DAMAGING
12	130855792	A	G	PIWIL1	coding	798	Y>C	nonsyn	0.01	DAMAGING	0.977	PROBABLY DAMAGING
12	20787953	C	T	PDE3A	coding	655	A>V	nonsyn	0.34	TOLERATED	0	BENIGN
12	8281876	T	G	CLEC4A	coding	72	Y>*	nonsyn:stop-gain	na	na	na	na
14	105417602	G	A	AHNAK2	coding	1396	L>F	nonsyn	0.23	TOLERATED	0.99	PROBABLY DAMAGING
14	105517794	T	G	GPR132	coding	227	K>T	nonsyn	0.47	TOLERATED	0.703	POSSIBLY DAMAGING
14	38092061	G	T	TTC6	coding	264	W>C	nonsyn	na	na	na	na
14	59961938	C	A	JKAMP	coding	166	P>T	nonsyn	0	DAMAGING	0.999	PROBABLY DAMAGING
14	74388787	G	A	ZNF410	coding	400	S>N	nonsyn	0.01	DAMAGING	0.07	BENIGN
15	101605839	C	T	LRRK1	coding	1733	P>S	nonsyn	0.07	TOLERATED	0.998	PROBABLY DAMAGING
15	51510816	T	G	CYP19A1	coding	222	D>A	nonsyn	0.12	TOLERATED	0.911	PROBABLY DAMAGING
16	31447264	G	A	ZNF843	coding	303	P>S	nonsyn	0	DAMAGING	0	UNKNOWN
16	67914641	C	G	EDC4	coding	760	A>G	nonsyn	0.34	TOLERATED	0.001	BENIGN
16	68156591	T	C	NFATC3	coding	269	S>P	nonsyn	0	DAMAGING	0.996	PROBABLY DAMAGING
16	84494366	G	A	ATP2C2	coding	843	A>T	nonsyn	0.23	TOLERATED	0	BENIGN
16	88706241	C	T	IL17C	coding	119	R>C	nonsyn	0	DAMAGING	1	PROBABLY DAMAGING
17	37884010	C	T	ERBB2	coding	1161	R>*	nonsyn:stop-gain	na	na	na	na
17	39881291	A	C	HAP1	coding	560	F>V	nonsyn	0.02	DAMAGING	0	BENIGN
17	71197935	A	C	COG1	coding	657	T>P	nonsyn	0.32	TOLERATED	0.046	BENIGN
19	19741303	T	A	GMIP	coding	839	D>V	nonsyn	0.17	TOLERATED	0.975	PROBABLY DAMAGING
19	45419479	T	C	APOC1	coding	31	S>P	nonsyn	0.02	DAMAGING	0.956	PROBABLY DAMAGING
19	7975396	TG	T	MAP2K7	coding	211	V>V	frameshift:stop-gain	na	na	na	na
2	152514561	T	C	NEB	coding	2040	Y>C	nonsyn	0.05	DAMAGING	0.999	PROBABLY DAMAGING
2	215839556	G	C	ABCA12	coding	1805	S>*	nonsyn:stop-gain	na	na	na	na
2	50758554	T	C	NRXN1	coding	760	S>G	nonsyn	0.09	TOLERATED	0.997	PROBABLY DAMAGING
2	55077223	G	T	EML6	coding	438	A>S	nonsyn	0.59	TOLERATED	0.16	BENIGN
2	62449947	C	A	B3GNT2	coding	198	L>M	nonsyn	0.03	DAMAGING	0.402	POSSIBLY DAMAGING
21	38525331	A	G	TTC3	coding	832	K>E	*nonsyn	0	DAMAGING	0.965	PROBABLY DAMAGING
22	21991190	C	A	CCDC116	coding	558	P>H	nonsyn	0.08	TOLERATED	0.553	POSSIBLY DAMAGING
3	10251344	A	G	IRAK2	coding	166	R>G	nonsyn	0.51	TOLERATED	0.047	BENIGN
3	180327887	T	A	TTC14	coding	624	S>T	nonsyn	0.01	DAMAGING	0.993	PROBABLY DAMAGING
3	62355885	G	C	FEZF2	coding	418	T>R	nonsyn	0.2	TOLERATED	0.759	POSSIBLY DAMAGING
4	103682008	C	A	MANBA	coding	15	G>V	nonsyn	0.07	TOLERATED	0	UNKNOWN
4	20736354	A	T	KCNIP4	coding	145	F>Y	nonsyn	0	DAMAGING	0.957	PROBABLY DAMAGING
4	56865526	A	G	CEP135	coding	690	K>E	nonsyn	0.98	TOLERATED	0.92	PROBABLY DAMAGING
4	6052337	G	A	JAKMIP1	coding	626	L>F	nonsyn	0.04	DAMAGING	0.889	PROBABLY DAMAGING
5	52097480	G	T	PELO	coding	322	D>Y	nonsyn	0.04	DAMAGING	0.284	POSSIBLY DAMAGING
5	78602211	C	T	JMY	coding	632	A>V	nonsyn	0.24	TOLERATED	0.953	PROBABLY DAMAGING
5	837524	C	T	ZDHHC11	coding	286	V>M	nonsyn	0.17	TOLERATED	0.84	POSSIBLY DAMAGING
6	39513406	C	A	KIF6	coding	414	V>F	nonsyn	0.4	TOLERATED	0.83	POSSIBLY DAMAGING
6	44224171	C	T	SLC35B2	coding	90	D>N	nonsyn	0.34	TOLERATED	0.095	BENIGN
8	103845356	A	G	AZIN1	coding	278	S>P	nonsyn	0.01	DAMAGING	0.992	PROBABLY DAMAGING
8	10465962	C	A	RP1L1	coding	1882	E>D	nonsyn	0.37	TOLERATED	0	UNKNOWN
8	10465990	T	C	RP1L1	coding	1873	D>G	nonsyn	0.41	TOLERATED	0	UNKNOWN
8	10466031	A	C	RP1L1	coding	1859	D>E	nonsyn	1	TOLERATED	0	UNKNOWN
8	110497292	T	A	PKHD1L1	coding	3199	I>K	nonsyn	0	DAMAGING	0.979	PROBABLY DAMAGING
8	94767182	TG	T	TMEM67	coding	14	W>C	frameshift:stop-gain	na	na	na	na
8	94767184	G	T	TMEM67	coding	14	W>C	nonsyn	0.08	TOLERATED	0.33	POSSIBLY DAMAGING
9	139735084	C	G	RABL6	coding	409	C>W	nonsyn	0	DAMAGING	0	UNKNOWN
9	6014884	C	A	RANBP6	coding	242	D>Y	nonsyn	0.01	DAMAGING	0.998	PROBABLY DAMAGING
9	8499826	G	T	PTPRD	coding	715	P>T	nonsyn	0.07	TOLERATED	1	PROBABLY DAMAGING
X	118108966	G	T	LONRF3	coding	75	D>Y	nonsyn	0.07	TOLERATED	1	PROBABLY DAMAGING
X	119388178	C	G	ZBTB33	coding	303	P>R	nonsyn	0.06	TOLERATED	0.001	BENIGN
X	131762534	C	T	HS6ST2	coding	552	R>Q	nonsyn	0.29	TOLERATED	0.966	PROBABLY DAMAGING
X	131762535	G	A	HS6ST2	coding	552	R>*	nonsyn:stop-gain	na	na	na	na
X	22132634	A	T	PHEX	coding	411	E>V	nonsyn	0	DAMAGING	0.818	POSSIBLY DAMAGING
X	92928282	T	C	NAP1L3	coding	8	M>V	nonsyn	0.49	TOLERATED	0	BENIGN

G3 resistant cells

Chr	Position	Reference	Alteration	Gene name	Location on transcript structure	Amino acid position	Amino acid change	Mutation type	Sift_Score	Sift_Prediction	Poly_Score	Poly_Prediction
1	144220807	A	C	NBPF8	coding	3576	D>A	nonsyn	0.54	TOLERATED	0.817	POSSIBLY DAMAGING
1	152083578	C	A	TCHH	coding	705	Q>H	nonsyn	0.3	TOLERATED	0	UNKNOWN
1	169541554	T	G	F5	coding	93	E>A	nonsyn	0	DAMAGING	0.7	POSSIBLY DAMAGING
1	171511168	G	T	PRRC2C	coding	1521	L>F	nonsyn	0.17	TOLERATED	0	UNKNOWN
1	89449390	T	C	RBMXL1	coding	40	I>M	nonsyn	1	TOLERATED	0	BENIGN
10	75276253	C	A	USP54	coding	1311	D>Y	nonsyn	0	DAMAGING	0.998	PROBABLY DAMAGING
12	56221541	C	A	DNAJC14	coding	301	W>L	nonsyn	0.03	DAMAGING	0.96	PROBABLY DAMAGING
14	106320630	C	A	IGHM	coding	394	A>S	nonsyn	0.2	TOLERATED	0.139	BENIGN
15	75763112	C	T	PTPN9	coding	423	R>Q	nonsyn	0.54	TOLERATED	0.004	BENIGN
16	77242422	G	A	SYCE1L	coding	81	R>K	nonsyn	0.85	TOLERATED	0.217	POSSIBLY DAMAGING
16	78064626	G	T	CLEC3A	coding	170	G>V	nonsyn	na	na	na	na
17	39240627	T	C	KRTAP4-7	coding	57	S>P	nonsyn	1	TOLERATED	0	UNKNOWN
17	62271174	G	C	TEX2	coding	641	Q>E	nonsyn	0.72	TOLERATED	0	BENIGN
18	6264019	TG	T	L3MBTL4	coding	49	S>QIK	*nonsynlframeshift:stop-gain	na	na	na	na
19	51535325	G	C	KLK12	coding	88	H>Q	nonsyn	0.39	TOLERATED	0.061	BENIGN
3	121383364	T	G	GOLGB1	coding	3258	H>P	nonsyn	0	DAMAGING	0.996	PROBABLY DAMAGING
5	74364388	G	T	ANKRD31	coding	1917	Q>K	nonsyn	0.04	DAMAGING	0.066	BENIGN
6	111912772	C	T	TRAF3IP2	coding	182	G>D	nonsyn	0.46	TOLERATED	0.013	BENIGN
6	155451057	C	T	TIAM2	coding	234	R>C	nonsyn	0.1	TOLERATED	0.004	BENIGN
6	35087005	C	A	TCP11	coding	440	D>Y	nonsyn	0.07	TOLERATED	0.988	PROBABLY DAMAGING
9	116811327	G	A	ZNF618	coding	582	G>D	nonsyn	0.05	DAMAGING	0.999	PROBABLY DAMAGING

Appendix 15

Quality control of phosphoproteomics MS data of MCF7 cells stimulated with 5 mM lactic acid, 0.97 mM HCl, 20 mM lactic acid or 9.7 mM HCl for 5, 15, 30 and 60 min (Chapter 7).

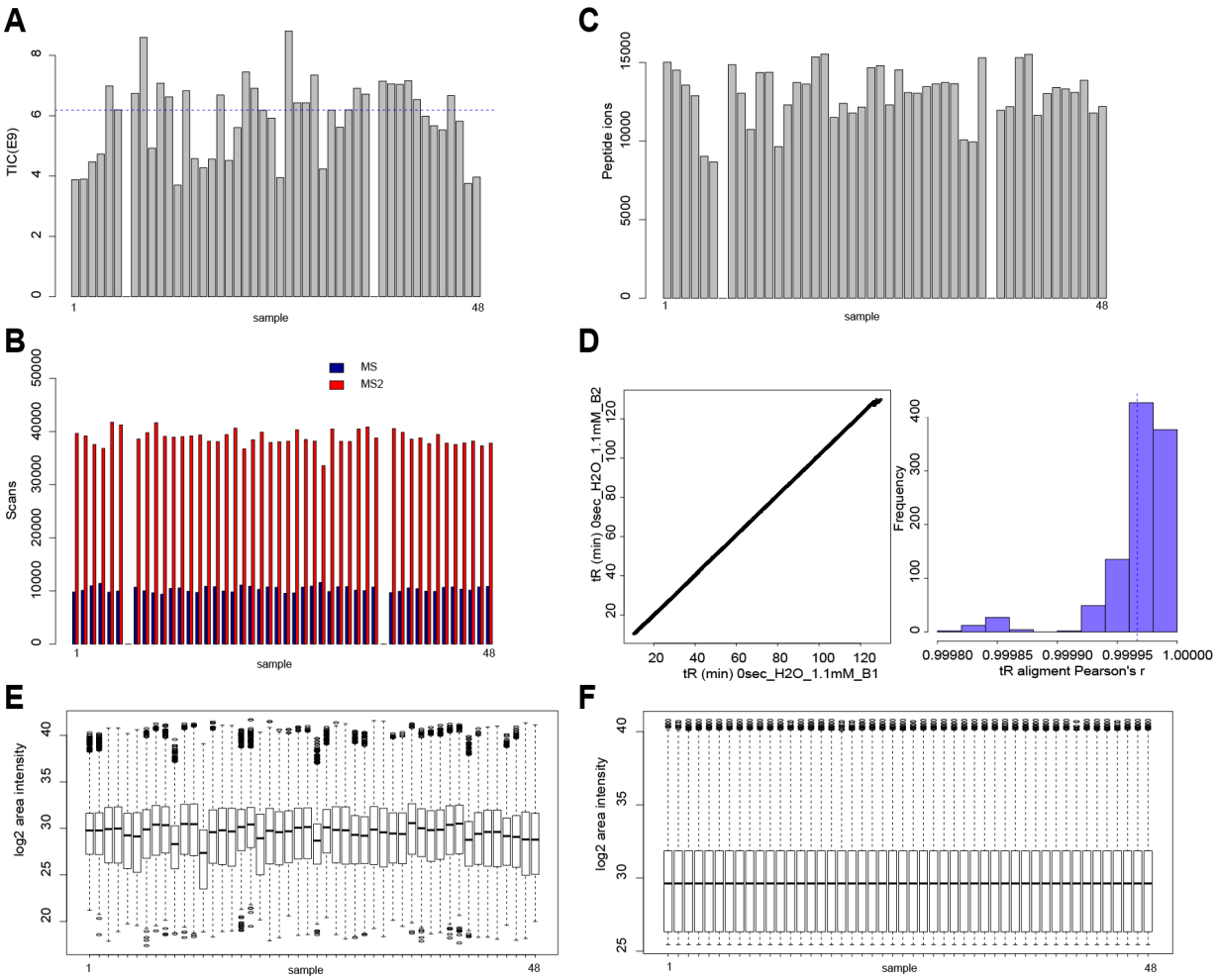

Appendix 15. (**A**) Quantification of total area under the chromatographic peaks contained in 72 phosphoproteomics MS runs. Two samples (15min_lactic_acid_5mM_B2_T2 and 30min_HCl_0.97mM_B2_T2) were run with an incorrect method, which resulted in chromatograms which intensity was below the detection threshold. (**B**) Number of MS and MS2 scans quantified by RawMeat. (**C**) Number of identified peptide ions (FDR<0.05) that generate the database created from the 72 MS runs. The two samples that did not contribute to the database population were substituted for the average of the additional replicates. (**D**) Representative alignment between retention times of two experimental samples (left panel) and histogram distribution of the correlation between the alignment of retention times of all experimental samples (right panel). (**E**) Box plots demonstrating the distribution of log_2-transformed phosphopeptide peak intensities pre-normalisation. (**F**) log_2 distribution of phosphopeptides peak intensities post-quantile normalisation.

Appendix 16

Summary of modulated phosphopeptides associated to structural constituents of cytoskeleton, structural molecule activity, Arf6 trafficking events, regulation of Rho GTPase activity or RAC1 signalling pathway (Chapter 7).

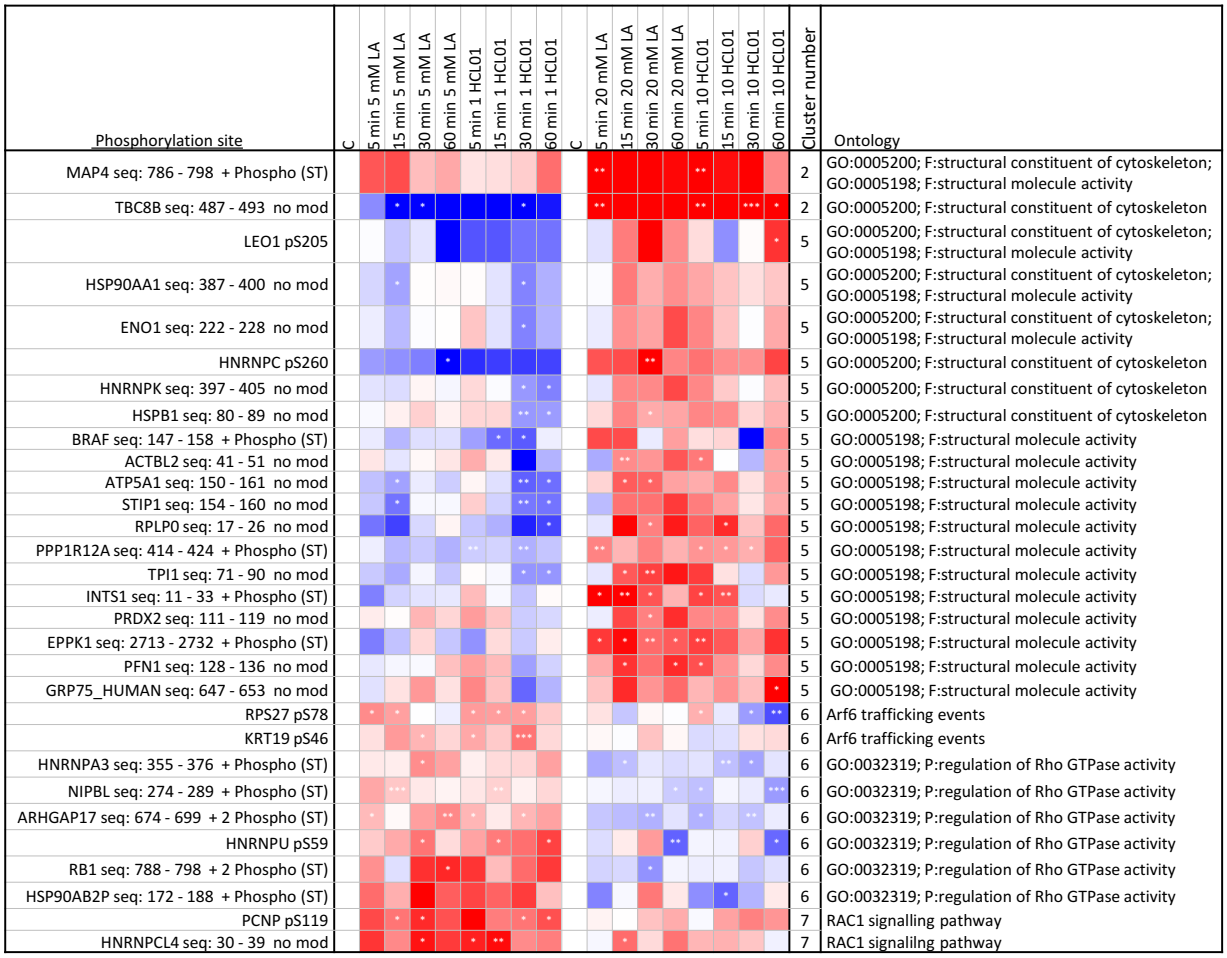

Appendix 17

Quality control of proteomics MS data of MCF7 cells treated with 20 mM lactic, 9.7 mM HCl or H_2Oacid for 4, 8 and 24 h (Chapter 7).

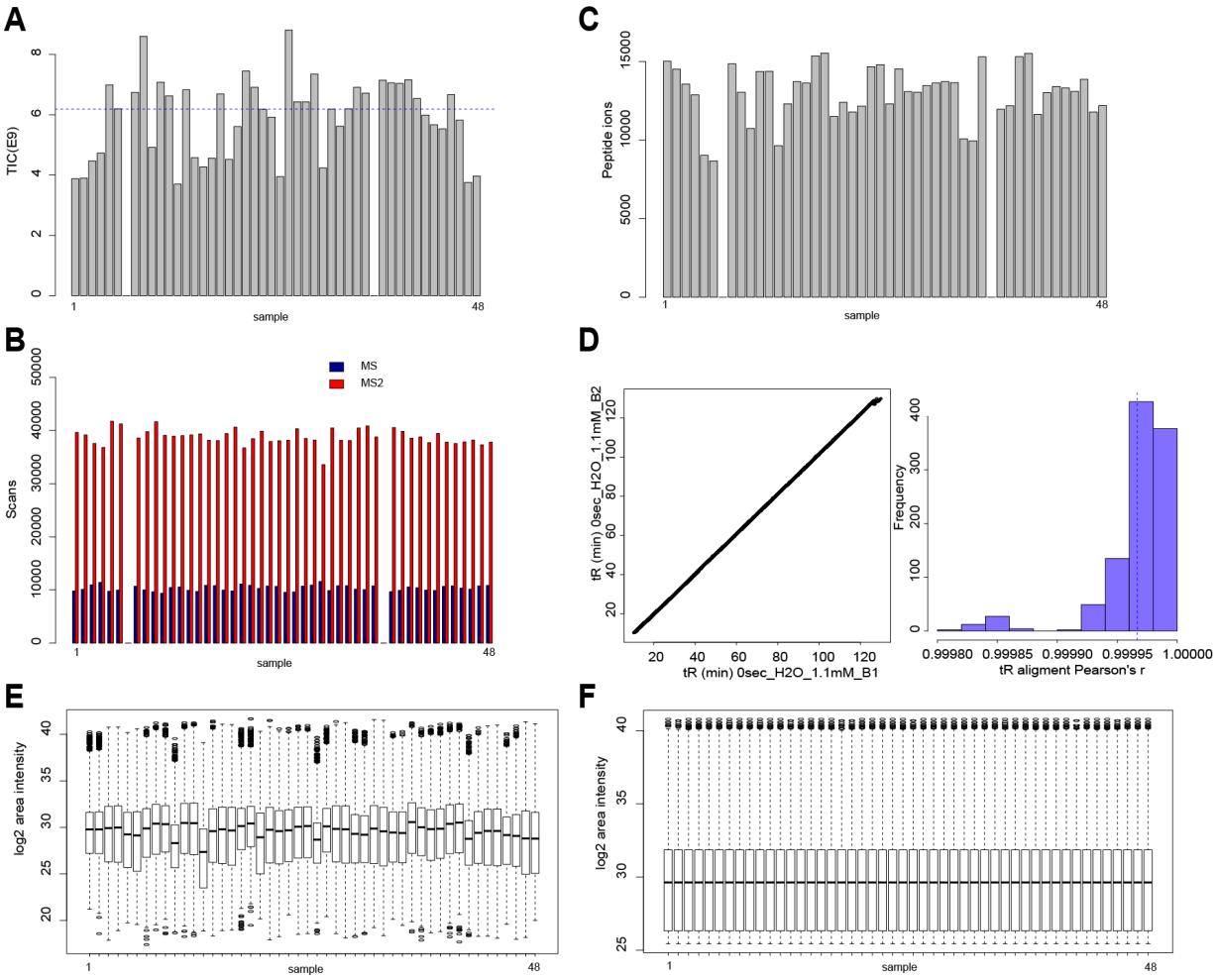

Appendix 17. (**A**) Quantification of total area under the chromatographic peaks contained in 48proteomics MS runs. Two samples (4h_H_2O_B2_T1 and 0h_HCl_B2_T2) were run with an incorrect method, which resulted in chromatograms which intensity was below the detection threshold. (**B**) Number of MS and MS2 scans quantified by RawMeat. (**C**) Number of identified peptide ions (FDR<0.05) that generate the database created from the 48 MS runs. The two samples that did not contribute to the database population were substituted for the average of the additional replicates. (**D**) Representative alignment between retention times of two experimental samples (left panel) and histogram distribution of the correlation between the alignment of retention times of all experimental samples (right panel). (**E**) Box plots demonstrating the distribution of log_2-transformed phosphopeptide peak intensities pre-normalisation. (**F**) log_2 distribution of phosphopeptides peak intensities post-quantile normalisation.

Appendix 18

Summary of the proteins modulated upon treatment with 20 mM lactic acid, 9.7 mM HCl or H_2O contained in the *K*-means clustering analysis (Chapter 7).

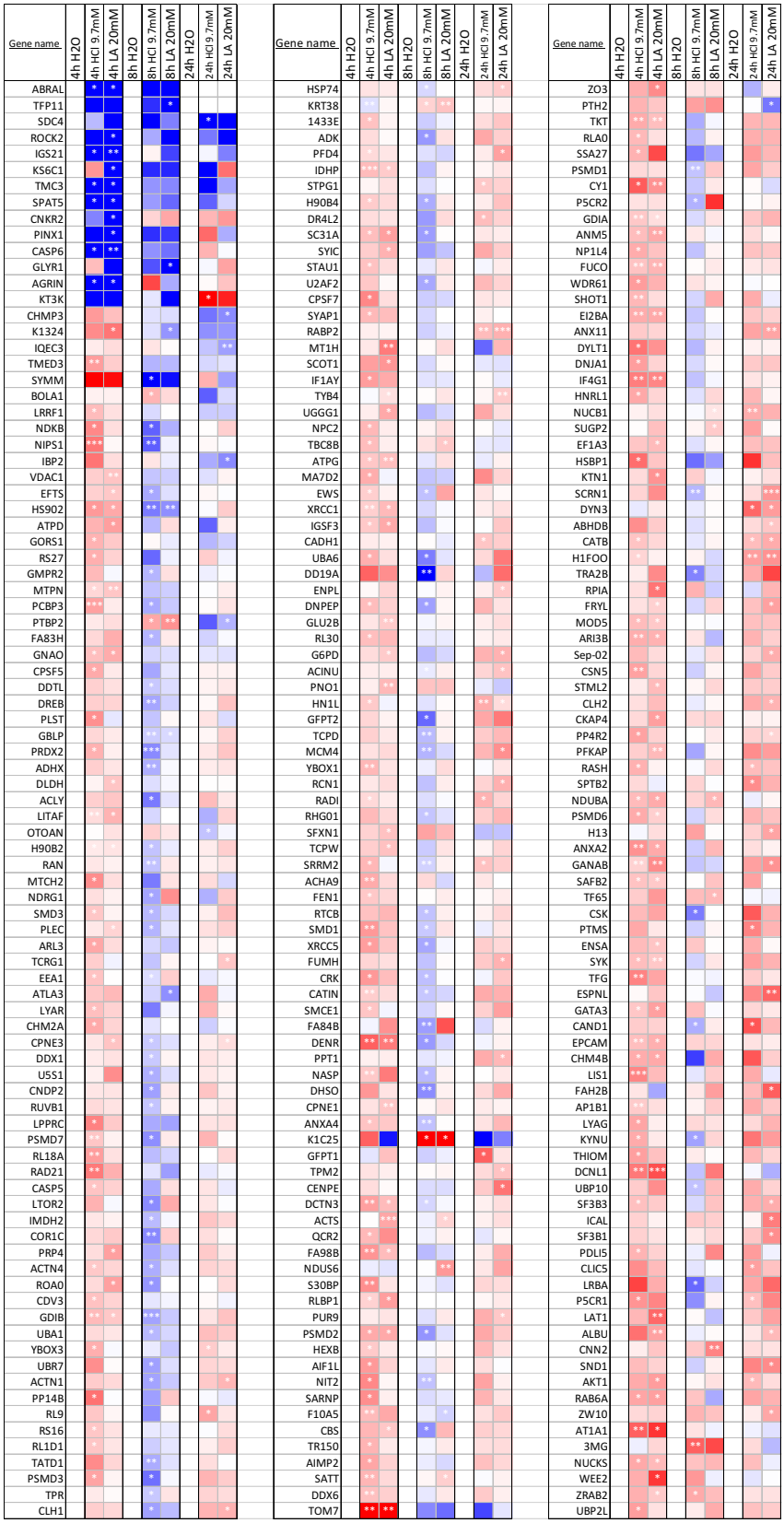

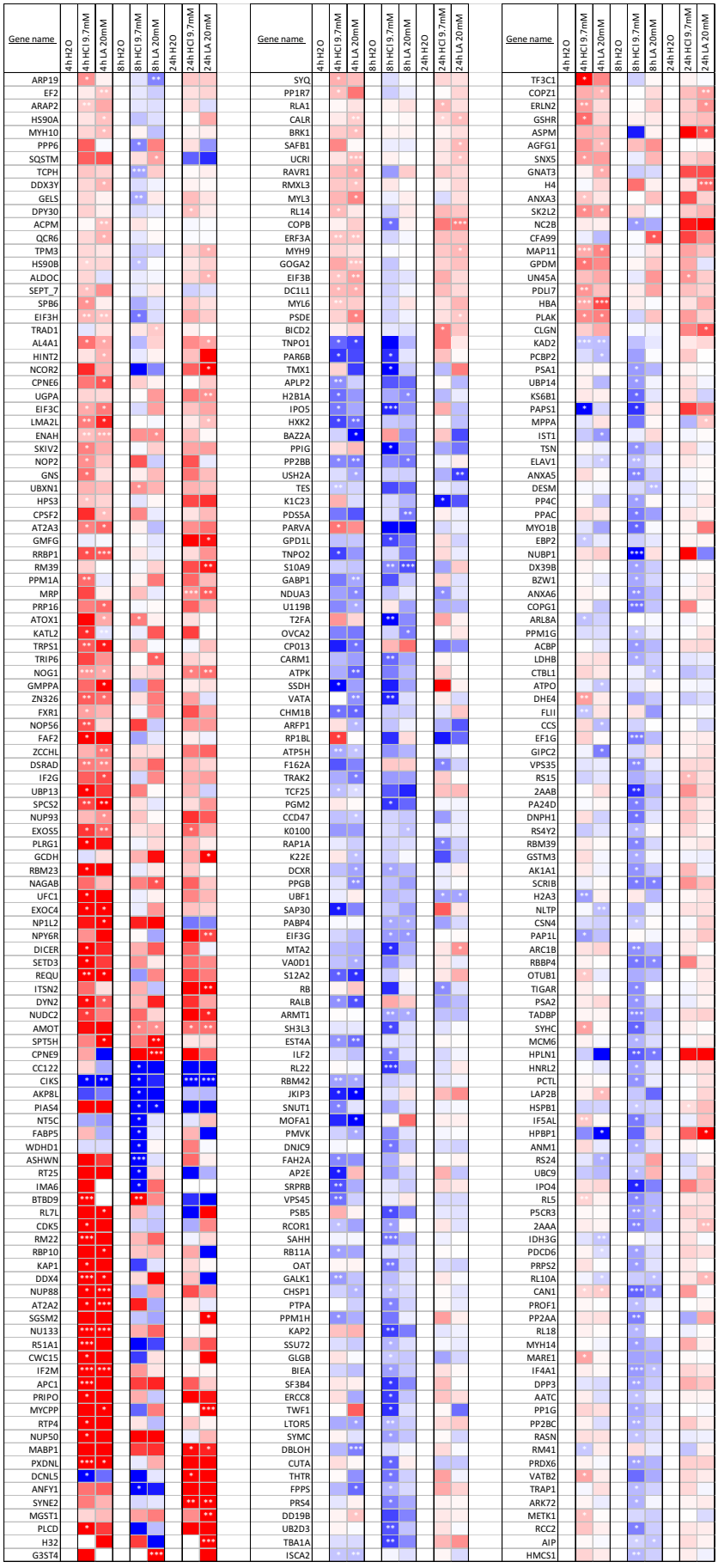
Gene name
4h H2O
4h HCl 9.7mM
4h LA 20mM
8h H2O
8h HCl 9.7mM
8h LA 20mM
24h H2O
24h HCl 9.7mM
24h LA 20mM
ARP19
EF2
ARAP2
HS90A
MYH10
PPP6
SQSTM
TCPH
DDX3Y
GELS
DPY30
ACPM
QCR6
TPM3
HS90B
ALDOC
SEPT_7
SPB6
EIF3H
TRAD1
AL4A1
HINT2
NCOR2
CPNE6
UGPA
EIF3C
LMA2L
ENAH
SKIV2
NOP2
GNS
UBXN1
HPS3
CPSF2
AT2A3
GMFG
RRBP1
RM39
PPM1A
MRP
PRP16
ATOX1
KATL2
TRPS1
TRIP6
NOG1
GMPPA
ZN326
FXR1
NOP56
FAF2
ZCCHL
DSRAD
IF2G
UBP13
SPCS2
NUP93
EXOS5
PLRG1
GCDH
RBM23
NAGAB
UFC1
EXOC4
NP1L2
NPY6R
DICER
SETD3
REQU
ITSN2
DYN2
NUDC2
AMOT
SPTSH
CPNE9
CC122
CIKS
AKP8L
PIAS4
NT5C
FABP5
WDHD1
ASHWN
RT25
IMA6
BTBD9
RL7L
CDK5
RM22
RBP10
KAP1
DDX4
NUP88
AT2A2
SGSM2
NU133
R51A1
CWC15
IF2M
APC1
PRIPO
MYCPP
RTP4
NUP50
MABP1
PXDNL
DCNL5
ANFY1
SYNE2
MGST1
PLCD
H32
G3ST4
SYQ
PP1R7
RLA1
CALR
BRK1
SAFB1
UCRI
RAVR1
RMXL3
MYL3
RL14
COPB
ERF3A
MYH9
GOGA2
EIF3B
DC1L1
MYL6
PSDE
BICD2
TNPO1
PAR6B
TMX1
APLP2
H2B1A
IPO5
HXK2
BAZ2A
PPIG
PP2BB
USH2A
TES
K1C23
PDS5A
PARVA
GPD1L
TNPO2
S10A9
GABP1
NDUA3
U119B
T2FA
OVCA2
CP013
CARM1
ATPK
SSDH
VATA
CHM1B
ARFP1
RP1BL
ATP5H
F162A
TRAK2
TCF25
PGM2
CCD47
K0100
RAP1A
K22E
DCXR
PPGB
UBF1
SAP30
PABP4
EIF3G
MTA2
VA0D1
S12A2
RB
RALB
ARMT1
SH3L3
EST4A
ILF2
RL22
RBM42
JKIP3
SNUT1
MOFA1
PMVK
DNJC9
FAH2A
AP2E
SRPRB
VPS45
PSB5
RCOR1
SAHH
RB11A
OAT
GALK1
CHSP1
PTPA
PPM1H
KAP2
SSU72
GLGB
BIEA
SF3B4
ERCC8
TWF1
LTOR5
SYMC
DBLOH
CUTA
THTR
FPPS
PRS4
DD19B
UB2D3
TBA1A
ISCA2
TF3C1
COPZ1
ERLN2
GSHR
ASPM
AGFG1
SNX5
GNAT3
H4
ANXA3
SK2L2
NC2B
CFA99
MAP11
GPDM
UN45A
PDLI7
HBA
PLAK
CLGN
KAD2
PCBP2
PSA1
UBP14
KS6B1
PAPS1
MPPA
IST1
TSN
ELAV1
ANXA5
DESM
PP4C
PPAC
MYO1B
EBP2
NUBP1
DX39B
BZW1
ANXA6
COPG1
ARL8A
PPM1G
ACBP
LDHB
CTBL1
ATPO
DHE4
FLII
CCS
EF1G
GIPC2
VPS35
RS15
2AAB
PA24D
DNPH1
RS4Y2
RBM39
GSTM3
AK1A1
SCRIB
H2A3
NLTP
CSN4
PAP1L
ARC1B
RBBP4
OTUB1
TIGAR
PSA2
TADBP
SYHC
MCM6
HPLN1
HNRL2
PCTL
LAP2B
HSPB1
IF5AL
HPBP1
ANM1
RS24
UBC9
IPO4
RL5
P5CR3
2AAA
IDH3G
PDCD6
PRPS2
RL10A
CAN1
PROF1
PP2AA
RL18
MYH14
MARE1
IF4A1
DPP3
AATC
PP1G
PP2BC
RASN
RM41
PRDX6
VATB2
TRAP1
ARK72
METK1
RCC2
AIP
HMCS1

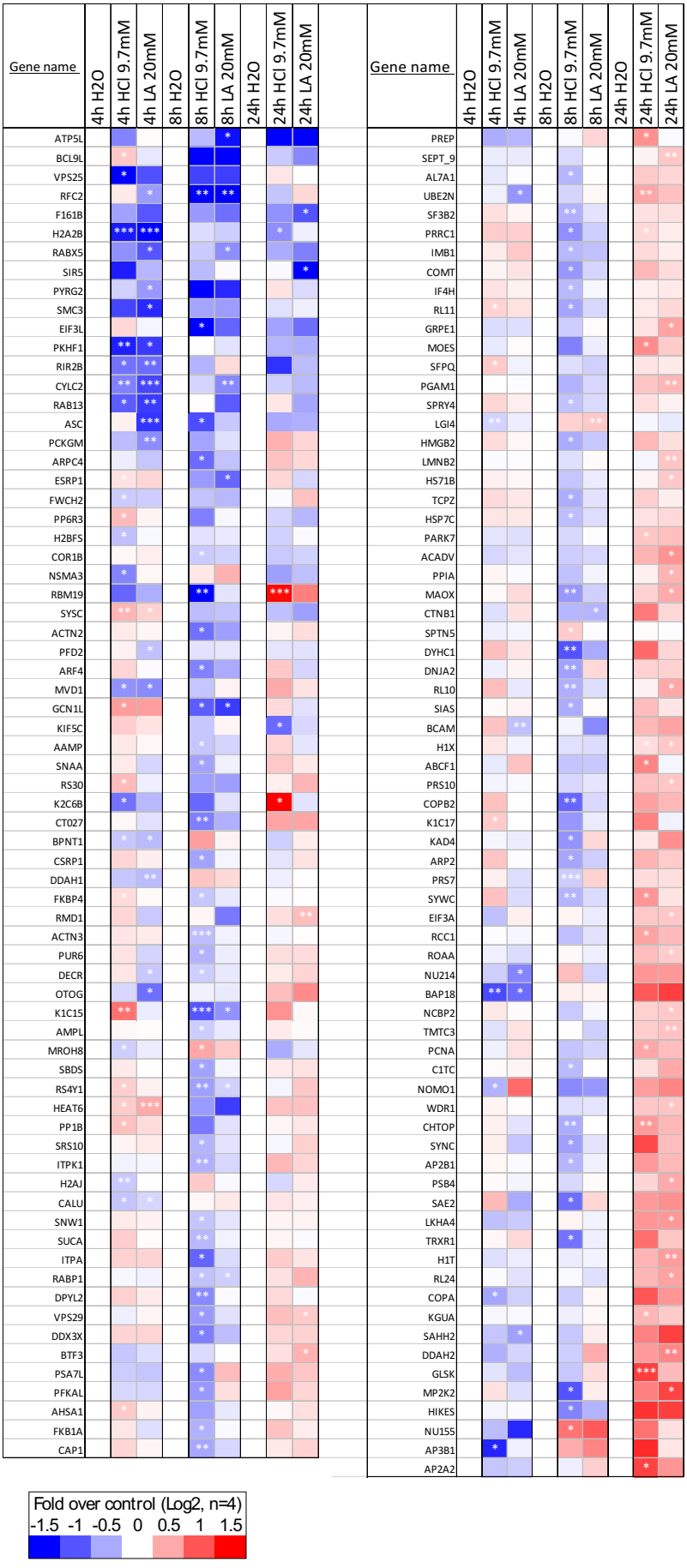
Gene name
4h H2O
4h HCl 9.7mM
4h LA 20mM
8h H2O
8h HCl 9.7mM
8h LA 20mM
24h H2O
24h HCl 9.7mM
24h LA 20mM
ATP5L
BCL9L
VPS25
RFC2
F161B
H2A2B
RABX5
SIR5
PYRG2
SMC3
EIF3L
PKHF1
RIR2B
CYLC2
RAB13
ASC
PCKGM
ARPC4
ESRP1
FWCH2
PP6R3
H2BFS
COR1B
NSMA3
RBM19
SYSC
ACTN2
PFD2
ARF4
MVD1
GCN1L
KIF5C
AAMP
SNAA
RS30
K2C6B
CT027
BPNT1
CSRP1
DDAH1
FKBP4
RMD1
ACTN3
PUR6
DECR
OTOG
K1C15
AMPL
MROH8
SBDS
RS4Y1
HEAT6
PP1B
SRS10
ITPK1
H2AJ
CALU
SNW1
SUCA
ITPA
RABP1
DPYL2
VPS29
DDX3X
BTF3
PSA7L
PFKAL
AHSA1
FKB1A
CAP1
Gene name
PREP
SEPT_9
AL7A1
UBE2N
SF3B2
PRRC1
IMB1
COMT
IF4H
RL11
GRPE1
MOES
SFPQ
PGAM1
SPRY4
LGI4
HMGB2
LMNB2
HS71B
TCPZ
HSP7C
PARK7
ACADV
PPIA
MAOX
CTNB1
SPTN5
DYHC1
DNJA2
RL10
SIAS
BCAM
H1X
ABCF1
PRS10
COPB2
K1C17
KAD4
ARP2
PRS7
SYWC
EIF3A
RCC1
ROAA
NU214
BAP18
NCBP2
TMTC3
PCNA
C1TC
NOMO1
WDR1
CHTOP
SYNC
AP2B1
PSB4
SAE2
LKHA4
TRXR1
H1T
RL24
COPA
KGUA
SAHH2
DDAH2
GLSK
MP2K2
HIKES
NU155
AP3B1
AP2A2
Fold over control (Log2, n=4)
-1.5 -1 -0.5 0 0.5 1 1.5

References

1. Di Paolo, G. and P. De Camilli, *Phosphoinositides in cell regulation and membrane dynamics.* Nature, 2006. **443**(7112): p. 651-7.
2. Thorpe, L.M., H. Yuzugullu, and J.J. Zhao, *PI3K in cancer: divergent roles of isoforms, modes of activation and therapeutic targeting.* Nat Rev Cancer, 2015. **15**(1): p. 7-24.
3. Vanhaesebroeck, B., et al., *The emerging mechanisms of isoform-specific PI3K signalling.* Nat Rev Mol Cell Biol, 2010. **11**(5): p. 329-41.
4. Auger, K.R., et al., *PDGF-dependent tyrosine phosphorylation stimulates production of novel polyphosphoinositides in intact cells.* Cell, 1989. **57**(1): p. 167-75.
5. Maehama, T. and J.E. Dixon, *The tumor suppressor, PTEN/MMAC1, dephosphorylates the lipid second messenger, phosphatidylinositol 3,4,5-trisphosphate.* J Biol Chem, 1998. **273**(22): p. 13375-8.
6. Yuan, T.L. and L.C. Cantley, *PI3K pathway alterations in cancer: variations on a theme.* Oncogene, 2008. **27**(41): p. 5497-510.
7. Arcaro, A., et al., *Class II phosphoinositide 3-kinases are downstream targets of activated polypeptide growth factor receptors.* Mol Cell Biol, 2000. **20**(11): p. 3817-30.
8. Katso, R.M., et al., *Phosphoinositide 3-Kinase C2beta regulates cytoskeletal organization and cell migration via Rac-dependent mechanisms.* Mol Biol Cell, 2006. **17**(9): p. 3729-44.
9. Burman, C. and N.T. Ktistakis, *Regulation of autophagy by phosphatidylinositol 3-phosphate.* FEBS Lett, 2010. **584**(7): p. 1302-12.
10. Franco, I., et al., *PI3K class II alpha controls spatially restricted endosomal PtdIns3P and Rab11 activation to promote primary cilium function.* Dev Cell, 2014. **28**(6): p. 647-58.
11. Alliouachene, S., et al., *Inactivation of the Class II PI3K-C2beta Potentiates Insulin Signaling and Sensitivity.* Cell Rep, 2015. **13**(9): p. 1881-94.
12. Jaber, N., et al., *Class III PI3K Vps34 plays an essential role in autophagy and in heart and liver function.* Proc Natl Acad Sci U S A, 2012. **109**(6): p. 2003-8.
13. Byfield, M.P., J.T. Murray, and J.M. Backer, *hVps34 is a nutrient-regulated lipid kinase required for activation of p70 S6 kinase.* J Biol Chem, 2005. **280**(38): p. 33076-82.
14. Johnson, E.E., et al., *Gene silencing reveals a specific function of hVps34 phosphatidylinositol 3-kinase in late versus early endosomes.* J Cell Sci, 2006. **119**(Pt 7): p. 1219-32.
15. Pattingre, S., et al., *Bcl-2 antiapoptotic proteins inhibit Beclin 1-dependent autophagy.* Cell, 2005. **122**(6): p. 927-39.
16. Bago, R., et al., *The hVps34-SGK3 pathway alleviates sustained PI3K/Akt inhibition by stimulating mTORC1 and tumour growth.* EMBO J, 2016. **35**(17): p. 1902-22.
17. Holt, K.H., et al., *Phosphatidylinositol 3-kinase activation is mediated by high-affinity interactions between distinct domains within the p110 and p85 subunits.* Mol Cell Biol, 1994. **14**(1): p. 42-9.
18. Huang, C.H., et al., *The structure of a human p110alpha/p85alpha complex elucidates the effects of oncogenic PI3Kalpha mutations.* Science, 2007. **318**(5857): p. 1744-8.
19. Guillermet-Guibert, J., et al., *The p110beta isoform of phosphoinositide 3-kinase signals downstream of G protein-coupled receptors and is functionally redundant with p110gamma.* Proc Natl Acad Sci U S A, 2008. **105**(24): p. 8292-7.
20. Cattaneo, F., et al., *Cell-surface receptors transactivation mediated by g protein-coupled receptors.* Int J Mol Sci, 2014. **15**(11): p. 19700-28.
21. Chang, M.T., et al., *Identifying recurrent mutations in cancer reveals widespread lineage diversity and mutational specificity.* Nat Biotechnol, 2016. **34**(2): p. 155-63.
22. Gupta, S., et al., *Binding of ras to phosphoinositide 3-kinase p110alpha is required for ras-driven tumorigenesis in mice.* Cell, 2007. **129**(5): p. 957-68.

23. Bunney, T.D. and M. Katan, *Phosphoinositide signalling in cancer: beyond PI3K and PTEN.* Nat Rev Cancer, 2010. **10**(5): p. 342-52.
24. Song, M.S., L. Salmena, and P.P. Pandolfi, *The functions and regulation of the PTEN tumour suppressor.* Nat Rev Mol Cell Biol, 2012. **13**(5): p. 283-96.
25. Barber, D.F., et al., *PTEN regulation, a novel function for the p85 subunit of phosphoinositide 3-kinase.* Sci STKE, 2006. **2006**(362): p. pe49.
26. Tessier, M. and J.R. Woodgett, *Role of the Phox homology domain and phosphorylation in activation of serum and glucocorticoid-regulated kinase-3.* J Biol Chem, 2006. **281**(33): p. 23978-89.
27. Chi, M.N., et al., *INPP4B is upregulated and functions as an oncogenic driver through SGK3 in a subset of melanomas.* Oncotarget, 2015. **6**(37): p. 39891-907.
28. Hnia, K., et al., *Myotubularin phosphoinositide phosphatases: cellular functions and disease pathophysiology.* Trends Mol Med, 2012. **18**(6): p. 317-27.
29. Hawkins, P.T., et al., *Signalling through Class I PI3Ks in mammalian cells.* Biochem Soc Trans, 2006. **34**(Pt 5): p. 647-62.
30. Andjelkovic, M., et al., *Role of translocation in the activation and function of protein kinase B.* J Biol Chem, 1997. **272**(50): p. 31515-24.
31. Manning, B.D. and L.C. Cantley, *AKT/PKB signaling: navigating downstream.* Cell, 2007. **129**(7): p. 1261-74.
32. Alessi, D.R., et al., *Molecular basis for the substrate specificity of protein kinase B; comparison with MAPKAP kinase-1 and p70 S6 kinase.* FEBS Lett, 1996. **399**(3): p. 333-8.
33. Hornbeck, P.V., et al., *PhosphoSitePlus, 2014: mutations, PTMs and recalibrations.* Nucleic Acids Res, 2015. **43**(Database issue): p. D512-20.
34. Datta, S.R., et al., *14-3-3 proteins and survival kinases cooperate to inactivate BAD by BH3 domain phosphorylation.* Mol Cell, 2000. **6**(1): p. 41-51.
35. Vanhaesebroeck, B. and D.R. Alessi, *The PI3K-PDK1 connection: more than just a road to PKB.* Biochem J, 2000. **346 Pt 3**: p. 561-76.
36. Larrea, M.D., et al., *Phosphorylation of p27Kip1 regulates assembly and activation of cyclin D1-Cdk4.* Mol Cell Biol, 2008. **28**(20): p. 6462-72.
37. Fang, X., et al., *Phosphorylation and inactivation of glycogen synthase kinase 3 by protein kinase A.* Proc Natl Acad Sci U S A, 2000. **97**(22): p. 11960-5.
38. Porstmann, T., et al., *SREBP activity is regulated by mTORC1 and contributes to Akt-dependent cell growth.* Cell Metab, 2008. **8**(3): p. 224-36.
39. Sun, Y., et al., *Rab8A and Rab13 are activated by insulin and regulate GLUT4 translocation in muscle cells.* Proc Natl Acad Sci U S A, 2010. **107**(46): p. 19909-14.
40. Laplante, M. and D.M. Sabatini, *mTOR signaling in growth control and disease.* Cell, 2012. **149**(2): p. 274-93.
41. Guertin, D.A. and D.M. Sabatini, *Defining the role of mTOR in cancer.* Cancer Cell, 2007. **12**(1): p. 9-22.
42. Sarbassov, D.D., et al., *Prolonged rapamycin treatment inhibits mTORC2 assembly and Akt/PKB.* Mol Cell, 2006. **22**(2): p. 159-68.
43. Jacinto, E., et al., *Mammalian TOR complex 2 controls the actin cytoskeleton and is rapamycin insensitive.* Nat Cell Biol, 2004. **6**(11): p. 1122-8.
44. Dibble, C.C. and B.D. Manning, *Signal integration by mTORC1 coordinates nutrient input with biosynthetic output.* Nat Cell Biol, 2013. **15**(6): p. 555-64.
45. Ma, X.M. and J. Blenis, *Molecular mechanisms of mTOR-mediated translational control.* Nat Rev Mol Cell Biol, 2009. **10**(5): p. 307-18.
46. Sunami, T., et al., *Structural basis of human p70 ribosomal S6 kinase-1 regulation by activation loop phosphorylation.* J Biol Chem, 2010. **285**(7): p. 4587-94.
47. Michels, A.A., et al., *mTORC1 directly phosphorylates and regulates human MAF1.* Mol Cell Biol, 2010. **30**(15): p. 3749-57.

48. Robitaille, A.M., et al., *Quantitative phosphoproteomics reveal mTORC1 activates de novo pyrimidine synthesis.* Science, 2013. **339**(6125): p. 1320-3.
49. Ben-Sahra, I., et al., *Stimulation of de novo pyrimidine synthesis by growth signaling through mTOR and S6K1.* Science, 2013. **339**(6125): p. 1323-8.
50. Dodd, K.M., et al., *mTORC1 drives HIF-1alpha and VEGF-A signalling via multiple mechanisms involving 4E-BP1, S6K1 and STAT3.* Oncogene, 2015. **34**(17): p. 2239-50.
51. Benita, Y., et al., *An integrative genomics approach identifies Hypoxia Inducible Factor-1 (HIF-1)-target genes that form the core response to hypoxia.* Nucleic Acids Res, 2009. **37**(14): p. 4587-602.
52. Horton, J.D., J.L. Goldstein, and M.S. Brown, *SREBPs: activators of the complete program of cholesterol and fatty acid synthesis in the liver.* J Clin Invest, 2002. **109**(9): p. 1125-31.
53. Peterson, T.R., et al., *mTOR complex 1 regulates lipin 1 localization to control the SREBP pathway.* Cell, 2011. **146**(3): p. 408-20.
54. Duvel, K., et al., *Activation of a metabolic gene regulatory network downstream of mTOR complex 1.* Mol Cell, 2010. **39**(2): p. 171-83.
55. Marino, M.L., et al., *Autophagy is a protective mechanism for human melanoma cells under acidic stress.* J Biol Chem, 2012. **287**(36): p. 30664-76.
56. Kim, J., et al., *AMPK and mTOR regulate autophagy through direct phosphorylation of Ulk1.* Nat Cell Biol, 2011. **13**(2): p. 132-41.
57. Settembre, C., et al., *A lysosome-to-nucleus signalling mechanism senses and regulates the lysosome via mTOR and TFEB.* EMBO J, 2012. **31**(5): p. 1095-108.
58. Inoki, K., et al., *Rheb GTPase is a direct target of TSC2 GAP activity and regulates mTOR signaling.* Genes Dev, 2003. **17**(15): p. 1829-34.
59. Ma, L., et al., *Phosphorylation and functional inactivation of TSC2 by Erk implications for tuberous sclerosis and cancer pathogenesis.* Cell, 2005. **121**(2): p. 179-93.
60. Manning, B.D., et al., *Identification of the tuberous sclerosis complex-2 tumor suppressor gene product tuberin as a target of the phosphoinositide 3-kinase/akt pathway.* Mol Cell, 2002. **10**(1): p. 151-62.
61. Kovacina, K.S., et al., *Identification of a proline-rich Akt substrate as a 14-3-3 binding partner.* J Biol Chem, 2003. **278**(12): p. 10189-94.
62. Carriere, A., et al., *Oncogenic MAPK signaling stimulates mTORC1 activity by promoting RSK-mediated raptor phosphorylation.* Curr Biol, 2008. **18**(17): p. 1269-77.
63. Mihaylova, M.M. and R.J. Shaw, *The AMPK signalling pathway coordinates cell growth, autophagy and metabolism.* Nat Cell Biol, 2011. **13**(9): p. 1016-23.
64. Inoki, K., T. Zhu, and K.L. Guan, *TSC2 mediates cellular energy response to control cell growth and survival.* Cell, 2003. **115**(5): p. 577-90.
65. Gwinn, D.M., et al., *AMPK phosphorylation of raptor mediates a metabolic checkpoint.* Mol Cell, 2008. **30**(2): p. 214-26.
66. Hawley, S.A., et al., *Calmodulin-dependent protein kinase kinase-beta is an alternative upstream kinase for AMP-activated protein kinase.* Cell Metab, 2005. **2**(1): p. 9-19.
67. Shaw, R.J., et al., *The tumor suppressor LKB1 kinase directly activates AMP-activated kinase and regulates apoptosis in response to energy stress.* Proc Natl Acad Sci U S A, 2004. **101**(10): p. 3329-35.
68. Mungai, P.T., et al., *Hypoxia triggers AMPK activation through reactive oxygen species-mediated activation of calcium release-activated calcium channels.* Mol Cell Biol, 2011. **31**(17): p. 3531-45.
69. Sofer, A., et al., *Regulation of mTOR and cell growth in response to energy stress by REDD1.* Mol Cell Biol, 2005. **25**(14): p. 5834-45.
70. Yoshida, S., et al., *Redox regulates mammalian target of rapamycin complex 1 (mTORC1) activity by modulating the TSC1/TSC2-Rheb GTPase pathway.* J Biol Chem, 2011. **286**(37): p. 32651-60.

71. Zhang, J., et al., *A tuberous sclerosis complex signalling node at the peroxisome regulates mTORC1 and autophagy in response to ROS.* Nat Cell Biol, 2013. **15**(10): p. 1186-96.
72. Thedieck, K., et al., *Inhibition of mTORC1 by astrin and stress granules prevents apoptosis in cancer cells.* Cell, 2013. **154**(4): p. 859-74.
73. Alexander, A., et al., *ATM signals to TSC2 in the cytoplasm to regulate mTORC1 in response to ROS.* Proc Natl Acad Sci U S A, 2010. **107**(9): p. 4153-8.
74. Sancak, Y., et al., *Ragulator-Rag complex targets mTORC1 to the lysosomal surface and is necessary for its activation by amino acids.* Cell, 2010. **141**(2): p. 290-303.
75. Nicklin, P., et al., *Bidirectional transport of amino acids regulates mTOR and autophagy.* Cell, 2009. **136**(3): p. 521-34.
76. Masui, K., W.K. Cavenee, and P.S. Mischel, *mTORC2 in the center of cancer metabolic reprogramming.* Trends Endocrinol Metab, 2014. **25**(7): p. 364-73.
77. Sarbassov, D.D., et al., *Rictor, a novel binding partner of mTOR, defines a rapamycin-insensitive and raptor-independent pathway that regulates the cytoskeleton.* Curr Biol, 2004. **14**(14): p. 1296-302.
78. Pearce, L.R., et al., *Protor-1 is required for efficient mTORC2-mediated activation of SGK1 in the kidney.* Biochem J, 2011. **436**(1): p. 169-79.
79. Liu, P., et al., *PtdIns(3,4,5)P3-Dependent Activation of the mTORC2 Kinase Complex.* Cancer Discov, 2015. **5**(11): p. 1194-209.
80. Oh, W.J., et al., *mTORC2 can associate with ribosomes to promote cotranslational phosphorylation and stability of nascent Akt polypeptide.* EMBO J, 2010. **29**(23): p. 3939-51.
81. Betz, C., et al., *Feature Article: mTOR complex 2-Akt signaling at mitochondria-associated endoplasmic reticulum membranes (MAM) regulates mitochondrial physiology.* Proc Natl Acad Sci U S A, 2013. **110**(31): p. 12526-34.
82. Hsu, P.P., et al., *The mTOR-regulated phosphoproteome reveals a mechanism of mTORC1-mediated inhibition of growth factor signaling.* Science, 2011. **332**(6035): p. 1317-22.
83. Liu, P., et al., *Sin1 phosphorylation impairs mTORC2 complex integrity and inhibits downstream Akt signalling to suppress tumorigenesis.* Nat Cell Biol, 2013. **15**(11): p. 1340-50.
84. Testa, J.R. and P.N. Tsichlis, *AKT signaling in normal and malignant cells.* Oncogene, 2005. **24**(50): p. 7391-3.
85. Dibble, C.C. and L.C. Cantley, *Regulation of mTORC1 by PI3K signaling.* Trends Cell Biol, 2015. **25**(9): p. 545-55.
86. Pavlova, N.N. and C.B. Thompson, *The Emerging Hallmarks of Cancer Metabolism.* Cell Metab, 2016. **23**(1): p. 27-47.
87. Hanahan, D. and R.A. Weinberg, *Hallmarks of cancer: the next generation.* Cell, 2011. **144**(5): p. 646-74.
88. Yamada, T. and P. Bork, *Evolution of biomolecular networks: lessons from metabolic and protein interactions.* Nat Rev Mol Cell Biol, 2009. **10**(11): p. 791-803.
89. Brand, K., et al., *Metabolic alterations associated with proliferation of mitogen-activated lymphocytes and of lymphoblastoid cell lines: evaluation of glucose and glutamine metabolism.* Immunobiology, 1986. **173**(1): p. 23-34.
90. Gonnella, R., et al., *Kaposi sarcoma associated herpesvirus (KSHV) induces AKT hyperphosphorylation, bortezomib-resistance and GLUT-1 plasma membrane exposure in THP-1 monocytic cell line.* J Exp Clin Cancer Res, 2013. **32**: p. 79.
91. Hirschey, M.D., et al., *Dysregulated metabolism contributes to oncogenesis.* Semin Cancer Biol, 2015. **35 Suppl**: p. S129-50.
92. Ying, H., et al., *Oncogenic Kras maintains pancreatic tumors through regulation of anabolic glucose metabolism.* Cell, 2012. **149**(3): p. 656-70.
93. Locasale, J.W., et al., *Phosphoglycerate dehydrogenase diverts glycolytic flux and contributes to oncogenesis.* Nat Genet, 2011. **43**(9): p. 869-74.

94. Possemato, R., et al., *Functional genomics reveal that the serine synthesis pathway is essential in breast cancer.* Nature, 2011. **476**(7360): p. 346-50.
95. Martinez-Outschoorn, U.E., et al., *Cancer metabolism: a therapeutic perspective.* Nat Rev Clin Oncol, 2017. **14**(1): p. 11-31.
96. Olson, A.L. and J.E. Pessin, *Structure, function, and regulation of the mammalian facilitative glucose transporter gene family.* Annu Rev Nutr, 1996. **16**: p. 235-56.
97. Wieman, H.L., J.A. Wofford, and J.C. Rathmell, *Cytokine stimulation promotes glucose uptake via phosphatidylinositol-3 kinase/Akt regulation of Glut1 activity and trafficking.* Mol Biol Cell, 2007. **18**(4): p. 1437-46.
98. Foster, R., et al., *Multiple metabolic alterations exist in mutant PI3K cancers, but only glucose is essential as a nutrient source.* PLoS One, 2012. **7**(9): p. e45061.
99. van Geldermalsen, M., et al., *ASCT2/SLC1A5 controls glutamine uptake and tumour growth in triple-negative basal-like breast cancer.* Oncogene, 2016. **35**(24): p. 3201-8.
100. Wise, D.R., et al., *Myc regulates a transcriptional program that stimulates mitochondrial glutaminolysis and leads to glutamine addiction.* Proc Natl Acad Sci U S A, 2008. **105**(48): p. 18782-7.
101. Rajeeve, V., et al., *Polyamine production is downstream and upstream of oncogenic PI3K signalling and contributes to tumour cell growth.* Biochem J, 2013. **450**(3): p. 619-28.
102. Nieman, K.M., et al., *Adipocytes promote ovarian cancer metastasis and provide energy for rapid tumor growth.* Nat Med, 2011. **17**(11): p. 1498-503.
103. Inoue, S., et al., *Mutant IDH1 Downregulates ATM and Alters DNA Repair and Sensitivity to DNA Damage Independent of TET2.* Cancer Cell, 2016. **30**(2): p. 337-48.
104. Baysal, B.E., et al., *Mutations in SDHD, a mitochondrial complex II gene, in hereditary paraganglioma.* Science, 2000. **287**(5454): p. 848-51.
105. Yuneva, M.O., et al., *The metabolic profile of tumors depends on both the responsible genetic lesion and tissue type.* Cell Metab, 2012. **15**(2): p. 157-70.
106. Davidson, S.M., et al., *Environment Impacts the Metabolic Dependencies of Ras-Driven Non-Small Cell Lung Cancer.* Cell Metab, 2016. **23**(3): p. 517-28.
107. Brooks, G.A., *Cell-cell and intracellular lactate shuttles.* J Physiol, 2009. **587**(Pt 23): p. 5591-600.
108. Ahmed, K., et al., *An autocrine lactate loop mediates insulin-dependent inhibition of lipolysis through GPR81.* Cell Metab, 2010. **11**(4): p. 311-9.
109. Halestrap, A.P. and M.C. Wilson, *The monocarboxylate transporter family--role and regulation.* IUBMB Life, 2012. **64**(2): p. 109-19.
110. Halestrap, A.P. and D. Meredith, *The SLC16 gene family-from monocarboxylate transporters (MCTs) to aromatic amino acid transporters and beyond.* Pflugers Arch, 2004. **447**(5): p. 619-28.
111. Ullah, M.S., A.J. Davies, and A.P. Halestrap, *The plasma membrane lactate transporter MCT4, but not MCT1, is up-regulated by hypoxia through a HIF-1alpha-dependent mechanism.* J Biol Chem, 2006. **281**(14): p. 9030-7.
112. Birsoy, K., et al., *MCT1-mediated transport of a toxic molecule is an effective strategy for targeting glycolytic tumors.* Nat Genet, 2013. **45**(1): p. 104-8.
113. Swietach, P., R.D. Vaughan-Jones, and A.L. Harris, *Regulation of tumor pH and the role of carbonic anhydrase 9.* Cancer Metastasis Rev, 2007. **26**(2): p. 299-310.
114. Justus, C.R., L. Dong, and L.V. Yang, *Acidic tumor microenvironment and pH-sensing G protein-coupled receptors.* Front Physiol, 2013. **4**: p. 354.
115. Wagner, W., W.M. Ciszewski, and K.D. Kania, *L- and D-lactate enhance DNA repair and modulate the resistance of cervical carcinoma cells to anticancer drugs via histone deacetylase inhibition and hydroxycarboxylic acid receptor 1 activation.* Cell Commun Signal, 2015. **13**: p. 36.

116. Fischer, K., et al., *Inhibitory effect of tumor cell-derived lactic acid on human T cells.* Blood, 2007. **109**(9): p. 3812-9.
117. Colegio, O.R., et al., *Functional polarization of tumour-associated macrophages by tumour-derived lactic acid.* Nature, 2014. **513**(7519): p. 559-63.
118. Panieri, E. and M.M. Santoro, *ROS homeostasis and metabolism: a dangerous liason in cancer cells.* Cell Death Dis, 2016. **7**(6): p. e2253.
119. Sundaresan, M., et al., *Regulation of reactive-oxygen-species generation in fibroblasts by Rac1.* Biochem J, 1996. **318 (Pt 2)**: p. 379-82.
120. Bae, Y.S., et al., *Epidermal growth factor (EGF)-induced generation of hydrogen peroxide. Role in EGF receptor-mediated tyrosine phosphorylation.* J Biol Chem, 1997. **272**(1): p. 217-21.
121. Sullivan, L.B. and N.S. Chandel, *Mitochondrial reactive oxygen species and cancer.* Cancer Metab, 2014. **2**: p. 17.
122. Trachootham, D., J. Alexandre, and P. Huang, *Targeting cancer cells by ROS-mediated mechanisms: a radical therapeutic approach?* Nat Rev Drug Discov, 2009. **8**(7): p. 579-91.
123. Leslie, N.R., et al., *Redox regulation of PI 3-kinase signalling via inactivation of PTEN.* EMBO J, 2003. **22**(20): p. 5501-10.
124. Ostman, A., et al., *Regulation of protein tyrosine phosphatases by reversible oxidation.* J Biochem, 2011. **150**(4): p. 345-56.
125. Sporn, M.B. and K.T. Liby, *NRF2 and cancer: the good, the bad and the importance of context.* Nat Rev Cancer, 2012. **12**(8): p. 564-71.
126. Banin, S., et al., *Enhanced phosphorylation of p53 by ATM in response to DNA damage.* Science, 1998. **281**(5383): p. 1674-7.
127. Takahashi, A., et al., *Mitogenic signalling and the p16INK4a-Rb pathway cooperate to enforce irreversible cellular senescence.* Nat Cell Biol, 2006. **8**(11): p. 1291-7.
128. Dalleau, S., et al., *Cell death and diseases related to oxidative stress: 4-hydroxynonenal (HNE) in the balance.* Cell Death Differ, 2013. **20**(12): p. 1615-30.
129. Dizdaroglu, M. and P. Jaruga, *Mechanisms of free radical-induced damage to DNA.* Free Radic Res, 2012. **46**(4): p. 382-419.
130. Holmstrom, K.M. and T. Finkel, *Cellular mechanisms and physiological consequences of redox-dependent signalling.* Nat Rev Mol Cell Biol, 2014. **15**(6): p. 411-21.
131. Sazanov, L.A., *A giant molecular proton pump: structure and mechanism of respiratory complex I.* Nat Rev Mol Cell Biol, 2015. **16**(6): p. 375-88.
132. Teissier, E., et al., *Peroxisome proliferator-activated receptor alpha induces NADPH oxidase activity in macrophages, leading to the generation of LDL with PPAR-alpha activation properties.* Circ Res, 2004. **95**(12): p. 1174-82.
133. Malhotra, J.D., et al., *Antioxidants reduce endoplasmic reticulum stress and improve protein secretion.* Proc Natl Acad Sci U S A, 2008. **105**(47): p. 18525-30.
134. Singh, A., et al., *Dysfunctional KEAP1-NRF2 interaction in non-small-cell lung cancer.* PLoS Med, 2006. **3**(10): p. e420.
135. Wu, P., T.E. Nielsen, and M.H. Clausen, *Small-molecule kinase inhibitors: an analysis of FDA-approved drugs.* Drug Discov Today, 2016. **21**(1): p. 5-10.
136. Folkes, A.J., et al., *The identification of 2-(1H-indazol-4-yl)-6-(4-methanesulfonyl-piperazin-1-ylmethyl)-4-morpholin-4-yl-t hieno[3,2-d]pyrimidine (GDC-0941) as a potent, selective, orally bioavailable inhibitor of class I PI3 kinase for the treatment of cancer.* J Med Chem, 2008. **51**(18): p. 5522-32.
137. Fritsch, C., et al., *Characterization of the novel and specific PI3Kalpha inhibitor NVP-BYL719 and development of the patient stratification strategy for clinical trials.* Mol Cancer Ther, 2014. **13**(5): p. 1117-29.
138. Vanhaesebroeck, B. and A. Khwaja, *PI3Kdelta inhibition hits a sensitive spot in B cell malignancies.* Cancer Cell, 2014. **25**(3): p. 269-71.

139. Gaude, E. and C. Frezza, *Tissue-specific and convergent metabolic transformation of cancer correlates with metastatic potential and patient survival.* Nat Commun, 2016. **7**: p. 13041.
140. Pieters, R., et al., *Pharmacokinetics, pharmacodynamics, efficacy, and safety of a new recombinant asparaginase preparation in children with previously untreated acute lymphoblastic leukemia: a randomized phase 2 clinical trial.* Blood, 2008. **112**(13): p. 4832-8.
141. Polanski, R., et al., *Activity of the monocarboxylate transporter 1 inhibitor AZD3965 in small cell lung cancer.* Clin Cancer Res, 2014. **20**(4): p. 926-37.
142. Doherty, J.R., et al., *Blocking lactate export by inhibiting the Myc target MCT1 Disables glycolysis and glutathione synthesis.* Cancer Res, 2014. **74**(3): p. 908-20.
143. Yang, Y., et al., *Different effects of LDH-A inhibition by oxamate in non-small cell lung cancer cells.* Oncotarget, 2014. **5**(23): p. 11886-96.
144. Le, A., et al., *Inhibition of lactate dehydrogenase A induces oxidative stress and inhibits tumor progression.* Proc Natl Acad Sci U S A, 2010. **107**(5): p. 2037-42.
145. Maschek, G., et al., *2-deoxy-D-glucose increases the efficacy of adriamycin and paclitaxel in human osteosarcoma and non-small cell lung cancers in vivo.* Cancer Res, 2004. **64**(1): p. 31-4.
146. Farber, S. and L.K. Diamond, *Temporary remissions in acute leukemia in children produced by folic acid antagonist, 4-aminopteroyl-glutamic acid.* N Engl J Med, 1948. **238**(23): p. 787-93.
147. Wilson, P.M., et al., *Standing the test of time: targeting thymidylate biosynthesis in cancer therapy.* Nat Rev Clin Oncol, 2014. **11**(5): p. 282-98.
148. Lo-Coco, F., et al., *Retinoic acid and arsenic trioxide for acute promyelocytic leukemia.* N Engl J Med, 2013. **369**(2): p. 111-21.
149. Fathi, A.T., et al., *Biochemical, Epigenetic, and Metabolic Approaches to Target IDH Mutations in Acute Myeloid Leukemia.* Semin Hematol, 2015. **52**(3): p. 165-71.
150. Yun, J., et al., *Vitamin C selectively kills KRAS and BRAF mutant colorectal cancer cells by targeting GAPDH.* Science, 2015. **350**(6266): p. 1391-6.
151. Porporato, P.E., et al., *A mitochondrial switch promotes tumor metastasis.* Cell Rep, 2014. **8**(3): p. 754-66.
152. Dang, C.V., et al., *The interplay between MYC and HIF in cancer.* Nat Rev Cancer, 2008. **8**(1): p. 51-6.
153. Kung, A.L., et al., *Small molecule blockade of transcriptional coactivation of the hypoxia-inducible factor pathway.* Cancer Cell, 2004. **6**(1): p. 33-43.
154. Lin, C.Y., et al., *Transcriptional amplification in tumor cells with elevated c-Myc.* Cell, 2012. **151**(1): p. 56-67.
155. Huang, M.J., et al., *A small-molecule c-Myc inhibitor, 10058-F4, induces cell-cycle arrest, apoptosis, and myeloid differentiation of human acute myeloid leukemia.* Exp Hematol, 2006. **34**(11): p. 1480-9.
156. Yin, X., et al., *Low molecular weight inhibitors of Myc-Max interaction and function.* Oncogene, 2003. **22**(40): p. 6151-9.
157. Albrecht, B.K., et al., *Identification of a Benzoisoxazoloazepine Inhibitor (CPI-0610) of the Bromodomain and Extra-Terminal (BET) Family as a Candidate for Human Clinical Trials.* J Med Chem, 2016. **59**(4): p. 1330-9.
158. Mayer, I.A., et al., *A Phase Ib Study of Alpelisib (BYL719), a PI3Kalpha-Specific Inhibitor, with Letrozole in ER+/HER2- Metastatic Breast Cancer.* Clin Cancer Res, 2016.
159. Rosell, R., et al., *Screening for epidermal growth factor receptor mutations in lung cancer.* N Engl J Med, 2009. **361**(10): p. 958-67.
160. Carracedo, A., et al., *Inhibition of mTORC1 leads to MAPK pathway activation through a PI3K-dependent feedback loop in human cancer.* J Clin Invest, 2008. **118**(9): p. 3065-74.
161. Casado, P., et al., *Kinase-substrate enrichment analysis provides insights into the heterogeneity of signaling pathway activation in leukemia cells.* Sci Signal, 2013. **6**(268): p. rs6.

162. Ng, K.P., et al., *A common BIM deletion polymorphism mediates intrinsic resistance and inferior responses to tyrosine kinase inhibitors in cancer.* Nat Med, 2012. **18**(4): p. 521-8.
163. Kobayashi, S., et al., *EGFR mutation and resistance of non-small-cell lung cancer to gefitinib.* N Engl J Med, 2005. **352**(8): p. 786-92.
164. Balak, M.N., et al., *Novel D761Y and common secondary T790M mutations in epidermal growth factor receptor-mutant lung adenocarcinomas with acquired resistance to kinase inhibitors.* Clin Cancer Res, 2006. **12**(21): p. 6494-501.
165. Zunder, E.R., et al., *Discovery of drug-resistant and drug-sensitizing mutations in the oncogenic PI3K isoform p110 alpha.* Cancer Cell, 2008. **14**(2): p. 180-92.
166. Wagle, N., et al., *Response and acquired resistance to everolimus in anaplastic thyroid cancer.* N Engl J Med, 2014. **371**(15): p. 1426-33.
167. Woyach, J.A., et al., *Resistance mechanisms for the Bruton's tyrosine kinase inhibitor ibrutinib.* N Engl J Med, 2014. **370**(24): p. 2286-94.
168. Juric, D., et al., *Convergent loss of PTEN leads to clinical resistance to a PI(3)Kalpha inhibitor.* Nature, 2015. **518**(7538): p. 240-4.
169. Holderfield, M., et al., *Targeting RAF kinases for cancer therapy: BRAF-mutated melanoma and beyond.* Nat Rev Cancer, 2014. **14**(7): p. 455-67.
170. Costa, C., et al., *Measurement of PIP3 levels reveals an unexpected role for p110beta in early adaptive responses to p110alpha-specific inhibitors in luminal breast cancer.* Cancer Cell, 2015. **27**(1): p. 97-108.
171. Engelman, J.A., et al., *Effective use of PI3K and MEK inhibitors to treat mutant Kras G12D and PIK3CA H1047R murine lung cancers.* Nat Med, 2008. **14**(12): p. 1351-6.
172. Shepherd, C., et al., *PI3K/mTOR inhibition upregulates NOTCH-MYC signalling leading to an impaired cytotoxic response.* Leukemia, 2013. **27**(3): p. 650-60.
173. !!! INVALID CITATION !!! .
174. Kuczynski, E.A., et al., *Drug rechallenge and treatment beyond progression--implications for drug resistance.* Nat Rev Clin Oncol, 2013. **10**(10): p. 571-87.
175. Stinchcombe, T.E. and M.A. Socinski, *Considerations for second-line therapy of non-small cell lung cancer.* Oncologist, 2008. **13 Suppl 1**: p. 28-36.
176. Blackwell, K.L., et al., *Randomized study of Lapatinib alone or in combination with trastuzumab in women with ErbB2-positive, trastuzumab-refractory metastatic breast cancer.* J Clin Oncol, 2010. **28**(7): p. 1124-30.
177. Bedard, P.L., et al., *A phase Ib dose-escalation study of the oral pan-PI3K inhibitor buparlisib (BKM120) in combination with the oral MEK1/2 inhibitor trametinib (GSK1120212) in patients with selected advanced solid tumors.* Clin Cancer Res, 2015. **21**(4): p. 730-8.
178. Lopez, J.S. and U. Banerji, *Combine and conquer: challenges for targeted therapy combinations in early phase trials.* Nat Rev Clin Oncol, 2016.
179. Sharma, S.V., et al., *A chromatin-mediated reversible drug-tolerant state in cancer cell subpopulations.* Cell, 2010. **141**(1): p. 69-80.
180. Weisberg, E., et al., *Reversible resistance induced by FLT3 inhibition: a novel resistance mechanism in mutant FLT3-expressing cells.* PLoS One, 2011. **6**(9): p. e25351.
181. Chmielecki, J., et al., *Optimization of dosing for EGFR-mutant non-small cell lung cancer with evolutionary cancer modeling.* Sci Transl Med, 2011. **3**(90): p. 90ra59.
182. Morales, C., et al., *Dihydrofolate reductase amplification and sensitization to methotrexate of methotrexate-resistant colon cancer cells.* Mol Cancer Ther, 2009. **8**(2): p. 424-32.
183. Sun, C., et al., *Reversible and adaptive resistance to BRAF(V600E) inhibition in melanoma.* Nature, 2014. **508**(7494): p. 118-22.
184. Hammers, H.J., et al., *Reversible epithelial to mesenchymal transition and acquired resistance to sunitinib in patients with renal cell carcinoma: evidence from a xenograft study.* Mol Cancer Ther, 2010. **9**(6): p. 1525-35.

185. Tang, T.C., et al., *Development of a resistance-like phenotype to sorafenib by human hepatocellular carcinoma cells is reversible and can be delayed by metronomic UFT chemotherapy.* Neoplasia, 2010. **12**(11): p. 928-40.
186. Rimawi, M.F., et al., *Reduced dose and intermittent treatment with lapatinib and trastuzumab for potent blockade of the HER pathway in HER2/neu-overexpressing breast tumor xenografts.* Clin Cancer Res, 2011. **17**(6): p. 1351-61.
187. Das Thakur, M., et al., *Modelling vemurafenib resistance in melanoma reveals a strategy to forestall drug resistance.* Nature, 2013. **494**(7436): p. 251-5.
188. Seghers, A.C., et al., *Successful rechallenge in two patients with BRAF-V600-mutant melanoma who experienced previous progression during treatment with a selective BRAF inhibitor.* Melanoma Res, 2012. **22**(6): p. 466-72.
189. Workman, P., et al., *How Much Longer Will We Put Up With $100,000 Cancer Drugs?* Cell, 2017. **168**(4): p. 579-583.
190. Iadevaia, S., et al., *Identification of optimal drug combinations targeting cellular networks: integrating phospho-proteomics and computational network analysis.* Cancer Res, 2010. **70**(17): p. 6704-14.
191. Foo, J., et al., *Effects of pharmacokinetic processes and varied dosing schedules on the dynamics of acquired resistance to erlotinib in EGFR-mutant lung cancer.* J Thorac Oncol, 2012. **7**(10): p. 1583-93.
192. Fenn, J.B., et al., *Electrospray ionization for mass spectrometry of large biomolecules.* Science, 1989. **246**(4926): p. 64-71.
193. Karas, M. and F. Hillenkamp, *Laser desorption ionization of proteins with molecular masses exceeding 10,000 daltons.* Anal Chem, 1988. **60**(20): p. 2299-301.
194. Wilm, M. and M. Mann, *Analytical properties of the nanoelectrospray ion source.* Anal Chem, 1996. **68**(1): p. 1-8.
195. Chelius, D., et al., *Global protein identification and quantification technology using two-dimensional liquid chromatography nanospray mass spectrometry.* Anal Chem, 2003. **75**(23): p. 6658-65.
196. Douglas, D.J., A.J. Frank, and D. Mao, *Linear ion traps in mass spectrometry.* Mass Spectrom Rev, 2005. **24**(1): p. 1-29.
197. Makarov, A., et al., *Performance evaluation of a hybrid linear ion trap/orbitrap mass spectrometer.* Anal Chem, 2006. **78**(7): p. 2113-20.
198. Canas, B., et al., *Trends in sample preparation for classical and second generation proteomics.* J Chromatogr A, 2007. **1153**(1-2): p. 235-58.
199. Wisniewski, J.R., A. Zougman, and M. Mann, *Combination of FASP and StageTip-based fractionation allows in-depth analysis of the hippocampal membrane proteome.* J Proteome Res, 2009. **8**(12): p. 5674-8.
200. Kulak, N.A., et al., *Minimal, encapsulated proteomic-sample processing applied to copy-number estimation in eukaryotic cells.* Nat Methods, 2014. **11**(3): p. 319-24.
201. Rodriguez, J., et al., *Does trypsin cut before proline?* J Proteome Res, 2008. **7**(1): p. 300-5.
202. Garcia, B.A., et al., *Chemical derivatization of histones for facilitated analysis by mass spectrometry.* Nat Protoc, 2007. **2**(4): p. 933-8.
203. Hyung, S.J. and B.T. Ruotolo, *Integrating mass spectrometry of intact protein complexes into structural proteomics.* Proteomics, 2012. **12**(10): p. 1547-64.
204. Shishkova, E., A.S. Hebert, and J.J. Coon, *Now, More Than Ever, Proteomics Needs Better Chromatography.* Cell Syst, 2016. **3**(4): p. 321-324.
205. Cutillas, P.R. and B. Vanhaesebroeck, *Quantitative profile of five murine core proteomes using label-free functional proteomics.* Mol Cell Proteomics, 2007. **6**(9): p. 1560-73.
206. Kim, M.S., et al., *A draft map of the human proteome.* Nature, 2014. **509**(7502): p. 575-81.
207. Wilhelm, M., et al., *Mass-spectrometry-based draft of the human proteome.* Nature, 2014. **509**(7502): p. 582-7.

208. Gillet, L.C., et al., *Targeted data extraction of the MS/MS spectra generated by data-independent acquisition: a new concept for consistent and accurate proteome analysis.* Mol Cell Proteomics, 2012. **11**(6): p. O111 016717.
209. Bilbao, A., et al., *Processing strategies and software solutions for data-independent acquisition in mass spectrometry.* Proteomics, 2015. **15**(5-6): p. 964-80.
210. Rost, H.L., et al., *OpenSWATH enables automated, targeted analysis of data-independent acquisition MS data.* Nat Biotechnol, 2014. **32**(3): p. 219-23.
211. Zhang, J., et al., *PEAKS DB: de novo sequencing assisted database search for sensitive and accurate peptide identification.* Mol Cell Proteomics, 2012. **11**(4): p. M111 010587.
212. Perkins, D.N., et al., *Probability-based protein identification by searching sequence databases using mass spectrometry data.* Electrophoresis, 1999. **20**(18): p. 3551-67.
213. Eng, J.K., A.L. McCormack, and J.R. Yates, *An approach to correlate tandem mass spectral data of peptides with amino acid sequences in a protein database.* J Am Soc Mass Spectrom, 1994. **5**(11): p. 976-89.
214. Craig, R. and R.C. Beavis, *TANDEM: matching proteins with tandem mass spectra.* Bioinformatics, 2004. **20**(9): p. 1466-7.
215. Gygi, S.P., et al., *Quantitative analysis of complex protein mixtures using isotope-coded affinity tags.* Nat Biotechnol, 1999. **17**(10): p. 994-9.
216. Thompson, A., et al., *Tandem mass tags: a novel quantification strategy for comparative analysis of complex protein mixtures by MS/MS.* Anal Chem, 2003. **75**(8): p. 1895-904.
217. Ross, P.L., et al., *Multiplexed protein quantitation in Saccharomyces cerevisiae using amine-reactive isobaric tagging reagents.* Mol Cell Proteomics, 2004. **3**(12): p. 1154-69.
218. Sandberg, A., et al., *Quantitative accuracy in mass spectrometry based proteomics of complex samples: the impact of labeling and precursor interference.* J Proteomics, 2014. **96**: p. 133-44.
219. Ong, S.E., et al., *Stable isotope labeling by amino acids in cell culture, SILAC, as a simple and accurate approach to expression proteomics.* Mol Cell Proteomics, 2002. **1**(5): p. 376-86.
220. Bantscheff, M., et al., *Quantitative mass spectrometry in proteomics: critical review update from 2007 to the present.* Anal Bioanal Chem, 2012. **404**(4): p. 939-65.
221. Strassberger, V., et al., *Chemical proteomic and bioinformatic strategies for the identification and quantification of vascular antigens in cancer.* J Proteomics, 2010. **73**(10): p. 1954-73.
222. Milac, T.I., T.W. Randolph, and P. Wang, *Analyzing LC-MS/MS data by spectral count and ion abundance: two case studies.* Stat Interface, 2012. **5**(1): p. 75-87.
223. Yang, F., et al., *Applying a targeted label-free approach using LC-MS AMT tags to evaluate changes in protein phosphorylation following phosphatase inhibition.* J Proteome Res, 2007. **6**(11): p. 4489-97.
224. Picotti, P. and R. Aebersold, *Selected reaction monitoring-based proteomics: workflows, potential, pitfalls and future directions.* Nat Methods, 2012. **9**(6): p. 555-66.
225. Montoya, A., et al., *Characterization of a TiO(2) enrichment method for label-free quantitative phosphoproteomics.* Methods, 2011. **54**(4): p. 370-8.
226. Wilkes, E.H., et al., *Empirical inference of circuitry and plasticity in a kinase signaling network.* Proc Natl Acad Sci U S A, 2015. **112**(25): p. 7719-24.
227. Terfve, C.D., et al., *Large-scale models of signal propagation in human cells derived from discovery phosphoproteomic data.* Nat Commun, 2015. **6**: p. 8033.
228. Sciacovelli, M., et al., *Fumarate is an epigenetic modifier that elicits epithelial-to-mesenchymal transition.* Nature, 2016. **537**(7621): p. 544-547.
229. Lin, J., et al., *Understanding protein phosphorylation on a systems level.* Brief Funct Genomics, 2010. **9**(1): p. 32-42.
230. Humphrey, S.J., S.B. Azimifar, and M. Mann, *High-throughput phosphoproteomics reveals in vivo insulin signaling dynamics.* Nat Biotechnol, 2015. **33**(9): p. 990-5.

231. Gnad, F., et al., *Evolutionary constraints of phosphorylation in eukaryotes, prokaryotes, and mitochondria.* Mol Cell Proteomics, 2010. **9**(12): p. 2642-53.
232. Tan, C.S., C. Jorgensen, and R. Linding, *Roles of "junk phosphorylation" in modulating biomolecular association of phosphorylated proteins?* Cell Cycle, 2010. **9**(7): p. 1276-80.
233. Beltrao, P., et al., *Systematic functional prioritization of protein posttranslational modifications.* Cell, 2012. **150**(2): p. 413-25.
234. Moses, A.M., et al., *Regulatory evolution in proteins by turnover and lineage-specific changes of cyclin-dependent kinase consensus sites.* Proc Natl Acad Sci U S A, 2007. **104**(45): p. 17713-8.
235. Cohen, P., *The regulation of protein function by multisite phosphorylation--a 25 year update.* Trends Biochem Sci, 2000. **25**(12): p. 596-601.
236. Sacco, F., et al., *The human phosphatase interactome: An intricate family portrait.* FEBS Lett, 2012. **586**(17): p. 2732-9.
237. Olsen, J.V., et al., *Global, in vivo, and site-specific phosphorylation dynamics in signaling networks.* Cell, 2006. **127**(3): p. 635-48.
238. Steeg, P.S., et al., *Histidine kinases and histidine phosphorylated proteins in mammalian cell biology, signal transduction and cancer.* Cancer Lett, 2003. **190**(1): p. 1-12.
239. Turner, N. and R. Grose, *Fibroblast growth factor signalling: from development to cancer.* Nat Rev Cancer, 2010. **10**(2): p. 116-29.
240. Copps, K.D. and M.F. White, *Regulation of insulin sensitivity by serine/threonine phosphorylation of insulin receptor substrate proteins IRS1 and IRS2.* Diabetologia, 2012. **55**(10): p. 2565-82.
241. Flight, M.H., *Neurodegenerative diseases: New kinase targets for Alzheimer's disease.* Nat Rev Drug Discov, 2013. **12**(10): p. 739.
242. Bodenmiller, B., et al., *Phosphoproteomic analysis reveals interconnected system-wide responses to perturbations of kinases and phosphatases in yeast.* Sci Signal, 2010. **3**(153): p. rs4.
243. Rowland, M.A., B. Harrison, and E.J. Deeds, *Phosphatase specificity and pathway insulation in signaling networks.* Biophys J, 2015. **108**(4): p. 986-96.
244. Thingholm, T.E., O.N. Jensen, and M.R. Larsen, *Analytical strategies for phosphoproteomics.* Proteomics, 2009. **9**(6): p. 1451-68.
245. Vosseller, K., et al., *Quantitative analysis of both protein expression and serine / threonine post-translational modifications through stable isotope labeling with dithiothreitol.* Proteomics, 2005. **5**(2): p. 388-98.
246. Gronborg, M., et al., *A mass spectrometry-based proteomic approach for identification of serine/threonine-phosphorylated proteins by enrichment with phospho-specific antibodies: identification of a novel protein, Frigg, as a protein kinase A substrate.* Mol Cell Proteomics, 2002. **1**(7): p. 517-27.
247. Zhang, G. and T.A. Neubert, *Use of detergents to increase selectivity of immunoprecipitation of tyrosine phosphorylated peptides prior to identification by MALDI quadrupole-TOF MS.* Proteomics, 2006. **6**(2): p. 571-8.
248. Blagoev, B., et al., *Temporal analysis of phosphotyrosine-dependent signaling networks by quantitative proteomics.* Nat Biotechnol, 2004. **22**(9): p. 1139-45.
249. Rush, J., et al., *Immunoaffinity profiling of tyrosine phosphorylation in cancer cells.* Nat Biotechnol, 2005. **23**(1): p. 94-101.
250. Chen, J., et al., *Low-bias phosphopeptide enrichment from scarce samples using plastic antibodies.* Sci Rep, 2015. **5**: p. 11438.
251. Beausoleil, S.A., et al., *Large-scale characterization of HeLa cell nuclear phosphoproteins.* Proc Natl Acad Sci U S A, 2004. **101**(33): p. 12130-5.

252. Han, G., et al., *Large-scale phosphoproteome analysis of human liver tissue by enrichment and fractionation of phosphopeptides with strong anion exchange chromatography.* Proteomics, 2008. **8**(7): p. 1346-61.
253. Nie, S., et al., *Comprehensive profiling of phosphopeptides based on anion exchange followed by flow-through enrichment with titanium dioxide (AFET).* J Proteome Res, 2010. **9**(9): p. 4585-94.
254. Hao, P., et al., *Novel application of electrostatic repulsion-hydrophilic interaction chromatography (ERLIC) in shotgun proteomics: comprehensive profiling of rat kidney proteome.* J Proteome Res, 2010. **9**(7): p. 3520-6.
255. McNulty, D.E. and R.S. Annan, *Hydrophilic interaction chromatography reduces the complexity of the phosphoproteome and improves global phosphopeptide isolation and detection.* Mol Cell Proteomics, 2008. **7**(5): p. 971-80.
256. Zarei, M., et al., *Fast and easy phosphopeptide fractionation by combinatorial ERLIC-SCX solid-phase extraction for in-depth phosphoproteome analysis.* Nat Protoc, 2016. **11**(1): p. 37-45.
257. de Graaf, E.L., et al., *Single-step enrichment by Ti4+-IMAC and label-free quantitation enables in-depth monitoring of phosphorylation dynamics with high reproducibility and temporal resolution.* Mol Cell Proteomics, 2014. **13**(9): p. 2426-34.
258. Tsai, C.F., et al., *Immobilized metal affinity chromatography revisited: pH/acid control toward high selectivity in phosphoproteomics.* J Proteome Res, 2008. **7**(9): p. 4058-69.
259. Pinkse, M.W., et al., *Selective isolation at the femtomole level of phosphopeptides from proteolytic digests using 2D-NanoLC-ESI-MS/MS and titanium oxide precolumns.* Anal Chem, 2004. **76**(14): p. 3935-43.
260. Larsen, M.R., et al., *Highly selective enrichment of phosphorylated peptides from peptide mixtures using titanium dioxide microcolumns.* Mol Cell Proteomics, 2005. **4**(7): p. 873-86.
261. Aryal, U.K. and A.R. Ross, *Enrichment and analysis of phosphopeptides under different experimental conditions using titanium dioxide affinity chromatography and mass spectrometry.* Rapid Commun Mass Spectrom, 2010. **24**(2): p. 219-31.
262. Zarei, M., et al., *Comparison of ERLIC-TiO2, HILIC-TiO2, and SCX-TiO2 for global phosphoproteomics approaches.* J Proteome Res, 2011. **10**(8): p. 3474-83.
263. Delom, F. and E. Chevet, *Phosphoprotein analysis: from proteins to proteomes.* Proteome Sci, 2006. **4**: p. 15.
264. Schroeder, M.J., et al., *A neutral loss activation method for improved phosphopeptide sequence analysis by quadrupole ion trap mass spectrometry.* Anal Chem, 2004. **76**(13): p. 3590-8.
265. Olsen, J.V., et al., *Higher-energy C-trap dissociation for peptide modification analysis.* Nat Methods, 2007. **4**(9): p. 709-12.
266. Hart-Smith, G., *A review of electron-capture and electron-transfer dissociation tandem mass spectrometry in polymer chemistry.* Anal Chim Acta, 2014. **808**: p. 44-55.
267. Palumbo, A.M. and G.E. Reid, *Evaluation of gas-phase rearrangement and competing fragmentation reactions on protein phosphorylation site assignment using collision induced dissociation-MS/MS and MS3.* Anal Chem, 2008. **80**(24): p. 9735-47.
268. Savitski, M.M., et al., *Confident phosphorylation site localization using the Mascot Delta Score.* Mol Cell Proteomics, 2011. **10**(2): p. M110 003830.
269. McAllister, F.E., et al., *Mass spectrometry based method to increase throughput for kinome analyses using ATP probes.* Anal Chem, 2013. **85**(9): p. 4666-74.
270. Hernandez-Armenta, C., et al., *Benchmarking substrate-based kinase activity inference using phosphoproteomic data.* Bioinformatics, 2017.
271. Clark, L.C., Jr., et al., *Continuous recording of blood oxygen tensions by polarography.* J Appl Physiol, 1953. **6**(3): p. 189-93.

272. Lanza, I.R. and K.S. Nair, *Functional assessment of isolated mitochondria in vitro.* Methods Enzymol, 2009. **457**: p. 349-72.
273. Xie, H., et al., *LDH-A inhibition, a therapeutic strategy for treatment of hereditary leiomyomatosis and renal cell cancer.* Mol Cancer Ther, 2009. **8**(3): p. 626-35.
274. Putri, S.P., et al., *Current metabolomics: practical applications.* J Biosci Bioeng, 2013. **115**(6): p. 579-89.
275. Sreekumar, A., et al., *Metabolomic profiles delineate potential role for sarcosine in prostate cancer progression.* Nature, 2009. **457**(7231): p. 910-4.
276. Zhou, B., et al., *LC-MS-based metabolomics.* Mol Biosyst, 2012. **8**(2): p. 470-81.
277. Scheijen, J.L., et al., *L(+) and D(-) lactate are increased in plasma and urine samples of type 2 diabetes as measured by a simultaneous quantification of L(+) and D(-) lactate by reversed-phase liquid chromatography tandem mass spectrometry.* Exp Diabetes Res, 2012. **2012**: p. 234812.
278. Patti, G.J., O. Yanes, and G. Siuzdak, *Innovation: Metabolomics: the apogee of the omics trilogy.* Nat Rev Mol Cell Biol, 2012. **13**(4): p. 263-9.
279. Metallo, C.M., et al., *Reductive glutamine metabolism by IDH1 mediates lipogenesis under hypoxia.* Nature, 2011. **481**(7381): p. 380-4.
280. Bamshad, M.J., et al., *Exome sequencing as a tool for Mendelian disease gene discovery.* Nat Rev Genet, 2011. **12**(11): p. 745-55.
281. Kumar, P., S. Henikoff, and P.C. Ng, *Predicting the effects of coding non-synonymous variants on protein function using the SIFT algorithm.* Nat Protoc, 2009. **4**(7): p. 1073-81.
282. Adzhubei, I.A., et al., *A method and server for predicting damaging missense mutations.* Nat Methods, 2010. **7**(4): p. 248-9.
283. McLaren, W., et al., *The Ensembl Variant Effect Predictor.* Genome Biol, 2016. **17**(1): p. 122.
284. Forbes, S.A., et al., *COSMIC: mining complete cancer genomes in the Catalogue of Somatic Mutations in Cancer.* Nucleic Acids Res, 2011. **39**(Database issue): p. D945-50.
285. Kalyanaraman, B., et al., *Measuring reactive oxygen and nitrogen species with fluorescent probes: challenges and limitations.* Free Radic Biol Med, 2012. **52**(1): p. 1-6.
286. Schwartz, J.C. and I. Jardine, *Quadrupole ion trap mass spectrometry.* Methods Enzymol, 1996. **270**: p. 552-86.
287. Li, H. and R. Durbin, *Fast and accurate short read alignment with Burrows-Wheeler transform.* Bioinformatics, 2009. **25**(14): p. 1754-60.
288. DePristo, M.A., et al., *A framework for variation discovery and genotyping using next-generation DNA sequencing data.* Nat Genet, 2011. **43**(5): p. 491-8.
289. Saunders, C.T., et al., *Strelka: accurate somatic small-variant calling from sequenced tumor-normal sample pairs.* Bioinformatics, 2012. **28**(14): p. 1811-7.
290. Koboldt, D.C., et al., *VarScan 2: somatic mutation and copy number alteration discovery in cancer by exome sequencing.* Genome Res, 2012. **22**(3): p. 568-76.
291. Van Loo, P., et al., *Allele-specific copy number analysis of tumors.* Proc Natl Acad Sci U S A, 2010. **107**(39): p. 16910-5.
292. Stratton, M.R., P.J. Campbell, and P.A. Futreal, *The cancer genome.* Nature, 2009. **458**(7239): p. 719-24.
293. Martincorena, I. and P.J. Campbell, *Somatic mutation in cancer and normal cells.* Science, 2015. **349**(6255): p. 1483-9.
294. Lu, C., et al., *Histone H3K36 mutations promote sarcomagenesis through altered histone methylation landscape.* Science, 2016. **352**(6287): p. 844-9.
295. Bonnet, D. and J.E. Dick, *Human acute myeloid leukemia is organized as a hierarchy that originates from a primitive hematopoietic cell.* Nat Med, 1997. **3**(7): p. 730-7.
296. Niepel, M., S.L. Spencer, and P.K. Sorger, *Non-genetic cell-to-cell variability and the consequences for pharmacology.* Curr Opin Chem Biol, 2009. **13**(5-6): p. 556-61.

297. Reymond, N., B.B. d'Agua, and A.J. Ridley, *Crossing the endothelial barrier during metastasis.* Nat Rev Cancer, 2013. **13**(12): p. 858-70.
298. Dennis, G., Jr., et al., *DAVID: Database for Annotation, Visualization, and Integrated Discovery.* Genome Biol, 2003. **4**(5): p. P3.
299. Ashburner, M., et al., *Gene ontology: tool for the unification of biology. The Gene Ontology Consortium.* Nat Genet, 2000. **25**(1): p. 25-9.
300. Schaefer, C.F., et al., *PID: the Pathway Interaction Database.* Nucleic Acids Res, 2009. **37**(Database issue): p. D674-9.
301. Liu, P., et al., *Oncogenic PIK3CA-driven mammary tumors frequently recur via PI3K pathway-dependent and PI3K pathway-independent mechanisms.* Nat Med, 2011. **17**(9): p. 1116-20.
302. Gupta, S., A. Seth, and R.J. Davis, *Transactivation of gene expression by Myc is inhibited by mutation at the phosphorylation sites Thr-58 and Ser-62.* Proc Natl Acad Sci U S A, 1993. **90**(8): p. 3216-20.
303. Qu, L., et al., *Endoplasmic reticulum stress induces p53 cytoplasmic localization and prevents p53-dependent apoptosis by a pathway involving glycogen synthase kinase-3beta.* Genes Dev, 2004. **18**(3): p. 261-77.
304. Posch, C., et al., *Combined targeting of MEK and PI3K/mTOR effector pathways is necessary to effectively inhibit NRAS mutant melanoma in vitro and in vivo.* Proc Natl Acad Sci U S A, 2013. **110**(10): p. 4015-20.
305. Elkabets, M., et al., *AXL mediates resistance to PI3Kalpha inhibition by activating the EGFR/PKC/mTOR axis in head and neck and esophageal squamous cell carcinomas.* Cancer Cell, 2015. **27**(4): p. 533-46.
306. Pelicano, H., et al., *Mitochondrial dysfunction in some triple-negative breast cancer cell lines: role of mTOR pathway and therapeutic potential.* Breast Cancer Res, 2014. **16**(5): p. 434.
307. Marcu, R., et al., *Mitochondrial matrix Ca(2)(+) accumulation regulates cytosolic NAD(+)/NADH metabolism, protein acetylation, and sirtuin expression.* Mol Cell Biol, 2014. **34**(15): p. 2890-902.
308. Wu, M., et al., *Multiparameter metabolic analysis reveals a close link between attenuated mitochondrial bioenergetic function and enhanced glycolysis dependency in human tumor cells.* Am J Physiol Cell Physiol, 2007. **292**(1): p. C125-36.
309. Liu, W., et al., *Targeted genes and interacting proteins of hypoxia inducible factor-1.* Int J Biochem Mol Biol, 2012. **3**(2): p. 165-78.
310. Burr, S.P., et al., *Mitochondrial Protein Lipoylation and the 2-Oxoglutarate Dehydrogenase Complex Controls HIF1alpha Stability in Aerobic Conditions.* Cell Metab, 2016. **24**(5): p. 740-752.
311. Gao, P., et al., *HIF-dependent antitumorigenic effect of antioxidants in vivo.* Cancer Cell, 2007. **12**(3): p. 230-8.
312. Birsoy, K., et al., *Metabolic determinants of cancer cell sensitivity to glucose limitation and biguanides.* Nature, 2014. **508**(7494): p. 108-12.
313. Muellner, M.K., et al., *A chemical-genetic screen reveals a mechanism of resistance to PI3K inhibitors in cancer.* Nat Chem Biol, 2011. **7**(11): p. 787-93.
314. Ilic, N., et al., *PI3K-targeted therapy can be evaded by gene amplification along the MYC-eukaryotic translation initiation factor 4E (eIF4E) axis.* Proc Natl Acad Sci U S A, 2011. **108**(37): p. E699-708.
315. Anderson, A.R., et al., *Tumor morphology and phenotypic evolution driven by selective pressure from the microenvironment.* Cell, 2006. **127**(5): p. 905-15.
316. Gerlinger, M., et al., *Intratumor heterogeneity and branched evolution revealed by multiregion sequencing.* N Engl J Med, 2012. **366**(10): p. 883-92.
317. Ramirez, M., et al., *Diverse drug-resistance mechanisms can emerge from drug-tolerant cancer persister cells.* Nat Commun, 2016. **7**: p. 10690.

318. Lee, W., et al., *The mutation spectrum revealed by paired genome sequences from a lung cancer patient.* Nature, 2010. **465**(7297): p. 473-7.
319. Dokmanovic, M., et al., *Trastuzumab-induced recruitment of Csk-homologous kinase (CHK) to ErbB2 receptor is associated with ErbB2-Y1248 phosphorylation and ErbB2 degradation to mediate cell growth inhibition.* Cancer Biol Ther, 2014. **15**(8): p. 1029-41.
320. Schramek, D., et al., *The stress kinase MKK7 couples oncogenic stress to p53 stability and tumor suppression.* Nat Genet, 2011. **43**(3): p. 212-9.
321. Cristobal, I., et al., *SETBP1 overexpression is a novel leukemogenic mechanism that predicts adverse outcome in elderly patients with acute myeloid leukemia.* Blood, 2010. **115**(3): p. 615-25.
322. Chen, D., et al., *LIFR is a breast cancer metastasis suppressor upstream of the Hippo-YAP pathway and a prognostic marker.* Nat Med, 2012. **18**(10): p. 1511-7.
323. Ryland, G.L., et al., *Loss of heterozygosity: what is it good for?* BMC Med Genomics, 2015. **8**: p. 45.
324. Zhou, L., et al., *FASN, ErbB2-mediated glycolysis is required for breast cancer cell migration.* Oncol Rep, 2016. **35**(5): p. 2715-22.
325. Pfister, A.B., et al., *Early response to ErbB2 over-expression in polarized Caco-2 cells involves partial segregation from ErbB3 by relocalization to the apical surface and initiation of survival signaling.* J Cell Biochem, 2010. **111**(3): p. 643-52.
326. Ishizawar, R.C., T. Miyake, and S.J. Parsons, *c-Src modulates ErbB2 and ErbB3 heterocomplex formation and function.* Oncogene, 2007. **26**(24): p. 3503-10.
327. Xu, H., et al., *Enhanced RAD21 cohesin expression confers poor prognosis and resistance to chemotherapy in high grade luminal, basal and HER2 breast cancers.* Breast Cancer Res, 2011. **13**(1): p. R9.
328. Nancolas, B., R.B. Sessions, and A.P. Halestrap, *Identification of key binding site residues of MCT1 for AR-C155858 reveals the molecular basis of its isoform selectivity.* Biochem J, 2015. **466**(1): p. 177-88.
329. Kapushesky, M., et al., *Gene expression atlas at the European bioinformatics institute.* Nucleic Acids Res, 2010. **38**(Database issue): p. D690-8.
330. van der Valk, J., et al., *Optimization of chemically defined cell culture media--replacing fetal bovine serum in mammalian in vitro methods.* Toxicol In Vitro, 2010. **24**(4): p. 1053-63.
331. Li, G., et al., *Distinct pathways of ERK1/2 activation by hydroxy-carboxylic acid receptor-1.* PLoS One, 2014. **9**(3): p. e93041.
332. Gupta, S.C., et al., *Acidosis promotes invasiveness of breast cancer cells through ROS-AKT-NF-kappaB pathway.* Oncotarget, 2014. **5**(23): p. 12070-82.
333. Haworth, R.S., S. Dashnyam, and M. Avkiran, *Ras triggers acidosis-induced activation of the extracellular-signal-regulated kinase pathway in cardiac myocytes.* Biochem J, 2006. **399**(3): p. 493-501.
334. Berwick, D.C., et al., *The identification of ATP-citrate lyase as a protein kinase B (Akt) substrate in primary adipocytes.* J Biol Chem, 2002. **277**(37): p. 33895-900.
335. Chen, C.H., et al., *ER stress inhibits mTORC2 and Akt signaling through GSK-3beta-mediated phosphorylation of rictor.* Sci Signal, 2011. **4**(161): p. ra10.
336. Foster, K.G., et al., *Regulation of mTOR complex 1 (mTORC1) by raptor Ser863 and multisite phosphorylation.* J Biol Chem, 2010. **285**(1): p. 80-94.
337. Amano, M., et al., *Formation of actin stress fibers and focal adhesions enhanced by Rho-kinase.* Science, 1997. **275**(5304): p. 1308-11.
338. Xie, J., et al., *Beyond Warburg effect--dual metabolic nature of cancer cells.* Sci Rep, 2014. **4**: p. 4927.
339. Jamali, S., et al., *Hypoxia-induced carbonic anhydrase IX facilitates lactate flux in human breast cancer cells by non-catalytic function.* Sci Rep, 2015. **5**: p. 13605.

340. Welshons, W.V., et al., *Control of proliferation of MCF-7 breast cancer cells in a commercial preparation of charcoal-stripped adult bovine serum.* Breast Cancer Res Treat, 1992. **23**(1-2): p. 97-104.
341. Damaghi, M., J.W. Wojtkowiak, and R.J. Gillies, *pH sensing and regulation in cancer.* Front Physiol, 2013. **4**: p. 370.
342. Das Thakur, M. and D.D. Stuart, *The evolution of melanoma resistance reveals therapeutic opportunities.* Cancer Res, 2013. **73**(20): p. 6106-10.
343. Carmona-Fontaine, C., et al., *Emergence of spatial structure in the tumor microenvironment due to the Warburg effect.* Proc Natl Acad Sci U S A, 2013. **110**(48): p. 19402-7.
344. Zhao, Y., et al., *Overcoming trastuzumab resistance in breast cancer by targeting dysregulated glucose metabolism.* Cancer Res, 2011. **71**(13): p. 4585-97.
345. Cantley, L.C., *The phosphoinositide 3-kinase pathway.* Science, 2002. **296**(5573): p. 1655-7.
346. Hata, A.N., et al., *Tumor cells can follow distinct evolutionary paths to become resistant to epidermal growth factor receptor inhibition.* Nat Med, 2016. **22**(3): p. 262-9.
347. Lipinski, K.A., et al., *Cancer Evolution and the Limits of Predictability in Precision Cancer Medicine.* Trends Cancer, 2016. **2**(1): p. 49-63.
348. Blount, Z.D., C.Z. Borland, and R.E. Lenski, *Historical contingency and the evolution of a key innovation in an experimental population of Escherichia coli.* Proc Natl Acad Sci U S A, 2008. **105**(23): p. 7899-906.
349. Gotink, K.J., et al., *Cross-resistance to clinically used tyrosine kinase inhibitors sunitinib, sorafenib and pazopanib.* Cell Oncol (Dordr), 2015. **38**(2): p. 119-29.
350. Missner, E., et al., *Off-target decoding of a multitarget kinase inhibitor by chemical proteomics.* Chembiochem, 2009. **10**(7): p. 1163-74.
351. Tan, S., Y. Ng, and D.E. James, *Next-generation Akt inhibitors provide greater specificity: effects on glucose metabolism in adipocytes.* Biochem J, 2011. **435**(2): p. 539-44.
352. Lindsley, C.W., et al., *Allosteric Akt (PKB) inhibitors: discovery and SAR of isozyme selective inhibitors.* Bioorg Med Chem Lett, 2005. **15**(3): p. 761-4.
353. Garcia-Martinez, J.M., et al., *Ku-0063794 is a specific inhibitor of the mammalian target of rapamycin (mTOR).* Biochem J, 2009. **421**(1): p. 29-42.
354. Wall, M., et al., *The mTORC1 inhibitor everolimus prevents and treats Emu-Myc lymphoma by restoring oncogene-induced senescence.* Cancer Discov, 2013. **3**(1): p. 82-95.
355. Sherk, A.B., et al., *Development of a small-molecule serum- and glucocorticoid-regulated kinase-1 antagonist and its evaluation as a prostate cancer therapeutic.* Cancer Res, 2008. **68**(18): p. 7475-83.
356. Dengler, M.A., et al., *Oncogenic stress induced by acute hyper-activation of Bcr-Abl leads to cell death upon induction of excessive aerobic glycolysis.* PLoS One, 2011. **6**(9): p. e25139.
357. Hanfstein, B., et al., *Dynamics of mutant BCR-ABL-positive clones after cessation of tyrosine kinase inhibitor therapy.* Haematologica, 2011. **96**(3): p. 360-6.
358. Amin, A.D., et al., *Evidence Suggesting That Discontinuous Dosing of ALK Kinase Inhibitors May Prolong Control of ALK+ Tumors.* Cancer Res, 2015. **75**(14): p. 2916-27.
359. Liu, P., et al., *Targeting the phosphoinositide 3-kinase pathway in cancer.* Nat Rev Drug Discov, 2009. **8**(8): p. 627-44.
360. Lawrence, R.T., et al., *The proteomic landscape of triple-negative breast cancer.* Cell Rep, 2015. **11**(4): p. 630-44.
361. Mertins, P., et al., *Proteogenomics connects somatic mutations to signalling in breast cancer.* Nature, 2016. **534**(7605): p. 55-62.
362. Zhang, H., et al., *Integrated Proteogenomic Characterization of Human High-Grade Serous Ovarian Cancer.* Cell, 2016. **166**(3): p. 755-65.
363. Ruscetti, M., et al., *HDAC inhibition impedes epithelial-mesenchymal plasticity and suppresses metastatic, castration-resistant prostate cancer.* Oncogene, 2016. **35**(29): p. 3781-95.

364. Geiger, T., et al., *Proteomic portrait of human breast cancer progression identifies novel prognostic markers.* Cancer Res, 2012. **72**(9): p. 2428-39.
365. Engelman, J.A., J. Luo, and L.C. Cantley, *The evolution of phosphatidylinositol 3-kinases as regulators of growth and metabolism.* Nat Rev Genet, 2006. **7**(8): p. 606-19.
366. Mottet, D., et al., *Regulation of hypoxia-inducible factor-1alpha protein level during hypoxic conditions by the phosphatidylinositol 3-kinase/Akt/glycogen synthase kinase 3beta pathway in HepG2 cells.* J Biol Chem, 2003. **278**(33): p. 31277-85.
367. Zhong, H., et al., *Modulation of hypoxia-inducible factor 1alpha expression by the epidermal growth factor/phosphatidylinositol 3-kinase/PTEN/AKT/FRAP pathway in human prostate cancer cells: implications for tumor angiogenesis and therapeutics.* Cancer Res, 2000. **60**(6): p. 1541-5.
368. Le Gal, K., et al., *Antioxidants can increase melanoma metastasis in mice.* Sci Transl Med, 2015. **7**(308): p. 308re8.
369. Jahangiri, A. and W.A. Weiss, *It takes two to tango: Dual inhibition of PI3K and MAPK in rhabdomyosarcoma.* Clin Cancer Res, 2013. **19**(21): p. 5811-3.
370. Bendall, S.C., et al., *Single-cell mass cytometry of differential immune and drug responses across a human hematopoietic continuum.* Science, 2011. **332**(6030): p. 687-96.
371. Wei, W., et al., *Single-Cell Phosphoproteomics Resolves Adaptive Signaling Dynamics and Informs Targeted Combination Therapy in Glioblastoma.* Cancer Cell, 2016. **29**(4): p. 563-73.
372. Baek, S.H., *When signaling kinases meet histones and histone modifiers in the nucleus.* Mol Cell, 2011. **42**(3): p. 274-84.
373. Chou, T.C., *Drug combination studies and their synergy quantification using the Chou-Talalay method.* Cancer Res, 2010. **70**(2): p. 440-6.
374. Maiso, P., et al., *Metabolic signature identifies novel targets for drug resistance in multiple myeloma.* Cancer Res, 2015. **75**(10): p. 2071-82.
375. Sancho, P., et al., *MYC/PGC-1alpha Balance Determines the Metabolic Phenotype and Plasticity of Pancreatic Cancer Stem Cells.* Cell Metab, 2015. **22**(4): p. 590-605.
376. Carracedo, A. and P.P. Pandolfi, *The PTEN-PI3K pathway: of feedbacks and cross-talks.* Oncogene, 2008. **27**(41): p. 5527-41.
377. Cao, Y., et al., *Tumor cells upregulate normoxic HIF-1alpha in response to doxorubicin.* Cancer Res, 2013. **73**(20): p. 6230-42.
378. Shroff, E.H., et al., *MYC oncogene overexpression drives renal cell carcinoma in a mouse model through glutamine metabolism.* Proc Natl Acad Sci U S A, 2015. **112**(21): p. 6539-44.
379. Muller, I., et al., *Targeting of the MYCN protein with small molecule c-MYC inhibitors.* PLoS One, 2014. **9**(5): p. e97285.
380. Campaner, S. and B. Amati, *Two sides of the Myc-induced DNA damage response: from tumor suppression to tumor maintenance.* Cell Div, 2012. **7**(1): p. 6.
381. Pourdehnad, M., et al., *Myc and mTOR converge on a common node in protein synthesis control that confers synthetic lethality in Myc-driven cancers.* Proc Natl Acad Sci U S A, 2013. **110**(29): p. 11988-93.
382. Castel, P., et al., *PDK1-SGK1 Signaling Sustains AKT-Independent mTORC1 Activation and Confers Resistance to PI3Kalpha Inhibition.* Cancer Cell, 2016. **30**(2): p. 229-42.
383. Faes, S. and O. Dormond, *PI3K and AKT: Unfaithful Partners in Cancer.* Int J Mol Sci, 2015. **16**(9): p. 21138-52.
384. De Saedeleer, C.J., et al., *Glucose deprivation increases monocarboxylate transporter 1 (MCT1) expression and MCT1-dependent tumor cell migration.* Oncogene, 2014. **33**(31): p. 4060-8.
385. Sounni, N.E., et al., *Blocking lipid synthesis overcomes tumor regrowth and metastasis after antiangiogenic therapy withdrawal.* Cell Metab, 2014. **20**(2): p. 280-94.
386. Siravegna, G., et al., *Clonal evolution and resistance to EGFR blockade in the blood of colorectal cancer patients.* Nat Med, 2015. **21**(7): p. 795-801.

387. Okosun, J., et al., *Recurrent mTORC1-activating RRAGC mutations in follicular lymphoma.* Nat Genet, 2016. **48**(2): p. 183-8.
388. Blau, C.A. and E. Liakopoulou, *Can we deconstruct cancer, one patient at a time?* Trends Genet, 2013. **29**(1): p. 6-10.
389. Nakanishi, Y., et al., *Activating Mutations in PIK3CB Confer Resistance to PI3K Inhibition and Define a Novel Oncogenic Role for p110beta.* Cancer Res, 2016. **76**(5): p. 1193-203.
390. White, S.L., et al., *Cellular responses to ErbB-2 overexpression in human mammary luminal epithelial cells: comparison of mRNA and protein expression.* Br J Cancer, 2004. **90**(1): p. 173-81.
391. Gould, S.J., *Wonderful life : the Burgess Shale and the nature of history*. 1st ed. 1989, New York: W.W. Norton. 347 p.
392. Warburg, O., *On the origin of cancer cells.* Science, 1956. **123**(3191): p. 309-14.
393. Hussien, R. and G.A. Brooks, *Mitochondrial and plasma membrane lactate transporter and lactate dehydrogenase isoform expression in breast cancer cell lines.* Physiol Genomics, 2011. **43**(5): p. 255-64.
394. Morais-Santos, F., et al., *Targeting lactate transport suppresses in vivo breast tumour growth.* Oncotarget, 2015. **6**(22): p. 19177-89.
395. Roland, C.L., et al., *Cell surface lactate receptor GPR81 is crucial for cancer cell survival.* Cancer Res, 2014. **74**(18): p. 5301-10.
396. Riemann, A., et al., *Acidic environment leads to ROS-induced MAPK signaling in cancer cells.* PLoS One, 2011. **6**(7): p. e22445.
397. Leprivier, G., et al., *The eEF2 kinase confers resistance to nutrient deprivation by blocking translation elongation.* Cell, 2013. **153**(5): p. 1064-79.
398. Chen, J.L., et al., *Lactic acidosis triggers starvation response with paradoxical induction of TXNIP through MondoA.* PLoS Genet, 2010. **6**(9): p. e1001093.
399. Bjorkoy, G., et al., *p62/SQSTM1 forms protein aggregates degraded by autophagy and has a protective effect on huntingtin-induced cell death.* J Cell Biol, 2005. **171**(4): p. 603-14.
400. Jeanson, Y., et al., *Lactate induces FGF21 expression in adipocytes through a p38-MAPK pathway.* Biochem J, 2016. **473**(6): p. 685-92.
401. Shiraishi, T., et al., *Glycolysis is the primary bioenergetic pathway for cell motility and cytoskeletal remodeling in human prostate and breast cancer cells.* Oncotarget, 2015. **6**(1): p. 130-43.
402. Chen, P., et al., *Gpr132 sensing of lactate mediates tumor-macrophage interplay to promote breast cancer metastasis.* Proc Natl Acad Sci U S A, 2017. **114**(3): p. 580-585.
403. Li, J., et al., *Ovarian cancer G protein coupled receptor 1 suppresses cell migration of MCF7 breast cancer cells via a Galpha12/13-Rho-Rac1 pathway.* J Mol Signal, 2013. **8**(1): p. 6.
404. Lauritzen, G., et al., *The Na+/H+ exchanger NHE1, but not the Na+, HCO3(-) cotransporter NBCn1, regulates motility of MCF7 breast cancer cells expressing constitutively active ErbB2.* Cancer Lett, 2012. **317**(2): p. 172-83.
405. Mardakheh, F.K., et al., *Proteomics profiling of interactome dynamics by colocalisation analysis (COLA).* Mol Biosyst, 2016. **13**(1): p. 92-105.
406. Ribeiro Ede, A., Jr., et al., *The structure and regulation of human muscle alpha-actinin.* Cell, 2014. **159**(6): p. 1447-60.
407. Schonichen, A., et al., *Considering protonation as a posttranslational modification regulating protein structure and function.* Annu Rev Biophys, 2013. **42**: p. 289-314.
408. Hong, C.S., et al., *MCT1 Modulates Cancer Cell Pyruvate Export and Growth of Tumors that Co-express MCT1 and MCT4.* Cell Rep, 2016. **14**(7): p. 1590-601.